Spring 5-15-2023

Ribosomes as Sensors: How Cells Utilize the Translational Process to Monitor Cellular Conditions

Kyusik Q. Kim

WASHINGTON UNIVERSITY IN ST. LOUIS

Division of Biology and Biomedical Sciences
Molecular Cell Biology

Dissertation Examination Committee:
Hani Zaher, Chair
Sergej Djuranovic
Michael B Major
Heather L True
Zhongsheng You

Ribosomes as Sensors: How Cells Utilize the Translational Process to Monitor Cellular Conditions

by

Kyusik Kim

A dissertation presented to
Washington University in St. Louis
in partial fulfillment of the
requirements for the degree
of Doctor of Philosophy

May 2023
St. Louis, Missouri

Table of Contents

List of Figures

List of Tables

Acknowledgments

The work described in this dissertation was supported by funding from the National Institutes of Health (R01GM112641, R00GM094210, R01GM141474 to H.S.Z.).

Kyusik Kim

Washington University in St. Louis

May 2023

Dedicated to my significant other, Nicolette, and all the friends and family that have helped me along the way.

ABSTRACT OF THE DISSERTATION

Ribosomes as Sensors: How Cells Utilize the Translational Process to Monitor Cellular Conditions

by

Kyusik Kim

Doctor of Philosophy in Biology and Biomedical Sciences

Molecular Cell Biology

Washington University in St. Louis, 2023

Hani Zaher, Chair

Cells must constantly modulate their gene expression in response to ever-shifting environmental conditions. In order to do so, cells require mechanisms to relay information from the environment to the gene expression machinery. Increasingly, evidence has come to suggest that the translational machinery is utilized by the cell to capture and convey these signals. In particular, cells appear to monitor collisions between ribosomes to select the appropriate response pathways.

We are just beginning to understand how disruptions in normal ribosome dynamics signal for various responses and how the ribosome contributes to this process. In this work, we find that inhibition of canonical initiation in yeast results in activation of a conserved eukaryotic stress response known as the integrated stress response (ISR). In investigating the consequences of modified nucleobases in the mRNA, we report that N1-methylpseudouridine, the modification used in the COVID-19 mRNA vaccines, is translated faithfully. On the other hand, we report that the presence of alkyl adducts on the transcript stall the ribosome and activates ribosome rescue

pathways in bacteria. For the No-Go Decay mRNA quality control pathway, we show that contacts between the ribosome and the mRNA are important for the ensuing cleavage events. Finally, we show that ISR activation may be more regulated than previously thought, involving two independent factors – Gcn2 and Mbf1 – to monitor ribosome collisions. Taken together, this work offers insights into how cells integrate signals from ribosomes in order to make wider decisions about allocation of cellular resources.

Chapter 1

Ribosomes as sensors of the cellular state

Kyusik Kim and Hani S Zaher

Abstract

The discovery that collisions between ribosomes are the key signaling event that triggers quality control and stress response pathways in eukaryotes has changed our understanding of how cells sense and respond to the environment. Collided eukaryotic ribosomes adopt a unique structure, providing a mechanistic basis for how environmental signals can be sensed by the translational machinery and propagated into wider reprogramming of gene expression. Indeed, the use of ribosomes as a signaling hub is quite apt, as ribosomes make intimate contact with both mRNA and tRNAs. This enables them to monitor the integrity of genetic information coming from the nucleus while simultaneously checking the availability of cellular resources, acting as a sentinel of the central dogma of biology. Here, we discuss the ribosome in the context of the broader translational cycle and how signals arise from disruptions to ribosome function. We also discuss the effects of modifications to the mRNA on the ribosome and the role of the ribosome in the response to these effects.

Introduction

Cellular function is predicated on the identities and concentration of proteins produced by the cell. Thus, cells devote a large portion of their metabolism to protein synthesis – comprising 30% of total metabolism for mammalian cells and 50% of total metabolism for bacterial cells (Buttgereit and Brand, 1995; Russell and Cook, 1995). In order to maintain this tremendous output, cells must be able to modulate their gene expression in response to dynamic environmental conditions. Such a task requires mechanisms to capture information about the environment and convey this information to the gene expression machinery. Increasingly, evidence has come to suggest that the ribosome, the biological machine directly responsible for translating encoded genetic information into proteins, plays the role of this environmental sensor.

Ribosomes are uniquely suited to this function as a sensor. Of the players of the central dogma, they are the most abundant, in the order of 10^6-10^7 for eukaryotic cells (Duncan and Hershey, 1983; Ho et al., 2018; Jonathan R. Warner, 1999), compared to 10^4 and 10^3 for RNA and DNA polymerase, respectively (Beck et al., 2011; Ho et al., 2018; Wiśniewski et al., 2014). They are also at the crux of a process which gauges the mRNA integrity, energy status, and nutrient availability. Furthermore, ribosomes are massive complexes composed of proteins in addition to their constituent rRNA, providing a means to integrate and transmit information via interfacing with other cellular proteins.

Initiation

To understand how ribosome dynamics contribute to regulation of gene expression, we must first discuss ribosomes in the broader context of the translational cycle: initiation,

elongation, termination, and recycling. The following discussion largely pertains to eukaryotes, as the work primarily concerns translation in eukaryotic systems.

Canonical initiation in eukaryotes begins with the formation of 43S preinitiation complexes (43S PICs). 43S PICs are comprised of the 40S ribosomal subunit bound by the initiation factors eIF1, eIF1A, eIF3, and ternary complex (TC) – initiator methionyl-tRNA and GTP in complex with the initiation factor eIF2 (Hinnebusch and Lorsch, 2012; Jackson et al., 2010; Pelletier and Sonenberg, 2019). Once assembled, 43S PICs are recruited to the 5'm7Gppp cap structure of a transcript by the eIF4F complex, which is comprised of the cap binding factor eIF4E, DEAD-box RNA helicase eIF4A, and scaffolding factor eIF4G (Hinnebusch and Lorsch, 2012; Jackson et al., 2010; Pelletier and Sonenberg, 2019). The 43S PIC then begins scanning for a start codon in the correct sequence context (Hinnebusch, 2017, 2014, 2011; Kolitz et al., 2009; Lomakin et al., 2006), and when found, results in hydrolysis of GTP and release of inorganic phosphate (P_i) from the ternary complex (Algire et al., 2005). Release of P_i and dissociation of eIF1, eIF1A, eIF3, and eIF2-GDP leads to eIF5B-mediated joining of the 60S ribosomal, leaving an 80S ribosome primed for elongation (Pestova et al., 2000).

Integrated Stress Response

Under conditions such as amino acid deprivation or detection of viral RNA, eukaryotes inhibit initiation via a conserved stress response known as the integrated stress response (ISR) (Harding et al., 2019; Hinnebusch, 2005; Pakos-Zebrucka et al., 2016). Signaling in this system begins with distinct protein kinases which monitor for unique stresses. Mammals have four such kinases: GCN2 for amino acid starvation, PERK for endoplasmic reticulum (ER) stress, PKR for viral infection, and HRI for heme insufficiency, while yeast have only Gcn2 (Baird and Wek, 2012; Jackson et al., 2010; Pavitt, 2005). Upon activation when their particular stress is detected,

the kinases phosphorylate Ser51 in the alpha subunit of eIF2 (Dever et al., 1992). Phosphorylation of eIF2α in turn converts eIF2 into an inhibitor of its guanine exchange factor eIF2B, inhibiting formation of new ternary complexes and thus, 43S PICs (Krishnamoorthy et al., 2001; Rowlands et al., 1988). As eIF2 is present at higher concentrations than eIF2B (Kulak et al., 2014; Von der Haar and McCarthy, 2002), even slightly elevated levels of phosphorylated eIF2α results in rapid inhibition of eIF2B, depletion of TC, and repression of initiation. At the same time, these conditions also promote translation of stress response genes. Key genes include transcription factors that are the master effectors of the downstream response, such as *GCN4* in yeast and *ATF4* in mammals.

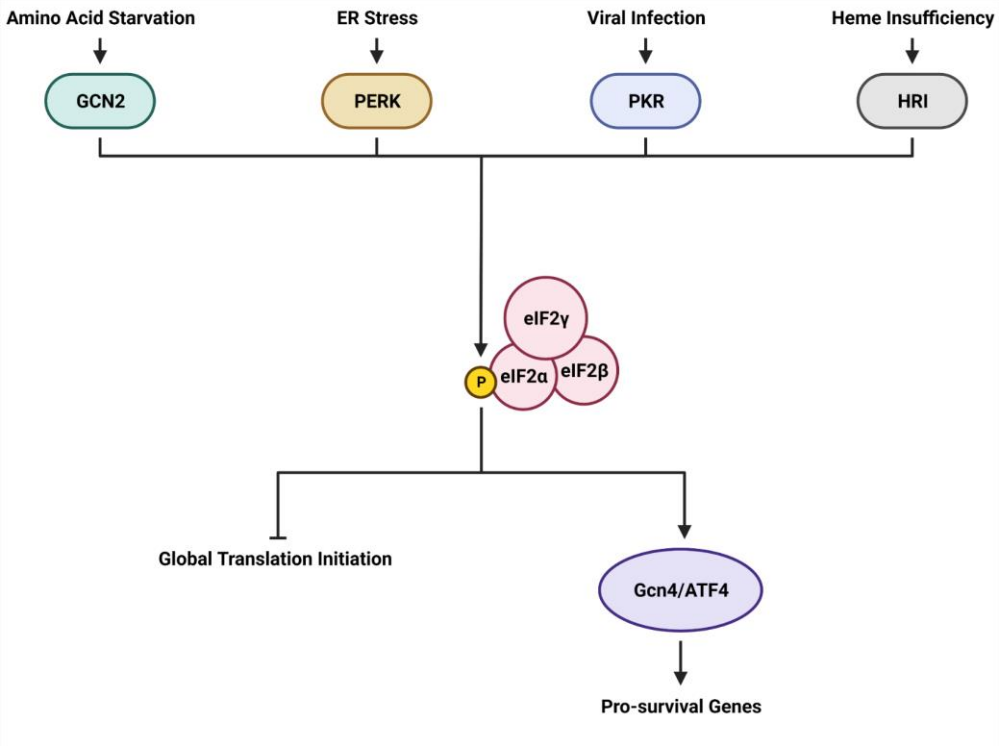

Figure 1: Overview of Integrated Stress Response signaling
In mammals, the kinases GCN2, PERK, PKR, and HRI monitor distinct stresses. Upon activation in response to their particular stress, the kinase phosphorylates the alpha subunit of eIF2. Phosphorylation of eIF2α then results in repression of global translation initiation while simultaneously enabling the selective translation of stress response genes such as ATF4. The ISR is conserved in yeast, but with the presence of only one kinase, Gcn2. The functional homolog of ATF4 in yeast is Gcn4.

Target of Rapamycin (TOR) Signaling Pathway

The TOR signaling pathway promotes anabolic metabolism while repressing catabolic processes in response to nutrients (González and Hall, 2017; Howell et al., 2013; Laplante and Sabatini, 2012; Loewith and Hall, 2011; Shimobayashi and Hall, 2014; Wullschleger et al., 2006). The pathway is comprised of two distinct complexes, TORC1 and TORC2 (mTOR1 and 2 in mammals), with only TORC1 sensitive to rapamycin and regulated by amino acids levels (Loewith et al., 2002). Upon sensing of amino acids, a conserved family of RAG small GTPases form heterodimers and activate TORC1 via an upstream factor (González and Hall, 2017; Nakashima et al., 1999; Sekiguchi et al., 2001). Activation of TORC1 then promotes growth by regulatory phosphorylation of downstream factors involved in pathways such as autophagy, cytoskeleton organization, lipid metabolism, cell migration, and cell division (Battaglioni et al., 2022).

The TOR pathway, in conjunction with the ISR, is also able to repress translation initiation in response to amino acid availability. One of the targets of TOR is eIF4E binding proteins (4E-BPs), which compete with eIF4E for binding to eIF4G (Gingras et al., 2001a, 2001b, 1999). TOR signaling maintains inhibitory phosphorylation of 4E-BPs, but under conditions where TOR signaling is inactivated, repression of 4E-BP activity is released (Gingras et al., 2001a, 2001b, 1999). In addition, TOR plays a role in the regulatory phosphorylation of other factors involved in translation (Fonseca et al., 2014).

Since both GCN2 and TOR regulate translation in response to amino acids, it is likely the pathways communicate with each another. In yeast, TOR inhibition by rapamycin can activate Gcn2 in an amino acid starvation-independent manner by dephosphorylating serine 577 via Sit4 (a Tap42-associated type 2 protein phosphatase 2A) (Cherkasova and Hinnebusch, 2003; Kubota

et al., 2003). By contrast, amino acid deprivation-mediated inhibition of mTORC1 in mammals appears to require GCN2 (Anthony et al., 2004; Xiao et al., 2011). However, it is unclear if GCN2 or ATF4 is the responsible factor (Averous et al., 2016; Ye et al., 2015).

Regardless of how the two pathways communicate with each other, stress response genes are upregulated under conditions where both pathways inhibit translation. This suggests that these genes harbor elements or are translated via mechanisms that are resistant to both loss of eIF4E activity and depletion of eIF2 ternary complexes. One potential class of elements are internal ribosome entry sites (IRESes), which are sequences that form structures able to directly recruit ribosomes (Jang et al., 1988; Lee et al., 2017; Martinez-Salas et al., 2018; Pelletier and Sonenberg, 1988). IRESes are prevalent among viruses as a means to bypass host regulatory mechanisms (Lee et al., 2017; Martinez-Salas et al., 2018), but the presence of IRESes, or alternative mechanisms of initiation, in eukaryotic genomes has yet to be widely characterized (Yang and Wang, 2019).

Elongation and tRNA selection

During elongation, the ribosome traverses across the transcript in discrete steps and decodes it by interrogating interactions between the codons of the mRNA and the anticodons of tRNAs, forming peptide bonds when the correct interactions are found (Dever et al., 2018; Rodnina, 2018). For accurate decoding, the ribosome must discriminate between cognate (no mismatch between the anticodon of the tRNA and the codon of the mRNA), near-cognate (one mismatch), and non-cognate (greater than one mismatch) amino-acylated tRNAs (aa-tRNAs). The ribosome is able to do so by utilizing differences in kinetics via a mechanism known as induced fit; matches accelerate forward rates while mismatches accelerate dissociation of the tRNA (Koshland, 1958; Pape, 1999; Pape et al., 2000; Rodnina and Wintermeyer, 2001). As

many of the mechanistic details were elucidated in bacteria (Dever et al., 2018; Rodnina, 2018), the following will describe tRNA selection in bacteria for simplicity.

Selection of tRNAs occurs in two phases: initial selection and kinetic proofreading (Rodnina et al., 2005). In initial selection, an aa-tRNA, in complex with EF-Tu • GTP, binds to the A-site of the ribosome, forming a complex that is readily reversible (Pape, 1999; Rodnina et al., 1996). Contacts occur between the tRNA and the mRNA in the decoding center of the ribosome small subunit, and if the pair do not form a duplex, the complex dissociates, and the process repeats with a new aa-tRNA • EF-Tu • GTP (Blanchard et al., 2004; Gromadski and Rodnina, 2004; Ogle et al., 2001; Pape, 1999). However, if the pair forms a duplex, then the universally conserved bases A1492, A1493, and G530 of the 16S rRNA change conformation to monitor the minor groove of the first two base pairs of the duplex (Ogle et al., 2001). If Watson-Crick base pairing geometry is then detected, A-minor interactions formed by these residues stabilize the complex and induce further conformational changes in the ribosome and EF-Tu, stimulating GTP hydrolysis (Gromadski et al., 2006; Gromadski and Rodnina, 2004; Ogle et al., 2002; Pape, 1999; Rodnina et al., 1995). Once GTP hydrolysis occurs, EF-Tu undergoes further conformational changes and is released from the aa-tRNA, enabling progress into the proofreading phase (Pape, 1999).

During proofreading, aa-tRNAs are either accommodated, moving completely into the A-site, or rejected, leading to their dissociation from the ribosome (Blanchard et al., 2004; Pape, 1999; Rodnina et al., 2005). The lower duplex stability of near-cognate tRNAs accelerates their rate of rejection, while cognate tRNAs accelerate the rate of accommodation (Blanchard et al., 2004; Gromadski and Rodnina, 2004; Pape, 1999). Accommodated aa-tRNAs then participate in

peptidyl transfer, incorporating the amino acid into the peptide chain (Ledoux and Uhlenbeck, 2008).

Pseudouridine and N1-methylpseudouridine

While the canonical bases of RNA are adenine (A), cytosine (C), guanosine (G), and uracil (U), various modified forms of these bases are also present in the cell. Pseudouridine (Ψ) is an isomer of uridine in which the nucleobase is connected to the ribose sugar through C5 rather than N1. The modified nucleotide is found across all types of RNA, and its widespread abundance in the cell has led it being termed the "fifth nucleotide" (Li et al., 2016). The isomerization of the base has functional implications, freeing the N1 proton to participate in hydrogen bonding, enhancing base stacking effects and allowing for base pairing with guanosine and uridine (Davis, 1995; Deb et al., 2019; Ejby et al., 2007; Hudson et al., 2013; Kierzek et al., 2014). Unsurprisingly, pseudouridine has been implicated as having important roles in the structural stability of tRNAs and rRNAs, as well as other functions such as splicing (Li et al., 2016).

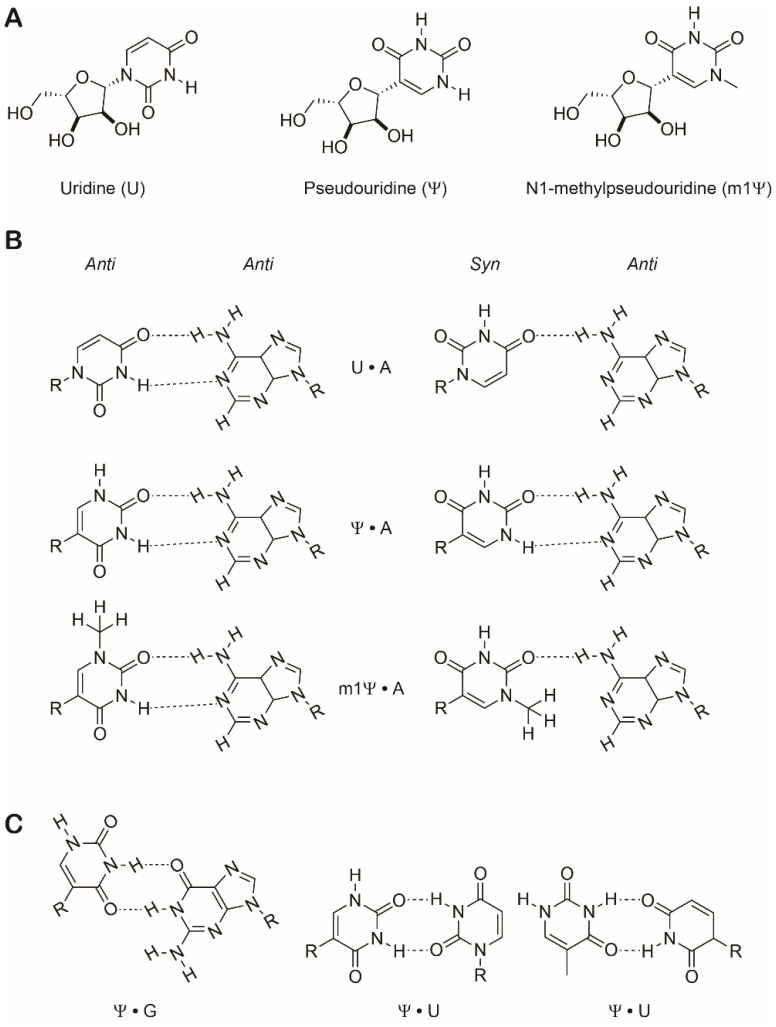

Figure 2: Overview of base pairing by uridine, pseudouridine, and N1-methylpseudouridine
A) Chemical structures of uridine, pseudouridine, and N1-methylpseudouridine. Pseudouridine is generated from uridine via the isomerization of the glycosidic bond from N1 to C5. **B)** Potential hydrogen bonding interactions of uridine, pseudouridine, and N1-methylpseudouridine (left) with adenosine (A; right) in both the *anti* and *syn* conformations. **C)** Hydrogen bonding interactions of pseudouridine with guanosine (G) and uridine (U).

The usage of modified nucleotides ("Messenger RNA Encoding the Full-Length SARS-CoV-2 Spike Glycoprotein," 2020) in Pfizer-BioNTech's BNT162b2 (Polack et al., 2020) and Moderna's mRNA-1273 (Baden et al., 2021) vaccines have sparked renewed interest in the field. Initial studies of RNA-based therapeutics showed the viability of producing proteins from exogenously introduced RNA (Jirikowski et al., 1992; Wolff et al., 1990). However, usage of

early forms of synthetic mRNAs was hampered by cellular anti-viral defenses, which inhibit translation upon detection of foreign RNA (Akira et al., 2006; Freund et al., 2019; Karikó et al., 2005, 2004; Weissman et al., 2000). Seminal work by Karikó et al. found that the presence of modified nucleotides such as 5-methylcytosine and pseudouridine alleviated these effects, reducing the immunogenicity of the RNA and increasing protein yield (Anderson et al., 2010; Freund et al., 2019; Karikó et al., 2012, 2011, 2008, 2005).

While much of the focus surrounding Ψ has been on characterizing characteristics important for the clinic, there has been considerably less attention on its effects on the decoding process. Current studies have reported conflicting results; work by the Yu group reported that introduction of Ψ to stop codons induced readthrough in vitro and in vivo (Adachi and Yu, 2020; Fernández et al., 2013; Karijolich and Yu, 2011), while others have reported minimal effect on fidelity (Eyler et al., 2019; Hoernes et al., 2019, 2016; Nir et al., 2022; Svidritskiy et al., 2016).

Even less is known of the related modification, N1-methylpseudouridine (m1Ψ), which is the modification used in the COVID-19 mRNA vaccines ("Messenger RNA Encoding the Full-Length SARS-CoV-2 Spike Glycoprotein," 2020). m1Ψ is used in place of Ψ due to its superior immunogenicity and protein yield characteristics (Andries et al., 2015; Parr et al., 2020; Svitkin et al., 2017), but its effects on tRNA selection have yet to be investigated. m1Ψ has the potential to affect decoding, given that its presence increases duplex stability, although no clear correlation was observed between luminescence and m1Ψ content in luciferase constructs (Mauger et al., 2019). However, only synonymous substitutions were implemented, potentially obscuring the influence of the modified nucleotide due to its position in the wobble position of the codon.

Alkylative Damage to mRNA

Nucleic acids are susceptible to modification by multiple types of chemical damage, whether it be from endogenous sources such as byproducts of cellular metabolism, or from exogenous agents such as environmental toxins (Wurtmann and Wolin, 2009). RNAs are particularly vulnerable to these insults due to exposure of the Watson Crick face, lack of associated protection from proteins, and increased exposure to damaging agents from their presence in the cytosol instead of the nucleus (Chen et al., 2022; Li et al., 2006).

One form of damage to RNA is the addition of alkyl adducts to various positions in the nucleobases. Several of these modifications alter the base pairing preferences of the nucleoside, such as in O6-methylguanosine (m6G) (Spratt and Levy, 1997). The presence of m6G in a codon impairs decoding, leading to increased miscoding and stalling the ribosome, depending on its position within the codon (Hudson and Zaher, 2015). Even modifications which do not appear to alter Watson-Crick base-pairing, such as N6-methyladenosine (m6A), can still destabilize duplexes, slow decoding, and reduce protein synthesis (Hoernes et al., 2019, 2016; Roost et al., 2015).

Our group has previously shown that treatment with alkylating agents such as methyl methanesulfonate (MMS) leads to a significant increase of alkyl adducts on RNAs (Yan et al., 2019). MMS reacts with RNA in a S_N2 type mechanism, of which the N1 of adenosine (m1A) and N3 of cytosine (m3C) are particularly vulnerable (Wyatt and Pittman, 2006). While there do not appear to be any investigations of the effects of m3C on decoding, the modification significantly decreases duplex stability (Mao et al., 2021), making it likely to impede translation. On the other hand, m1A has already been shown to impair translation in mammalian cell culture

and reconstituted *E. coli* translation systems (Hoernes et al., 2019; You et al., 2017), suggesting that it stalls the ribosome.

tmRNA ribosome rescue system in Bacteria

Prolonged stalling of ribosomes is deleterious to the cell due to formation of non-productive queues of energetically expensive ribosomes and accumulation of toxic peptide products (Inada, 2020; Müller et al., 2021). Bacteria have evolved pathways to rescue stalled ribosomes, returning them to the active pool while degrading the nascent peptide (Müller et al., 2021). One widely conserved and well-studied pathway is the transfer-messenger RNA (tmRNA) system, which rescues ribosomes stalled at the 3' end of transcripts (Hudson et al., 2014; Karzai, 1999; Keiler et al., 1996; Tu et al., 1995). tmRNA, which is encoded by the *ssrA* gene (Chauhan and Apirion, 1989; Oh et al., 1990), binds to the A-site of stalled ribosomes in a manner dependent on the accessory factor SmpB (Barends et al., 2001; Hanawa-Suetsugu, 2002; Karzai, 1999). The tmRNA contains both a short open reading frame (ORF) and a tRNA-like domain, leading to transfer of the nascent peptide chain and resumption of translation on its ORF in a process known as *trans*-translation (Hudson et al., 2014; Janssen and Hayes, 2012; Moore and Sauer, 2007, 2005) . The ORF codes for the ssrA signal peptide, which targets the nascent chain for degradation by proteases, and is terminated by a stop codon, allowing the ribosome to complete translation, terminate, and be recycled (Hudson et al., 2014; Janssen and Hayes, 2012; Moore and Sauer, 2007, 2005). While truncated transcripts lacking a stop codon have been the classical target of the tmRNA system, it is unknown if stalling induced by alkylative damage activates this system.

Communication with the transcript

In the course of normal elongation, the ribosome can encounter various roadblocks, such as inhibitory codons, stable secondary structures, or chemical damage to the transcript, that cause it to stall (D'Orazio and Green, 2021; Letzring et al., 2013, 2010; Simms et al., 2017a). Ribosomes stalled in this manner are highly deleterious to the cell, causing trailing ribosomes to collide and form queues of non-productive ribosomes (D'Orazio and Green, 2021; Inada, 2020). In yeast, these collisions activate the No-Go Decay (NGD) quality control pathway to degrade the transcript and prevent further loss of valuable ribosomes (Doma and Parker, 2006; D'Orazio and Green, 2021; Ikeuchi et al., 2019; Simms et al., 2019, 2017b). Mapping of NGD cleavage products revealed a major cleavage site approximately 45 nt upstream of the stall site (Simms et al., 2017b), placing the site within upstream collided ribosomes. This suggested that communication was occurring either between ribosomes or between the ribosome and the transcript. The universally conserved ribosomal protein Rps3 stands out as a likely factor mediating ribosome-mRNA communication, as the residues that contact the mRNA near the entry tunnel are widely conserved (Takyar et al., 2005). Conserved residues of Rps3 have previously been implicated in other important functions such as start codon selection (Dong et al., 2017) and unwinding of the mRNA (Takyar et al., 2005), but the same as yet to be shown for NGD.

Termination and Recycling

Upon recognition of a stop codon, the ribosome must halt further translation and be separated from the transcript and nascent peptide. In eukaryotes, termination is mediated by the release factors eRF1 and eRF3 (Alkalaeva et al., 2006). The two form a complex, along with GTP, that binds to the stop codon in the A-site (Cheng et al., 2009; des Georges et al., 2015;

Preis et al., 2014; Shao et al., 2016). Hydrolysis of GTP by eRF3 then leads to conformational changes in eRF1 such that it induces release of the nascent peptide from the peptidyl-tRNA in the P-site of the ribosome (Brown et al., 2015; Matheisl et al., 2015; Muhs et al., 2015; Preis et al., 2014; Shao et al., 2016).

Afterwards, the ribosome must be recycled to return energetically expensive ribosomes back to the available pool, enabling them to go through another cycle of translation. Post-termination ribosomes are recycled by the factor ABCE1, which splits the ribosome via an ATP-hydrolysis dependent mechanism (Becker et al., 2012; Pisarev et al., 2010; Pisareva et al., 2011; Shoemaker and Green, 2011). However, after splitting, deacylated tRNA and the transcript remain bound to the 40S; these are then released by eIF1, eIF1A, eIF3 and eIF3J (Pisarev et al., 2010, 2007).

Signaling on the Ribosome

Many studies have focused on understanding initiation, as it is thought to be the most heavily regulated step in eukaryotic translation (Sonenberg and Hinnebusch, 2009). However, recent work has uncovered how disruptions during elongation are key signaling events in triggering various quality control and stress response pathways. Here, we discuss the mechanisms underlying the signaling network and the fate of the ribosome as a result. The following discussion is published in Trends in Biochemical Sciences as Kyusik Q Kim and Hani S Zaher (2022). Canary in a coal mine: collided ribosomes as sensors of cellular conditions.

Ribosome collisions are inevitable

In all organisms, the expression and maintenance of the genetic information relies on molecular machines that traverse linear nucleic acid templates for long distances. Oftentimes,

multiple machines share the same template and even move in opposing trajectories. To avoid conflicts, organisms have evolved a host of mechanisms to coordinate the activity of its various machines (García-Muse and Aguilera, 2016). However, a key challenge for the organism is how to respond when machines become stuck and run into one another. Collisions must be promptly resolved to restore proper gene expression and return to homeostasis. This is evident during replication and transcription, during which collisions can occur between replisomes and transcribing RNA polymerases (García-Muse and Aguilera, 2016). Such events can be highly deleterious, resulting in genomic instability and even cell death (García-Muse and Aguilera, 2016). However, organisms have also taken advantage of these events to monitor genomic integrity and maintain the fidelity of the genomic information. Indeed, signaling as a result of disruptions in the movement of DNA and RNA polymerases is utilized for various DNA repair pathways (García-Muse and Aguilera, 2016).

Translation of mRNA on the other hand, only involves ribosomes that move in the same direction – from the 5' to the 3' end of the mRNA. Even so, the stochastic nature of the translational process results in ribosomes sometimes slowing down and running into one another (Mitarai et al., 2008; Sørensen and Pedersen, 1991). Slowed or stopped translation is also used as a regulatory mechanism for frameshifting and folding (Farabaugh, 1996; Richter and Coller, 2015). Indeed, modeling studies in bacteria found that protein output could not be explained without a collision-centric model (Ferrin and Subramaniam, 2017; Mitarai et al., 2008). Comprehensive looks at ribosome occupancy in yeast and human cells have also found collisions to be widespread (Han et al., 2020; Meydan and Guydosh, 2020). These naturally occurring stalls and collisions are not the focus of this review. Instead, we focus on stalling and collisions arising from defects in the mRNA. These defects, whether due to misprocessing or chemical damage,

can cause the ribosome to arrest and lead to non-productive queues of stalled ribosomes (Yan and Zaher, 2019). It was known that, similar to how polymerases act as sensors of DNA damage, such events led to the activation of ribosome-associated quality control (RQC) and mRNA-surveillance pathways in eukaryotes (Doma and Parker, 2006; Howard and Frost, 2021; Simms et al., 2017a).

However, it remained unclear how eukaryotic cells recognized stalled ribosomes to trigger destruction of the defective transcript and recover the valuable ribosomes. It was not until recently that we came to realize that additional ribosomes colliding into a stalled ribosome was the key event for initiating these pathways (Simms et al., 2017b). Subsequent structural studies have uncovered that collided eukaryotic ribosomes adopt a unique structure that can be readily distinguished from normal ribosomes (Ikeuchi et al., 2019; Juszkiewicz et al., 2018). The ubiquitin signaling that occurs on the collided ribosomes are the basis for various downstream quality-control processes. In this review, we will discuss the role of this ubiquitin signaling and its consequences for the ribosome. Downstream processes will be briefly discussed but are more extensively covered in several recent reviews (see (D'Orazio and Green, 2021; Inada, 2017; Yip and Shao, 2021)). Furthermore, signaling on collided ribosomes appears to have consequences beyond that of just ribosome rescue and mRNA quality control, including sensing environmental changes to trigger stress responses and cell-fate decisions (Sinha et al., 2020; Wu et al., 2020). We will delve into how cells might monitor the global collision frequency to activate the most appropriate response pathway.

Ribosome collision leads to ubiquitination of ribosomal proteins

Ribosomal stalling and collisions seem to be a feature of the eukaryotic transcriptome (Han et al., 2020; Meydan and Guydosh, 2020). Naturally occurring stalls arising from certain

transcript elements appear to be dealt with by the translation factor eIF5A (Han et al., 2020) and typically result in resumption of translation. In contrast, upon detection of non-productive stalls which block continued translation, three critical steps must occur in order to prevent accumulation of toxic peptide products: ribosome dissociation and rescue, decay of the defective mRNA, and degradation of the incomplete peptide (for reviews, see (D'Orazio and Green, 2021; Inada, 2017; Yip and Shao, 2021)). The discovery in yeast that RQC and the mRNA surveillance pathway of No-Go Decay (NGD) were dependent on the presence of the E3 ligase Hel2 (Brandman et al., 2012; Letzring et al., 2013; Matsuo et al., 2017; Saito et al., 2015; Simms et al., 2017b; Sitron et al., 2017; Winz et al., 2019), suggested that the factor is the first to respond to ribosome stalling. The factor harbors a RING-finger ubiquitin-ligase domain and was initially characterized for its role in ubiquitination of excess histones (Singh et al., 2012). Subsequent studies determined that Hel2 ubiquitinated ribosomal proteins uS3 and uS10 in response to collisions (Ikeuchi et al., 2019; Matsuo et al., 2017; Simms et al., 2017b). At the same time, several groups identified ZNF598 as the mammalian homologue of Hel2 and found it to play a similar role in resolving ribosome stalls (Garzia et al., 2017; Juszkiewicz et al., 2018; Juszkiewicz and Hegde, 2017; Sundaramoorthy et al., 2017).

In a yeast cell, the number of Hel2 molecules has been estimated to be ~2000 (Ho et al., 2018), about 1% of the number of ribosomes (Jonathan R Warner, 1999). As a result, efficient ribosome rescue requires the factor to display high specificity for stalled ribosomes over elongating ones. Structural studies revealed that stalled ribosomes adopt distinct conformations relative to translating ones, which in principle can rationalize how the factor recognizes stalled ribosomes specifically (Matsuo et al., 2017). A number of clues, however, argued for a different mode of recognition, including the observation that stalling is used as a regulatory mechanism

for several processes such as protein targeting and programmed frameshifting (Farabaugh, 1996; Richter and Coller, 2015). Furthermore, stalled ribosomes adopt different conformations depending on the nature of the stall (D'Orazio and Green, 2021; Wilson et al., 2016), making it difficult to reconcile how one factor can recognize all these conformations. So how does Hel2/ZNF598 bind ribosomes stalled on problematic mRNAs only? An important observation in uncovering the answer was the finding that robust NGD requires the stall to occur well downstream of the start codon and that cleavage of the aberrant mRNA can be mapped further upstream of the initial stalling site (Chen et al., 2010; Simms et al., 2017b; Tsuboi et al., 2012). This suggested that the signal for triggering NGD was the collision and subsequent pileup of ribosomes. This model was further bolstered by the observation that Hel2-mediated ubiquitination of ribosomal proteins was found to be activated in response to ribosome collisions (Matsuo et al., 2017; Simms et al., 2017b). For instance, even though addition of compounds such as cycloheximide and emetine to high concentrations does not result in activation of Hel2/ZNF598, their addition to intermediate concentrations – during which partial stalling occurs – is accompanied by ubiquitination of ribosomal proteins (Juszkiewicz et al., 2018; Simms et al., 2017b).

Although the idea of collided ribosomes acting as the master signal for downstream ribosome rescue pathways was an appealing one, the mechanics of how this might occur was not immediately obvious. In a series of structural studies, cryo-electron microscopy (cryo-EM) analysis of the minimal collision unit of two ribosomes, or disome, revealed that collided ribosomes adopt a unique structure (Ikeuchi et al., 2019; Juszkiewicz et al., 2018). In the disome structure, the lead ribosome is stabilized in a post-translocation state, with an empty A site but occupied P and E sites, while the collided ribosome adopts a rotated state with hybrid A/P and

P/E-tRNAs. The conformations of the two ribosomes result in various contacts being made between the ribosomal 40S subunits. The key interactions appear to be between RACK1 and uS3 of the stalled ribosome with RACK1 and uS10 of the collided ribosome in yeast, and between RACK1 of the stalled ribosome with eS10, uS10, and uS3 of the collided ribosome in mammals. It is thought that the interface between the collided 40S subunits is recognized by Hel2/ZNF598 (Ikeuchi et al., 2019; Juszkiewicz et al., 2018). However, a structure of the factor in complex with ribosomes is yet to be determined.

Biochemical reconstitution of Hel2/ZNF598-mediated ubiquitination provided further support for *in vivo* observations; disomes are sufficient for activity but higher-order structures of collided ribosomes – trisomes or longer polyribosome chains – appear to be more efficiently ubiquitinated (Juszkiewicz et al., 2018; Matsuo et al., 2020). A recent cryo-EM analysis of trisomes on the natural stalling sequence of the yeast *SDD1* mRNA suggests that this may be due to the fact that the second and third ribosome form an interface similar to the one observed in disomes (Matsuo et al., 2020). Since the second and third ribosome form the recognition interface in the trisome structure, subsequently collided ribosomes in longer polyribosome chains may also generate more of these interfaces (Matsuo et al., 2020). If the 40S-40S interfaces are indeed recognized by Hel2/ZNF598, this would provide a structural basis for the observed increase in ubiquitination efficiency.

One important note is it remains unknown which ribosomes in a pileup are ubiquitinated. If Hel2/ZNF598 is indeed recognizing the rotated state or unique interfaces of collided ribosomes, it is possible that only the collided ribosomes are ubiquitinated, leaving the stalled ribosome unmarked. This would serve to distinguish the lead ribosome and could also further

explain how trisomes show more efficient ubiquitination compared to disomes. However, other ubiquitin signals, discussed later in this review, may exhibit alternative patterns.

The role of ribosomal protein-ubiquitination in dissociation of the stalled ribosome

Upon ubiquitination, ribosomes undergo rescue and recycling of their subunits. For disassembly of the stalled ribosome, recent work suggests that after ubiquitination by Hel2/ZNF598, the lead ribosome of a pileup is disassembled by the Ribosome-Quality Control Trigger (RQT) complex (Juszkiewicz et al., 2020b; Matsuo et al., 2020). The complex is composed of the helicase Slh1, Cue3/Rqt3, and Rqt4 in yeast, and its homologs ASCC3, ASCC2, and TRIP4, respectively, in mammals. The mammalian complex also contains the factor ASCC1 (Hashimoto et al., 2020; Juszkiewicz et al., 2020b), whose yeast homolog is yet to be identified. Disassembly of the lead ribosome is dependent on the helicase action of Slh1/ASCC3 (Hashimoto et al., 2020; Juszkiewicz et al., 2020b; Matsuo et al., 2020), after which the peptidyl-tRNA-bound 60S subunit is handled by the RQC pathway for destruction of the nascent peptide and recycling of the 60S (Brandman et al., 2012; Chu et al., 2009). The 40S subunit on the other hand, is presumably returned to the free 40S pool.

While it is now clear that ubiquitination is needed for rescue of stalled ribosomes, how the ribosome rescue machinery utilizes the ubiquitin marks to properly target the stalled ribosome remains undetermined. Cue3 of the RQT complex possesses a CUE domain (Matsuo et al., 2017) (ubiquitin-binding domain) which readily provides a molecular rationale for how the complex can associate with ubiquitinated ribosomes. However, deletion of Cue3 does not completely abolish RQC, suggesting that Slh1 can still correctly target the stalled ribosome, albeit at reduced efficiencies (Matsuo et al., 2017; Sitron et al., 2017). It also appears that ubiquitination of ribosomal proteins is not necessary for Slh1/ASCC3 association with disomes,

even though ubiquitination of uS10/eS10 is required for their downstream function in ribosome disassembly (Hashimoto et al., 2020; Juszkiewicz et al., 2020b; Matsuo et al., 2020). Complicating the matter further is the unknown ubiquitination status of each ribosome in the pileup. If the lead ribosome is indeed unmarked, this would provide a mechanism for how the stalled ribosome is recognized, but not the mechanism by which Slh1/ASCC3 is targeted to said ribosome. In this model, it is feasible that Slh1/ASCC3 recognizes the stalled ribosome in a collided-ribosome context.

To complete the rescue process, ubiquitin marks must be removed such that previously-collided ribosomes can later be properly recognized in the event of another stall. In humans, the de-ubiquitinating enzymes OTUD3 and USP21 can remove ubiquitin placed by ZNF598 (Garshott et al., 2020). However, significant de-ubiquitination after UV-induced ubiquitination of uS10/eS10 required several hours (Garshott et al., 2020). While it is possible that de-ubiquitination after UV damage does not reflect more basal conditions, as a large number of stalls might overwhelm the deubiquitinases, if de-ubiquitination is indeed a slow process, it is difficult to imagine that these enzymes can act to remove ubiquitin before a ribosome stalls again. Also, the model does not explain how these enzymes would be specifically targeted to collided ribosomes or at what stage in the rescue pathway they act. It is abundantly clear that more work is needed to understand how the addition and removal of ubiquitin during and after stalling are coordinated to maintain ribosome stasis.

eS7 ubiquitination as a pathway for alternative NGD and mRNA degradation

In yeast, the small ribosomal protein eS7 is ubiquitinated in addition to uS10 (Buschauer et al., 2020; Ikeuchi et al., 2019). Unlike uS10, which is a target of Hel2, eS7 is initially monoubiquitinated by Not4 (Panasenko and Collart, 2012), a factor that has multiple functions

(for review see (Collart, 2013)). How and when Not4 targets ribosomes for eS7 monoubiquitination is not clear, but the addition of K63-linked polyubiquitination on monoubiquitinated eS7 by Hel2 occurs during stalling (Ikeuchi et al., 2019). eS7 polyubiquitination seems to operate as a signal for a secondary mechanism for degrading the aberrant mRNA termed NGD^{RQC-}, in which decay is decoupled from RQC. This mechanism is characterized by an initial cleavage of the mRNA well upstream of the stall sequence, relative to cleavages observed during normal RQC-coupled NGD (Ikeuchi et al., 2019). While NGD^{RQC-} appears to be only a minor contributor to NGD under normal conditions, it becomes increasingly active when uS10 ubiquitination is inhibited or Slh1 is absent. Therefore, it has been proposed that under normal conditions, ubiquitination of uS10 is required for Slh1 activity in ribosome disassembly, which in turn is required for NGD. When Slh1 is overwhelmed, eS7 polyubiquitination serves as a secondary signal for mRNA degradation (Ikeuchi et al., 2019), possibly by the Ccr4-Not complex.

Interestingly, in addition to its role in quality control of aberrant mRNA, eS7 monoubiquitination appears to play an additional role in decay of normal mRNAs (Buschauer et al., 2020). Emerging evidence suggests that mRNA decay in eukaryotes is intimately coupled to ribosome speed, whereby slowed translation is a determinant for increased mRNA turnover (Presnyak et al., 2015). In a recent study, Buschauer and Matsuo et al. found that eS7 ubiquitination is required to recruit the Ccr4-Not deadenylase complex to slowly translating ribosomes (Buschauer et al., 2020). Not5 is a core subunit of Ccr4-Not that binds to the ribosome and inspects the occupancy of the E site as a proxy for ribosome speed; an empty E site indicates that A-site decoding is slow and in turn results in Not5-mediated recruitment of the DEAD-box helicase Dhh1 for decapping and decay (Buschauer et al., 2020).

How eS7 ubiquitination can be used for two seemingly distinct pathways of mRNA decay is not completely understood. It is possible, however, that the level of eS7 polyubiquitination is used as a measure of how much ribosome speed is reduced. The more linked-ubiquitin chains are added, the more likely the mRNA is defective. Alternatively, a Not5-dependent decay pathway for defective mRNAs would add redundancy and provide a means to initiate decay for stalls near the start codon, which do not robustly activate NGD. To add more complexity to the interplay between these processes, activation of the Unfolded Protein Response (UPR) also leads to Not4-mediated ubiquitination of eS7 (Matsuki et al., 2020). It is entirely possible that the signal here is not the same as observed in collision or slowed translation, as activation of UPR can also lead to ubiquitination of uS5 in mammals (Higgins et al., 2015). In addition, it is unknown how ribosomes are rescued in these pathways. More work is needed to determine how Not4 and Not5 are participating in the resolution of stalls, mRNA decay, and stress responses.

uS3 ubiquitination as a marker for ribosome competency

Thus far, we have only discussed stalling in the context of defective mRNAs, but in principle, defects in the ribosome would also lead to similar consequences. It is important for cells to correctly identify the source of the defect to degrade the appropriate molecule. In eukaryotes, defective ribosomes are degraded through a process termed non-functional rRNA decay (NRD) (LaRiviere et al., 2006). Briefly, the process by which aberrant ribosomes are recognized and targeted for degradation critically depends on the position of the defect within the rRNA species. 25S NRD is responsible for degrading defective large subunits while 18S NRD is responsible for degrading defective small subunits. Intriguingly, many of the factors involved during ribosome collisions are also involved in 18S NRD (Limoncelli et al., 2017; Sugiyama et

al., 2019), suggesting interplay between the two processes. In contrast, 25S NRD shares few such factors (Fujii et al., 2009).

In yeast, 18S NRD is initiated by mono-ubiquitination of uS3 K212 by the E3 ligase Mag2, followed by K63-polyubiquitination by Hel2 or Rsp5 (Sugiyama et al., 2019). After 80S splitting in an alternative ribosome rescue factor, Dom34, and Slh1-dependent manner, the 18S rRNA is degraded by a yet uncharacterized pathway that requires the major exonuclease Xrn1 (Sugiyama et al., 2019). Ubiquitination of uS3 does not appear to commit the 18S to destruction, however. In humans, the G3BP1-USP10 complex was found to remove ubiquitin from ribosomal proteins uS3, uS5, and eS10, which prevented lysosome degradation of the 18S rRNA (Meyer et al., 2020). The homologous complex in yeast, Bre5-Ubp3p, de-ubiquitinates uS3 and eS7 (Jung et al., 2017; Matsuki et al., 2020). These findings indicate that uS3 signaling is part of a complex system regulating ribosome stasis.

It is unclear how activation of 18S NRD is coordinated with that of RQC, as uS3 ubiquitination is necessary for 18S NRD but is dispensable for RQC. The work on 18S NRD utilized a mutant 18S rRNA (Sugiyama et al., 2019), but cycloheximide-induced collisions and UPR also lead to ubiquitination of uS3 (Higgins et al., 2015; Matsuki et al., 2020; Simms et al., 2017b). In this case, the overall ubiquitin signaling or uS5 ubiquitination status might serve as unique signature to delineate when the 18S rRNA is targeted for recycling or for degradation. Ubiquitination also appears to be hierarchical, at least in human, where uS10 and eS10 ubiquitination events are needed for uS3 and uS5 ubiquitination, and uS3 is potentially ubiquitinated before uS5 (Garshott et al., 2020). Perhaps uS3 is initially ubiquitinated on collided ribosomes as a signal for quality-control pathways to further probe translational competency of ribosomes. Subsequent

ubiquitination of other uS3 lysine residues, uS5, or other ribosomal proteins could then act as downstream checkpoints for 18S status.

Alternatively, since non-functional ribosomes are expected to lead in a ribosome pileup distinct from pileups that occur on aberrant mRNAs, it might be possible to differentiate between the two types of stalls. Specifically, mutations in the decoding center of the small subunit, which have been used to probe 18S NRD, inhibit tRNA selection altogether (Yoshizawa et al., 1999). Therefore, ribosomes harboring these mutations are expected to stall on the start codon and cause collisions different than ones occurring further downstream. In this case, it is possible that a collision between the initiating small subunit and the defective ribosome is used to activate 18S NRD.

Preventing further translation on aberrant mRNAs

A pressing problem for the cell is preventing ribosomes from initiating on defective transcripts. Although the transcript can be degraded through mRNA-surveillance pathways after a collision is detected, additional ribosomes might continue to initiate on the transcript during the intervening period before decay. This would incur costs in the loss of competent ribosomes and the energy expended to rescue them from the transcript. It follows that cells would have evolved mechanisms to suppress further initiation on aberrant mRNAs. A recent study by Hickey and colleagues used a genome-wide CRISPR-Cas9 screen to identify mammalian factors whose absence contributed to increased protein production on stalling reporters (Hickey et al., 2020). Interestingly, in addition to known RQC factors, the factors GIGYF2 and 4EHP (eIF4E2) were identified as some of the top hits in the screen (Hickey et al., 2020). These factors are part of an initiation-repressor complex that inhibits recognition of the mRNA cap structure by the translation initiation factor eIF4E, preventing translation initiation (Morita et al., 2012). In

agreement with a role for these factors in RQC, both were previously shown to interact with ZNF598 (Morita et al., 2012).

At first glance, this interaction could explain how they might be specifically recruited to stalled ribosomes. However, it turns out that neither ZNF598 nor ZNF598-mediated ubiquitination are required for GIGYF2/4EHP recruitment to aberrant mRNAs (Juszkiewicz et al., 2020a; Sinha et al., 2020). Instead, two independent studies identified the requirement for the transcriptional coactivator EDF1 in recruiting the repressor complex to ribosomes (Juszkiewicz et al., 2020a; Sinha et al., 2020). In both studies, unbiased mass-spectrometry approaches showed that EDF1 bound collided ribosomes (Juszkiewicz et al., 2020a; Sinha et al., 2020). Notably, Mbf1, the yeast homologue of EDF1, was previously shown to prevent +1 frameshifting, resulting from ribosomal collisions, on stalling sequences (Simms et al., 2019; Wang et al., 2018). Cryo-EM structures of Mbf1 and EDF1 in complex with collided ribosomes revealed that the factors display identical modes of binding; both bind along the entry tunnel of the mRNA of collided ribosomes that have adopted a rotated state (Sinha et al., 2020). Mbf1/EDF1 also makes extensive contacts with uS3, a factor known to be important for reading-frame maintenance by the ribosome (Simms et al., 2018; Wang et al., 2018). While these structures provide important clues about how Mbf1/EDF1 may prevent frameshifting, they do not tell us about how they contribute to RQC.

Activating stress responses when the quality control machinery is overwhelmed

It is unlikely that RQC is the primary system for dealing with ribosome collisions since Hel2/ZNF598 is substoichiometric to ribosomes (Garzia et al., 2017; Ho et al., 2018). One can easily see how the RQC machinery would be overwhelmed under stress conditions that lead to an elevated frequency of ribosome collisions. For instance, amino-acid deprivation, which leads

to depletion of aminoacylated tRNAs, and alkylation and oxidation stresses, which globally damage RNA, have been documented to increase levels of ribosome collisions (Yan et al., 2019; Yan and Zaher, 2021). Under these conditions, cells instead appear to activate pro-survival pathways such as the integrated stress response (ISR), and if the stress is severe, programmed-cell death (apoptosis).

The ISR is a conserved eukaryotic stress response triggered by a diverse set of endogenous and exogenous signals. In mammals, various stresses are monitored by distinct protein kinases that, upon activation, phosphorylate the α subunit of the translation initiation factor eIF2. Phosphorylation of eIF2α promotes the selective translation of a subset of mRNAs required for survival and recovery from stress (for reviews, see (Costa-Mattioli and Walter, 2020; Donnelly et al., 2013; Pakos-Zebrucka et al., 2016)). *Saccharomyces cerevisiae* has been used as a model for studying the ISR, owing to the conserved mechanism of its activation and the presence of only one known eIF2a kinase, Gcn2 (Hinnebusch, 2005). Gcn2 is typically activated in response to amino-acid starvation and robust activation requires the presence of two coactivators, Gcn1 and Gcn20 (Garcia-Barrio, 2000; Marton et al., 1997; Sattlegger and Hinnebusch, 2005). In the classical model, it is thought that Gcn2 is activated by binding to deacylated tRNAs on the ribosome, with Gcn1 and Gcn20 aiding in the delivery of the deacylated tRNA to its tRNA-synthetase-like domain (Garcia-Barrio, 2000; Marton et al., 1997; Sattlegger and Hinnebusch, 2005). However, Gcn2 can also be robustly activated by conditions that would not be expected to increase levels of deacylated tRNAs (Hughes et al., 2000; Natarajan et al., 2001; Yan and Zaher, 2021), suggesting that the kinase can be activated via alternative mechanisms.

The clue for these alternative mechanisms came when Ishimura and Nagy et al. reported that ribosome stalling also activates GCN2 and subsequently the ISR in mammals (Ishimura et al., 2016). Neurons from mice containing a loss-of-function mutation in the rescue factor GTPBP2 were found to activate GCN2 in the presence of reduced levels of $tRNA^{Arg}_{UCU}$ (Ishimura et al., 2016). Importantly, elevated levels of ribosome stalling occurred on AGA codons without an accompanying increase in deacylated tRNAs levels (Ishimura et al., 2016). These observations pointed to a ribosome-centric mode for ISR activation by GCN2. Soon afterwards, two groups provided further support for this model. Inglis and Mason et al. reconstituted GCN2-mediated phosphorylation of eIF2a in vitro and found that ribosomes activate the kinase much more robustly than deacylated tRNAs (Inglis et al., 2019). Further analysis using hydrogen-deuterium exchange mass spectrometry (HDX-MS) revealed that the P stalk of the ribosome interacts with GCN2 and that the P stalk in isolation is sufficient to stimulate kinase activity. Independently, using a CRISPR-Cas9 mutagenesis screen in Chinese hamster ovary cells, Harding and colleagues identified components of the P stalk to be important for GCN2 function (Harding et al., 2019). In-vitro reconstitution experiments further supported these observations, whereby wild-type ribosomes stimulated GCN2 activity but not ribosomes isolated from P-stalk mutant cells (Harding et al., 2019).

A stalling-induced activation model was appealing since many stress conditions cause widespread stalling and activate the ISR (Hughes et al., 2000; Natarajan et al., 2001; Simms et al., 2014; Yan et al., 2019; Yan and Zaher, 2021; You et al., 2017). However, at least three important questions remained unaddressed: what conformation of the ribosome activates the ISR, how conserved is the activation mechanism, and how is ISR activation coordinated with that of RQC? Two very recent studies partially addressed these questions (Pochopien et al., 2021; Yan

and Zaher, 2021). In a study from our group, yeast Gcn2 was found to be activated by conditions that promote ribosome collisions (Yan and Zaher, 2021). Similar to what was observed for Hel2-mediated ubiquitination of ribosomal proteins, addition of antibiotics and stalling agents only at concentrations that promote collisions were found to promote eIF2a phosphorylation by Gcn2. These observations suggest that collided ribosomes activate Gcn2 and that stalling-induced activation of the ISR is a conserved mechanism across eukaryotes. Indeed, Gcn2's coactivator, Gcn1, appears to preferentially bind to collided ribosomes in mammals and yeast (Lee et al., 2015; Pochopien et al., 2021; Sattlegger and Hinnebusch, 2005). A recent cryo-EM structure of yeast Gcn1 in complex with a collided disome provided an important molecular basis for this specificity (Pochopien et al., 2021). Gcn1 was found to snake its way across the disome unit, making interactions with the stalled and collided ribosomes. Although the structure of the complex represents an inactivated state in which the repressors Rpg2/Gir2 are bound in the A site of the lead ribosome, presumably preventing Gcn2 from binding, it provided some important clues about how Gcn2 and its coactivators recognize stalled ribosomes. In the future, it will be interesting to identify how recognition of collided ribosomes is relayed by Gcn1 to activate the kinase domain of Gcn2.

The observation that RQC and the ISR are activated via the same ribosome stalling signal suggests that the two processes must coordinate the activation of their factors, especially given that they lead to distinct cellular responses. Transcriptomic profiling from the Guydosh group (Meydan and Guydosh, 2020) and our group (Yan and Zaher, 2021) revealed that RQC suppresses the premature activation of Gcn2 in the absence of stress conditions. Furthermore, our data showed that the presence of Hel2 attenuates the activation of Gcn2 in response to several stressors, suggesting that activation of RQC suppresses that of the ISR. By contrast, when the

ISR is inhibited, RQC is overactivated – as judged by increased Hel2-mediated ubiquitination – suggesting that the two processes are in apparent competition. Interestingly, although Hel2 has no preference for the nature of the stalled ribosome, Gcn2 and/or its coactivators appear to prefer stalled ribosomes with an empty A site (Yan and Zaher, 2021). These observations indicate that although both pathways recognize collided ribosomes, they are not in direct competition with each other and instead bind to distinct regions on the ribosome. However, Hel2 appears to be more sensitive to changes to the translational machinery and responds more robustly to lower collision frequencies than does Gcn2, suggesting that RQC is activated more rapidly than ISR (Yan and Zaher, 2021). This presents a model in which low numbers of collided ribosomes, as a result of defects in a few mRNAs, are rescued through RQC before they can activate Gcn2. Under stress conditions in which collisions are more frequent and widespread, Hel2 is likely to get overwhelmed, enabling activation of Gcn2 and subsequent activation of the ISR.

Long-term signaling consequences via MAPKKKs

The observations that collided ribosomes are recognized by numerous factors involved in distinct downstream processes suggest that they are widely used to gauge cellular conditions. The appeal of such a mechanism stems from the observation that the translational machinery is exquisitely sensitive to cellular status, functioning as a sort of molecular sentinel to alert cells to environmental changes. Thus far, we have discussed how the frequency of ribosome collisions is potentially used to mount a quality-control process versus a stress-response pathway. But what if conditions are so severe that neither of these pathways can mitigate the impact on translation? Typically, these conditions prompt cells to arrest the cell cycle and/or activate programmed cell death (Kurokawa and Kornbluth, 2009). Interestingly, we have known for a while that conditions that alter ribosome function in mammals robustly activate the stress-activated kinases (SAPKs),

p38 and c-Jun N-terminal kinase (JNK), in a process termed the ribotoxic stress response (RSR) (Iordanov et al., 1998, 1997). Activation of SAPKs then lead to cell-cycle arrest and apoptosis (Darling and Cook, 2014; Duch et al., 2012; Iordanov et al., 1998, 1997). Studies have implicated the Mitogen Activated Protein Kinase Kinase Kinase (MAPKKK) ZAK as the upstream kinase of p38 and JNK (Jandhyala et al., 2008; Wang et al., 2005).

Up until recently, an important question that remained unresolved was how ZAK was activated to trigger the RSR. Two studies suggested that the ribosome itself plays a direct role in ZAK activation, in which the long isoform of the protein, ZAKa, interacts with the ribosome to sense perturbance to its function (Vind et al., 2020; Wu et al., 2020). However, the studies reached conflicting conclusions about how the perturbed ribosome is probed by ZAKa. Vind et al. argued that the factor associates with ribosomes and under ribotoxic stress, uses sensor domains to inspect alterations to functional sites on the ribosome, irrespective of collisions (Vind et al., 2020). In contrast, Wu et al. argued that even though ZAKa interacts with elongating ribosomes, it is auto-phosphorylated in response to ribosome collisions, and consequently activates RSR (Wu et al., 2020). In addition, the authors also suggested that robust activation of ISR by GCN2 requires the presence of ZAKa (Wu et al., 2020). The distinct conclusions reached by the two groups on the conformation of the ribosome responsible for ZAKa activation cannot not be readily reconciled, especially since the studies also reached differing conclusions regarding the interplay between ZAKa and RQC. As noted in Wu et al., differences in experimental conditions may explain some of these discrepancies (Wu et al., 2020), but more studies are needed to hammer out the exact molecular mechanism by which RSR is activated during stalling.

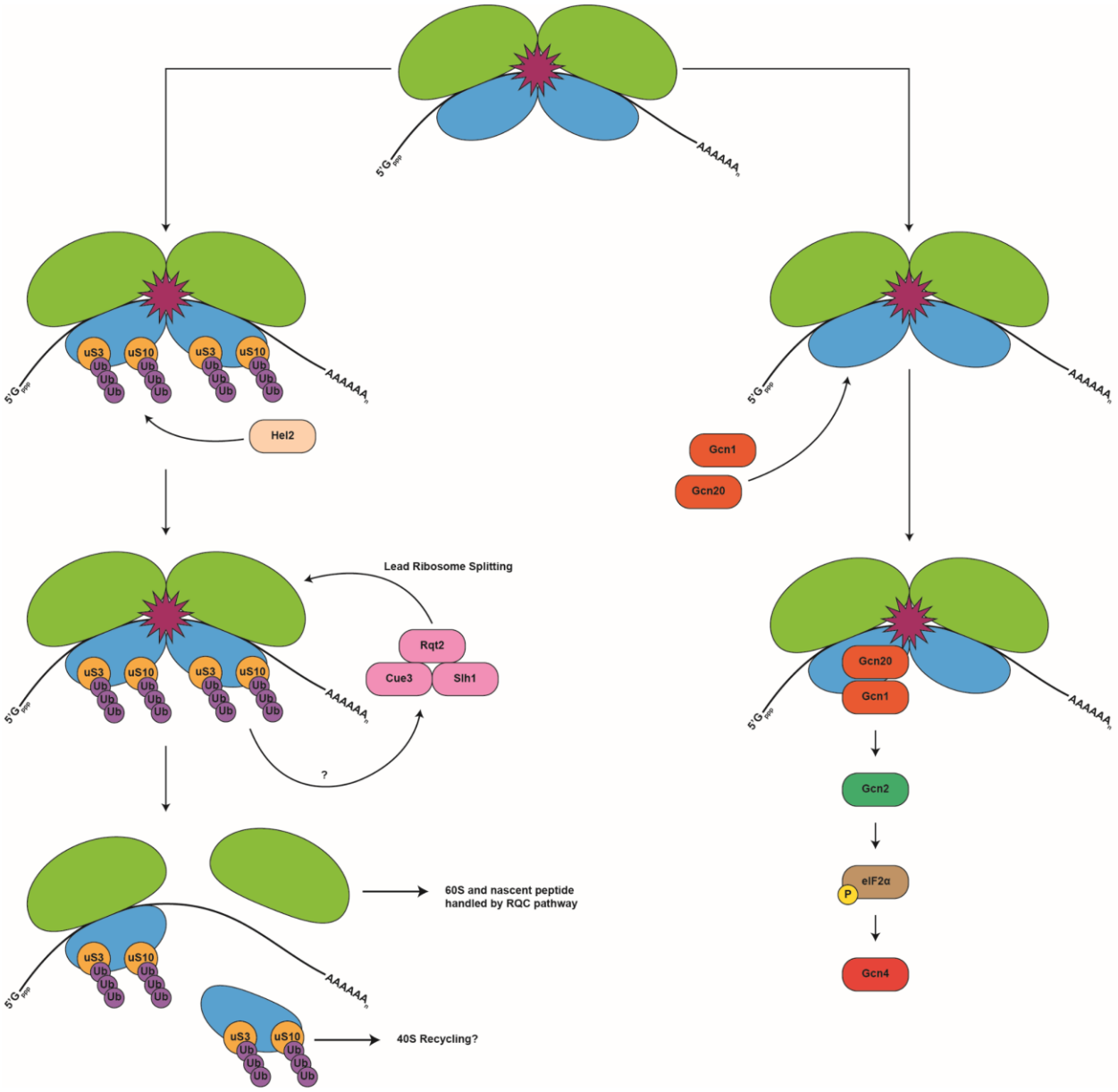

Figure 3: Model for potential signaling on collided ribosomes in yeast
Collided ribosomes are recognized by Hel2, which ubiquitinates the ribosomal proteins uS3 and uS10 (Left). It remains unknown if the lead, collided, or both ribosomes are ubiquitinated. Ubiquitination then triggers splitting of the lead ribosome by the RQT complex. The mechanism of the signaling and recruitment of the RQT complex is still undetermined. The resulting 60S containing the nascent peptide is dealt with by the RQC pathway, while the 40S is presumably returned to the free 40S pool. How the ubiquitin marks are removed before recycling, or how the process is regulated, is not completely understood. In the event this system is overwhelmed, collided ribosomes are recognized and bound by Gcn1 and Gcn2. Gcn1 and Gcn20 then activate Gcn2, leading to phosphorylation of eIF2a and activation of the ISR.

Conclusion

Initial biological studies elucidated the mechanisms of how the gene expression machinery operates, while following studies fleshed out how cells reprogram gene expression in response to a various array of stresses. However, how these diverse stresses were sensed and how the signal was transmitted to the gene expression machinery was not fully understood. Growing evidence suggests that cells utilize ribosomes as sensors of internal conditions, monitoring collisions between them as a sort of rheostat to guide selection of critical cell fate decisions (Wu et al., 2020; Yan and Zaher, 2021). Indeed, ribosomal collisions have now been implicated in coactivation of the innate immune response (Wan et al., 2021) and RQC pathways in bacteria (Cerullo et al., 2022; Saito et al., 2022).

It is clear that we have only just begun to uncover the role of the ribosome as a key player in maintaining homeostasis, in addition to their function of translating mRNA into protein. One area in need of investigation is the mechanisms by which stress response genes remain resistant to disruptions in translation, given that they are critical for recovery from the stress that induced their expression in the first place. Meanwhile, during elongation, it is unknown how the presence of certain modified nucleotides in transcript are decoded by the ribosome. The alkyl adduct m1A has been shown to stall the ribosome (Hoernes et al., 2019; You et al., 2017), but whether ribosome rescue pathways in bacteria are activated as a result remains undetermined. On the other hand, information regarding how N1-methylpseudouridine is decoded by the ribosome is lacking, while studies on the related modification, pseudouridine, have reported conflicting results (Adachi and Yu, 2020; Eyler et al., 2019; Fernández et al., 2013; Hoernes et al., 2019, 2016; Karijolich and Yu, 2011; Nir et al., 2022; Svidritskiy et al., 2016). Finally, it is apparent that signaling on the collided ribosome is important for activation of downstream response

pathways (Garzia et al., 2017; Ikeuchi et al., 2019; Juszkiewicz et al., 2018; Matsuo et al., 2017; Simms et al., 2017b; Sundaramoorthy et al., 2017). However, whether contact with the mRNA by the ribosome is important to the signaling, or for the downstream quality control processes, is unknown. In addition, our understanding of the factors that recognize and report on collisions, and the mechanisms by which they do so, is incomplete. By answering these questions, we will gain deeper insight into how cells sense and respond to their environment.

Contributions to Works

Alyklative damage of mRNA leads to ribosome stalling and rescue by trans translation in bacteria

I collected and analyzed the mass spectrometry data investigating changes in the level of alkylated RNAs in the cell. I also conducted the rifampicin pre-treatment experiments to isolate the effects of ribosomes stalled by damage to the mRNA rather than those stalled on truncated transcripts produced as a result of DNA damage.

Interactions between the mRNA and Rps3/uS3 at the entry tunnel of the ribosomal small subunit are important for no-go decay

I was responsible for analysis of high-throughput sequencing data of 5'-no-go-decay (NGD) fragments in *rps3-R116A, R117AΔski2Δ*, *dom34Δski2Δ*, and *asc1-R38D, K40Eski2Δ* mutants to understand how these mutations affected NGD cleavage patterns.

References

1. Adachi H, Yu YT. 2020. Pseudouridine-mediated stop codon readthrough in s. cerevisiae is sequence context–independent. *Rna* **26**:1247–1256. doi:10.1261/RNA.076042.120

2. Akira S, Uematsu S, Takeuchi O. 2006. Pathogen recognition and innate immunity. *Cell* **124**:783–801. doi:10.1016/j.cell.2006.02.015

3. Algire MA, Maag D, Lorsch JR. 2005. Pi release from eIF2, not GTP hydrolysis, is the step controlled by start-site selection during eukaryotic translation initiation. *Molecular Cell* **20**:251–262. doi:10.1016/j.molcel.2005.09.008

4. Alkalaeva EZ, Pisarev AV, Frolova LY, Kisselev LL, Pestova TV. 2006. In Vitro Reconstitution of Eukaryotic Translation Reveals Cooperativity between Release Factors eRF1 and eRF3. *Cell* **125**:1125–1136. doi:10.1016/j.cell.2006.04.035

5. Anderson BR, Muramatsu H, Nallagatla SR, Bevilacqua PC, Sansing LH, Weissman D, Karikó K. 2010. Incorporation of pseudouridine into mRNA enhances translation by diminishing PKR activation. *Nucleic Acids Research* **38**:5884–5892. doi:10.1093/nar/gkq347

6. Andries O, Mc Cafferty S, De Smedt SC, Weiss R, Sanders NN, Kitada T. 2015. N1-methylpseudouridine-incorporated mRNA outperforms pseudouridine-incorporated mRNA by providing enhanced protein expression and reduced immunogenicity in mammalian cell lines and mice. *Journal of Controlled Release* **217**:337–344. doi:10.1016/j.jconrel.2015.08.051

7. Anthony TG, McDaniel BJ, Byerley RL, McGrath BC, Cavener DB, McNurlan MA, Wek RC. 2004. Preservation of liver protein synthesis during dietary leucine deprivation occurs at

the expense of skeletal muscle mass in mice deleted for eIF2 kinase GCN2. *Journal of Biological Chemistry* **279**:36553–36561. doi:10.1074/jbc.M404559200

8. Averous J, Lambert-Langlais S, Mesclon F, Carraro V, Parry L, Jousse C, Bruhat A, Maurin AC, Pierre P, Proud CG, Fafournoux P. 2016. GCN2 contributes to mTORC1 inhibition by leucine deprivation through an ATF4 independent mechanism. *Scientific Reports* **6**:1–10. doi:10.1038/srep27698

9. Baden LR, El Sahly HM, Essink B, Kotloff K, Frey S, Novak R, Diemert D, Spector SA, Rouphael N, Creech CB, McGettigan J, Khetan S, Segall N, Solis J, Brosz A, Fierro C, Schwartz H, Neuzil K, Corey L, Gilbert P, Janes H, Follmann D, Marovich M, Mascola J, Polakowski L, Ledgerwood J, Graham BS, Bennett H, Pajon R, Knightly C, Leav B, Deng W, Zhou H, Han S, Ivarsson M, Miller J, Zaks T. 2021. Efficacy and Safety of the mRNA-1273 SARS-CoV-2 Vaccine. *New England Journal of Medicine* **384**:403–416. doi:10.1056/nejmoa2035389

10. Baird TD, Wek RC. 2012. Eukaryotic initiation factor 2 phosphorylation and translational control in metabolism. *Advances in Nutrition* **3**:307–321. doi:10.3945/an.112.002113

11. Barends S, Karzai AW, Sauer RT, Wower J, Kraal B. 2001. Simultaneous and functional binding of SmpB and EF-Tu·GTP to the alanyl acceptor arm of tmRNA. *Journal of Molecular Biology* **314**:9–21. doi:10.1006/jmbi.2001.5114

12. Battaglioni S, Benjamin D, Wälchli M, Maier T, Hall MN. 2022. mTOR substrate phosphorylation in growth control. *Cell* **185**:1814–1836. doi:10.1016/j.cell.2022.04.013

13. Beck M, Schmidt A, Malmstroem J, Claassen M, Ori A, Szymborska A, Herzog F, Rinner O, Ellenberg J, Aebersold R. 2011. The quantitative proteome of a human cell line. *Molecular Systems Biology* **7**:549–549. doi:10.1038/MSB.2011.82

14. Becker T, Franckenberg S, Wickles S, Shoemaker CJ, Anger AM, Armache J-P, Sieber H, Ungewickell C, Berninghausen O, Daberkow I, Karcher A, Thomm M, Hopfner K-P, Green R, Beckmann R. 2012. Structural basis of highly conserved ribosome recycling in eukaryotes and archaea. *Nature* **482**:501–506. doi:10.1038/nature10829

15. Blanchard SC, Gonzalez RL, Kim HD, Chu S, Puglisi JD. 2004. tRNA selection and kinetic proofreading in translation. *Nat Struct Mol Biol* **11**:1008–1014. doi:10.1038/nsmb831

16. Brandman O, Stewart-Ornstein J, Wong D, Larson A, Williams CC, Li GW, Zhou S, King D, Shen PS, Weibezahn J, Dunn JG, Rouskin S, Inada T, Frost A, Weissman JS. 2012. A Ribosome-Bound Quality Control Complex Triggers Degradation of Nascent Peptides and Signals Translation Stress. *Cell* **151**:1042–1054. doi:10.1016/j.cell.2012.10.044

17. Brown A, Shao S, Murray J, Hegde RS, Ramakrishnan V. 2015. Structural basis for stop codon recognition in eukaryotes. *Nature* **524**:493–496. doi:10.1038/nature14896

18. Buschauer R, Matsuo Y, Sugiyama T, Chen YH, Alhusaini N, Sweet T, Ikeuchi K, Cheng J, Matsuki Y, Nobuta R, Gilmozzi A, Berninghausen O, Tesina P, Becker T, Coller J, Inada T, Beckmann R. 2020. The Ccr4-Not complex monitors the translating ribosome for codon optimality. *Science* **368**. doi:10.1126/science.aay6912

19. Buttgereit F, Brand MD. 1995. A hierarchy of ATP-consuming processes in mammalian cells. *Biochemical Journal* **312**:163–167. doi:10.1042/BJ3120163

20. Cerullo F, Filbeck S, Patil PR, Hung HC, Xu H, Vornberger J, Hofer FW, Schmitt J, Kramer G, Bukau B, Hofmann K, Pfeffer S, Joazeiro CAP. 2022. Bacterial ribosome collision sensing by a MutS DNA repair ATPase paralogue. *Nature 2022 603:7901* **603**:509–514. doi:10.1038/S41586-022-04487-6

21. Chauhan AK, Apirion D. 1989. The gene for a small stable RNA (10Sa RNA) of Escherichia coli. *Mol Microbiol* **3**:1481–1485. doi:10.1111/j.1365-2958.1989.tb00133.x

22. Chen L, Muhlrad D, Hauryliuk V, Cheng Z, Lim MK, Shyp V, Parker R, Song H. 2010. Structure of the Dom34-Hbs1 complex and implications for no-go decay. *Nature Structural and Molecular Biology* **17**:1233–1240. doi:10.1038/nsmb.1922

23. Chen X, Yu H, Li Z, Ye W, Liu Z, Gao J, Wang Y, Li X, Zhang L, Alenina N, Bader M, Ding H, Li P, Aung LHH. 2022. Oxidative RNA Damage in the Pathogenesis and Treatment of Type 2 Diabetes. *Front Physiol* **13**:725919. doi:10.3389/fphys.2022.725919

24. Cheng Z, Saito K, Pisarev AV, Wada M, Pisareva VP, Pestova TV, Gajda M, Round A, Kong C, Lim M, Nakamura Y, Svergun DI, Ito K, Song H. 2009. Structural insights into eRF3 and stop codon recognition by eRF1. *Genes Dev* **23**:1106–1118. doi:10.1101/gad.1770109

25. Cherkasova VA, Hinnebusch AG. 2003. Translational control by TOR and TAP42 through dephosphorylation of eIF2α kinase GCN2. *Genes and Development* **17**:859–872. doi:10.1101/gad.1069003

26. Chu J, Hong NA, Masuda CA, Jenkins BV, Nelms KA, Goodnow CC, Glynne RJ, Wu H, Masliah E, Joazeiro CAPP, Kay SA. 2009. A mouse forward genetics screen identifies

LISTERIN as an E3 ubiquitin ligase involved in neurodegeneration. *Proceedings of the National Academy of Sciences of the United States of America* **106**:2097–2103. doi:10.1073/pnas.0812819106

27. Collart MA. 2013. The Not4 RING E3 Ligase: A Relevant Player in Cotranslational Quality Control. *ISRN Molecular Biology* **2013**:1–19. doi:10.1155/2013/548359

28. Costa-Mattioli M, Walter P. 2020. The integrated stress response: From mechanism to disease. *Science (New York, NY)* **368**. doi:10.1126/science.aat5314

29. Darling NJ, Cook SJ. 2014. The role of MAPK signalling pathways in the response to endoplasmic reticulum stress. *Biochimica et Biophysica Acta - Molecular Cell Research* **1843**:2150–2163. doi:10.1016/j.bbamcr.2014.01.009

30. Davis DR. 1995. Stabilization of RNA stacking by pseudouridine. *Nucleic Acids Research* **23**:5020–5026. doi:10.1093/nar/23.24.5020

31. Deb I, Popenda Ł, Sarzyńska J, Małgowska M, Lahiri A, Gdaniec Z, Kierzek R. 2019. Computational and NMR studies of RNA duplexes with an internal pseudouridine-adenosine base pair. *Scientific Reports* **9**:1–13. doi:10.1038/s41598-019-52637-0

32. des Georges A, Dhote V, Kuhn L, Hellen CUT, Pestova TV, Frank J, Hashem Y. 2015. Structure of mammalian eIF3 in the context of the 43S preinitiation complex. *Nature* **525**:491–495. doi:10.1038/nature14891

33. Dever TE, Dinman JD, Green R. 2018. Translation Elongation and Recoding in Eukaryotes. *Cold Spring Harb Perspect Biol* **10**:a032649. doi:10.1101/cshperspect.a032649

34. Dever TE, Feng L, Wek RC, Cigan AM, Donahue TF, Hinnebusch AG. 1992. Phosphorylation of initiation factor 2 alpha by protein kinase GCN2 mediates gene-specific translational control of GCN4 in yeast. *Cell* **68**:585–596. doi:10.1016/0092-8674(92)90193-g

35. Doma MK, Parker R. 2006. Endonucleolytic cleavage of eukaryotic mRNAs with stalls in translation elongation. *Nature* **440**:561–564. doi:10.1038/nature04530

36. Dong J, Aitken CE, Thakur A, Shin B-S, Lorsch JR, Hinnebusch AG. 2017. Rps3/uS3 promotes mRNA binding at the 40S ribosome entry channel and stabilizes preinitiation complexes at start codons. *Proc Natl Acad Sci USA* **114**. doi:10.1073/pnas.1620569114

37. Donnelly N, Gorman AM, Gupta S, Samali A. 2013. The eIF2α kinases: Their structures and functions. *Cellular and Molecular Life Sciences* **70**:3493–3511. doi:10.1007/s00018-012-1252-6

38. D'Orazio KN, Green R. 2021. Ribosome states signal RNA quality control. *Molecular Cell* **81**:1372–1383. doi:10.1016/j.molcel.2021.02.022

39. Duch A, De Nadal E, Posas F. 2012. The p38 and Hog1 SAPKs control cell cycle progression in response to environmental stresses. *FEBS Letters* **586**:2925–2931. doi:10.1016/j.febslet.2012.07.034

40. Duncan R, Hershey JWB. 1983. Identification and Quantitation of Levels of Protein Synthesis Initiation Factors in Crude HeLa Cell Lysates by Two-dimensional Polyacrylamide Gel Electrophoresis*. *THE JOURNAL OF BIOLOGICAL CHEMISTRY* **258**:7228–7235. doi:10.1016/S0021-9258(18)32356-1

41. Ejby M, Sørensen MA, Pedersen S. 2007. Pseudouridylation of helix 69 of 23S rRNA is necessary for an effective translation termination. *Proceedings of the National Academy of Sciences of the United States of America* **104**:19410–19415. doi:10.1073/pnas.0706558104

42. Eyler DE, Franco MK, Batool Z, Wu MZ, Dubuke ML, Dobosz-Bartoszek M, Jones JD, Polikanov YS, Roy B, Koutmou KS. 2019. Pseudouridinylation of mRNA coding sequences alters translation. *Proceedings of the National Academy of Sciences of the United States of America* **116**:23068–23074. doi:10.1073/pnas.1821754116

43. Farabaugh PJ. 1996. Programmed translational frameshifting. *Annual Review of Genetics* **30**:507–528. doi:10.1146/annurev.genet.30.1.507

44. Fernández IS, Ng CL, Kelley AC, Wu G, Yu YT, Ramakrishnan V. 2013. Unusual base pairing during the decoding of a stop codon by the ribosome. *Nature* **500**:107–110. doi:10.1038/nature12302

45. Ferrin MA, Subramaniam AR. 2017. Kinetic modeling predicts a stimulatory role for ribosome collisions at elongation stall sites in bacteria. *eLife* **6**:1–19. doi:10.7554/eLife.23629

46. Fonseca BD, Smith EM, Yelle N, Alain T, Bushell M, Pause A. 2014. The ever-evolving role of mTOR in translation. *Seminars in Cell & Developmental Biology* **36**:102–112. doi:10.1016/j.semcdb.2014.09.014

47. Freund I, Eigenbrod T, Helm M, Dalpke AH. 2019. RNA modifications modulate activation of innate toll-like receptors. *Genes* **10**. doi:10.3390/genes10020092

48. Fujii K, Kitabatake M, Sakata T, Miyata A, Ohno M. 2009. A role for ubiquitin in the clearance of nonfunctional rRNAs. *Genes and Development* **23**:963–974. doi:10.1101/gad.1775609

49. Garcia-Barrio M. 2000. Association of GCN1-GCN20 regulatory complex with the N-terminus of eIF2alpha kinase GCN2 is required for GCN2 activation. *The EMBO Journal* **19**:1887–1899. doi:10.1093/emboj/19.8.1887

50. García-Muse T, Aguilera A. 2016. Transcription-replication conflicts: How they occur and how they are resolved. *Nature Reviews Molecular Cell Biology* **17**:553–563. doi:10.1038/nrm.2016.88

51. Garshott DM, Sundaramoorthy E, Leonard M, Bennett EJ. 2020. Distinct regulatory ribosomal ubiquitylation events are reversible and hierarchically organized. *eLife* **9**:1–22. doi:10.7554/eLife.54023

52. Garzia A, Jafarnejad SM, Meyer C, Chapat C, Gogakos T, Morozov P, Amiri M, Shapiro M, Molina H, Tuschl T, Sonenberg N. 2017. The E3 ubiquitin ligase and RNA-binding protein ZNF598 orchestrates ribosome quality control of premature polyadenylated mRNAs. *Nature Communications* **8**. doi:10.1038/ncomms16056

53. Gingras A-C, Gygi SP, Raught B, Polakiewicz RD, Abraham RT, Hoekstra MF, Aebersold R, Sonenberg N. 1999. Regulation of 4E-BP1 phosphorylation: a novel two-step mechanism. *Genes & Development* **13**:1422–1437. doi:10.1101/gad.13.11.1422

54. Gingras A-C, Raught B, Gygi SP, Niedzwiecka A, Miron M, Burley SK, Polakiewicz RD, Wyslouch-Cieszynska A, Aebersold R, Sonenberg N. 2001a. Hierarchical phosphorylation of the translation inhibitor 4E-BP1. *Genes Dev* **15**:2852–2864. doi:10.1101/gad.912401

55. Gingras A-C, Raught B, Sonenberg N. 2001b. Regulation of translation initiation by FRAP/mTOR. *Genes Dev* **15**:807–826. doi:10.1101/gad.887201

56. González A, Hall MN. 2017. Nutrient sensing and TOR signaling in yeast and mammals. *The EMBO Journal* **36**:397–408. doi:10.15252/embj.201696010

57. Gromadski KB, Daviter T, Rodnina MV. 2006. A Uniform Response to Mismatches in Codon-Anticodon Complexes Ensures Ribosomal Fidelity. *Molecular Cell* **21**:369–377. doi:10.1016/j.molcel.2005.12.018

58. Gromadski KB, Rodnina MV. 2004. Kinetic Determinants of High-Fidelity tRNA Discrimination on the Ribosome. *Molecular Cell* **13**:191–200. doi:10.1016/S1097-2765(04)00005-X

59. Han P, Shichino Y, Schneider-Poetsch T, Mito M, Hashimoto S, Udagawa T, Kohno K, Yoshida M, Mishima Y, Inada T, Iwasaki S. 2020. Genome-wide Survey of Ribosome Collision. *Cell Reports* **31**:107610. doi:10.1016/j.celrep.2020.107610

60. Hanawa-Suetsugu K. 2002. SmpB functions in various steps of trans-translation. *Nucleic Acids Research* **30**:1620–1629. doi:10.1093/nar/30.7.1620

61. Harding HP, Ordonez A, Allen F, Parts L, Inglis AJ, Williams RL, Ron D. 2019. The ribosomal P-stalk couples amino acid starvation to GCN2 2 activation in mammalian cells. *eLife* **8**:1–19. doi:10.7554/eLife.50149

62. Hashimoto S, Sugiyama T, Yamazaki R, Nobuta R, Inada T. 2020. Identification of a novel trigger complex that facilitates ribosome-associated quality control in mammalian cells. *Scientific reports* **10**:3422. doi:10.1038/s41598-020-60241-w

63. Hickey KL, Dickson K, Cogan JZ, Replogle JM, Schoof M, D'Orazio KN, Sinha NK, Hussmann JA, Jost M, Frost A, Green R, Weissman JS, Kostova KK. 2020. GIGYF2 and 4EHP Inhibit Translation Initiation of Defective Messenger RNAs to Assist Ribosome-Associated Quality Control. *Molecular Cell* **79**:950-962.e6. doi:10.1016/j.molcel.2020.07.007

64. Higgins RR, Gendron JM, Rising L, Mak R, Webb K, Kaiser SE, Zuzow N, Riviere P, Yang B, Fenech E, Tang X, Lindsay SA, Christianson JC, Hampton RY, Wasserman SA, Bennett EJ. 2015. The Unfolded Protein Response Triggers Site-Specific Regulatory Ubiquitylation of 40S Ribosomal Proteins. *Molecular Cell* **59**:35–49. doi:10.1016/j.molcel.2015.04.026

65. Hinnebusch AG. 2017. Structural Insights into the Mechanism of Scanning and Start Codon Recognition in Eukaryotic Translation Initiation. *Trends in biochemical sciences* **42**:589–611. doi:10.1016/j.tibs.2017.03.004

66. Hinnebusch AG. 2014. The scanning mechanism of eukaryotic translation initiation. *Annual Review of Biochemistry* **83**:779–812. doi:10.1146/annurev-biochem-060713-035802

67. Hinnebusch AG. 2011. Molecular mechanism of scanning and start codon selection in eukaryotes. *Microbiology and molecular biology reviews : MMBR* **75**:434–67, first page of table of contents. doi:10.1128/MMBR.00008-11

68. Hinnebusch AG. 2005. Translational regulation of GCN4 and the general amino acid control of yeast. *Annual Review of Microbiology* **59**:407–450. doi:10.1146/annurev.micro.59.031805.133833

69. Hinnebusch AG, Lorsch JR. 2012. The mechanism of eukaryotic translation initiation: new insights and challenges. *Cold Spring Harbor perspectives in biology* **4**. doi:10.1101/cshperspect.a011544

70. Ho B, Baryshnikova A, Brown GW. 2018. Unification of Protein Abundance Datasets Yields a Quantitative Saccharomyces cerevisiae Proteome. *Cell Systems* **6**:192-205.e3. doi:10.1016/j.cels.2017.12.004

71. Hoernes TP, Clementi N, Faserl K, Glasner H, Breuker K, Lindner H, Hüttenhofer A, Erlacher MD. 2016. Nucleotide modifications within bacterial messenger RNAs regulate their translation and are able to rewire the genetic code. *Nucleic Acids Research* **44**:852–862. doi:10.1093/nar/gkv1182

72. Hoernes TP, Heimdörfer D, Köstner D, Faserl K, Nußbaumer F, Plangger R, Kreutz C, Lindner H, Erlacher MD. 2019. Eukaryotic Translation Elongation is Modulated by Single Natural Nucleotide Derivatives in the Coding Sequences of mRNAs. *Genes 2019, Vol 10, Page 84* **10**:84. doi:10.3390/GENES10020084

73. Howard CJ, Frost A. 2021. Ribosome-associated quality control and CAT tailing. *Critical Reviews in Biochemistry and Molecular Biology* 1–18. doi:10.1080/10409238.2021.1938507

74. Howell JJ, Ricoult SJH, Ben-Sahra I, Manning BD. 2013. A growing role for mTOR in promoting anabolic metabolism. *Biochemical Society Transactions* **41**:906–912. doi:10.1042/BST20130041

75. Hudson BH, Zaher HS. 2015. O6-Methylguanosine leads to position-dependent effects on ribosome speed and fidelity. *RNA* **21**:1648–1659. doi:10.1261/rna.052464.115

76. Hudson CM, Lau BY, Williams KP. 2014. Ends of the line for tmRNA-SmpB. *Front Microbiol* **5**. doi:10.3389/fmicb.2014.00421

77. Hudson GA, Bloomingdale RJ, Znosko BM. 2013. Thermodynamic contribution and nearest-neighbor parameters of pseudouridine-adenosine base pairs in oligoribonucleotides. *Rna* **19**:1474–1482. doi:10.1261/rna.039610.113

78. Hughes TR, Marton MJ, Jones AR, Roberts CJ, Stoughton R, Armour CD, Bennett HA, Coffey E, Dai H, He YD, Kidd MJ, King AM, Meyer MR, Slade D, Lum PY, Stepaniants SB, Shoemaker DD, Gachotte D, Chakraburtty K, Simon J, Bard M, Friend SH. 2000. Functional Discovery via a Compendium of Expression Profiles. *Cell* **102**:109–126. doi:10.1016/S0092-8674(00)00015-5

79. Ikeuchi K, Tesina P, Matsuo Y, Sugiyama T, Cheng J, Saeki Y, Tanaka K, Becker T, Beckmann R, Inada T. 2019. Collided ribosomes form a unique structural interface to induce Hel2-driven quality control pathways. *The EMBO Journal* **38**:1–21. doi:10.15252/embj.2018100276

80. Inada T. 2020. Quality controls induced by aberrant translation. *Nucleic Acids Research* **48**:1084–1096. doi:10.1093/NAR/GKZ1201

81. Inada T. 2017. The Ribosome as a Platform for mRNA and Nascent Polypeptide Quality Control. *Trends in Biochemical Sciences* **42**:5–15. doi:10.1016/j.tibs.2016.09.005

82. Inglis AJ, Masson GR, Shao S, Perisic O, McLaughlin SH, Hegde RS, Williams RL. 2019. Activation of GCN2 by the ribosomal P-stalk. *Proceedings of the National Academy of Sciences of the United States of America* **116**:4946–4954. doi:10.1073/pnas.1813352116

83. Iordanov MS, Pribnow D, Magun JL, Dinh TH, Pearson JA, Chen SL, Magun BE. 1997. Ribotoxic stress response: activation of the stress-activated protein kinase JNK1 by inhibitors of the peptidyl transferase reaction and by sequence-specific RNA damage to the alpha-sarcin/ricin loop in the 28S rRNA. *Molecular and Cellular Biology* **17**:3373–3381. doi:10.1128/mcb.17.6.3373

84. Iordanov MS, Pribnow D, Magun JL, Dinh TH, Pearson JA, Magun BE. 1998. Ultraviolet radiation triggers the ribotoxic stress response in mammalian cells. *Journal of Biological Chemistry* **273**:15794–15803. doi:10.1074/jbc.273.25.15794

85. Ishimura R, Nagy G, Dotu I, Chuang JH, Ackerman SL. 2016. Activation of GCN2 kinase by ribosome stalling links translation elongation with translation initiation. *eLife* **5**:1–22. doi:10.7554/eLife.14295

86. Jackson RJ, Hellen CUT, Pestova TV. 2010. The mechanism of eukaryotic translation initiation and principles of its regulation. *Nature Reviews Molecular Cell Biology* **11**:113–127. doi:10.1038/nrm2838

87. Jandhyala DM, Ahluwalia A, Obrig T, Thorpe CM. 2008. ZAK: A MAP3Kinase that transduces Shiga toxin- and ricin-induced proinflammatory cytokine expression. *Cellular Microbiology* **10**:1468–1477. doi:10.1111/j.1462-5822.2008.01139.x

88. Jang SK, Kräusslich HG, Nicklin MJ, Duke GM, Palmenberg AC, Wimmer E. 1988. A segment of the 5' nontranslated region of encephalomyocarditis virus RNA directs internal entry of ribosomes during in vitro translation. *J Virol* **62**:2636–2643. doi:10.1128/jvi.62.8.2636-2643.1988

89. Janssen BD, Hayes CS. 2012. The tmRNA ribosome-rescue systemAdvances in Protein Chemistry and Structural Biology. Elsevier. pp. 151–191. doi:10.1016/B978-0-12-386497-0.00005-0

90. Jirikowski GF, Sanna PP, Maciejewski-Lenoir D, Bloom FE, F. JG, Paolo SP, Dominique M-L, E. BF. 1992. Reversal of Diabetes Insipidus in Brattleboro Rats: Intrahypothalamic Injection of Vasopressin mRNA. *Science (New York, NY)* **255**:996–998. doi:10.1126/science.1546298

91. Jung Y, Kim HDHJ, Yang HW, Kim HDHJ, Jang CY, Kim J. 2017. Modulating cellular balance of Rps3 mono-ubiquitination by both Hel2 E3 ligase and Ubp3 deubiquitinase regulates protein quality control. *Experimental and Molecular Medicine* **49**:e390-12. doi:10.1038/emm.2017.128

92. Juszkiewicz S, Chandrasekaran V, Lin Z, Kraatz S, Ramakrishnan V, Hegde RS. 2018. ZNF598 Is a Quality Control Sensor of Collided Ribosomes. *Molecular Cell* **72**:469-481.e7. doi:10.1016/j.molcel.2018.08.037

93. Juszkiewicz S, Hegde RSS. 2017. Initiation of Quality Control during Poly(A) Translation Requires Site-Specific Ribosome Ubiquitination. *Molecular Cell* **65**:743-750.e4. doi:10.1016/j.molcel.2016.11.039

94. Juszkiewicz S, Slodkowicz G, Lin Z, Freire-Pritchett P, Peak-Chew SY, Hegde RS. 2020a. Ribosome collisions trigger cis-acting feedback inhibition of translation initiation. *eLife* **9**:1–29. doi:10.7554/eLife.60038

95. Juszkiewicz S, Speldewinde SH, Wan L, Svejstrup JQ, Hegde RS. 2020b. The ASC-1 Complex Disassembles Collided Ribosomes. *Molecular Cell* **79**:603-614.e8. doi:10.1016/j.molcel.2020.06.006

96. Karijolich J, Yu YT. 2011. Converting nonsense codons into sense codons by targeted pseudouridylation. *Nature* **474**:395–399. doi:10.1038/nature10165

97. Karikó K, Buckstein M, Ni H, Weissman D. 2005. Suppression of RNA recognition by Toll-like receptors: The impact of nucleoside modification and the evolutionary origin of RNA. *Immunity* **23**:165–175. doi:10.1016/j.immuni.2005.06.008

98. Karikó K, Muramatsu H, Keller JM, Weissman D. 2012. Increased erythropoiesis in mice injected with submicrogram quantities of pseudouridine-containing mRNA encoding erythropoietin. *Molecular Therapy* **20**:948–953. doi:10.1038/mt.2012.7

99. Karikó K, Muramatsu H, Ludwig J, Weissman D. 2011. Generating the optimal mRNA for therapy: HPLC purification eliminates immune activation and improves translation of nucleoside-modified, protein-encoding mRNA. *Nucleic Acids Research* **39**:1–10. doi:10.1093/nar/gkr695

100. Karikó K, Muramatsu H, Welsh FA, Ludwig J, Kato H, Akira S, Weissman D. 2008. Incorporation of pseudouridine into mRNA yields superior nonimmunogenic vector with increased translational capacity and biological stability. *Molecular therapy : the journal of the American Society of Gene Therapy* **16**:1833–1840. doi:10.1038/mt.2008.200

101. Karikó K, Ni H, Capodici J, Lamphier M, Weissman D. 2004. mRNA Is an Endogenous Ligand for Toll-like Receptor 3. *Journal of Biological Chemistry* **279**:12542–12550. doi:10.1074/jbc.M310175200

102. Karzai AW. 1999. SmpB, a unique RNA-binding protein essential for the peptide-tagging activity of SsrA (tmRNA). *The EMBO Journal* **18**:3793–3799. doi:10.1093/emboj/18.13.3793

103. Keiler KC, Waller PRH, Sauer RT. 1996. Role of a peptide tagging system in degradation of proteins synthesized from damaged messenger RNA. *Science* **271**:990–993. doi:10.1126/science.271.5251.990

104. Kierzek E, Malgowska M, Lisowiec J, Turner DH, Gdaniec Z, Kierzek R. 2014. The contribution of pseudouridine to stabilities and structure of RNAs. *Nucleic Acids Research* **42**:3492–3501. doi:10.1093/nar/gkt1330

105. Kolitz SE, Takacs JE, Lorsch JR. 2009. Kinetic and thermodynamic analysis of the role of start codon/anticodon base pairing during eukaryotic translation initiation. *RNA (New York, NY)* **15**:138–152. doi:10.1261/rna.1318509

106. Koshland DE. 1958. Application of a Theory of Enzyme Specificity to Protein Synthesis. *Proc Natl Acad Sci USA* **44**:98–104. doi:10.1073/pnas.44.2.98

107. Krishnamoorthy T, Pavitt GD, Zhang F, Dever TE, Hinnebusch AG. 2001. Tight Binding of the Phosphorylated α Subunit of Initiation Factor 2 (eIF2α) to the Regulatory Subunits of Guanine Nucleotide Exchange Factor eIF2B Is Required for Inhibition of Translation Initiation. *Molecular and Cellular Biology* **21**:5018–5030. doi:10.1128/mcb.21.15.5018-5030.2001

108. Kubota H, Obata T, Ota K, Sasaki T, Ito T. 2003. Rapamycin-induced translational derepression of GCN4 mRNA involves a novel mechanism for activation of the eIF2α kinase GCN2. *Journal of Biological Chemistry* **278**:20457–20460. doi:10.1074/jbc.C300133200

109. Kulak NA, Pichler G, Paron I, Nagaraj N, Mann M. 2014. Minimal, encapsulated proteomic-sample processing applied to copy-number estimation in eukaryotic cells. *Nature Methods* **11**:319–324. doi:10.1038/nmeth.2834

110. Kurokawa M, Kornbluth S. 2009. Caspases and Kinases in a Death Grip. *Cell* **138**:838–854. doi:10.1016/j.cell.2009.08.021

111. Laplante M, Sabatini DM. 2012. MTOR signaling in growth control and disease. *Cell* **149**:274–293. doi:10.1016/j.cell.2012.03.017

112. LaRiviere FJ, Cole SE, Ferullo DJ, Moore MJ. 2006. A late-acting quality control process for mature eukaryotic rRNAs. *Molecular Cell* **24**:619–626. doi:10.1016/j.molcel.2006.10.008

113. Ledoux S, Uhlenbeck OC. 2008. Different aa-tRNAs Are Selected Uniformly on the Ribosome. *Molecular Cell* **31**:114–123. doi:10.1016/j.molcel.2008.04.026

114. Lee K-M, Chen C-J, Shih S-R. 2017. Regulation Mechanisms of Viral IRES-Driven Translation. *Trends in Microbiology* **25**:546–561. doi:10.1016/j.tim.2017.01.010

115. Lee SJ, Swanson MJ, Sattlegger E. 2015. Gcn1 contacts the small ribosomal protein Rps10, which is required for full activation of the protein kinase Gcn2. *Biochemical Journal* **466**:547–559. doi:10.1042/BJ20140782

116. Letzring DP, Dean KM, Grayhack EJ. 2010. Control of translation efficiency in yeast by codon-anticodon interactions. *Rna* **16**:2516–2528. doi:10.1261/rna.2411710

117. Letzring DP, Wolf AS, Brule CE, Grayhack EJ. 2013. Translation of CGA codon repeats in yeast involves quality control components and ribosomal protein L1. *Rna* **19**:1208–1217. doi:10.1261/rna.039446.113

118. Li X, Ma S, Yi C. 2016. Pseudouridine: the fifth RNA nucleotide with renewed interests. *Current Opinion in Chemical Biology* **33**:108–116. doi:10.1016/J.CBPA.2016.06.014

119. Li Z, Wu J, DeLeo C. 2006. RNA damage and surveillance under oxidative stress. *IUBMB Life (International Union of Biochemistry and Molecular Biology: Life)* **58**:581–588. doi:10.1080/15216540600946456

120. Limoncelli KA, Merrikh CN, Moore MJ. 2017. ASC1 and RPS3: New actors in 18S nonfunctional rRNA decay. *Rna* **23**:1946–1960. doi:10.1261/rna.061671.117

121. Loewith R, Hall MN. 2011. Target of rapamycin (TOR) in nutrient signaling and growth control. *Genetics* **189**:1177–1201. doi:10.1534/genetics.111.133363

122. Loewith R, Jacinto E, Wullschleger S, Lorberg A, Crespo JL, Bonenfant D, Oppliger W, Jenoe P, Hall MN. 2002. Two TOR complexes, only one of which is rapamycin sensitive, have distinct roles in cell growth control. *Molecular Cell* **10**:457–468. doi:10.1016/S1097-2765(02)00636-6

123. Lomakin IB, Shirokikh NE, Yusupov MM, Hellen CUT, Pestova TV. 2006. The fidelity of translation initiation: reciprocal activities of eIF1, IF3 and YciH. *The EMBO Journal* **25**:196–210. doi:https://doi.org/10.1038/sj.emboj.7600904

124. Mao S, Haruehanroengra P, Ranganathan SV, Shen F, Begley TJ, Sheng J. 2021. Base Pairing and Functional Insights into N 3-Methylcytidine (m 3 C) in RNA. *ACS Chem Biol* **16**:76–85. doi:10.1021/acschembio.0c00735

125. Martinez-Salas E, Francisco-Velilla R, Fernandez-Chamorro J, Embarek AM. 2018. Insights into Structural and Mechanistic Features of Viral IRES Elements. *Front Microbiol* **8**:2629. doi:10.3389/fmicb.2017.02629

126. Marton MJ, Vazquez de Aldana CR, Qiu H, Chakraburtty K, Hinnebusch AG. 1997. Evidence that GCN1 and GCN20, translational regulators of GCN4, function on elongating ribosomes in activation of eIF2alpha kinase GCN2. *Molecular and Cellular Biology* **17**:4474–4489. doi:10.1128/mcb.17.8.4474

127. Matheisl S, Berninghausen O, Becker T, Beckmann R. 2015. Structure of a human translation termination complex. *Nucleic Acids Res* **43**:8615–8626. doi:10.1093/nar/gkv909

128. Matsuki Y, Matsuo Y, Nakano Y, Iwasaki S, Yoko H, Udagawa T, Li S, Saeki Y, Yoshihisa T, Tanaka K, Ingolia NT, Inada T. 2020. Ribosomal protein S7 ubiquitination during ER stress in yeast is associated with selective mRNA translation and stress outcome. *Scientific Reports* **10**:1–15. doi:10.1038/s41598-020-76239-3

129. Matsuo Y, Ikeuchi K, Saeki Y, Iwasaki S, Schmidt C, Udagawa T, Sato F, Tsuchiya H, Becker T, Tanaka K, Ingolia NTT, Beckmann R, Inada T. 2017. Ubiquitination of stalled

ribosome triggers ribosome-associated quality control. *Nature Communications* **8**:1–13. doi:10.1038/s41467-017-00188-1

130. Matsuo Y, Tesina P, Nakajima S, Mizuno M, Endo A, Buschauer R, Cheng J, Shounai O, Ikeuchi K, Saeki Y, Becker T, Beckmann R, Inada T. 2020. RQT complex dissociates ribosomes collided on endogenous RQC substrate SDD1. *Nature Structural and Molecular Biology* **27**:323–332. doi:10.1038/s41594-020-0393-9

131. Mauger DM, Joseph Cabral B, Presnyak V, Su SV, Reid DW, Goodman B, Link K, Khatwani N, Reynders J, Moore MJ, McFadyen IJ. 2019. mRNA structure regulates protein expression through changes in functional half-life. *Proceedings of the National Academy of Sciences of the United States of America* **116**:24075–24083. doi:10.1073/pnas.1908052116

132. Messenger RNA Encoding the Full-Length SARS-CoV-2 Spike Glycoprotein. 2020. World Health Organization: International Nonproprietary Names Programme. p. 11889.

133. Meydan S, Guydosh NR. 2020. Disome and Trisome Profiling Reveal Genome-wide Targets of Ribosome Quality Control. *Molecular Cell* **79**:588-602.e6. doi:10.1016/j.molcel.2020.06.010

134. Meyer C, Garzia A, Morozov P, Molina H, Tuschl T. 2020. The G3BP1-Family-USP10 Deubiquitinase Complex Rescues Ubiquitinated 40S Subunits of Ribosomes Stalled in Translation from Lysosomal Degradation. *Molecular Cell* **77**:1193-1205.e5. doi:10.1016/j.molcel.2019.12.024

135. Mitarai N, Sneppen K, Pedersen S. 2008. Ribosome Collisions and Translation Efficiency: Optimization by Codon Usage and mRNA Destabilization. *Journal of Molecular Biology* **382**:236–245. doi:10.1016/j.jmb.2008.06.068

136. Moore SD, Sauer RT. 2007. The tmRNA System for Translational Surveillance and Ribosome Rescue. *Annu Rev Biochem* **76**:101–124. doi:10.1146/annurev.biochem.75.103004.142733

137. Moore SD, Sauer RT. 2005. Ribosome rescue: tmRNA tagging activity and capacity in Escherichia coli. *Molecular Microbiology* **58**:456–466. doi:10.1111/j.1365-2958.2005.04832.x

138. Morita M, Ler LW, Fabian MR, Siddiqui N, Mullin M, Henderson VC, Alain T, Fonseca BD, Karashchuk G, Bennett CF, Kabuta T, Higashi S, Larsson O, Topisirovic I, Smith RJ, Gingras A-C, Sonenberg N. 2012. A Novel 4EHP-GIGYF2 Translational Repressor Complex Is Essential for Mammalian Development. *Molecular and Cellular Biology* **32**:3585–3593. doi:10.1128/mcb.00455-12

139. Muhs M, Hilal T, Mielke T, Skabkin MA, Sanbonmatsu KY, Pestova TV, Spahn CMT. 2015. Cryo-EM of Ribosomal 80S Complexes with Termination Factors Reveals the Translocated Cricket Paralysis Virus IRES. *Molecular Cell* **57**:422–432. doi:10.1016/j.molcel.2014.12.016

140. Müller C, Crowe-McAuliffe C, Wilson DN. 2021. Ribosome Rescue Pathways in Bacteria. *Front Microbiol* **12**:652980. doi:10.3389/fmicb.2021.652980

141. Nakashima N, Noguchi E, Nishimoto T. 1999. Saccharomyces cerevisiae putative G protein, Gtr1p, which forms complexes with itself and a novel protein designated as Gtr2p, negatively regulates the Ran/Gsp1p G protein cycle through Gtr2p. *Genetics* **152**:853–867. doi:10.1093/genetics/152.3.853

142. Natarajan K, Meyer MR, Jackson BM, Slade D, Roberts C, Hinnebusch AG, Marton MJ. 2001. Transcriptional Profiling Shows that Gcn4p Is a Master Regulator of Gene Expression during Amino Acid Starvation in Yeast. *Molecular and Cellular Biology* **21**:4347–4368. doi:10.1128/mcb.21.13.4347-4368.2001

143. Nir R, Hoernes TP, Muramatsu H, Faserl K, Karikó K, Erlacher MD, Sas-Chen A, Schwartz S. 2022. A systematic dissection of determinants and consequences of snoRNA-guided pseudouridylation of human mRNA. *Nucleic Acids Research* **50**:4900–4916. doi:10.1093/nar/gkac347

144. Ogle JM, Brodersen DE, Clemons WM, Tarry MJ, Carter AP, Ramakrishnan V. 2001. Recognition of Cognate Transfer RNA by the 30 *S* Ribosomal Subunit. *Science* **292**:897–902. doi:10.1126/science.1060612

145. Ogle JM, Murphy FV, Tarry MJ, Ramakrishnan V. 2002. Selection of tRNA by the Ribosome Requires a Transition from an Open to a Closed Form. *Cell* **111**:721–732. doi:10.1016/S0092-8674(02)01086-3

146. Oh BK, Chauhan AK, Isono K, Apirion D. 1990. Location of a gene (ssrA) for a small, stable RNA (10Sa RNA) in the Escherichia coli chromosome. *J Bacteriol* **172**:4708–4709. doi:10.1128/jb.172.8.4708-4709.1990

147. Pakos-Zebrucka K, Koryga I, Mnich K, Ljujic M, Samali A, Gorman AM. 2016. The integrated stress response. *EMBO reports* **17**:1374–1395. doi:10.15252/embr.201642195

148. Panasenko OO, Collart MA. 2012. Presence of Not5 and ubiquitinated Rps7A in polysome fractions depends upon the Not4 E3 ligase. *Molecular Microbiology* **83**:640–653. doi:10.1111/j.1365-2958.2011.07957.x

149. Pape T. 1999. Induced fit in initial selection and proofreading of aminoacyl-tRNA on the ribosome. *The EMBO Journal* **18**:3800–3807. doi:10.1093/emboj/18.13.3800

150. Pape T, Wintermeyer W, Rodnina MV. 2000. Conformational switch in the decoding region of 16S rRNA during aminoacyl-tRNA selection on the ribosome. *Nature Structural Biology* **7**:104–107. doi:10.1038/72364

151. Parr CJC, Wada S, Kotake K, Kameda S, Matsuura S, Sakashita S, Park S, Sugiyama H, Kuang Y, Saito H. 2020. N 1-Methylpseudouridine substitution enhances the performance of synthetic mRNA switches in cells. *Nucleic Acids Research* **48**:E35. doi:10.1093/nar/gkaa070

152. Pavitt GD. 2005. eIF2B, a mediator of general and gene-specific translational control. *Biochemical Society Transactions* **33**:1487–1492. doi:10.1042/BST0331487

153. Pelletier J, Sonenberg N. 2019. The Organizing Principles of Eukaryotic Ribosome Recruitment. *Annual review of biochemistry* **88**:307–335. doi:10.1146/annurev-biochem-013118-111042

154. Pelletier J, Sonenberg N. 1988. Internal initiation of translation of eukaryotic mRNA directed by a sequence derived from poliovirus RNA. *Nature* **334**:320–325. doi:10.1038/334320a0

155. Pestova TV, Lomakin IB, Lee JH, Choi SK, Dever TE, Hellen CU. 2000. The joining of ribosomal subunits in eukaryotes requires eIF5B. *Nature* **403**:332–335. doi:10.1038/35002118

156. Pisarev AV, Hellen CUT, Pestova TV. 2007. Recycling of Eukaryotic Posttermination Ribosomal Complexes. *Cell* **131**:286–299. doi:10.1016/j.cell.2007.08.041

157. Pisarev AV, Skabkin MA, Pisareva VP, Skabkina OV, Rakotondrafara AM, Hentze MW, Hellen CUT, Pestova TV. 2010. The Role of ABCE1 in Eukaryotic Posttermination Ribosomal Recycling. *Molecular Cell* **37**:196–210. doi:10.1016/j.molcel.2009.12.034

158. Pisareva VP, Skabkin MA, Hellen CUT, Pestova TV, Pisarev AV. 2011. Dissociation by Pelota, Hbs1 and ABCE1 of mammalian vacant 80S ribosomes and stalled elongation complexes. *EMBO Journal* **30**:1804–1817. doi:10.1038/emboj.2011.93

159. Pochopien AA, Beckert B, Kasvandik S, Berninghausen O, Beckmann R, Tenson T, Wilson DN. 2021. Structure of Gcn1 bound to stalled and colliding 80S ribosomes. *Proceedings of the National Academy of Sciences of the United States of America* **118**. doi:10.1073/pnas.2022756118

160. Polack FP, Thomas SJ, Kitchin N, Absalon J, Gurtman A, Lockhart S, Perez JL, Pérez Marc G, Moreira ED, Zerbini C, Bailey R, Swanson KA, Roychoudhury S, Koury K, Li P, Kalina WV, Cooper D, Frenck RW, Hammitt LL, Türeci Ö, Nell H, Schaefer A, Ünal S, Tresnan DB, Mather S, Dormitzer PR, Şahin U, Jansen KU, Gruber WC. 2020. Safety and Efficacy of the BNT162b2 mRNA Covid-19 Vaccine. *New England Journal of Medicine* **383**:2603–2615. doi:10.1056/nejmoa2034577

161. Preis A, Heuer A, Barrio-Garcia C, Hauser A, Eyler DE, Berninghausen O, Green R, Becker T, Beckmann R. 2014. Cryoelectron Microscopic Structures of Eukaryotic Translation Termination Complexes Containing eRF1-eRF3 or eRF1-ABCE1. *Cell Reports* **8**:59–65. doi:10.1016/j.celrep.2014.04.058

162. Presnyak V, Alhusaini N, Chen Y-HH, Martin S, Morris N, Kline N, Olson S, Weinberg D, Baker KE, Graveley BR, Coller J. 2015. Codon optimality is a major determinant of mRNA stability. *Cell* **160**:1111–1124. doi:10.1016/j.cell.2015.02.029

163. Richter JD, Coller J. 2015. Pausing on Polyribosomes: Make Way for Elongation in Translational Control. *Cell* **163**:292–300. doi:10.1016/j.cell.2015.09.041

164. Rodnina MV. 2018. Translation in Prokaryotes. *Cold Spring Harb Perspect Biol* **10**:a032664. doi:10.1101/cshperspect.a032664

165. Rodnina MV, Fricke R, Kuhn L, Wintermeyer W. 1995. Codon-dependent conformational change of elongation factor Tu preceding GTP hydrolysis on the ribosome. *The EMBO Journal* **14**:2613–2619. doi:10.1002/j.1460-2075.1995.tb07259.x

166. Rodnina MV, Gromadski KB, Kothe U, Wieden H-J. 2005. Recognition and selection of tRNA in translation. *FEBS Letters* **579**:938–942. doi:10.1016/j.febslet.2004.11.048

167. Rodnina MV, Pape T, Fricke R, Kuhn L, Wintermeyer W. 1996. Initial Binding of the Elongation Factor Tu·GTP·Aminoacyl-tRNA Complex Preceding Codon Recognition on the Ribosome. *Journal of Biological Chemistry* **271**:646–652. doi:10.1074/jbc.271.2.646

168. Rodnina MV, Wintermeyer W. 2001. Ribosome fidelity: tRNA discrimination, proofreading and induced fit. *Trends in Biochemical Sciences* **26**:124–130. doi:10.1016/S0968-0004(00)01737-0

169. Roost C, Lynch SR, Batista PJ, Qu K, Chang HY, Kool ET. 2015. Structure and thermodynamics of N6-methyladenosine in RNA: A spring-loaded base modification. *Journal of the American Chemical Society* **137**:2107–2115. doi:10.1021/JA513080V/SUPPL_FILE/JA513080V_SI_001.PDF

170. Rowlands AG, Panniers R, Henshaw EC. 1988. The catalytic mechanism of guanine nucleotide exchange factor action and competitive inhibition by phosphorylated eukaryotic initiation factor 2. *Journal of Biological Chemistry* **263**:5526–5533. doi:10.1016/s0021-9258(18)60596-4

171. Russell JB, Cook GM. 1995. Energetics of bacterial growth: balance of anabolic and catabolic reactions. *Microbiological Reviews* **59**:48–62. doi:10.1128/MR.59.1.48-62.1995

172. Saito K, Horikawa W, Ito K. 2015. Inhibiting K63 Polyubiquitination Abolishes No-Go Type Stalled Translation Surveillance in Saccharomyces cerevisiae. *PLoS Genetics* **11**:1–18. doi:10.1371/journal.pgen.1005197

173. Saito K, Kratzat H, Campbell A, Buschauer R, Burroughs AM, Berninghausen O, Aravind L, Green R, Beckmann R, Buskirk AR. 2022. Ribosome collisions induce mRNA cleavage and ribosome rescue in bacteria. *Nature 2022 603:7901* **603**:503–508. doi:10.1038/S41586-022-04416-7

174. Sattlegger E, Hinnebusch AG. 2005. Polyribosome binding by GCN1 is required for full activation of eukaryotic translation initiation factor 2α kinase GCN2 during amino acid starvation. *Journal of Biological Chemistry* **280**:16514–16521. doi:10.1074/jbc.M414566200

175. Sekiguchi T, Hirose E, Nakashima N, Ii M, Nishimoto T. 2001. Novel G Proteins, Rag C and Rag D, Interact with GTP-binding Proteins, Rag A and Rag B. *Journal of Biological Chemistry* **276**:7246–7257. doi:10.1074/jbc.M004389200

176. Shao S, Murray J, Brown A, Taunton J, Ramakrishnan V, Hegde RS. 2016. Decoding Mammalian Ribosome-mRNA States by Translational GTPase Complexes. *Cell* **167**:1229-1240.e15. doi:10.1016/j.cell.2016.10.046

177. Shimobayashi M, Hall MN. 2014. Making new contacts: The mTOR network in metabolism and signalling crosstalk. *Nature Reviews Molecular Cell Biology* **15**:155–162. doi:10.1038/nrm3757

178. Shoemaker CJ, Green R. 2011. Kinetic analysis reveals the ordered coupling of translation termination and ribosome recycling in yeast. *Proc Natl Acad Sci USA* **108**. doi:10.1073/pnas.1113956108

179. Simms CL, Hudson BH, Mosior JW, Rangwala AS, Zaher HS. 2014. An Active Role for the Ribosome in Determining the Fate of Oxidized mRNA. *Cell Reports* **9**:1256–1264. doi:10.1016/j.celrep.2014.10.042

180. Simms CL, Kim KQ, Yan LL, Qiu J, Zaher HS. 2018. Interactions between the mRNA and Rps3/uS3 at the entry tunnel of the ribosomal small subunit are important for no-go decay. *PLoS Genetics* **14**:1–25. doi:10.1371/journal.pgen.1007818

181. Simms CL, Thomas EN, Zaher HS. 2017a. Ribosome-based quality control of mRNA and nascent peptides. *WIREs RNA* **8**:e1366. doi:10.1002/wrna.1366

182. Simms CL, Yan LL, Qiu JK, Zaher HS. 2019. Ribosome Collisions Result in +1 Frameshifting in the Absence of No-Go Decay. *Cell Reports* **28**:1679-1689.e4. doi:10.1016/j.celrep.2019.07.046

183. Simms CL, Yan LL, Zaher HS. 2017b. Ribosome Collision Is Critical for Quality Control during No-Go Decay. *Molecular Cell* **68**:361-373.e5. doi:10.1016/j.molcel.2017.08.019

184. Singh RK, Gonzalez M, Kabbaj MHM, Gunjan A. 2012. Novel E3 ubiquitin ligases that regulate histone protein levels in the budding yeast saccharomyces cerevisiae. *PLoS ONE* **7**. doi:10.1371/journal.pone.0036295

185. Sinha NK, Ordureau A, Best KM, Saba JA, Zinshteyn B, Sundaramoorthy E, Fulzele A, Garshott DM, Denk T, Thoms M, Paulo JA, Harper JW, Bennett EJ, Beckmann R, Green R, Harper W, Bennett EJ, Beckmann R, Green R. 2020. EDF1 coordinates cellular responses to ribosome collisions. *eLife* **9**:1–84. doi:10.7554/ELIFE.58828

186. Sitron CSS, Park JHH, Brandman O. 2017. Asc1, Hel2, and Slh1 couple translation arrest to nascent chain degradation. *Rna* **23**:798–810. doi:10.1261/rna.060897.117

187. Sonenberg N, Hinnebusch AG. 2009. Regulation of Translation Initiation in Eukaryotes: Mechanisms and Biological Targets. *Cell* **136**:731–745. doi:https://doi.org/10.1016/j.cell.2009.01.042

188. Sørensen MA, Pedersen S. 1991. Absolute in vivo translation rates of individual codons in Escherichia coli. The two glutamic acid codons GAA and GAG are translated with a

threefold difference in rate. *Journal of Molecular Biology* **222**:265–280. doi:10.1016/0022-2836(91)90211-N

189. Spratt TE, Levy DE. 1997. Structure of the hydrogen bonding complex of O6-methylguanine with cytosine and thymine during DNA replication. *Nucleic Acids Research* **25**:3354–3361. doi:10.1093/NAR/25.16.3354

190. Sugiyama T, Li S, Kato M, Ikeuchi K, Ichimura A, Matsuo Y, Inada T. 2019. Sequential Ubiquitination of Ribosomal Protein uS3 Triggers the Degradation of Non-functional 18S rRNA. *Cell Reports* **26**:3400-3415.e7. doi:10.1016/j.celrep.2019.02.067

191. Sundaramoorthy E, Leonard M, Mak R, Liao J, Fulzele A, Bennett EJJ. 2017. ZNF598 and RACK1 Regulate Mammalian Ribosome-Associated Quality Control Function by Mediating Regulatory 40S Ribosomal Ubiquitylation. *Molecular Cell* **65**:751-760.e4. doi:10.1016/j.molcel.2016.12.026

192. Svidritskiy E, Madireddy R, Korostelev AA. 2016. Structural Basis for Translation Termination on a Pseudouridylated Stop Codon. *Journal of Molecular Biology* **428**:2228–2236. doi:https://doi.org/10.1016/j.jmb.2016.04.018

193. Svitkin YV, Cheng YM, Chakraborty T, Presnyak V, John M, Sonenberg N. 2017. N1-methyl-pseudouridine in mRNA enhances translation through eIF2α-dependent and independent mechanisms by increasing ribosome density. *Nucleic Acids Research* **45**:6023–6036. doi:10.1093/nar/gkx135

194. Takyar S, Hickerson RP, Noller HF. 2005. mRNA Helicase Activity of the Ribosome. *Cell* **120**:49–58. doi:10.1016/j.cell.2004.11.042

195. Tsuboi T, Kuroha K, Kudo K, Makino S, Inoue E, Kashima I, Inada T. 2012. Dom34: Hbs1 Plays a General Role in Quality-Control Systems by Dissociation of a Stalled Ribosome at the 3' End of Aberrant mRNA. *Molecular Cell* **46**:518–529. doi:10.1016/j.molcel.2012.03.013

196. Tu G-F, Reid GE, Zhang J-G, Moritz RL, Simpson RJ. 1995. C-terminal Extension of Truncated Recombinant Proteins in Escherichia coli with a 10Sa RNA Decapeptide. *Journal of Biological Chemistry* **270**:9322–9326. doi:10.1074/jbc.270.16.9322

197. Vind AC, Snieckute G, Blasius M, Tiedje C, Krogh N, Bekker-Jensen DB, Andersen KL, Nordgaard C, Tollenaere MAX, Lund AH, Olsen JV, Nielsen H, Bekker-Jensen S. 2020. ZAKα Recognizes Stalled Ribosomes through Partially Redundant Sensor Domains. *Molecular cell* **78**:700–713. doi:10.1016/j.molcel.2020.03.021

198. Von der Haar T, McCarthy JEG. 2002. Intracellular translation initiation factor levels in Saccharomyces cerevisiae and their role in cap-complex function. *Molecular Microbiology* **46**:531–544. doi:10.1046/j.1365-2958.2002.03172.x

199. Wan L, Juszkiewicz S, Blears D, Bajpe PK, Han Z, Faull P, Mitter R, Stewart A, Snijders AP, Hegde RS, Svejstrup JQ. 2021. Translation stress and collided ribosomes are co-activators of cGAS. *Molecular Cell* **81**:2808-2822.e10. doi:10.1016/j.molcel.2021.05.018

200. Wang J, Zhou J, Yang Q, Grayhack EJ. 2018. Multi-protein bridging factor 1(Mbf1), Rps3 and Asc1 prevent stalled ribosomes from frameshifting. *eLife* **7**:1–26. doi:10.7554/eLife.39637

201. Wang X, Mader MM, Toth JE, Yu X, Jin N, Campbell RM, Smallwood JK, Christe ME, Chatterjee A, Goodson T, Vlahos CJ, Matter WF, Bloem LJ. 2005. Complete inhibition of anisomycin and UV radiation but not cytokine induced JNK and p38 activation by an aryl-substituted dihydropyrrolopyrazole quinoline and mixed lineage kinase 7 small interfering RNA. *Journal of Biological Chemistry* **280**:19298–19305. doi:10.1074/jbc.M413059200

202. Warner Jonathan R. 1999. The economics of ribosome biosynthesis in yeast. *Trends in Biochemical Sciences* **24**:437–440. doi:10.1016/S0968-0004(99)01460-7

203. Warner Jonathan R. 1999. The economics of ribosome biosynthesis in yeast. *Trends in Biochemical Sciences* **24**:437–440. doi:10.1016/S0968-0004(99)01460-7

204. Weissman D, Ni H, Scales D, Dude A, Capodici J, McGibney K, Abdool A, Isaacs SN, Cannon G, Karikó K. 2000. HIV Gag mRNA Transfection of Dendritic Cells (DC) Delivers Encoded Antigen to MHC Class I and II Molecules, Causes DC Maturation, and Induces a Potent Human In Vitro Primary Immune Response. *The Journal of Immunology* **165**:4710–4717. doi:10.4049/jimmunol.165.8.4710

205. Wilson DN, Arenz S, Beckmann R. 2016. Translation regulation via nascent polypeptide-mediated ribosome stalling. *Current Opinion in Structural Biology* **37**:123–133. doi:10.1016/j.sbi.2016.01.008

206. Winz ML, Peil L, Turowski TW, Rappsilber J, Tollervey D. 2019. Molecular interactions between Hel2 and RNA supporting ribosome-associated quality control. *Nature Communications* **10**:1–15. doi:10.1038/s41467-019-08382-z

207. Wiśniewski JR, Hein MY, Cox J, Mann M. 2014. A “proteomic ruler” for protein copy number and concentration estimation without spike-in standards. *Molecular and Cellular Proteomics* **13**:3497–3506. doi:10.1074/mcp.M113.037309

208. Wolff JA, Malone RW, Williams P, Chong W, Acsadi G, Jani A, Felgner PL. 1990. Direct gene transfer into mouse muscle in vivo. *Science (New York, NY)* **247**:1465–1468. doi:10.1126/science.1690918

209. Wu CCC, Peterson A, Zinshteyn B, Regot S, Green R. 2020. Ribosome Collisions Trigger General Stress Responses to Regulate Cell Fate. *Cell* **182**:404-416.e14. doi:10.1016/j.cell.2020.06.006

210. Wullschleger S, Loewith R, Hall MN. 2006. TOR signaling in growth and metabolism. *Cell* **124**:471–484. doi:10.1016/j.cell.2006.01.016

211. Wurtmann EJ, Wolin SL. 2009. RNA under attack: Cellular handling of RNA damage. *Critical Reviews in Biochemistry and Molecular Biology* **44**:34–49. doi:10.1080/10409230802594043

212. Wyatt MD, Pittman DL. 2006. Methylating agents and DNA repair responses: Methylated bases and sources of strand breaks. *Chemical Research in Toxicology* **19**:1580–1594. doi:10.1021/TX060164E/ASSET/IMAGES/MEDIUM/TX060164EN00001.GIF

213. Xiao F, Huang Z, Li H, Yu J, Wang C, Chen S, Meng Q, Cheng Y, Gao X, Li J, Liu Y, Guo F. 2011. Leucine deprivation increases hepatic insulin sensitivity via GCN2/mTOR/S6K1 and AMPK pathways. *Diabetes* **60**:746–756. doi:10.2337/db10-1246

214. Yan LL, Simms CL, McLoughlin F, Vierstra RD, Zaher HS. 2019. Oxidation and alkylation stresses activate ribosome-quality control. *Nature Communications* **10**:1–15. doi:10.1038/s41467-019-13579-3

215. Yan LL, Zaher HS. 2021. Ribosome quality control antagonizes the activation of the integrated stress response on colliding ribosomes. *Molecular Cell* **81**:614-628.e4. doi:10.1016/j.molcel.2020.11.033

216. Yan LL, Zaher HS. 2019. How do cells cope with RNA damage and its consequences? *Journal of Biological Chemistry* **294**:15158–15171. doi:10.1074/jbc.REV119.006513

217. Yang Y, Wang Z. 2019. IRES-mediated cap-independent translation, a path leading to hidden proteome. *Journal of Molecular Cell Biology* **11**:911–919. doi:10.1093/jmcb/mjz091

218. Ye J, Palm W, Peng M, King B, Lindsten T, Li MO, Koumenis C, Thompson CB. 2015. GCN2 sustains mTORC1 suppression upon amino acid deprivation by inducing Sestrin2. *Genes and Development* **29**:2331–2336. doi:10.1101/gad.269324.115

219. Yip MCJ, Shao S. 2021. Detecting and Rescuing Stalled Ribosomes. *Trends in Biochemical Sciences* 1–13. doi:10.1016/j.tibs.2021.03.008

220. Yoshizawa S, Fourmy D, Puglisi JD. 1999. Recognition of the codon-anticodon helix by ribosomal RNA. *Science* **285**:1722–1725. doi:10.1126/science.285.5434.1722

221. You C, Dai X, Wang Y. 2017. Position-dependent effects of regioisomeric methylated adenine and guanine ribonucleosides on translation. *Nucleic Acids Research* **45**:9059–9067. doi:10.1093/nar/gkx515

Chapter 2

Loss of eIF4E in yeast results in induction of the integrated stress response in an eIF2α phosphorylation-independent manner

Kyusik Q Kim, Alison C Greenlaw, Benjamin H Hudson, and Hani S Zaher

Abstract

Eukaryotes have evolved at least two seemingly independent conserved pathways to regulate translation initiation in response to stress. One is the activation of the integrated stress response (ISR) through the phosphorylation of the alpha subunit of initiation factor eIF2 by kinases that sense biotic and abiotic stresses. This leads to global inhibition of initiation while promoting the translation of pro-survival effector genes, such as *GCN4* in yeast. The other is inhibition of the Target of Rapamycin (TOR) signaling pathway, which leads to sequestration of the initiation factor eIF4E and subsequent inhibition of canonical initiation. Here we probe translational control in the absence of eIF4E by utilizing a temperature-sensitive allele of the factor in Saccharomyces cerevisiae. Intriguingly, we find that loss of eIF4E leads to translation of *GCN4*. In addition, we find that translation of *GCN4* is not accompanied by eIF2α phosphorylation. Our data suggest that when eIF4E levels are depleted, *GCN4* translation is de-repressed via a unique mechanism that may involve the reduction of eIF2 levels. Overall, our findings add to the emerging evidence that the conserved ISR and TOR signaling pathways communicate with each other to ensure organisms mount a cohesive response to stress.

Introduction

Careful control of which genes are expressed enables organisms to maintain homeostasis under dynamic environmental conditions. When resources are abundant, cells devote much of their energy and resources to protein synthesis (1). As such, the process of translation is highly regulated to ensure protein output is properly tuned (2). Of the four phases of translation – initiation, elongation, termination, and recycling – initiation appears to be the most regulated step in eukaryotes (3). In eukaryotes, canonical initiation begins with the formation of 43S preinitiation complexes (43S PICs) by the binding of ternary complex (TC), composed of initiator methionyl-tRNA and the GTP-bound form of the factor eIF2, and several other initiation factors to the 40S ribosomal subunit (4, 5). 43S PICs are then recruited to the 5'm7Gppp cap structure of the transcript by the eIF4F complex, composed of the cap-binding factor eIF4E, helicase eIF4A, and the scaffolding factor eIF4G. Once loaded onto the transcript, the 43S PIC begins scanning for a start codon in an appropriate context (6–10). Upon recognition of such a start codon, the GDP-bound eIF2, together with inorganic phosphate, is released (11). This in turn enables eIF5B to catalyze joining of the large 60S ribosomal subunit to form an 80S initiating ribosome ready to engage in elongation (12).

While eukaryotes have evolved various mechanisms to regulate assembly and recruitment of the 80S subunit, a key conserved mechanism is the phosphorylation of Ser51 in the α subunit of eIF2 in response to various stress conditions (13). Phosphorylation of eIF2α activates the integrated stress response (ISR), a genetic reprogram of survival genes which enables cells to respond to and recover from the stress (14, 15). The phosphorylation of eIF2α is carried out by upstream kinases which monitor distinct stresses. Mammals have four such kinases: GCN2, PERK, HRI, and PKR, which are activated in response to nutrient deprivation, ER stress,

cytoplasmic protein misfolding, and viral infection, respectively, while budding yeast has only one, Gcn2 (16–18). Upon phosphorylation, eIF2 becomes a competitive inhibitor of its own guanine exchange factor (GEF) eIF2B (19, 20), preventing the exchange of GDP for GTP, binding of initiator methionyl tRNA, and participation of eIF2 in a new round of initiation. Since eIF2B levels are substoichiometric to those of eIF2 (21, 22), a slight increase in the levels of phosphorylated eIF2α inhibits the exchange activity of eIF2B, leading to rapid depletion of available ternary complex levels and repression of global translation. However, reduced ternary complex levels also drives increased translation of *GCN4* in yeast (ATF4 mammals), the key effector of the ISR (13). Translation of *GCN4* and ATF4 are regulated through a mechanism where under condition of abundant ternary complex levels, inhibitory upstream open reading frames (uORFs) in the transcript repress translation of the main open reading frame. When ternary complex levels are depleted, ribosomes are able to bypass these inhibitory uORFs and initiate on the main ORF (for review, see (14, 15)). De-repression of *GCN4* or ATF4 translation then leads to upregulation of amino acid biosynthesis and other stress response genes.

In addition to GCN2, eukaryotes evolved an independent pathway to regulate translation in response to nutrient availability. The target of rapamycin (TOR) signaling pathway promotes growth and proliferation in response to nutrients, particularly amino acids (23–28). Both yeast and mammals contain two distinct complexes, TORC1 and TORC2. Of the two complexes, only TORC1 is regulated by amino acids levels and sensitive to rapamycin (29). In the presence of amino acids, a conserved family of RAG small GTPases form active heterodimers, bind activators of TORC1, and switch on the pathway (23, 30, 31). TOR then phosphorylates several substrates that regulate pathways including autophagy, cytoskeleton organization, lipid metabolism, cell migration, and cell division (32). In addition to these pathways, TOR regulates

protein synthesis at the initiation and elongation phases by directly or indirectly phosphorylating ribosomal proteins, translation factors, and translational regulators (33). One such target is eIF4E binding proteins (eIF4E-BPs), which sequester eIF4E away from eIF4G (34). Under nutrient-rich conditions, TOR signaling inactivates eIF4E-BPs, enabling canonical initiation to proceed.

Given that both GCN2 and TOR regulate translation in response to nutrient availability, it seems logical that cells would have evolved means for the pathways to communicate with one another. Remarkably, potential crosstalk between the two pathways has only been investigated in a few studies showing indirect regulation between GCN2 and TORC1. In yeast, it was shown that TOR inhibition by rapamycin derepressed the activity of Sit4 (a Tap42-associated type 2 protein phosphatase 2A), which then dephosphorylates serine 577 of Gcn2 and activates it in an amino acid starvation-independent manner (35, 36). Conversely, in mammals it was shown that amino acid deprivation-mediated inhibition of mTORC1 required GCN2 (37, 38). However, the mechanism is not entirely clear as conflicting data exists as to whether the crosstalk is directly mediated by GCN2 or by the downstream factor ATF4 (39, 40).

Here we utilize a temperature-sensitive allele of the cap-binding factor eIF4E (*cdc33-ts4-2*) (41) to characterize translational control in the absence of eIF4F in *Saccharomyces cerevisiae*. Our goal was to enrich for alternative cap-dependent or cap-independent mechanisms of translation in a systematic and unbiased manner. Inhibiting eIF4E activity also allowed us to mimic the effect of TOR inhibition on translation initiation without directly inhibiting the TOR pathway. Using ribosome profiling, we find that loss of eIF4E leads to translation of *GCN4*. In agreement with these observations, transcriptomic and subsequent quantitative reverse transcription PCR (qRT-PCR) analyses showed induction of the Gcn4 regulon for the *cdc33-ts4-2* strain under the restrictive temperature, but not for the wild-type strain under the same

conditions. Western-blot analysis of the mutant strain further confirmed the accumulation of Gcn4 when eIF4E function was compromised. Interestingly, increased translation of *GCN4* was not accompanied by phosphorylation of eIF2α, suggesting a noncanonical mechanism for ISR activation when eIF4E levels are depleted. Indeed, deleting Gcn2 had no effect on the induction of Gcn4 under these conditions. Instead, translation of *GCN4* appears to be due to decreased levels of ternary complex via an unknown mechanism. Together, our findings offer a link between eIF4E levels and *GCN4* translation, which in turn may provide a previously unappreciated mechanism for crosstalk between TOR signaling and the ISR in nutrient sensing.

Materials and Methods

Yeast Strains and Plasmids

Strains, plasmids, and primers used in this study are listed in Tables 1, 2, and 3, respectively. The HIS3 cassette was amplified from pFA6a-6xGLY-FLAG-HIS3 (42). *CDC33-HIS3* and *cdc33-ts4-2-HIS3* (E73K, G179D) yeast strains were constructed in the BY4741 background (MATa; *his3Δ1*; leu2Δ0; met15Δ0; ura3Δ0) using standard PCR-based techniques. Plasmids pDB-CDC123 and pC2873 were transformed into BY4741 *CDC33-HIS3* and *cdc33-ts4-2-HIS3*. *CDC33-HIS3* and *cdc33-ts4-2-HIS3* strains were also constructed in the J292 background (*MATα leu2-3,-112 ura3-52 his3 gcn2Δ::loxP gcd11Δ::KanMX* p[*GCD11, URA3*]) (43). pC2872 was transformed into the *CDC33/cdc33-ts4-2* J292 background via plasmid shuffling to replace the [*GCD11, URA3*] plasmid (44). p713 and p722 were transformed into J292 *CDC33/cdc33-ts4-2* pC2872. Plasmids were transformed using a lithium acetate method (45). Cells were either grown in YPD or synthetic complete medium with all amino acids except histidine or histidine and uracil. For cells treated with 3-Amino-1,2,4-triazole (3-AT; Millipore Sigma; cat#A8056), cells were grown at 25°C to OD ~0.5 in synthetic complete medium minus histidine or histidine and uracil, then treated with 30 mM 3-AT for an hour. Plasmid pDB-CDC123 was constructed via Gibson assembly using the Gibson Assembly Master Mix (NEB; cat#E2611S), following manufacturer's instructions.

Polysome Profiling

CDC33 and *cdc33-4-2* cells were grown in YPD at 25°C to OD ~0.5. Cultures were split in two, with half remaining at 25°C and the other half shaken in a pre-warmed 37°C water bath. After an hour, cycloheximide was added to a final concentration of 100 μg/mL. After incubation with cycloheximide for 2 minutes, cells were pelleted and flash frozen on dry ice. Cell pellets were

resuspended in polysome-lysis buffer (20 mM Tris pH 7.5, 140 mM KCl, 1.5 mM $MgCl_2$, 0.5 mM DTT, 100 μg/mL cycloheximide, 200 μg/mL heparin, 1% Triton), washed once, and lysed with glass beads using a FastPrep-24 (MP Biomedical). For RNAse treatment, supernatants from cleared lysates corresponding to ~20 A_{260} of total RNA were first treated with 300 U of RNase I (ThermoFisher Scientific; cat#AM2294) at 25°C for 1 hour. Lysates were then layered over a sucrose cushion (1.1 M sucrose, 20 mM Tris pH 7.5, 500 mM NH_4Cl, 10 mM $MgCl_2$, and 0.5 mM EDTA pH 7.5) in an MLA-130 rotor (Eppendorf) and centrifuged at 267,000 × g for 2 h at 4°C. After centrifugation, RNA was extracted using a hot phenol method (46).

mRNA PolyA Purification and Fragmentation

CNBr-activated Sepharose beads (Cytiva; cat#17098101) were coupled to polydT_{25} using the method in Chockalingam et al. 2001 (47). Total RNA was heated at 65°C, incubated with polydT beads in binding buffer (10 mM Tris pH 7.5, 400 mM NaCl, 1 mM EDTA, 0.1% SDS) at room temperature for 10 minutes, washed twice with wash buffer (10 mM Tris pH 7.5, 40 mM NaCl, 1 mM EDTA, 0.1% SDS), and eluted with 20 mM KOH. Eluted samples were neutralized via addition of 3M sodium acetate pH 5.2 to a final concentration of 300 mM and ethanol precipitated. polyA selected RNAs were fragmented by incubation at 95°C for 20 minutes in fragmentation buffer (50 mM sodium bicarbonate pH 9.2, 1 mM EDTA). Reactions were stopped by the addition of 3M sodium acetate pH 5.2 to a final concentration of 300 mM and samples were ethanol precipitated.

RNA-seq and Ribosome Profiling Library Preparation

Following PAGE purification and size selection (21-34 nt) on a 15% urea PAGE gel, ribosome-protected RNA fragments were subjected to ribosomal blanking by annealing with biotinylated primers (Table 2) and incubation with streptavidin beads (ThermoFisher Scientific; cat#88816)

following manufacturer's instructions. Blanked ribosome protected fragments and fragmented mRNAs were dephosphorylated using T4 polynucleotide kinase (NEB; cat#M0201S). Fragments were then ligated to a short adenylated DNA oligonucleotide – 5'rAppCTGTAGGCACCATCAAT/3ddC/3' – at their 3' end using T4 RNA ligase 2, truncated (NEB; cat#M0242S). Ligated products were purified using denaturing urea PAGE and reverse transcribed using M-MLV (Promega; cat#M1701) and RS-1 primer (/5Phos/AGATCGGAAGAGCGTCGTGTAGGGAAAGAGT GTAGATCTCGGTGGTCGC/iSp18/CACTCA/iSp18/TTCAGACGTGTGCTCTTCCG ATCTATTGATGGTGCCTACAG. cDNA products were circularized using CircLigase (Lucigen; cat#CL4111K). Optimal amplification cycle number was determined via pilot PCR before PCR amplification with Phusion polymerase (NEB; cat#M0530S) and unique barcoded primers. DNA libraries were purified using native PAGE and then analyzed for length and purity using Agilent Bioanalyzer.

Sequencing and Quality Control of Reads

Prepared cDNAs were sequenced on a HiSeq 2500 at the Genome Technology Access Center (GTAC) of Washington University in St. Louis. Samples were demultiplexed based on their 6-nt barcode, allowing for 1 mismatch, using Flexbar 3.5 (48) and checked for initial quality using FastQC 0.11.9 (49). Reads were then processed with Cutadapt 4.2 (50) to remove the 17-nt linker sequence, requiring at least 15 nt of overlap. For ribosome profiling reads, any reads not containing the linker were discarded, while for the RNA-seq reads, any reads containing the linker were discarded. rRNAs, tRNAs, snoRNAs, and other ncRNAs were filtered out by mapping to the R64-1-1 release ncRNA fasta file from SGD using Hisat2 2.2.1 (51).

Analysis of Genome Mapped Reads

Filtered reads were mapped to the R64-1-1 genome (SGD) using STAR 2.7.10b (52), allowing for 2 mismatches in the RNA-seq reads or 1 mismatch in the ribosome profiling reads, with only uniquely mapping reads kept. Output sam files were converted into bam files using Samtools 1.16.1 (53, 54). Ribosome profiling reads were uploaded to the RiboA webtool (55) and analyzed for frame using the "sacCer3_R64-2-1_20150113.gff" annotation, "sacCer3_R64-2-1_genome.fa" fasta file, and quantification from the 3' end, with all other options kept as their default. Bam files were analyzed using FeatureCounts 2.0.1 (56) to count reads mapping to 5'UTRs, CDSes, introns, and 3'UTRs with strandedness enforced and requiring at least 50% of the read to map to the feature. Features were annotated in a custom R64-1-1 (SGD) annotation file with the addition of 5' and 3'UTR annotations from the Pelechano study (57), using the longest UTR, or default 5' and 3'UTRs of 120 and 200 nt, respectively. Reads mapping to 5'UTRs, introns, and 3'UTRs were normalized by feature length, and then normalized again by the average coverage of the corresponding CDS. All analyzed features were filtered for outliers using the ROUT method in GraphPad Prism with Q = 0.1%. Bam files were also converted to bed files and coverage across unique, non-overlapping features was counted using Bedtools 2.30.0 (58), with reads containing introns mapped as independent fragments and matching strandedness enforced. For ribosome profiling reads, coverage was determined using a "pseudo-A" site coordinate, which was calculated by taking the midpoint of the mapped read coordinates, with weighting towards the 5'end of the fragment if the midpoint fell between bases. Coverage was then extracted for all genes with 5'UTR, CDS, and 3'UTR of at least 100 nt in length and at least 128 reads mapping to the CDS. The coverage at each position was normalized by the mean coverage across the gene. Coverage corresponding to each feature was divided evenly across 100

bins and averaged among all features of the same type across all analyzed genes. Coverage calculations were done in custom Python scripts using Biopython (59) and SciPy (60).

Analysis of Transcriptome Mapped Reads

Filtered reads were mapped to the transcriptome using Salmon 1.9.0 (61), with 50 nt upstream and downstream of annotated CDSes included and the whole genome used as a decoy. Reads were mapped with the stranded forward (SF) library option, k-mer values of 11 and 21 for the ribosome profiling and RNA-seq reads, respectively, and fldMean and fldSD values taken from the Bioanalyzer results for each sample (Table 4). Salmon quantified reads were converted into a count matrix and imported into DESeq2 1.32.0 (62) using tximport 1.20.0 (63). Counts were transformed using a variance-stabilizing transformation method (62) with blind set to true. Transformed counts were plotted on a heatmap with clustering by Euclidean distances, as well as subjected to principal component analysis, using the base functions in R 4.2.1 (64). Differential gene expression was determined for all combinations of strain and temperature analyzed using DESeq2. All reported Log_2 fold changes were first shrunk using the ashr algorithm (65). The comparisons tested in DESeq2 can be found in the Zenodo repository.

Downstream Bioinformatic Analysis

The sequences of all transcripts (CDS plus 5'UTR and 3'UTR sequences from the Pelechano annotation, or default 5' and 3'UTR sequences of length 120 and 200, respectively, extracted from the genome) showing a Log2 fold change >= 1 in response to loss of eIF4E were compiled into a fasta file and analyzed using STREME (66) from the online MEME suite with default settings. The top 100 upregulated genes as a result of loss of eIF4E in the RNA-seq and Ribosome Profiling datasets were analyzed using the Gene Ontology Term Finder on SGD (v 0.86) with default settings. For the Pearson correlation matrix, GC content was calculated using

the sequence of the whole transcript (CDS plus 5'UTR and 3'UTR sequences from the Pelechano annotation, or default 5' and 3'UTR sequences of length 120 and 200, respectively, extracted from the genome). ΔG was calculated using the same sequences from above using the ViennaRNA RNAFold program 2.5.1 (67). Genes marked as part of the Gcn4 regulon were classified based on the UC and T dataset in Rawal et al. 2018 (68).

Immunoblotting

Whole cell lysates were harvested and lysed in 1 mL of ice-cold lysis buffer (300 mM NaOH, 1% β-mercaptoethanol). Proteins were precipitated through the addition of TCA to 10% concentration by volume and resuspended in HU buffer (8 M Urea, 5% SDS, 200 mM Tris pH 6.8, 100 mM DTT, 1 mM ethylenediaminetetraacetic acid (EDTA), bromophenol blue) using a volume normalized to the harvested OD. Proteins were separated by SDS–PAGE and analyzed by immunoblotting. The following antibodies were used at the following volume by volume dilutions: 1:3000 rabbit anti-phospho-eIF2α (Ser51) (Cell Signaling Technology;cat#9721), 1:3000 rabbit anti-Gcn4 (a gift from the Hinnebusch lab), 1:5000 mouse anti-PGK1 (ThermoFisher Scientific; cat#459250), 1:3000 rabbit anti-HA (Santa Cruz Biotechnology; sc-805), 1:3000 mouse anti-His (Santa Cruz Biotechnology; sc-8036), 1:10000 goat anti mouse IgG HRP (ThermoFisher Scientific; cat#31430), 1:5000 goat anti rabbit IgG HRP (ThermoFisher Scientific; cat#31460). Blots were quantified in ImageQuant TL (Cytiva) by comparing Gcn4 band intensity with the corresponding Pgk1 band intensity.

Real-Time Quantitative Reverse Transcription PCR

Total RNA was isolated using a hot phenol method (46) and treated with DNase I (ThermoFisher Scientific; cat#EN0525). M-MuLV reverse transcriptase (Promega; cat#M1701) was used to generate cDNA from ~2 ug of total RNA and random hexamers (ThermoFisher Scientific,

cat#SO142) following manufacturer's instructions. Quantitative RT-PCR was conducted using iTaq Universal SYBR Green Supermix (Bio-Rad; cat#1725120) following manufacturer's instructions. The fold change for each gene was calculated by using the ΔΔCt method; expression at 37°C was normalized to expression of *TAF10*, then compared to the corresponding value calculated at 25°C. All measurements were done in biological triplicates. Differences were tested for statistical significance using the multiple t-tests analysis in GraphPad Prism with default settings.

Measurement of Renilla and Firefly Luminescence

Luminescence was measured as described in Simms et al. 2019 (69). Briefly, cells were grown in synthetic complete medium minus uracil to OD ~0.5 at 25C°. Half the culture was then shifted to 37°C for an hour before both cultures were collected by centrifugation and washed once with TE. Cells were then resuspended in zymolyase buffer (50 mM Tris pH 7.5, 10 mM $MgCl_2$, 1 M Sorbitol, 30 mM DTT) and incubated with lyticase from *Arthrobacter luteus* (Millipore Sigma; cat#L4025) at 37°C for 30 minutes. Cells were lysed by the addition of passive lysis buffer (Promega; cat#E1941). Samples were pelleted by centrifugation at 4000 × g for 5 minutes at room temperature and cleared lysates were transferred to 96-well plates. Luminescence was measured using the Dual-Luciferase Reporter Assay System (Promega; cat#E1910) following manufacturer's instructions on an Infinite F200 Pro plate reader (Tecan).

Results

Translation is greatly diminished but not completely abolished in *cdc33-ts4-2* cells under restrictive conditions

In an effort to characterize translation events in yeast in the absence of cap recognition by eIF4E, we took advantage of a temperature-sensitive allele of this factor, *cdc33-ts4-2* (70, 71). Under permissive conditions (25°C) the factor is stable and functions properly, but under restrictive conditions (37°C) the factor is degraded (72, 73), inhibiting formation of the eIF4F complex (Figure 1A). To generate our own *cdc33-ts4-2* strains, we introduced the E73K and G179D mutations into the BY7471 background using an integrating plasmid targeting the native *CDC33* locus. To generate a control strain, we used a plasmid bearing the wild-type sequence and integrated it into the same locus. Sequencing of the *CDC33* locus confirmed that the mutations were introduced as intended. Plating assays confirmed that the E73K and G179D mutations in *CDC33* render yeast temperature sensitive; at 25°C, the wild-type and mutant strains grew similarly, but at 37°C, the mutant strain failed to grow, in contrast to the control strain (Figure 1B). Prior work characterizing the *cdc33-ts4-2* mutant showed significant inhibition in [^{35}S] methionine incorporation compared to a wild-type strain when shifted to 37°C (41). To assess how the mutant factor affects translation in the BY4741 background, we conducted polysome profiling analysis of wild-type and mutant cells under permissive and restrictive conditions (Figure 1C). As expected, *CDC33* and *cdc33-ts4-2* cell profiles looked largely similar under permissive conditions at 25°C. Also as expected, *cdc33-ts4-2* cells showed a significant loss of polysomes when shifted to restrictive conditions, whereas *CDC33* cells nearly completely retained their polysome levels. Interestingly, in the *cdc33-ts4-2* cells, the 40S and 60S populations appeared largely unaffected while the 80S peak grew, suggesting ongoing

translation but broader loss of translational activity. In addition, while polysomes were largely lost, some polysomes were still observed, suggesting that a small population of transcripts remain actively translated even under eIF4E-depleted conditions (Figure 1C).

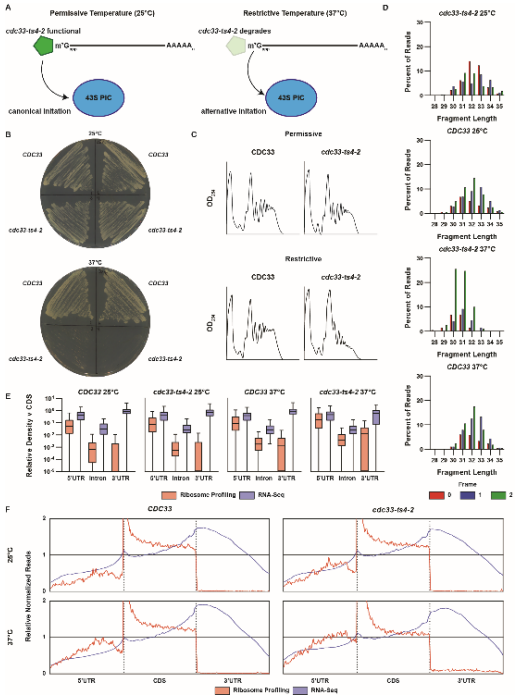

Figure 1: Marginal translation is maintained even under eIF4E-depleted conditions.
A) Schematic of translation initiation under permissive (25°C) and restrictive (37°C) conditions in the *cdc33-ts4-2* strain. Under normal conditions, the cap-binding factor is stable and translation initiation proceeds as normal. Under restrictive conditions, the factor degrades, inhibiting canonical initiation. **B)** *CDC33* and *cdc33-ts4-2* strains grown on YPD plates at 25°C and 37°C. The E73K and G179D mutations render the yeast temperature sensitive. **C)** Polysome profiles of whole cell extracts from *CDC33* and *cdc33-ts4-2* cells under permissive and restrictive conditions. Cells were first grown at 25°C to OD ~0.5, then the culture was split in two, with half the culture shifted to the restrictive condition for an hour before both cultures were collected. Absorbance readings were taken continuously at OD_{254}. **D)** Bar graphs plotting the percent of reads which map to the indicated frame for the given fragment length. The frame for each read was assigned by offsetting from the 3' end of the fragment, with the offset for each fragment length calculated based on the distance from the mapped 3' end to the annotated start of the CDS. The plots here show one replicate of biological duplicates. **E)** Box and whisker plots showing the relative density of reads mapping to the indicated feature, normalized by the feature length and the mean coverage of the associated CDS. Before plotting, outliers were removed using GraphPad Prism due to high variance in the distribution of densities, indicating outsized contribution from a small subset of genes. The plots show the average of biological duplicates for ribosome profiling and the average of biological triplicates for RNA-seq. **F)** Plots displaying metagene analysis of ribosome profiling and RNA-seq reads. Coverage by ribosomes was calculated by using the midpoint of the ribosome protected fragments as a "pseudo A-site." For RNA-seq reads, coverage across the entire mapped fragment was utilized. Coverage at each position in genes with 5' UTR, CDS, and 3' UTR of at least 100 nt in length were normalized by the mean coverage across the whole gene. Normalized coverages were then separated by the feature they mapped to, distributed evenly across 100 bins, and averaged across all analyzed genes. Relative normalized reads were plotted against a model gene 300 nt in length, with the first 100 nt representing the 5' UTR and the last 100 nt representing the 3' UTR. The dashed vertical lines indicate the start and stop of the CDS in the model gene, respectively.

Ribosome profiling of *CDC33* and *cdc33-ts4-2* cells

To identify transcripts whose translation is resistant to depletion of eIF4E, we conducted ribosome profiling (74) on *CDC33* and *cdc33-ts4-2* cells subjected to both permissive and restrictive conditions. In parallel, we subjected the same samples to RNA-seq. One of the hallmarks of ribosome profiling is a distribution of fragments centered around 28 nt with an enrichment of in-frame reads. However, initial quality control of ribosome profiling reads mapped to the genome did not show the typical distribution around 28 nt, nor an enrichment of in-frame reads (Figure 1D), possibly due to incomplete RNase digestion. To confirm that our ribosome profiling reads faithfully reflected ribosome protected fragments and not free mRNAs, we conducted metagenomic analysis of both our ribosome profiling and RNA-seq data. Reassuringly, metagenomic analysis of our ribosome profiling reads showed enrichment of reads mapping to gene coding sequences and 5'UTRs, with minimal coverage of introns or 3'UTRs (Figure 1E). Analysis of positional coverages also showed coverage centered around the annotated start of the CDS (Figure 1F), characteristic of ribosome protected fragments (74). While we note that we used cycloheximide to stabilize polysomes, which is known to introduce artifacts to ribosome position on transcripts (75), given that we were interested in transcripts which maintained ribosome occupancy even under eIF4E-depleted conditions and not the precise position of ribosomes on those transcripts, cycloheximide use should not confound our analysis.

Confident that our ribosome profiling results reflected true ribosome occupied fragments, we proceeded with differential gene analysis using the Salmon – DESeq2 pipeline (61, 62). Quality-control analysis of ribosome profiling and RNA-seq reads mapped to the transcriptome showed expected clustering of replicates, both by Euclidean distance and PCA (Figure 2A and 2B). Since our samples clustered closer by temperature rather than strain (Figure 2A), we

suspected that the majority of observed change in gene expression was due to the heat shock response. However, pairwise comparison between *cdc33-ts4-2* and *CDC33* at the restrictive condition, normalized to their counterparts at the permissive condition, was able to isolate changes in gene expression that were due to loss of eIF4E. Indeed, we observed that for genes annotated as part of the heat shock response in the Panther GO database, the expected increase in expression of heat shock factors disappears (Figure 2C). We plotted changes in transcript abundance, ribosome occupancy, and translational efficiency (TE) – ribosome occupancy normalized to transcript abundance (Figure 3A). We then searched for motifs in those genes which had at least a 2-fold change in expression for each dataset. No motifs were detected as significant for upregulated genes in the ribosome profiling or translational efficiency datasets, but several motifs were detected for genes in the RNA-seq dataset. Here, only the efficiency element necessary for polyadenylation of mRNAs stood out (Figure 3B) (76), indicating that mRNAs were enriched in the RNA-seq data set, as expected. Further analysis of transcript features also did not yield any obvious grouping of upregulated genes; no strong correlation was observed between differential TE, 5'UTR length, coding sequence length, 3'UTR length, GC content, number of uORFs, or folding energy (Figure 3C). Similarly, gene-ontology (GO) analysis of genes failed to detect any process as significant for genes with increased TE. Our data suggest that yeast may not employ cap-independent initiation as pervasively as mammals.

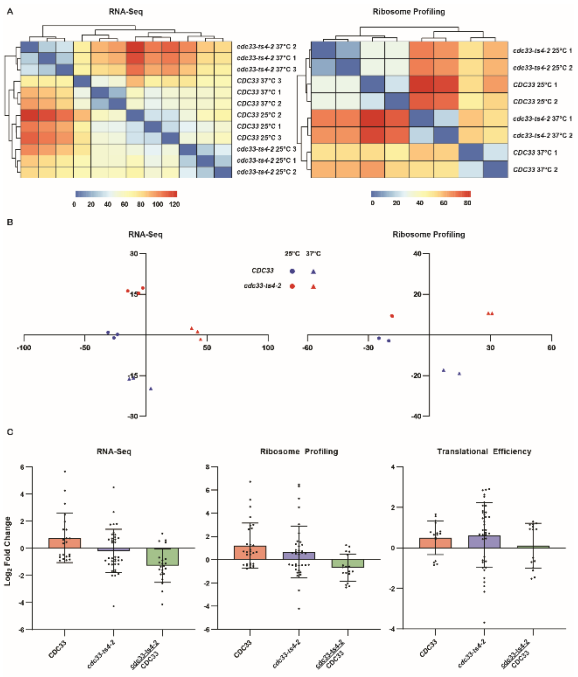

Figure 2: Differential gene expression analysis can account for changes due to heat shock
A) Heat map and clustering of Euclidean distances for variance stabilized transformed count data for RNA-seq and ribosome profiling samples. Counts were determined using the Salmon – DESeq2 pipeline. **B)** PCA plot of the transformed counts analyzed in A) **C)** Bar graphs of mean fold changes in mRNA expression (RNA-seq), ribosome occupancy (Ribosome Profiling), or ribosome occupancy normalized to mRNA levels (Translational Efficiency) for genes annotated under "response to heat" in Panther GO. Fold changes were calculated using DESeq2 by comparing the indicated strain at the restrictive condition to the strain at the permissive condition, except for the *cdc33-ts4-2/CDC33* comparison, which compares the strains at the restrictive condition normalized to their counterparts at the permissive condition. Only genes whose fold changes were marked as significant (adjusted p-value ≤ 0.05) were plotted.

Depletion of eIF4E activates the integrated stress response

Intriguingly, our analysis revealed that *GCN4*, the key regulator of the ISR, as one of the top genes showing increased ribosome occupancy and translational efficiency as a result of loss of eIF4E (Figure 3A). As our analysis reflects changes in expression of the CDS of genes, this indicated that the main ORF was being translated, rather than an increase in occupancy of the uORFs. In support of these results, genome mapped reads showed a significant increase in coverage of the main ORF of *GCN4* only in the *cdc33-ts4-2* strain under the restrictive condition (Figure 4A). In agreement with increased translation of *GCN4*, RNA-seq analysis also showed

that the Gcn4 regulon was significantly induced (Figure 4B). Moreover, GO analysis of RNA-seq and ribosome profiling data showed that the biological processes of amino acid synthesis to be significantly enriched in the mutant cells (Figure 3D). We validated our transcriptomic analysis by conducting qRT-PCR analysis of wild type and mutant cells, which showed significant increases in expression of Gcn4 regulon transcripts only in the mutant cells under restrictive conditions (Figure 4C). These results are consistent with previous reports on the related *cdc33-1* mutant (70), where an amino acid starvation phenotype was observed under restrictive conditions (70, 77, 78).

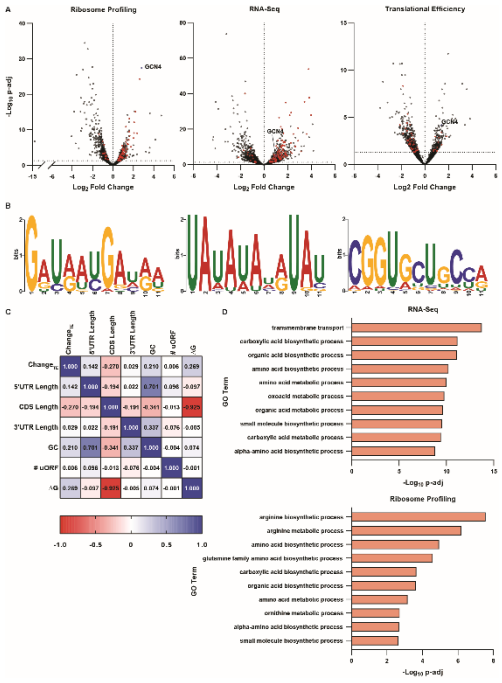

Figure 3: Loss of eIF4E leads to activation of the integrated stress response
A) Volcano plots of the fold change in mRNA expression (RNA-seq), ribosome occupancy (Ribosome Profiling), or ribosome occupancy normalized to mRNA levels (Translational Efficiency) plotted against the statistical significance of that change. Changes reflect changes in gene expression due to loss of eIF4E, for all genes passing automatic filtering in DESeq2. The vertical dashed line denotes a Log2 fold change of 0, while the horizontal dashed line denotes an adjusted p-value of 0.05. Genes which belong to the Gcn4 regulon are marked in red, while *GCN4* is marked in blue. **B)** Motifs found in genes upregulated due to loss of eIF4E (LFC ≥ 1) in the RNA-seq dataset, as determined by STREME from the MEME Suite software. No motifs passing statistical significance were found for genes which showed increased ribosome occupancy or translational efficiency. **C)** Pearson correlation matrix of the indicated features measured against one another. $Change_{TE}$ refers to the calculated differential translational efficiency values as plotted in A). **D)** GO term search results for upregulated genes as a result of loss of eIF4E in the RNA-seq and ribosome profiling datasets. Searches were done using the SGD GO Term Finder tool on the 100 most upregulated genes (LFC ≥ 1) in each dataset. Displayed are the top 10 terms from each search.

GCN4 translation is de-repressed via a non-canonical mechanism

Given the translational mechanism by which *GCN4* is regulated, the most parsimonious explanation for *GCN4* translation in our *cdc33-ts4-2* cells is that depletion of eIF4E leads to phosphorylation of eIF2α. To answer this question, we conducted immunoblot analysis of eIF2α-phosphorylation levels in wild-type and mutant cells under both permissive and restrictive conditions. To our surprise, we did not observe increased eIF2α-phosphorylation in *cdc33-ts4-2* cells under restrictive conditions (Figure 5A), indicating that de-repression of *GCN4* translation appeared to be the result of an alternative mechanism. To provide support for an eIF2α-phosphorylation independent mechanism for *GCN4* translation under these conditions, we introduced the *cdc33-ts4-2* mutations into a *gcn2Δ* background (43). As expected, deletion of Gcn2 completely abrogated the accumulation of Gcn4 and phosphorylation of eIF2α in response to treatment with 3-aminotriazole (3-AT; an inducer of histidine starvation), regardless of the eIF4E background. Complementing *gcn2*Δ with a plasmid-borne gene restored responsiveness to 3-AT. In contrast, depletion of eIF4E resulted in increased Gcn4 levels (without concordant eIF2α phosphorylation) irrespective of the presence of Gcn2 (Figure 5B). Together, our data suggest that eIF4E depletion leads to *GCN4* translation in a Gcn2-eIF2α-phosphorylation independent manner.

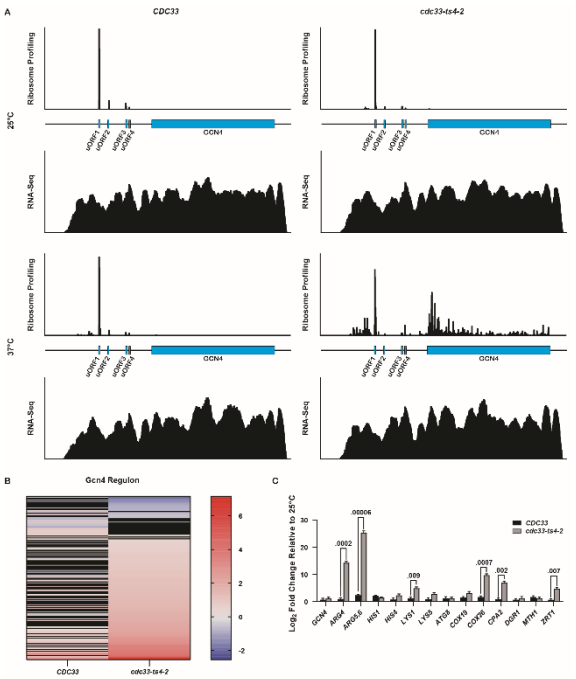

Figure 4: *GCN4* is translated under eIF4E-depleted conditions
A) Ribosome occupancy and RNA-seq coverage plots of the *GCN4* transcript. Coverage by ribosomes was calculated by using the midpoint of the ribosome protected fragments as a "pseudo A-site." For RNA-seq reads, coverage across the entire mapped fragment was utilized. **B)** Heat map of Log2 fold changes for genes belonging to the Gcn4 regulon in the RNA-seq dataset. Both strains at the restrictive condition were compared to the permissive condition. Rows colored in black indicate a fold change that did not have an adjusted p-value ≤ 0.05. **C)** qRT-PCR of the indicated genes in the *CDC33* and *cdc33-ts4-2* strains in the restrictive condition compared to the permissive condition. The expression of each gene was first normalized to expression of *TAF10*. Plotted are the average values of three biological replicates with error bars representing the standard deviation around the mean.

eIF2 levels may contribute to *GCN4* de-repression when eIF4E is depleted

While the standard model for *GCN4* de-repression is through phosphorylation of eIF2α, ultimately any mechanism which depletes ternary complex levels would also result in de-repression. A previous report on *cdc33-1* cells showed a slight reduction in initiator methionyl tRNA and eIF2 subunits under restrictive conditions (79). Fortuitously, the *gcn2Δ* parent strain had the gamma subunit of eIF2 (Gcd11) tagged with 6xHis. On our immunoblots, we observed what appeared to be a slight decrease in eIF2γ levels under restrictive conditions, suggesting that depletion of eIF4E may led to a depletion of eIF2γ levels (Figure 5B), and hence increased *GCN4* translation. If loss of eIF2γ levels is indeed responsible for observed de-repression of

GCN4, then overexpression of eIF2γ should restore translational control of *GCN4*. To test this hypothesis, we overexpressed eIF2γ in our *cdc33-ts4-2* cells. However, overexpression of eIF2γ did not fully suppress *GCN4* de-repression (Figure 5C), possibly indicating the presence of an upstream pathway responsible for observed *GCN4* de-repression or a feedback mechanism between eIF2γ levels and overall ternary complex levels. To approach rescue of eIF2γ levels in an orthogonal manner, we overexpressed Cdc123 in the same background. Cdc123 is an upstream factor responsible for eIF2γ maturation and proper ternary complex formation (80, 81). Furthermore, temperature-sensitive mutants of *cdc123* also exhibit *GCN4* de-repression and a G1 arrest phenotype similar to *cdc33-1* cells (77, 78, 81). Notably, overexpression of Cdc123 had no detectable effect on Gcn4 accumulation when eIF4E levels were depleted (Figure 5D). Collectively, our data suggest that eIF4E levels may alter the concentration of ternary complex, but that this decrease cannot fully explain the increased translation of *GCN4*.

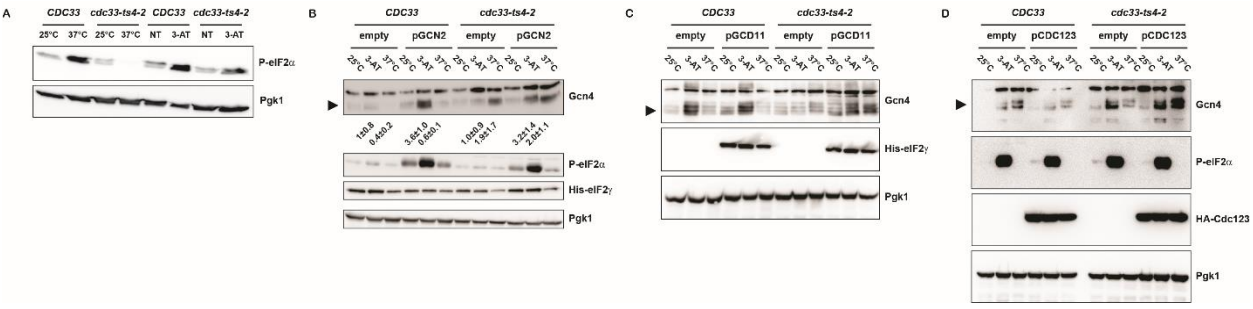

Figure 5: *GCN4* translation is de-repressed without concordant eIF2a-phosphorylation
Immunoblots of whole cell extracts collected from the indicated strains and conditions. Whole cell extracts were collected using an alkaline hydrolysis and trichloroacetic acid precipitation method. In A), cells were grown in YPD for lanes labeled 25°C and 37°C, while cells were grown in synthetic complete medium minus histidine for lanes marked NT and 3-AT. For all other immunoblots, cells were grown in synthetic complete medium minus uracil and histidine. Cells were grown at 25°C until OD ~0.5, at which point the culture was split and either shifted to 37°C or treated with 30 mM 3-AT for an hour. Blots are representative of at least duplicates. For B), the numbers below the Gcn4 blot represent the protein level of Gcn4 normalized to Pgk1 for each condition, relative to its corresponding no-treatment level from three biological replicates.

The 5' UTR of *GCN4* does not promote internal initiation of translation

Another intriguing explanation for the increased translation of *GCN4* in the absence of eIF4E is that the *GCN4* 5'-UTR can recruit the ribosome independent of the cap structure. To test this hypothesis, we constructed a polycistronic dual luciferase reporter with a Renilla luciferase and Firefly luciferase separated by a stop codon (Figure 6A). We inserted the 5'-UTR of *GCN4*, including the 4 uORFs, with or without the first 20 codons of the main GCN4 ORF, between the two genes. As a positive control, we generated a fusion dual luciferase protein, where the sequence of the two luciferase genes is separated by the first 20 codons of *GCN4* without any stop codons between the two genes. We transformed the plasmids into our *cdc33-ts-4-2* cells. As expected, the ratio of Firefly to Renilla luminescence was ~1% for the polycistronic reporter, relative to the ratio measured for the translation fusion reporter at both the permissive and restrictive temperature, suggesting little to no stop-codon readthrough in this strain (Figure 6B). Introducing the 5'-UTR of *GCN4* had no detectable effect on firefly luminescence, suggesting that it cannot drive internal initiation regardless of whether eIF4E is active or not (Figure 6B).

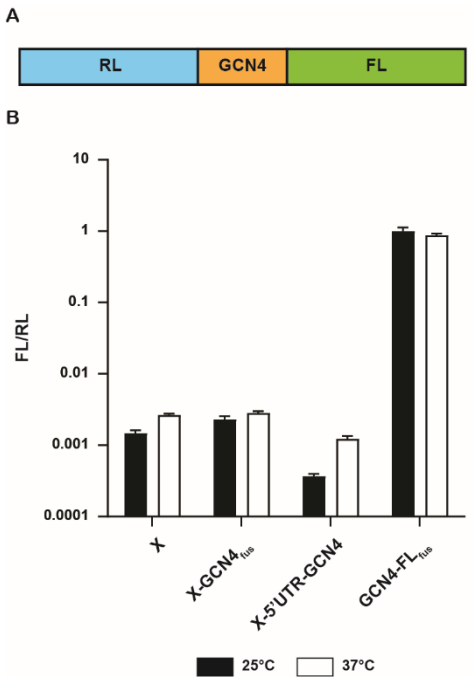

Figure 6: The *GCN4* 5' UTR is insufficient to drive cap-independent initiation.
A) Diagram of the dual-luciferase reporter construct **B)** Firefly luciferase luminescence normalized to renilla luciferase luminescence for the indicated reporter constructs and conditions. Cells were grown in synthetic complete medium minus uracil to OD ~0.5 at 25°C. Half the culture was shifted to 37°C for an hour before both cultures were collected. For reporter constructs: X refers to an in-frame stop codon placed between luciferases, X-GCN4fus refers to an in-frame stop codon plus the first 60 nt of the *GCN4* coding sequence, while X-5' UTR-GCN4 refers to an in-frame stop codon plus the 5' UTR of *GCN4* with all four uORFs included, along with the first 60 nt of the *GCN4* coding sequence. A reporter construct with only the first 60 nt of the *GCN4* coding sequence placed between luciferases (GCN4-FLfus) was used as a positive control. Plotted are the average values of three biological replicates with error bars representing the standard deviation around the mean.

Discussion

In eukaryotes, canonical initiation requires the coordinated effort of a multitude of initiation factors. These factors recruit the small ribosomal subunit to the 5'-cap of the mRNA and aid in identifying the correct start codon (3, 4, 17). On the other hand, while canonical initiation is responsible for translating the majority of mRNAs, multiple lines of evidence suggest that cap-independent mechanisms play critical roles in health and disease. Since many of the mechanisms appear to be highly conserved and necessary for cell survival under stress conditions, much effort has been directed at trying to elucidate their function and usage, particularly in the case of diseases with dysregulated translation such as autoimmune diseases, neurodegeneration, and cancer (82, 83). However, many studies have limited their focus to a particular transcript and the features that allow it to evade cap dependence during initiation (84, 85). The few studies that have attempted to define the global landscape of cap-independent translation have not used unbiased and systematic approaches, precluding the ability to glean important data about biologically relevant processes (86). To circumvent these issues, we used a temperature-sensitive allele of eIF4E to systematically disrupt cap recognition in yeast in an unbiased manner. We confirmed that under the restrictive temperature, the mutant allele leads to significant reduction in translation as judged by polysome profiling (Figure 1C). To identify transcripts whose translation is resistant to eIF4E loss, we subjected wild type and mutant cells under permissive and restrictive conditions to ribosome profiling. Notably, even though we found that the translation of several transcripts was resistant to loss of eIF4E (Figure 3A), a mechanism for how this might occur was not readily discernable. In particular, we observed no obvious correlation between translation efficiencies and CDS length, UTR length, structure, GC

content, or number of upstream open reading frames (Figure 3C). Our data suggest that cap-independent translation in yeast may not be as pervasive as it appears to be in mammals.

Our ribosome profiling, however, revealed that loss of eIF4E leads to increased translation of *GCN4*; we measured an almost 8-fold increase in ribosome occupancy in the mutant strain at 37°C compared to the wild-type strain (Figure 3A). This was consistent with our transcriptomic analysis, which showed an induction of the Gcn4 regulon (Figure 4B). In addition, qRT-PCR analysis of a number of Gcn4 targets showed that their RNA levels increase by as much as 30-fold in the mutant strain under the restrictive temperature, relative to the wild-type strain (Figure 4C). In agreement with the ribosome profiling data, immunoblot analysis revealed that Gcn4 levels increase only in the mutant strain when both strains are subjected to the restrictive condition (Figure 5B). By contrast, histidine deprivation through the use of the imidazoleglycerol-phosphate dehydratase (HIS3 gene product) inhibitor 3-AT resulted in increased accumulation of Gcn4 in both strains (Figure 5B).

Intriguingly, *GCN4* is primarily regulated at the translation level via a unique mechanism. Briefly, the *GCN4* mRNA harbors four additional reading frames (uORFs) in its 5' leader sequence (14). After initiating on the first uORF, cis- and trans-acting elements on the *GCN4* mRNA enable some of the terminating ribosomes to remain attached and continue scanning as 40S subunits. Under normal conditions, these scanning 40S subunits are able to rebind another initiator tRNA ternary complex and initiate again on one or more of the downstream uORFs in a process termed reinitiation. Translation of the third and/or fourth uORF results in near complete dissociation of any remaining ribosomes, preventing translation of the main ORF and repressing expression of the Gcn4 protein. When initiator tRNA ternary complex levels are depleted, some of the scanning 40S subunits are able to bypass uORFs 3 and 4 before rebinding a new ternary

complex, enabling reinitiation on the main ORF and de-repression of *GCN4* translation. Thus, any mechanism that reduces the concentration of initiator tRNA ternary complex would result in increased translation of *GCN4* (14). To the best of our knowledge, the only mechanism cells utilize to deplete ternary complex levels has been through phosphorylation of eIF2α. As a result, we were surprised to observe no accumulation of phosphorylated eIF2α in the *cdc33-ts4-2* mutant under the restrictive temperature (Figure 5A), suggesting that *GCN4* is translated via a distinct mechanism when eIF4E is depleted. In accordance with a novel mechanism, deletion of Gcn2 had no detectible effect on Gcn4 levels under these conditions, but completely inhibited its accumulation under conditions that depleted the amino acid histidine (Figure 5B).

Given the lack of eIF2α phosphorylation, the simplest explanation for observed de-repression of *GCN4* is that depletion of eIF4E also leads to depletion of ternary complex. These observations appeared to be borne out in work with *cdc33-1* cells, as well as with our observations of slight reductions in eIF2γ levels in our immunoblots. However, direct overexpression of eIF2γ did not restore translational control of *GCN4* under restrictive conditions (Figure 5C), suggesting that regulatory control may occur via an upstream mechanism. To test this, we overexpressed the eIF2 assembly factor Cdc123. Cdc123 has been documented to also be regulated by nutrient availability and the cell cycle (81). Furthermore, the factor directly binds eIF2γ and regulates its abundance through ubiquitination (81, 87). Cdc123 overexpression also failed to restore *GCN4* translational control under restrictive conditions, suggesting that the effects of eIF4E-depletion on eIF2γ are not mediated through Cdc123 (Figure 5D). Thus, how eIF4E levels contribute to *GCN4* de-repression is not currently understood.

Regardless of how eIF4E contributes to de-repression of *GCN4*, the ribosomal small subunit still needs to be recruited to the 5'-end of the transcript; thus, *GCN4* must be resistant to

inhibition of eIF4E. We hypothesized that the 5'-UTR of GCN4 might be able to directly recruit the ribosomal small subunit in the absence of eIF4E, in a manner similar to IRES-containing mRNAs. However, we failed to observe increased internal initiation on the *GCN4* 5'-UTR using a dual-luciferase polycistronic reporter (Figure 6B). The mechanism by which *GCN4* is able to recruit 43S PICs, such as cis- and trans- acting elements on the *GCN4* mRNA that could promote canonical initiation even with a minimal pool of available eIF4E, requires further investigation.

Our observation that *GCN4* translation is de-repressed under conditions of eIF4E depletion provides a potential connection between TOR signaling and the ISR. Under amino acid starvation, eIF2α phosphorylation by Gcn2 lowers available ternary complex levels, enabling scanning 40S subunits to reinitiate on the main ORF of *GCN4*. At the same time, amino acid starvation also inhibits TOR, leading to sequestration of eIF4E by eIF4E-binding proteins and inhibition of canonical cap recognition by 43S PICs (88). Both of these processes respond to nutrient availability and, as a result, must coordinate their efforts during reprogramming of gene expression (23). If depletion of eIF4E does indeed lead to depletion of ternary complex levels, this would provide a potential mechanism by which the two pathways are interconnected. Curiously, studies in human cell culture showed that mTOR activation, and not its inhibition, can lead to ATF4 translation (89–91). In contrast, in yeast, inhibition of TORC1 by rapamycin leads to *GCN4* translation, albeit in a Gcn2-mediated and eIF2α phosphorylation-dependent manner (35, 36). Further investigations are clearly needed to elucidate the mechanisms which enable a unified response by these two pathways to nutrient availability in the environment.

Data and Software Availability

Sequencing data have been deposited at the Gene Expression Omnibus under accession number GSE223465. Custom python scripts are available in the Zenodo repository at https://doi.org/10.5281/zenodo.7617427

Acknowledgments

The authors are grateful to Drs. Thomas Dever and Alan Hinnebusch for sharing yeast strains, plasmids, and Gcn4 antibody. We would also like to thank Dr. Nima Mosammaparast for careful reading of the manuscript and members of the Zaher laboratory for useful discussion and comments. This work was supported by an NIH grant (R00GM094210).

Supplementary Figures and Tables

Supplementary Table 1: Yeast strains used in this study

Name	Genotype	Reference/Source
BY4741 (*MATa*)	*MATa his3Δ1 leu2Δ0 met15Δ0 ura3Δ0*	Dharmacon
BY4741 *CDC33*	*BY4741; CDC33-HIS3*	This Study
BY4741 *cdc33-ts4-2*	*BY4741; cdc33-ts4-2-HIS3*	This Study
J292	*MATα leu2-3,-112 ura3-52 his3 gcn2Δ::loxP gcd11Δ::KanMX GCD11-URA3*	(43)
J292 *CDC33-HIS3*	*J292; CDC33-HIS3*	This Study
J292 *cdc33-ts4-2*	*J292; cdc33-ts4-2-HIS3*	This Study

Supplementary Table 2: Plasmids used in this study

Plasmid	Description	Reference/Source
pFA-CDC33-HIS3	pFA6a-6xGLY-FLAG-HIS3MX6	(42)
pDB-RL-X-FL	Renilla-Firefly luciferase fusion construct with an in-frame stop codon placed between; constructed with the pDB688 backbone	This Study; pDB688 (92)
pDB-RL-X-GCN4-FL	Same as pDB-RL-X-FL except the first 60 nt of the *GCN4* coding sequence placed after the in-frame stop codon; constructed with the pDB688 backbone	This Study; pDB688 (92)
pDB-RL-X-5'UTR-GCN4-FL	Same as pDB-RL-X-GCN4-FL except the 5' UTR of *GCN4* with all four uORFs placed between the in-frame stop codon and the first 60 nt of the *GCN4* coding sequence; constructed with the pDB688 backbone	This Study; pDB688 (92)
pDB-RL-GCN4-FL	Renilla-Firefly luciferase fusion construct with the first 60 nt of the *GCN4* coding sequence placed between; constructed with the pDB688 backbone	This Study; pDB688 (92)

pDB-CDC123	$_{GPD}$CDC123-HA-URA3; constructed with the pDB688 backbone	This Study; pDB688 (92)
pC2872	*His_8-GCD11 (eIF2γ), LEU2, CEN4/ARS*	(43)
pC2873	*His_8-GCD11 (eIF2γ), LEU2, pRS425*	(43)
P713	*URA3, CEN6*	(93)
p722	*GCN2, URA3, CEN6*	(93)

Supplementary Table 3: Primers used in this study

Primer	**Sequence**	**Reference/Source**
eIF4E-F-HindIII	TGAGTTCAAGCTTGCAAGAGGTAGTGTTAATTCTGG	This Study
eIF4E-R-BglII	AATGACAGATCTGTGGTGCGTCTTTCATACC	This Study
eIF4E-UTR-F-SacI	TGAGTTCGAGCTCATGTACATATCACGTAAGATGTTCC	This Study
eIF4E-UTR-R-EcoRI	AATGACGAATTCGTGCTGAGTTCGTCGAACC	This Study
eIF4E-G179D-F	CTATTGAGAATTGACGGTAAATTCAAGC	This Study
eIF4E-G179D-R	GCTTGAATTTACCGTCAATTCTCAATAG	This Study
eIF4E-E73K-F	CCAAACTGTTGAAAAATTTTGGGCTATC	This Study
eIF4E-E73K-R	GATAGCCCAAAATTTTTCAACAGTTTGG	This Study
FL-GCN4-Fusion-F(SalI)	CGTATGTCGACAATGTCCGAATATCAGCCAAG	This Study

RL-all-stop-R(SalI)	AAGAATTAGTCGACATTTATTGTTCATTTTTGAGAACTCGCTC	This Study
RL-all-F(AgeI)	AGGTCAACCGGTCAAACGTTCGGATCCTTCAAC	This Study
GCN4-F1	AGGTCAGTCGACTAATTCTTATATAATAGATATACAAAACAAAACAAAAC	This Study
GCN4-R(AgeI)	AGGTCAACCGGTATCCAATGGTGAGAAACCC	This Study
RL(X)FL-5'	CAAATGTCGACGTGCGATCAATGAACGTTCGGATCCTTCAACTTC	This Study
RL(X)FL-3'	GAAGTTGAAGGATCCGAACGTTCATTGATCGCACGTCGACATTTG	This Study
pDB-CDC123-R	GGCGGTGGGTACCCATACGATGTTCCTGACTATGCGTAGCACGTGTAATTCTAGAGC	This Study
pDB-CDC123-F	TATATCTATAAAAGTTGTATATTCTTGTGAGGACATGGATCCTTGCTCGAGGTATATTTG	This Study
CDC123-pDB-R	TACAACAAATATACCTCGAGCAAGGATCCATGTCCTCACAAGAATATACAACTTTAT	This Study
CDC123-pDB-F	ACGCATAGTCAGGAACATCGTATGGGTACCCACCGCCAGTTTCATTCTCACTATCACT	This Study
ARG4 F	ACTCCATGCTGATTGCCACA	This Study
ARG4 R	AGCAGTAGCGACACACTCAC	This Study
ARG5,6 F	GGTGGGTGGTGCCATTATCA	This Study
ARG5,6 R	AGTCTGGCTCAATTCCCTGC	This Study
HIS4 F	GCTATCGCAAGCTGAACACG	This Study
HIS4 R	GGGCTTCTTCGTAACCGTCA	This Study
CPA2 F	TGTCAAGGCATTTTTGGGCG	This Study
CPA2 R	AGAAAGGATCTGCACCAGCC	This Study

ZRT1 F	GGGCCCTATGTGTTGCGTAT	This Study
ZRT1 R	CAAGCGCAGTGTAAGAACCG	This Study
GCN4 F	TGCTTACAACCGCAAACAGC	This Study
GCN4 R	GCACGTTTTAGAGCAGCAGG	This Study
DGR1 F	CAGACCAACTGCCGTTCCTT	This Study
DGR1 R	ACGATCGTTGCCGTTGACT	This Study
COX26 F	GCTGCCCCAATCAAGAGGTA	This Study
COX26 R	TATACAGCACCAGGCCAACC	This Study
MTH1 F	CGCGGAAAAACAGCACAGAA	This Study
MTH1 R	CTTGTGCCTGACATTGCGAC	This Study
COX19 F	TGAGACCTACTCCACCCGAG	This Study
COX19 R	TTTCGTTCTGCACAAGCTGC	This Study
LYS5 F	AGCGTCTGATCCATGCACAA	This Study
LYS5 R	CATAGAAGCTCCCTCAGCCG	This Study
ATG8 F	GGAGTCGGAGAGGATTGCTG	This Study
ATG8 R	GAAGATGGCCTTCTCAGGGG	This Study
HIS1 F	TGAGACAATGAGGGCAGCAG	This Study
HIS1 R	TCAGGCAGCTTGTCTTCAGG	This Study
LYS1 F	TGCAGCCCTTGGTGTAAGAG	This Study
LYS1 R	ATTGGGGTAAGGCGACACTG	This Study
TAF10 F	CGGGTTTAACGTAGCAGATG	This Study
TAF10 R	CGCCTGACTGTTGTTAGCAT	This Study
Biotinylated rRNA depletio	/5Biosg/GGGGGGATGCGTGCATTTATCAGATCA	This Study

n oligos 1		
Biotinylated rRNA depletion oligos 2	/5Biosg/TTGGTGACTCTAGATAACCTCGGGCCGATCGCACG	This Study
Biotinylated rRNA depletion oligos 3	/5Biosg/GAGCCGCCTGGATACCGCAGCTAGGAATAATGGAAT	This Study
Biotinylated rRNA depletion oligos 4	/5Biosg/TCGTGGGGGGCCCAAGTCCTTCTGATCGAGGCCC	This Study
Biotinylated rRNA depletion oligos 5	/5Biosg/GCACTCGCCGAATCCCGGGGCCGAGGGAGCGA	This Study
Biotinylated rRNA depletion oligos 6	/5Biosg/GGGGCCGGGCCGCCCCTCCCACGGCGCG	This Study
Biotinylated rRNA depletion oligos 7	/5Biosg/CCCAGTGCGCCCCGGGCGTCGTCGCGCCGTCGGGTCCCGGG	This Study
Biotinylated	/5Biosg/TCCGCCGAGGGCGCACCACCGGCCCGTCTCGCC	This Study

rRNA depletion oligos 8		
Biotinylated rRNA depletion oligos 9	/5Biosg/AGGGGCTCTCGCTTCTGGCGCCAAGCGT	This Study
Biotinylated rRNA depletion oligos 10	/5Biosg/GAGCCTCGGTTGGCCCCGGATAGCCGGGTCCCCGT	This Study
Biotinylated rRNA depletion oligos 11	/5Biosg/GAGCCTCGGTTGGCCTCGGATAGCCGGTCCCCCGC	This Study
Biotinylated rRNA depletion oligos 12	/5Biosg/TCGCTGCGATCTATTGAAAGTCAGCCCTCGACACA	This Study
Biotinylated rRNA depletion oligos 13	/5Biosg/TCCTCCCGGGGCTACGCCTGTCTGAGCGTCGCT	This Study
Biotinylated rRNA depletion oligos 14	/5Biosg/GGGGCCGGGCCACCCCTCCCACGGCGCG	This Study

Supplementary Table 4: Bioanalyzer Results

Sample	Mean Fragment Length	Fragment Length Standard Deviation
rna_wt_25_1	236	89
rna_wt_25_2	209	13
rna_wt_25_3	212	22
rna_ts_25_1	212	20
rna_ts_25_2	209	14
rna_ts_25_3	216	33
rna_wt_37_1	239	82
rna_wt_37_2	221	43
rna_wt_37_3	229	64
rna_ts_37_1	210	12
rna_ts_37_2	223	58
rna_ts_37_3	211	9
rpf_ts_25_1	32	2
rpf_ts_25_2	31	2
rpf_ts_37_1	30	2
rpf_ts_37_2	30	2
rpf_wt_25_1	32	2
rpf_wt_25_2	32	2
rpf_wt_37_1	32	2
rpf_wt_37_2	32	2

References

1. Buttgereit,F. and Brand,M.D. (1995) A hierarchy of ATP-consuming processes in mammalian cells. *Biochemical Journal*, **312**, 163–167.

2. Hershey,J.W.B., Sonenberg,N. and Mathews,M.B. (2012) Principles of translational control: an overview. *Cold Spring Harbor perspectives in biology*, **4**.

3. Sonenberg,N. and Hinnebusch,A.G. (2009) Regulation of Translation Initiation in Eukaryotes: Mechanisms and Biological Targets. *Cell*, **136**, 731–745.

4. Hinnebusch,A.G. and Lorsch,J.R. (2012) The mechanism of eukaryotic translation initiation: new insights and challenges. *Cold Spring Harbor perspectives in biology*, **4**.

5. Pelletier,J. and Sonenberg,N. (2019) The Organizing Principles of Eukaryotic Ribosome Recruitment. *Annual review of biochemistry*, **88**, 307–335.

6. Hinnebusch,A.G. (2014) The scanning mechanism of eukaryotic translation initiation. *Annual Review of Biochemistry*, **83**, 779–812.

7. Hinnebusch,A.G. (2017) Structural Insights into the Mechanism of Scanning and Start Codon Recognition in Eukaryotic Translation Initiation. *Trends in biochemical sciences*, **42**, 589–611.

8. Lomakin,I.B., Shirokikh,N.E., Yusupov,M.M., Hellen,C.U.T. and Pestova,T.V. (2006) The fidelity of translation initiation: reciprocal activities of eIF1, IF3 and YciH. *The EMBO Journal*, **25**, 196–210.

9. Kolitz,S.E., Takacs,J.E. and Lorsch,J.R. (2009) Kinetic and thermodynamic analysis of the role of start codon/anticodon base pairing during eukaryotic translation initiation. *RNA (New York, N.Y.)*, **15**, 138–152.

10. Hinnebusch,A.G. (2011) Molecular mechanism of scanning and start codon selection in eukaryotes. *Microbiology and molecular biology reviews : MMBR*, **75**, 434–67, first page of table of contents.

11. Algire,M.A., Maag,D. and Lorsch,J.R. (2005) Pi release from eIF2, not GTP hydrolysis, is the step controlled by start-site selection during eukaryotic translation initiation. *Molecular Cell*, **20**, 251–262.

12. Pestova,T.V., Lomakin,I.B., Lee,J.H., Choi,S.K., Dever,T.E. and Hellen,C.U. (2000) The joining of ribosomal subunits in eukaryotes requires eIF5B. *Nature*, **403**, 332–335.

13. Dever,T.E., Feng,L., Wek,R.C., Cigan,A.M., Donahue,T.F. and Hinnebusch,A.G. (1992) Phosphorylation of initiation factor 2 alpha by protein kinase GCN2 mediates gene-specific translational control of GCN4 in yeast. *Cell*, **68**, 585–596.

14. Hinnebusch,A.G. (2005) Translational regulation of GCN4 and the general amino acid control of yeast. *Annual Review of Microbiology*, **59**, 407–450.

15. Pakos-Zebrucka,K., Koryga,I., Mnich,K., Ljujic,M., Samali,A. and Gorman,A.M. (2016) The integrated stress response. *EMBO reports*, **17**, 1374–1395.

16. Pavitt,G.D. (2005) eIF2B, a mediator of general and gene-specific translational control. *Biochemical Society Transactions*, **33**, 1487–1492.

17. Jackson,R.J., Hellen,C.U.T. and Pestova,T.V. (2010) The mechanism of eukaryotic translation initiation and principles of its regulation. *Nature Reviews Molecular Cell Biology*, **11**, 113–127.

18. Baird,T.D. and Wek,R.C. (2012) Eukaryotic initiation factor 2 phosphorylation and translational control in metabolism. *Advances in Nutrition*, **3**, 307–321.

19. Krishnamoorthy,T., Pavitt,G.D., Zhang,F., Dever,T.E. and Hinnebusch,A.G. (2001) Tight Binding of the Phosphorylated α Subunit of Initiation Factor 2 (eIF2α) to the Regulatory Subunits of Guanine Nucleotide Exchange Factor eIF2B Is Required for Inhibition of Translation Initiation. *Molecular and Cellular Biology*, **21**, 5018–5030.

20. Rowlands,A.G., Panniers,R. and Henshaw,E.C. (1988) The catalytic mechanism of guanine nucleotide exchange factor action and competitive inhibition by phosphorylated eukaryotic initiation factor 2. *Journal of Biological Chemistry*, **263**, 5526–5533.

21. Von der Haar,T. and McCarthy,J.E.G. (2002) Intracellular translation initiation factor levels in Saccharomyces cerevisiae and their role in cap-complex function. *Molecular Microbiology*, **46**, 531–544.

22. Kulak,N.A., Pichler,G., Paron,I., Nagaraj,N. and Mann,M. (2014) Minimal, encapsulated proteomic-sample processing applied to copy-number estimation in eukaryotic cells. *Nature Methods*, **11**, 319–324.

23. González,A. and Hall,M.N. (2017) Nutrient sensing and TOR signaling in yeast and mammals. *The EMBO Journal*, **36**, 397–408.

24. Wullschleger,S., Loewith,R. and Hall,M.N. (2006) TOR signaling in growth and metabolism. *Cell*, **124**, 471–484.

25. Loewith,R. and Hall,M.N. (2011) Target of rapamycin (TOR) in nutrient signaling and growth control. *Genetics*, **189**, 1177–1201.

26. Howell,J.J., Ricoult,S.J.H., Ben-Sahra,I. and Manning,B.D. (2013) A growing role for mTOR in promoting anabolic metabolism. *Biochemical Society Transactions*, **41**, 906–912.

27. Laplante,M. and Sabatini,D.M. (2012) MTOR signaling in growth control and disease. *Cell*, **149**, 274–293.

28. Shimobayashi,M. and Hall,M.N. (2014) Making new contacts: The mTOR network in metabolism and signalling crosstalk. *Nature Reviews Molecular Cell Biology*, **15**, 155–162.

29. Loewith,R., Jacinto,E., Wullschleger,S., Lorberg,A., Crespo,J.L., Bonenfant,D., Oppliger,W., Jenoe,P. and Hall,M.N. (2002) Two TOR complexes, only one of which is rapamycin sensitive, have distinct roles in cell growth control. *Molecular Cell*, **10**, 457–468.

30. Nakashima,N., Noguchi,E. and Nishimoto,T. (1999) Saccharomyces cerevisiae putative G protein, Gtr1p, which forms complexes with itself and a novel protein designated as Gtr2p, negatively regulates the Ran/Gsp1p G protein cycle through Gtr2p. *Genetics*, **152**, 853–867.

31. Sekiguchi,T., Hirose,E., Nakashima,N., Ii,M. and Nishimoto,T. (2001) Novel G Proteins, Rag C and Rag D, Interact with GTP-binding Proteins, Rag A and Rag B. *Journal of Biological Chemistry*, **276**, 7246–7257.

32. Battaglioni,S., Benjamin,D., Wälchli,M., Maier,T. and Hall,M.N. (2022) mTOR substrate phosphorylation in growth control. *Cell*, **185**, 1814–1836.

33. Wang,X., Janmaat,M., Beugnet,A., Paulin,F.E.M. and Proud,C.G. (2002) Evidence that the dephosphorylation of Ser535 in the ε-subunit of eukaryotic initiation factor (eIF) 2B is insufficient for the activation of eIF2B by insulin. *Biochemical Journal*, **367**, 475–481.

34. Gingras,A.C., Raught,B., Gygi,S.P., Niedzwiecka,A., Miron,M., Burley,S.K., Polakiewicz,R.D., Wyslouch-Cieszynska,A., Aebersold,R. and Sonenberg,N. (2001) Hierarchical phosphorylation of the translation inhibitor 4E-BP1. *Genes & development*, **15**, 2852–2864.

35. Cherkasova,V.A. and Hinnebusch,A.G. (2003) Translational control by TOR and TAP42 through dephosphorylation of eIF2α kinase GCN2. *Genes and Development*, **17**, 859–872.

36. Kubota,H., Obata,T., Ota,K., Sasaki,T. and Ito,T. (2003) Rapamycin-induced translational derepression of GCN4 mRNA involves a novel mechanism for activation of the eIF2α kinase GCN2. *Journal of Biological Chemistry*, **278**, 20457–20460.

37. Anthony,T.G., McDaniel,B.J., Byerley,R.L., McGrath,B.C., Cavener,D.B., McNurlan,M.A. and Wek,R.C. (2004) Preservation of liver protein synthesis during dietary leucine deprivation occurs at the expense of skeletal muscle mass in mice deleted for eIF2 kinase GCN2. *Journal of Biological Chemistry*, **279**, 36553–36561.

38. Xiao,F., Huang,Z., Li,H., Yu,J., Wang,C., Chen,S., Meng,Q., Cheng,Y., Gao,X., Li,J., *et al.* (2011) Leucine deprivation increases hepatic insulin sensitivity via GCN2/mTOR/S6K1 and AMPK pathways. *Diabetes*, **60**, 746–756.

39. Ye,J., Palm,W., Peng,M., King,B., Lindsten,T., Li,M.O., Koumenis,C. and Thompson,C.B. (2015) GCN2 sustains mTORC1 suppression upon amino acid deprivation by inducing Sestrin2. *Genes and Development*, **29**, 2331–2336.

40. Averous,J., Lambert-Langlais,S., Mesclon,F., Carraro,V., Parry,L., Jousse,C., Bruhat,A., Maurin,A.C., Pierre,P., Proud,C.G., *et al.* (2016) GCN2 contributes to mTORC1 inhibition by leucine deprivation through an ATF4 independent mechanism. *Scientific Reports*, **6**, 1–10.

41. Altmann,M., Sonenberg,N., Trachsel,H., Universitat,M. Der and Bern,C.- (1989) Translation in Saccharomyces cerevisiae: initiation factor 4E-dependent cell-free system. *Molecular and Cellular Biology*, **9**, 4467–4472.

42. Funakoshi,M. and Hochstrasser,M. (2009) Small epitope-linker modules for PCR-based C-terminal tagging in Saccharomyces cerevisiae. *Yeast (Chichester, England)*, **26**, 185–192.

43. Alone,P.V., Cao,C. and Dever,T.E. (2008) Translation Initiation Factor 2γ Mutant Alters Start Codon Selection Independent of Met-tRNA Binding. *Molecular and Cellular Biology*, **28**, 6877–6888.

44. Boeke,J.D., Trueheart,J., Natsoulis,G. and Fink,G.R. (1987) [10] 5-Fluoroorotic acid as a selective agent in yeast molecular genetics. *Methods in Enzymology*, **154**, 164–175.

45. Gietz,R.D., Schiestl,R.H., Willems,A.R. and Woods,R.A. (1995) Studies on the transformation of intact yeast cells by the LiAc/SS-DNA/PEG procedure. *Yeast (Chichester, England)*, **11**, 355–360.

46. Köhrer,K. and Domdey,H.B.T.-M. in E. (1991) [27] Preparation of high molecular weight RNA. In *Guide to Yeast Genetics and Molecular Biology*. Academic Press, Vol. 194, pp. 398–405.

47. Chockalingam,P.S., Jurado,L.A. and Jarrett,H.W. (2001) DNA affinity chromatography. *Molecular Biotechnology*, **19**, 189–199.

48. Roehr,J.T., Dieterich,C. and Reinert,K. (2017) Flexbar 3.0 - SIMD and multicore parallelization. *Bioinformatics*, **33**, 2941–2942.

49. Andrews,S., Krueger,F., Segonds-Pichon,A., Biggins,L., Krueger,C. and Wingett,S. (2010) FastQC.

50. Martin,M. (2011) Cutadapt removes adapter sequences from high-throughput sequencing reads. *EMBnet.journal*, **17**, 10.

51. Kim,D., Paggi,J.M., Park,C., Bennett,C. and Salzberg,S.L. (2019) Graph-based genome alignment and genotyping with HISAT2 and HISAT-genotype. *Nature Biotechnology*, **37**, 907–915.

52. Dobin,A., Davis,C.A., Schlesinger,F., Drenkow,J., Zaleski,C., Jha,S., Batut,P., Chaisson,M. and Gingeras,T.R. (2013) STAR: Ultrafast universal RNA-seq aligner. *Bioinformatics*, **29**, 15–21.

53. Danecek,P., Bonfield,J.K., Liddle,J., Marshall,J., Ohan,V., Pollard,M.O., Whitwham,A., Keane,T., McCarthy,S.A., Davies,R.M., *et al.* (2021) Twelve years of SAMtools and BCFtools. *GigaScience*, **10**, 1–4.

54. Li,H., Handsaker,B., Wysoker,A., Fennell,T., Ruan,J., Homer,N., Marth,G., Abecasis,G. and Durbin,R. (2009) The Sequence Alignment/Map format and SAMtools. *Bioinformatics*, **25**, 2078–2079.

55. Shao,D., Ahmed,N., Soni,N. and O'Brien,E.P. (2021) RiboA: a web application to identify ribosome A-site locations in ribosome profiling data. *BMC Bioinformatics*, **22**, 1–8.

56. Liao,Y., Smyth,G.K. and Shi,W. (2014) FeatureCounts: An efficient general purpose program for assigning sequence reads to genomic features. *Bioinformatics*, **30**, 923–930.

57. Pelechano,V., Wei,W. and Steinmetz,L.M. (2013) Extensive transcriptional heterogeneity revealed by isoform profiling. *Nature*, **497**, 127–131.

58. Quinlan,A.R. and Hall,I.M. (2010) BEDTools: A flexible suite of utilities for comparing genomic features. *Bioinformatics*, **26**, 841–842.

59. Cock,P.J.A., Antao,T., Chang,J.T., Chapman,B.A., Cox,C.J., Dalke,A., Friedberg,I., Hamelryck,T., Kauff,F., Wilczynski,B., *et al.* (2009) Biopython: Freely available Python tools for computational molecular biology and bioinformatics. *Bioinformatics*, **25**, 1422–1423.

60. Virtanen,P., Gommers,R., Oliphant,T.E., Haberland,M., Reddy,T., Cournapeau,D., Burovski,E., Peterson,P., Weckesser,W., Bright,J., *et al.* (2020) SciPy 1.0: fundamental algorithms for scientific computing in Python. *Nature Methods*, **17**, 261–272.

61. Patro,R., Duggal,G., Love,M.I., Irizarry,R.A. and Kingsford,C. (2017) Salmon provides fast and bias-aware quantification of transcript expression. *Nature methods*, **14**, 417–419.

62. Love,M.I., Huber,W. and Anders,S. (2014) Moderated estimation of fold change and dispersion for RNA-seq data with DESeq2. *Genome Biology*, **15**, 1–21.

63. Soneson,C., Love,M.I. and Robinson,M.D. (2016) Differential analyses for RNA-seq: Transcript-level estimates improve gene-level inferences. *F1000Research*, **4**, 1–23.

64. R Core Team (2022) R: A Language and Environment for Statistical Computing.

65. Stephens,M. (2017) False discovery rates: A new deal. *Biostatistics*, **18**, 275–294.

66. Bailey,T.L. (2021) STREME: accurate and versatile sequence motif discovery. *Bioinformatics*, **37**, 2834–2840.

67. Lorenz,R., Bernhart,S.H., Höner zu Siederdissen,C., Tafer,H., Flamm,C., Stadler,P.F. and Hofacker,I.L. (2011) ViennaRNA Package 2.0. *Algorithms for Molecular Biology*, **6**, 26.

68. Rawal,Y., Chereji,R.V., Valabhoju,V., Qiu,H., Ocampo,J., Clark,D.J. and Hinnebusch,A.G. (2018) Gcn4 Binding in Coding Regions Can Activate Internal and Canonical 5′ Promoters in Yeast. *Molecular Cell*, **70**, 297-311.e4.

69. Simms,C.L., Yan,L.L., Qiu,J.K. and Zaher,H.S. (2019) Ribosome Collisions Result in +1 Frameshifting in the Absence of No-Go Decay. *Cell Reports*, **28**, 1679-1689.e4.

70. Altmann,M. and Trachsel,H. (1989) Altered mRNA cap recognition activity of initiation factor 4E in the yeast cell cyde division mutant cdc33. *Nucleic Acids Research*, **17**, 5923–5931.

71. Altmann,M., Sonenberg,N. and Trachsel,H. (1989) Translation in Saccharomyces cerevisiae: initiation factor 4E-dependent cell-free system. *Molecular and Cellular Biology*, **9**, 4467–4472.

72. Ross,D., Saxena,M. and Altmann,M. (2012) eIF4E Is an Important Determinant of Adhesion and Pseudohyphal Growth of the Yeast S. cerevisiae. *PLOS ONE*, **7**, e50773.

73. Lavoie,C., Tam,R., Clark,M., Lee,H., Sonenberg,N. and Lasko,P. (1994) Suppression of a temperature-sensitive cdc33 mutation of yeast by a multicopy plasmid expressing a Drosophila ribosomal protein. *Journal of Biological Chemistry*, **269**, 14625–14630.

74. Ingolia,N.T., Ghaemmaghami,S., Newman,J.R.S. and Weissman,J.S. (2009) Genome-wide analysis in vivo of translation with nucleotide resolution using ribosome profiling. *Science*, **324**, 218–223.

75. Weinberg,D.E., Shah,P., Eichhorn,S.W., Hussmann,J.A., Plotkin,J.B. and Bartel,D.P. (2016) Improved Ribosome-Footprint and mRNA Measurements Provide Insights into Dynamics and Regulation of Yeast Translation. *Cell Reports*, **14**, 1787–1799.

76. Guo,Z. and Sherman,F. (1996) Signals sufficient for 3'-end formation of yeast mRNA. *Molecular and Cellular Biology*, **16**, 2772–2776.

77. Danaie,P., Altmann,M., Hall,M.N., Trachsel,H. and Helliwell,S.B. (1999) CLN3 expression is sufficient to restore G1-to-S-phase progression in Saccharomyces cerevisiae mutants defective in translation initiation factor eIF4E. *Biochemical Journal*, **340**, 135–141.

78. Iida,H. and Yahara,I. (1984) Specific early-G1 blocks accompanied with stringent response in Saccharomyces cerevisiae lead to growth arrest in resting state similar to the G0 of higher eucaryotes. *Journal of Cell Biology*, **98**, 1185–1193.

79. Nielsen,K.H., Szamecz,B., Valášek,L., Jivotovskaya,A., Shin,B.S. and Hinnebusch,A.G. (2004) Functions of eIF3 downstream of 48S assembly impact AUG recognition and GCN4 translational control. *EMBO Journal*, **23**, 1166–1177.

80. Perzlmaier,A.F., Richter,F. and Seufert,W. (2013) Translation initiation requires cell division cycle 123 (Cdc123) to facilitate biogenesis of the eukaryotic initiation factor 2 (eIF2). *Journal of Biological Chemistry*, **288**, 21537–21546.

81. Bieganowski,P., Shilinski,K., Tsichlis,P.N. and Brenner,C. (2004) Cdc123 and checkpoint forkhead associated with RING proteins control the cell cycle by controlling eIF2γ abundance. *Journal of Biological Chemistry*, **279**, 44656–44666.

82. Shi,Y., Yang,Y., Hoang,B., Bardeleben,C., Holmes,B., Gera,J. and Lichtenstein,A. (2016) Therapeutic potential of targeting IRES-dependent c-myc translation in multiple myeloma cells during ER stress. *Oncogene*, **35**, 1015–1024.

83. Philippe,C., Dubrac,A., Quelen,C., Desquesnes,A., Van Den Berghe,L., Ségura,C., Filleron,T., Pyronnet,S., Prats,H., Brousset,P., *et al.* (2016) PERK mediates the IRES-dependent translational activation of mRNAs encoding angiogenic growth factors after ischemic stress. *Science signaling*, **9**, ra44.

84. Holčík,M., Gordon,B.W. and Korneluk,R.G. (2003) The Internal Ribosome Entry Site-Mediated Translation of Antiapoptotic Protein XIAP Is Modulated by the Heterogeneous Nuclear Ribonucleoproteins C1 and C2. *Molecular and Cellular Biology*, **23**, 280–288.

85. Dobbyn,H.C., Hill,K., Hamilton,T.L., Spriggs,K.A., Pickering,B.M., Coldwell,M.J., De Moor,C.H., Bushell,M. and Willis,A.E. (2008) Regulation of BAG-1 IRES-mediated translation following chemotoxic stress. *Oncogene*, **27**, 1167–1174.

86. Shatsky,I.N., Terenin,I.M., Smirnova,V.V. and Andreev,D.E. (2018) Cap-Independent Translation: What's in a Name? *Trends in biochemical sciences*, **43**, 882–895.

87. Panvert,M., Dubiez,E., Arnold,L., Perez,J., Mechulam,Y., Seufert,W. and Schmitt,E. (2015) Cdc123, a Cell Cycle Regulator Needed for eIF2 Assembly, Is an ATP-Grasp Protein with Unique Features. *Structure*, **23**, 1596–1608.

88. Hay,N. and Sonenberg,N. (2004) Upstream and downstream of mTOR. *Genes and Development*, **18**, 1926–1945.

89. Torrence,M.E., Macarthur,M.R., Hosios,A.M., Valvezan,A.J., Asara,J.M., Mitchell,J.R. and Manning,B.D. (2021) The mtorc1-mediated activation of atf4 promotes protein and glutathione synthesis downstream of growth signals. *eLife*, **10**, 1–33.

90. Park,Y., Reyna-Neyra,A., Philippe,L. and Thoreen,C.C. (2017) mTORC1 Balances Cellular Amino Acid Supply with Demand for Protein Synthesis through Post-transcriptional Control of ATF4. *Cell Reports*, **19**, 1083–1090.

91. Ben-Sahra,I., Hoxhaj,G., Ricoult,S.J.H., Asara,J.M. and Manning,B.D. (2016) mTORC1 induces purine synthesis through control of the mitochondrial tetrahydrofolate cycle. *Science (New York, N.Y.)*, **351**, 728–733.

92. Salas-Marco,J. and Bedwell,D.M. (2005) Discrimination between defects in elongation fidelity and termination efficiency provides mechanistic insights into translational readthrough. *Journal of Molecular Biology*, **348**, 801–815.

93. Wek,R.C., Ramirez,M., Jackson,B.M. and Hinnebusch,A.G. (1990) Identification of positive-acting domains in GCN2 protein kinase required for translational activation of GCN4 expression. *Molecular and Cellular Biology*, **10**, 2820–2831.

Chapter 3

N1-methylpseudouridine found within COVID-19 mRNA vaccines produces faithful protein products

This chapter is currently published in Cell Reports as Kyusik Q Kim, Bhagyashri D Burgute, Shin-Cheng Tzeng, Crystal Jing, Courtney Jungers, Junya Zhang, Liewei L Yan, Richard D Vierstra, Sergej Djuranovic, Bradley S Evans, and Hani S Zaher (2022). N1-methylpseudouridine found within COVID-19 mRNA vaccines produces faithful protein products

Abstract

Synthetic mRNA technology is a promising avenue for treating and preventing disease. Key to the technology is the incorporation of modified nucleotides such as N1-methylpseudouridine (m1Ψ) to decrease immunogenicity of the RNA. However, relatively few studies have addressed the effects of modified nucleotides on the decoding process. Here we investigate the effect of m1Ψ and the related modification pseudouridine (Ψ) on translation. In a reconstituted system, we find that m1Ψ does not significantly alter decoding accuracy. More importantly, we do not detect an increase in miscoded peptides when mRNA containing m1Ψ is translated in cell culture, compared to unmodified mRNA. We also find that m1Ψ does not stabilize mismatched RNA-duplex formation and only mildly promotes errors during reverse transcription. Overall, our results suggest that m1Ψ does not significantly impact translational fidelity, a welcome sign for future RNA therapeutics.

.

Introduction

The remarkable effectiveness of the mRNA vaccines against SARS-CoV-2, and their record-setting approval (Baden et al., 2021; Polack et al., 2020), have generated considerable interest in synthetic mRNA therapeutics. This technology promises many advantages, including simplicity of production, ease of customization, and relatively low cost, as RNA can be readily made in vitro with high yields (Baronti et al., 2018). Importantly, RNAs produced in this manner can be synthesized with a cap structure just like eukaryotic mRNAs. These synthetic "mRNAs", when successfully delivered to the cytoplasm of eukaryotic cells, are well recognized as templates for protein synthesis by the ribosomes. Unlike direct delivery of proteins – which are typically limited to the extracellular space – proteins translated from synthetic mRNAs can be targeted to remain within the cell, directed for export, or even deposited in membranes. Furthermore, these mRNAs are non-integrating and readily degraded by ubiquitous cellular RNases, presumably making them safer than comparable DNA therapeutics (Sahin et al., 2014).

The potential of mRNA therapeutics has been documented in the literature for several decades. In one of the first reports, Wolff and colleagues demonstrated that injection of mRNAs for several reporter genes into the muscles of mice could produce protein products with yields similar to comparable injections of DNA plasmids (Wolff et al., 1990). Two years later, Jirikowski and colleagues showed that injection of vasopressin mRNA into the hypothalamus of Brattleboro rats resulted in expression of the protein and temporary reversal of their diabetes insipidus (Jirikowski et al., 1992). However, various obstacles hindered development of the technology until present times. Key challenges were the lack of an efficient delivery method and the instability and immunogenicity of in vitro transcribed mRNAs (Damase et al., 2021; Van Hoecke and Roose, 2019; Sahin et al., 2014).

Over the past decade, advances in lipid nanotechnology and material sciences have provided efficient and safe delivery systems for synthetic mRNAs (Damase et al., 2021; Guan and Rosenecker, 2017; Kaczmarek et al., 2017). At the same time, increased understanding of mRNA biochemistry and cellular mechanisms have addressed stability and immunogenicity concerns. In particular, the immunogenicity of in-vitro transcribed mRNA has been attributed to the activation of cell surface, endosomal, and cytoplasmic RNA sensors (Akira et al., 2006; Freund et al., 2019; Karikó et al., 2004, 2005; Weissman et al., 2000) that monitor for the presence of viral RNAs. Incorporation of modified nucleotide monophosphates into mRNA during its synthesis, along with careful purification of the modified mRNA, were found to suppress the activation of these sensors (Freund et al., 2019; Karikó et al., 2005, 2008, 2011). Substitution of uridine by pseudouridine (Ψ), a modification abundant in tRNAs and rRNAs, was one of the first modifications found to exhibit such effects on the innate immune response (Anderson et al., 2010; Karikó et al., 2008). Later studies documented similar effects for 5-methylcytidine and 2-thiouridine and observed that modified mRNAs produced 10 to 100-fold more protein compared to unmodified mRNAs (Kormann et al., 2011). Recently, N1-methylpseudouridine (m1Ψ), the modification used in the current mRNA SARS-CoV-2 vaccines, was found to possess superior characteristics to Ψ; m1Ψ elicited less immunogenicity and increased protein production by more than an order of magnitude relative to Ψ (Andries et al., 2015; Parr et al., 2020; Svitkin et al., 2017).

While much effort has been devoted to understanding the mechanisms by which nucleotides modifications suppress the innate immune response and increase protein yield, relatively few studies have investigated their effects on the fidelity of protein synthesis. The accuracy of tRNA selection by the ribosome when encountering modified mRNAs is an

important consideration, as the fidelity of the protein product might be a critical factor in RNA-based treatments. In the case of Ψ, studies have reported conflicting results as that to the effect of the modification on ribosome accuracy. Studies by the Yu group found that introduction of Ψ to stop codons induced readthrough in vitro and in vivo (Adachi and Yu, 2020; Fernández et al., 2013; Karijolich and Yu, 2011)– an effect rationalized as unusual base pairing between the codon and anticodon that is only allowed when modified bases are used (Fernández et al., 2013; Parisien et al., 2012). Studies from other groups examining the effects of Ψ on amino acid misincorporation provided conflicting results and suggested that the modification has little effect on the fidelity of protein synthesis (Eyler et al., 2019; Hoernes et al., 2016, 2019; Nir et al., 2022; Svidritskiy et al., 2016). To the best of our knowledge however, there have been no such studies on the effects of m1Ψ on tRNA selection by the ribosome and subsequent translation, even though m1Ψ is the current choice for mRNA vaccines.

To address this knowledge gap, we explored the effect of m1Ψ and Ψ on decoding using various in vitro systems. In a reconstituted system, the substitution of a single uridine with m1Ψ in a model mRNA was found to slightly decrease the observed rate of peptide-bond formation. However, m1Ψ did not significantly alter the overall accuracy of tRNA selection by the ribosome, whereas Ψ marginally increased the incorporation of near- and non-cognate amino acids. LC-MS/MS analysis of SARS-CoV-2 spike protein products produced in HEK 293 cells via electroporation of mRNAs containing only uridine, Ψ or m1Ψ, showed that translation of either modified mRNA did not lead to a detectable increase in miscoded proteins. High-resolution melt analysis found that Ψ, but not m1Ψ, increased the stability of mismatched duplexes. Primer extension assays and quantification of reverse transcriptase errors across the modifications via deep sequencing revealed that the modifications are read differently by reverse

transcriptases. Taken together, our findings provide important insights into the effects of m1Ψ on translation and its usage in future mRNA therapeutics.

Results

Validation of pseudouridine and N1-methylpseudouridine modifications in synthetic model mRNAs

Our initial goal was to determine how mRNA modifications in synthetic mRNAs modify their base-pairing properties and impact the decoding process. In particular, we sought to systemically examine how the modifications alter the incorporation of all near-cognate and non-cognate amino acids. To do so, we resorted to our reconstituted bacterial system, which allowed us to carry out well-defined reactions with each of the 20 tRNA isoacceptors as well as release factors (Keedy et al, 2018). To program ribosomes with modified mRNAs, we obtained three chemically synthesized model mRNAs – one with no modification and the other two having a single substitution of uridine for Ψ or m1Ψ (**Figure 1**). Before proceeding, we verified that each model mRNA contained the correct modification using liquid chromatography with tandem mass spectrometry (LC-MS/MS) analysis. To generate standards for Ψ and m1Ψ, we treated their respective nucleotide triphosphate with calf intestinal phosphatase (CIP). Standards for the four canonical nucleotides, along with Ψ and m1Ψ, were analyzed with an Agilent 6490 QQQ triple-quadrupole LC mass spectrometer to validate mass transitions and retention times. We then subjected our mRNAs to P1 nuclease digestion and CIP treatment to generate single nucleosides.

Using the parameters determined from analysis of the standards, analysis of the digested RNAs yielded peaks with distinct retention times and/or mass transitions for U, Ψ, and m1Ψ. Furthermore, Ψ and m1Ψ peaks were only observed in the respective RNA (**Supplementary Figure 1**). Analysis of the A, C, G, and U peaks confirmed that the base composition of each mRNA was correct (**Supplementary Figure 1D**).

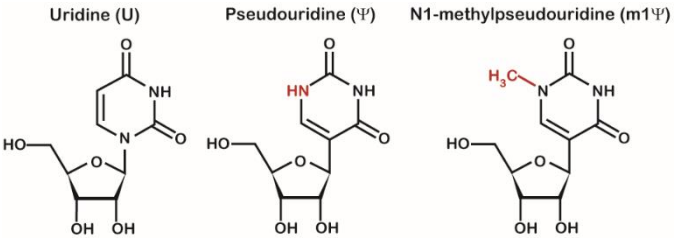

Figure 1: Chemical structures of uridine and its modifications.
Chemical structure of uridine, pseudouridine, and N1-methylpseudouridine. The N1 of both modified nucleosides are marked in red.

N1-methylpseudouridine slightly decreases the rate of peptide-bond formation

Using our reconstituted bacterial translation system, we measured the observed rates of peptide-bond formation (k_{pep}) (Zaher and Green, 2010) in the presence of our model mRNAs. Briefly, programmed ribosomes displayed either UAC, ΨAC, or m1ΨAC in the A site, which codes for the incorporation of tyrosine (Tyr). The initiation complexes also carried f-[^{35}S]-Met-tRNA^{fMet} in the P site, which allowed us to follow dipeptide formation by electrophoretic TLC (Youngman et al., 2004). As expected, in the presence of a Tyr-tRNA^{Tyr}•EFTu•GTP ternary complex, we observe robust accumulation of dipeptide products for all three initiation complexes after 10 seconds of incubation (**Figure 2A**).

Next, we used a pre-steady-state quench approach to measure the observed k_{pep} in the presence of 1 mM ribosome complexes and 2.5 mM tRNA^{Tyr}•EFTu•GTP ternary complex. At this sub-saturating concentration of reactants, changes to the observed k_{pep} reflect alterations to k_{cat} and $K_{1/2}$ (Zhang et al., 2016), allowing us to monitor contributions from both parameters. Ψ, and to a greater extent, m1Ψ, were found to reduce k_{pep} in the presence of the cognate ternary complex, with measured k_{pep} values of 40 s^{-1}, 31 s^{-1} and 25 s^{-1} for the UAC-, ΨAC- and m1ΨAC-programmed complexes, respectively (**Figure 2B, C**). This is consistent with reports from multiple groups showing that Ψ slows translation (Eyler et al., 2019; Hoernes et al., 2016; Karikó

et al., 2008). Similarly, we observe modest, but significant, reductions in the end point of the reactions, from ~0.7 for the unmodified mRNA to ~0.5 for the mRNA containing m1Ψ (**Figure 2D**). However, given that other steps during protein synthesis, including translocation, have been estimated to be much slower that peptide-bond formation, it is highly likely that the reduction in k_{pep} seen here is inconsequential to the overall protein yield from the modified mRNAs. Indeed, in eukaryotic extracts, the modifications appear not to affect overall protein synthesis yield (Hoernes et al., 2019).

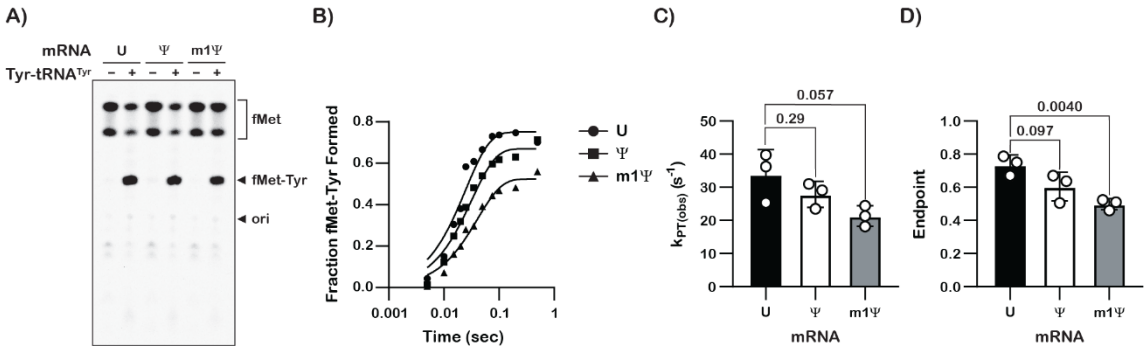

Figure 2: Pseudouridine and N1-methylpseudouridine slow down peptidyl transfer by the ribosome. **A)** A representative electrophoretic TLC of triplicates showing the translation products of three different initiation complexes -- UAC mRNA, ΨAC mRNA, or m1ΨAG mRNA – in the absence and presence of cognate tRNA (Tyr-tRNA^{Tyr} tRNA) ternary complex. **B)** A representative time-course plot of triplicates showing the kinetics of f-Met-Tyr peptide formation in the presence of unmodified (U), pseudouridine-containing (Ψ), and N1-methylpseudouridine-containing (m1Ψ) A-site UAC codon. **C-D)** Bar graph showing the measured observed rates of peptide-bond formation and reaction end points, respectively, in the presence of 1 mM initiation complex and 2.5 mM tRNA^{Tyr}•EFTu•GTP ternary complex. Plotted are the average values determined from three independent time courses with error bars representing the standard deviation around the mean. P values are denoted above the plots.

N1-methylpseudouridine preserves the fidelity of tRNA selection by the ribosome

Having established that Ψ and m1Ψ only modestly affect the cognate codon-anticodon interaction, we next sought to assess whether the modifications alter the incorporation frequency of near-cognate and non-cognate aminoacyl-tRNAs (aa-tRNAs). As mentioned earlier, conflicting data exist as to whether or not Ψ promotes miscoding (Adachi and Yu, 2020; Eyler et al., 2019; Fernández et al., 2013; Hoernes et al., 2016, 2019; Karijolich and Yu, 2011; Nir et al.,

2022; Svidritskiy et al., 2016). This raises the possibility that m1Ψ may also stabilize mismatched codon-anticodon interactions and allow ribosomes to accept near or non-cognate tRNAs. To address this, we conducted a peptidyl-transfer (PT) reactivity survey between the initiation complexes and all 19 near/non-cognate aa-tRNA isoacceptors (Keedy et al., 2018). The survey revealed that, with few exceptions, the overall reactivity profile was similar among the different initiation complexes after 10 seconds of incubation with ternary complexes (**Figure 3A**). We note that Tyr-tRNA^{Tyr} is present at low concentration in the tRNA mix – even after many attempts to deacylate it prior to aminoacylation – as evidenced by detection of a contaminating fMet-Tyr dipeptide in all reactions. However, this contaminant was readily distinguished by its distinct electrophoretic TLC migration (**Figure 3A**). Furthermore, we have previously shown that each dipeptide has a unique retention factor (Rf) on our eTLC assay, thus allowing identification (Keedy et al., 2018; Pierson et al., 2016; Simms et al., 2014). Altogether, the reactivity survey suggested that the modifications have little impact on overall accuracy of translation.

To better understand the effect of the modifications on miscoding, we focused on near-cognate aa-tRNAs and other aa-tRNAs that exhibited reactivity with the initiation complexes. We initially measured the observed k_{pep} values for the near-cognate Asp-tRNA^{Asp}, His-tRNA^{His}, Asn-tRNA^{Asn}, and Ser-tRNA^{Ser} substrates (**Figure 3B-F**). Of note, the first three aa-tRNAs correspond to mismatches involving the modification itself (U•C, U•G, and U•U, respectively), whereas the latter corresponds to an A•A mismatch 3’ to the modification. For all four reactions, Ψ and m1Ψ did not alter the observed k_{pep} values significantly (**Figure 3F**). Interestingly, Ψ was found to increase the end-point for the near-cognate interactions, especially in the presence of the Asn-tRNA^{Asn} ternary complex, which involves a U:U mismatch, whereas m1Ψ did not (**Figure**

3G). These observations suggest that Ψ modestly promotes miscoding by altering the proofreading phase of tRNA selection. Miscoding was not limited to these near-cognate aa-tRNAs, as similar observations were made for the remaining near-cognate aa-tRNAs: Cys-tRNA^{Cys} and Phe-tRNA^{Phe} (**Supplementary Figure 2J, K**). Interestingly, Ψ had the most dramatic impact on a mismatch involving its neighbor, i.e., reactions with Ser-tRNA^{Ser}, having an A•A mismatch to its 3' (**Figure 3E**), suggesting that Ψ alters the base-pairing properties of the entire codon-anticodon interaction. Supporting this proposal is the observation that Ψ increased end-point values for many non-cognate aa-tRNAs, which harbor more than one mismatch (**Supplementary Figure 2**). By contrast, m1Ψ did not increase k_{pep} or end-point values significantly for all tested near- and non-cognate aa-tRNAs (**Figure 3**, **Supplementary Figure 2**). Ultimately, our data suggest that although Ψ modestly increases mispairing during tRNA selection, m1Ψ behaves similarly to uridine.

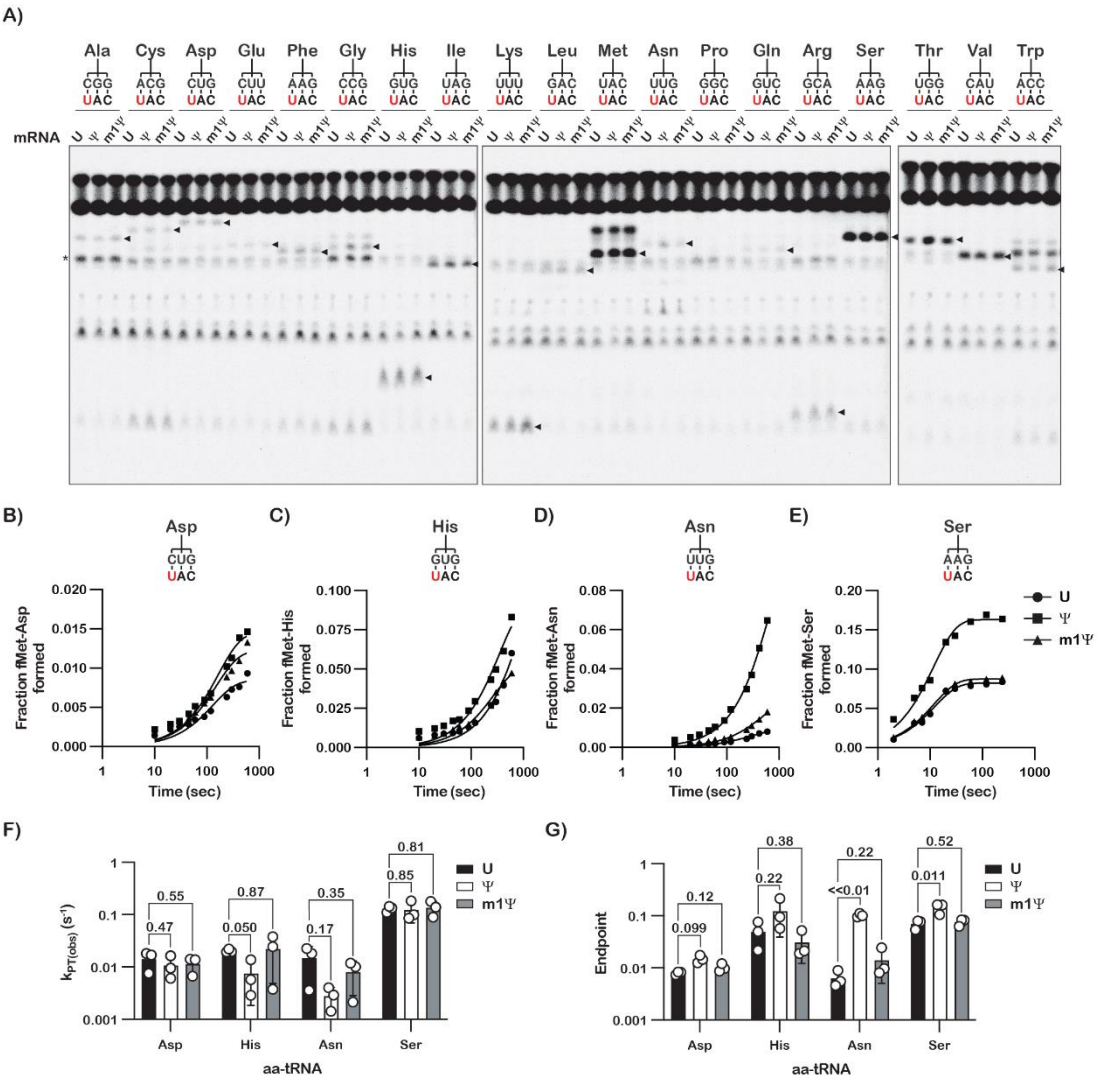

Figure 3: Unlike pseudouridine, N1-methylpseudouridine has little to no effect on the accuracy of tRNA selection

A) Representative electrophoretic TLCs of triplicates showing dipeptide formation reactions (10-second time point) of near/non- cognate tRNAs with UAC, ΨAC, or m1ΨAG initiation complexes. Arrowheads denote the translation product of each respective aa-tRNA. **B-E)** Representative time courses of triplicates of near-cognate tRNA ternary complexes (Asp, His, Asn, and Ser) and UAC, ΨAC, or Met-m1ΨmAG initiation complexes. The codon (UAC; modification in red) and near-cognate tRNA are indicated. **F, G)** Bar graph showing the measured observed rates of peptide-bond formation and reaction end points, respectively, in the presence of 1 mM initiation complex and 2.5 mM denoted ternary complex. Plotted are the average values determined from three independent time courses with error bars representing the standard deviation around the mean. P values are denoted above the plots.

N1-methylpseudouridine suppresses near-stop codon recognition by release factors

In addition to RNA-RNA interactions that occur within the decoding center between the codon of mRNAs and anticodon of tRNAs, RNA-protein interactions also occur during stop-

codon recognition by release factors (RFs). In fact, decoding of the stop codons is completely distinct than that of sense codons (Youngman et al., 2004). Fortuitously, our choice of the UAC A-site codon above, which is a near-stop codon for UAA and UAG, allowed us to evaluate how Ψ and m1Ψ impact misreading of sense codons by RFs (**Supplementary Figure 3A)**. Bacteria have two RFs (Youngman et al., 2004), with overlapping specificities: RF1, which recognizes UAA and UAG, and RF2, which recognizes UAA and UGA. RF1 was observed to react much faster with the UAC complex than did RF2 (**Supplementary Figure 3B-D**), with rates of hydrolysis of 0.2 s^{-1} and 0.03 s^{-1}, respectively. This was expected since RF1 exhibits promiscuity towards the third base of the stop codon – the same position where "mismatches" occur as the factor decodes the UAC near-stop codon. We also observed that m1Ψ significantly inhibited near-stop codon recognition by both factors, as we measured an endpoint of 0.3-0.4 compared to ~0.7 observed for uridine (**Supplementary Figure 3E**). Ψ, by contrast, only slightly decreased the rate of hydrolysis by RF1 (0.08 s^{-1}) and not by RF2 (0.04 s^{-1}) and had no effect on the end point (**Supplementary Figure 3D, E**). These observations not only reinforce the distinctions between the interactions of Ψ and m1Ψ with the decoding center, but also suggest that m1Ψ suppresses premature termination during protein synthesis.

N1-methylpseudouridine modified SARS-CoV-2 spike protein mRNA is translated faithfully by eukaryotic ribosomes.

So far, our analysis of the decoding process in the presence of modified mRNA focused on short model mRNAs added to a reconstituted bacterial system. These chemically synthesized mRNAs harbor a single modification, which allows us to systemically characterize their impact on the overall accuracy of tRNA selection. However, they are not ideal when evaluating how therapeutic mRNAs, which can harbor thousands of modified nucleotides, are translated. For

example, all the constituent uridines in the mRNA vaccines are substituted with m1Ψ. To probe whether such pervasive modification alters the accuracy of the ribosome in conditions more closely resembling those found in vivo, we generated SARS-CoV-2 spike protein mRNAs in which all constituent uridines remained unmodified or were completely replaced with Ψ or m1Ψ (**Figure 4A**). The template sequence is identical to that used in the BNT162b2 (Pfizer) mRNA Covid-19 vaccine (Jeong et al., 2021; Polack et al., 2020), except for the addition of sequences encoding His and FLAG tags at the 5' and 3' end (**Supplementary Table 1**), respectively, and the mRNAs were similarly capped.

To assess the integrity of spike protein products produced in human cells, we electroporated the unmodified and modified mRNAs into HEK 293 cells. Electroporation of a GFP plasmid control measured electroporation efficiency, which was estimated at 90% (**Supplementary Figure 4A**). More importantly, immunoblot analysis showed that the yields of spike protein products were similar regardless of modification status of the electroporated mRNA (**Figure 4B, Supplementary Figure 4B**). This was expected, as HEK 293 cells do not express TLR3, the receptor responsible for activating the innate immune response to unmodified mRNAs (Andries et al., 2015). Moreover, previous studies investigating translation of Ψ-containing mRNAs in HEK 293 cells reported similar results (Eyler et al., 2019; Hoernes et al., 2019). In addition to comparable yields, we also noted that regardless of the modification status of the mRNA, the resultant spike protein appeared to be processed into smaller products in the HEK 293 cells (**Figure 4B**), as has been previously noted (Ou et al., 2020). Additionally, the processed protein products migrated as heterogeneous bands (**Figure 4B**), suggesting that protein glycosylation also occurred as expected (Watanabe et al., 2020). Having established that incorporation of Ψ and m1Ψ into the mRNAs have little to no effect on protein yield under our

experimental conditions, we next sought to assess the impact of the modifications on miscoding using mass-spectrometry (MS) approaches. Spike protein products were purified with anti-FLAG magnetic beads, with a GFP-electroporated sample serving as a negative control. Following extensive washing, the samples were subjected to on-bead trypsin digestion and analyzed by LC-MS/MS.

After searching the datasets against the spike protein in the presence of the human proteome, we successfully identified 39% of the spike protein sequence (**Supplementary Figure 4D**). Reassuringly, label-free quantification of spike protein abundance did not detect significant levels of spike protein in the GFP control sample (<100-fold relative to the spike protein mRNA samples) (**Figure 4C**). Additionally, spike protein abundance was largely similar across all U, Ψ, and m1Ψ samples (**Figure 4C**), consistent with the immunoblot analysis (**Figure 4B, Supplementary Figure 4B**), which suggested that the modifications did not significantly alter protein yield.

To identify miscoded peptides, we conducted an error-tolerant search to identify candidates for further analysis. Results were checked in Scaffold to select the highest confidence candidates. To further ensure that we did not miss any miscoded peptides, we also conducted a second search against an in silico generated spike protein library, comprised of all single substitution protein products arising from miscoding events at every uridine in the spike protein sequence, to identify additional candidates. The sequences of all chosen candidates were then combined and added to the search library for a final confirmation search of the datasets.

Miscoded peptides identified in the final search were quantified from the MS1 scans using Proteome Discoverer and were further validated using Skyline. Miscoded peptides that

were not assigned quantitation values by Proteome Discoverer were manually quantified using Skyline if good peaks could be found. An example set of predicted fragmentation spectra for a wild-type peptide and its miscoded substituent is shown in **Figure 4D**. We then estimated the error frequency by dividing the abundance of the miscoded peptide by that of the parent faithful peptide (**Figure 4E, Supplementary Table 2**). Contrary to previous reports, which documented an increase in miscoding frequency when Ψ-containing luciferase mRNA was translated in HEK 293 cells (Eyler et al., 2019), we did not observe an increase in miscoding frequency for our Ψ-containing spike protein mRNA (**Figure 4F**). These distinctions could be due to the different proteins being analyzed. It is also feasible that our analysis missed rare miscoding events due to low coverage of any single miscoded peptide species. As such, the frequency of such events may be higher in the presence of Ψ-containing mRNA than we observe. However, our data suggest that for the most abundant miscoding events, Ψ does not significantly alter their frequency. Given the lack of observed effect for Ψ, the presence of the modification in the mRNA is not likely to have a biological impact on the fidelity of the protein products. More importantly, we do not observe an increase for our m1Ψ-containing mRNA (**Figure 4F**).

To add further confidence in our observations that the modifications do not significantly affect translational fidelity, we conducted a more sensitive assessment of miscoding in the presence of Ψ- and m1Ψ-containing mRNAs using a dual-luciferase reporter assay system (Kramer and Farabaugh, 2007). For this reporter, we mutated a critical lysine residue, encoded by AAA, in the active site of firefly luciferase, to an asparagine encoded by AAU (**Figure 4G**). Any observed firefly luciferase signal is then the result of miscoding events where the asparagine is miscoded as a lysine. By normalizing the signal to a wild-type control, we were able to assess how the presence of Ψ or m1Ψ affected miscoding frequency. The reporter construct RNA

(**Supplementary Table 1**) was transcribed in vitro and electroporated into HEK 293 cells using the same methods as for the spike protein mRNA. We found that neither the presence of Ψ nor the presence of m1Ψ in the RNA induced a detectable and/or significant increase in miscoding (**Figure 4G**), consistent with our LC-MS/MS analysis.

We also tested the mRNAs in a wheat germ system to broadly investigate how the modifications affect other eukaryotic systems. The protein yields were assessed by measuring ^{35}S-methionine incorporation into full-length polypeptides. Consistent with our results in the HEK 293 system, we did not observe significant differences in spike protein yield in the presence of either Ψ or m1Ψ-containing mRNAs relative to unmodified mRNA (**Supplementary Figure 5A**). We then subjected affinity-purified spike protein to LC-MS/MS analysis to assess miscoding events. Here, we searched the datasets against the computationally generated library used to search the HEK 293 datasets. An example set of predicted fragmentation spectra for a wild-type peptide and its miscoded substituent is shown in **Supplementary Figure 5C**. As before, we estimated the error frequency by dividing the abundance of the miscoded peptide by that of the parent faithful peptide (**Supplementary Table 3**). In wheat germ, translation of Ψ-containing mRNA induced a modest increase in miscoding frequency for some peptides (~1.5 fold) (**Supplementary Figure 5D**). However, and similar to what we observe in HEK 293 cells (**Figure 4F**), the relative abundance of most miscoded peptides did not change significantly in the presence of Ψ-containing mRNA. More importantly, as seen with the HEK 293 dataset, translation of the m1Ψ-containing mRNA in wheat germ extracts did not increase miscoding frequency (**Supplementary Figure 5D**). A second MS analysis found similar trends in a different set of miscoded peptides, with only marginal increases in miscoded peptides over wild-type peptides (**Supplementary Figure 5D**). While the relative abundance values were much

higher in the second test, this could be due to inaccurate quantification as the abundance of overall protein was very low. Collectively, our findings indicate that m1Ψ does not significantly increase miscoding during translation.

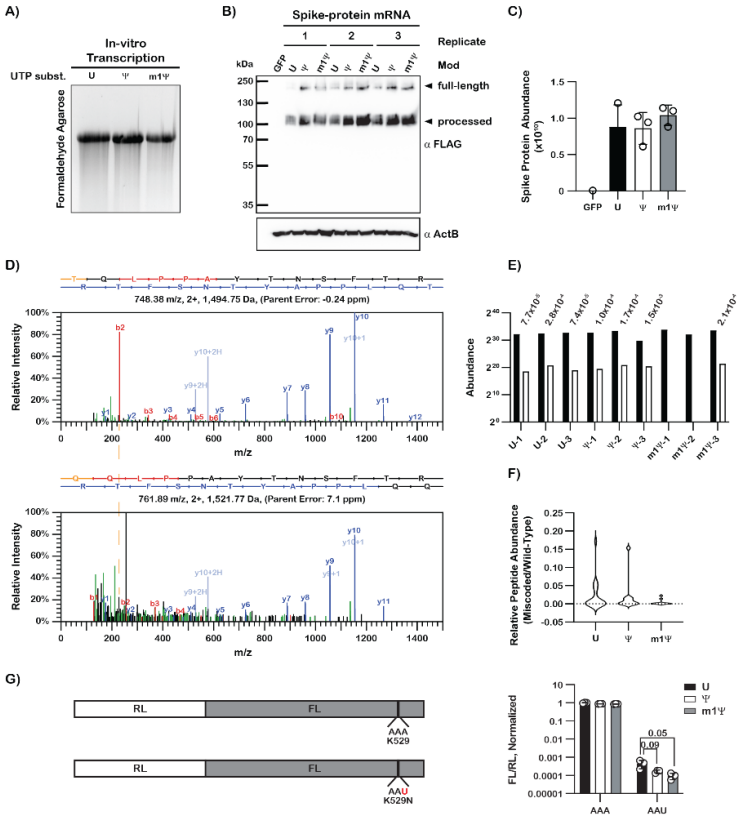

Figure 4: The presence of N1-methylpseudouride in mRNA does not increase amino-acid misincorporation frequency during translation in human cells

A) UV-transillumination image of an ethidium bromide-stained formaldehyde agarose gel used to visualize the mRNA constructs transfected into HEK 293 cells. **B)** Western blot analysis of total cell lysate from transfected HEK 293 cells. The SARS-CoV-2 spike protein is known to undergo post-translational processing and products corresponding to their respective sizes can be seen, as denoted by the arrows **C)** Bar graphs showing the abundance of the wild-type SARS-CoV-2 spike protein isolated from on-bead digestion. **D)** Fragmentation spectra of the wild-type peptide TQLPPAYTNSFTR and its substituent miscoded product, QQLPPAYTNSFTR. B and y ions are denoted in red and blue, respectively, while the substituted amino acid is denoted in orange. The difference in the m/z for the b_2-b_4 peaks between the wild-type peptide (top) and miscoded product (bottom) corresponds to a threonine to glutamine substitution. The dashed orange line indicates the shift in the mass of the b_2 ion. The nominal mass difference between threonine and glutamine is 27 Da. **E)** Bar graphs showing the abundance of TQLPPAYTNSFTR and its miscoded substituent, QQLPPAYTNSFTR. The miscoded peptide was not detected in samples m1Ψ-1 and m1Ψ-2. The relative peptide abundance is denoted above each pair **F)** Violin plots showing the distribution of relative peptide abundances for miscoded spike protein peptides translated from unmodified, Ψ-containing, or m1Ψ-containing mRNA. **G)** On the left is a schematic of the dual-luciferase reporter system used to assess miscoding frequency in HEK 293 cells. On the right are bar graphs showing normalized luminescence values for U, Ψ, and m1Ψ-containing mRNA. Plotted are the average values of three biological replicates with error bars representing the standard deviation around the mean. Unpaired t-tests did not show statistically significant differences in miscoding frequency between the U, Ψ, and m1Ψ-containing mRNA.

Unlike pseudouridine, N1-methylpseudouridine does not stabilize mismatches during RNA duplex formation

Our data on the error frequency by the ribosome during the decoding of Ψ implied that this modification stabilizes mismatches between the codon and anticodon while m1Ψ does not. This distinction between the two modified bases might be due to their interactions with the ribosome decoding center, in which Ψ is allowed to sample different conformations, while m1Ψ is sterically restricted to fewer conformations. Alternatively, the distinctions could arise from inherent differences between the two modifications, irrespective of the environment. Indeed, previous studies on Ψ suggest that its introduction increased that stability of UA, UG, and UU base pairs by 0.3-0.8 kcal/mol (Kierzek et al., 2014). Interestingly, Ψ was reported to stabilize mRNA structure regardless of the sequence context while the impact of m1Ψ on mRNA stability was dependent on the identity of its neighbors (Mauger et al., 2019), in agreement with the idea that the modifications differently alter RNA-duplex formation. As the effect of m1Ψ on mismatch stability remained unclear, we examined the effect of Ψ and m1Ψ on the stability of mismatched duplexes by measuring the melting-point temperatures (T_m) of duplex RNAs created by pairing our three model mRNAs with variants of their reverse complement. We initially generated 4 reverse complement RNAs, containing A, U, C, and G opposite to the nucleotide of interest. Consistent with earlier studies, Ψ was found to have no effect on the stability of the Watson-Crick UA base pair as we measured a T_m of 84.9°C for the UA duplex and a T_m of 84.8°C for the YA duplex (**Figure 5A**). By contrast, m1Ψ was found to decrease the T_m by more than 1°C (**Figure 5B**). More importantly, whereas Ψ increased that stability of all tested mismatches – especially for the UU pairing (T_m of ~79.5°C for UU compared to a T_m of > 81°C for YU) – m1Ψ significantly decreased their T_m by as much as by 3°C (**Figures 5A-D,**

Supplementary Figure 6A-D). These observations hint that stabilization of mismatched codon-anticodon pairings by Ψ may be the reason for the slight increase in near and non-cognate tRNA binding.

We also noticed that in addition to miscoding events that correspond to mismatches between Ψ and the aa-tRNA anticodon, we observed errors caused by mismatches that did not involve the modification itself but its neighbors (**Figure 3**). As a result, we speculated that Ψ stabilizes mismatches involving its neighbor bases. To test this hypothesis, we generated a reverse complement that, when paired with our model mRNA, harbored a GU mismatch 5' immediate to the modification. We found that Ψ increased the T_m of this neighbor-mismatched duplex by more than 1°C, whereas m1Ψ significantly decreased the T_m by more than 2°C (**Figure 5E, F**).

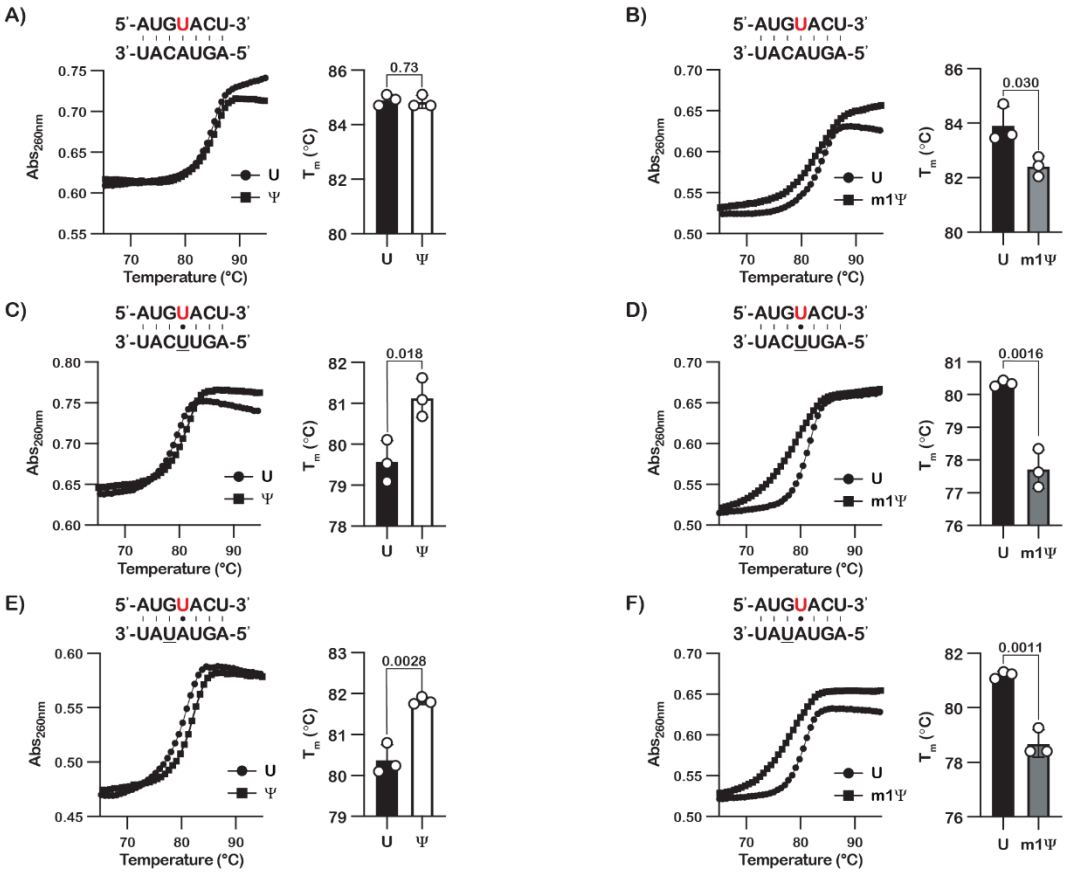

Figure 5: Pseudouridine stabilizes formation of mismatched RNA duplexes, including neighboring mismatches, whereas N1-methylpseudourdine does not.
A-F) Scatterplots showing the change in absorbance at 254 nm as a function of temperature for the indicated duplexes, with an accompanying bar graph showing the determined melting temperature for the same duplexes. Plotted are the means of three replicates with the error bars representing the standard deviation around the mean. P values are denoted above the bar graphs. **A, C, E)** correspond to duplexes containing Ψ while **B, D, F)** correspond to duplexes containing m1Ψ. The modified base is denoted in red.

Pseudouridine, but not N1-methylpseudouridine, increases errors by reverse transcriptases

Our data on the relative stability of mismatched duplexes containing Ψ and m1Ψ suggested that these modifications are likely to alter the accuracy of other processes which utilize RNA templates or nucleotide triphosphates (NTPs). Previous reports have documented increased error frequency during reverse transcription of RNAs containing Ψ (Potapov et al., 2018). Similarly, RNA polymerases were found to increase the frequency of misincorporation events when incorporating YTP instead of UTP (Potapov et al., 2018). It is worth noting, however, that

these studies used enzymatic reactions to generate the modified mRNA. Since the modification is likely to affect the accuracy of neighboring nucleotide incorporation during transcription, the source of error during reverse transcription could be ambiguous. Our model mRNAs bypass these issues since they only harbor a single modification that was synthetically incorporated. As a result, we could isolate the effects of the modifications on the error rate of reverse transcription (RT). To this end, we first investigated the effects of the modification on the accuracy of M-MLV reverse transcriptase using a primer-extension assay. A radiolabeled primer complementary to all bases upstream of the modified base was annealed to the three model mRNAs. Reverse transcription was initiated by adding either only one of the four canonical deoxynucleotide triphosphates (dNTPs), no dNTPs, or all four dNTPs. PAGE analysis of the resultant cDNA products revealed that uridine and its two substituents allowed for efficient incorporation of dAMP, as expected (**Figure 6A**). By contrast, and consistent with our analysis of duplex stability for Ψ-neighbor mismatches, a second event of dAMP incorporation was observed to occur more robustly for the Ψ-containing mRNA. Hence, even when correctly base paired with A, Ψ increases the misincorporation frequency downstream. Testing the incorporation of the other three nucleotides also allowed for a direct assessment of how the modifications alter mispairing frequency in the active site of the reverse transcriptase. As expected and consistent with earlier reports (Potapov et al., 2018), Ψ was found to increase the levels of misincorporation products, particularly those corresponding to U•C and U•T mismatches.

For reverse transcription of the mRNA containing m1Ψ, we also detected an increase in misincorporated products, albeit to a much lesser level compared to the mRNA containing Ψ. Interestingly, for RT reactions containing dTMP, we observed significant accumulation of high-

order cDNA products corresponding to 10-11 incorporation events only in the presence of the Ψ-containing mRNA, suggesting that the enzyme successfully crossed the stretch of adenosines in the mRNA template. In turn, this suggests that the enzyme was able to carry out three misincorporations of dTMP across Ψ, G, and U before successfully crossing the stretch of As. These observations add support to our proposal that Ψ dramatically affects the base pairing properties of its neighbors.

While the primer-extension assay above enabled the assessment of increased misincorporation events that occur on Ψ and m1Ψ, it did not enable quantification of the error rate of reverse transcription in the presence of all nucleotides. To quantify this error rate for each modification, we conducted deep sequencing of reverse transcription cDNA products for each mRNA. Briefly, an oligonucleotide linker was ligated to each of our model mRNAs and cDNA synthesis was carried out using a primer complementary to the ligated adapter. We used both Avian Myeloblastosis Virus (AMV) and Moloney Murine Leukemia Virus (M-MLV) reverse transcriptases for 1st-strand synthesis, as each RT is known to have distinct error profiles (Potapov et al., 2018). We attempted to amplify our cDNAs with primers containing unique molecular identifiers (UMIs) but were unable to do so. Instead, we proceeded with conventional deep sequencing and acquired between 10 to 15 million reads per sample. Reads were then processed to remove adapters and the linker from the 5' and 3' ends. Since we were unable to utilize UMIs to account for library amplification and sequencing artifacts, we processed our data as if searching for subclonal variants to better discriminate variation from sequencing error. To go about this, we mapped our processed reads to the reference sequence and searched for variants using deepSNV (Gerstung et al., 2014). While this method could not calculate a true error rate, it did provide clues as to how the modifications influence transcriptase error during

library construction. The Ψ and m1Ψ reads were compared to their corresponding U reads for each reaction. Interestingly, similar to the ribosome, reactions with the mRNA containing Ψ increased error frequency while reactions with the mRNA containing m1Ψ had a much lesser effect. For M-MLV, Ψ induced a greater incidence of T->A and T->G substitutions, as well as increasing the error rate of the upstream base from G->A (**Figure 6B**). m1Ψ induced a similar error profile but with frequencies that were an order of magnitude smaller (**Figure 6C**). Ψ also had similar effects on AMV reactions, albeit with lower frequencies than with M-MLV (**Figure 6D**). However, the same error profile was not observed in analysis of the AMV m1Ψ dataset, with none of the mentioned substitutions detected. Thus, our deep sequencing data corroborates our primer extension results, showing an increased rate of mutation from T to A and T to G, particularly for Ψ. This also explains why we observe higher molecular weight products when conducting primer extension assays with only TTP or CTP. The increased rate of G to A mutation in the preceding base, which is downstream to the modified base during reverse transcription, also supports the presence of the polyT products observed after gel electrophoresis. Likewise, the difference in error rates between Ψ and m1Ψ we saw in our sequencing data is consistent with differences in the frequency of misincorporated products that we observed in our primer extension assays.

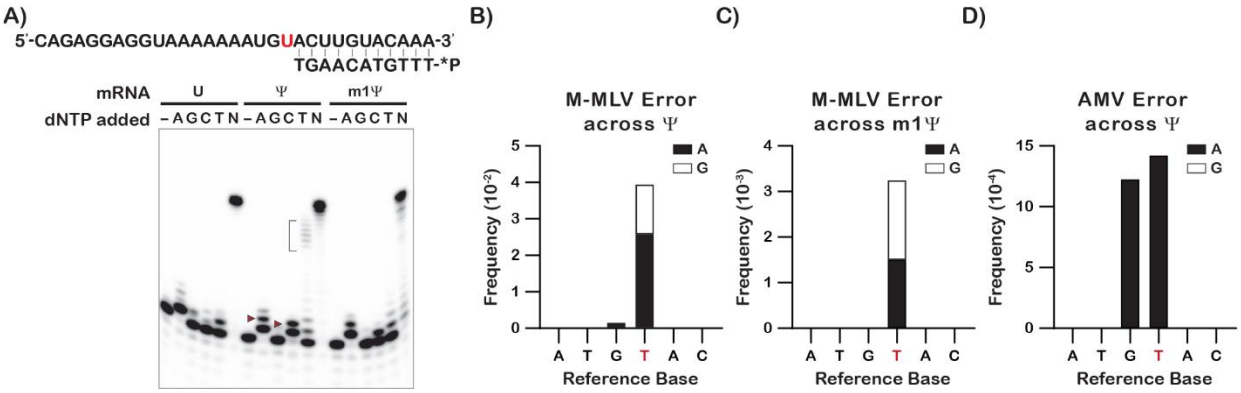

Figure 6: The fidelity of reverse transcriptase enzymes is altered in the presence of pseudouridine.
A) Phosphorimage of a denaturing urea gel used to follow primer extension by M-MLV in the presence of the indicated modified template and dNTP substrates. Shown is a representative gel of duplicates. **B)** Bar graphs showing the frequency of variant bases in the codon containing the modified base, as well as the previous codon, as detected by deep sequencing. Bars represent the sum of all variant frequencies, with the proportion for each variant denoted by color. Reference bases are shown below, with the modified base denoted in red. No variants in the two-codon window were detected as statistically significant for the AMV-reverse transcribed m1Ψ RNA.

Discussion

Here, we systemically characterized the effects of m1Ψ and Ψ on protein synthesis in well-defined in vitro systems and assessed whether these effects are relevant to the application of these modification in real-life examples, such as mRNA vaccines. We first investigated the effect of nucleotide modifications on the rate of peptide-bond formation in the context of our model mRNAs. We found m1Ψ to reduce the overall rate of peptide-bond formation in a bacterial reconstituted system (**Figure 2**). However, this decrease in k_{pep} did not seem to affect the overall yield of protein synthesis in eukaryotic cells or extracts (**Figure 4B, Supplementary Figure 4B, Supplementary Figure 5A)**. These results highlight an interesting pattern also seen with Ψ, where studies utilizing in vitro bacterial systems report a significant reduction for the rate of peptide-bond formation in the presence of the modification (Hoernes et al., 2016), whereas studies employing eukaryotic extracts document no decrease in the overall protein yield when modified RNA is used (Eyler et al., 2019; Hoernes et al., 2019). There are at least two non-mutually exclusive models that could explain this discrepancy between the bacterial system and eukaryotic cell-free extracts. Firstly, it is highly possible that even with the significant decrease in k_{pep}, translation remains rate limited by another step during initiation or elongation. Secondly, the overall elongation rate (including peptide-bond formation and translocation) of eukaryotic ribosomes has been estimated to be at least fourfold slower than that of bacterial ribosomes (Dennis and Bremer, 1974; Riba et al., 2019; Vogel and Jensen, 1994; Young and Bremer, 1976), suggesting that eukaryotic ribosomes may be less affected by changes to k_{pep}.

Regardless of whether or not the modifications slow translation , it has been shown that mRNAs harboring m1Ψ can produce as much as tenfold more protein compared to unmodified mRNAs (Andries et al., 2015; Parr et al., 2020; Svitkin et al., 2017). At least two mechanisms have

been proposed for this increased protein production: 1) unlike unmodified mRNAs, mRNAs with m1Ψ are more effective at evading Toll-like receptors (TLRs) (Andries et al., 2015), and 2) modified mRNAs mitigate PKR-mediated activation of the integrated stress response, which in turn prevents repression of translation initiation (Anderson et al., 2010; Svitkin et al., 2017).

We next assessed the effect of m1Ψ on the accuracy of tRNA selection by the ribosome by systematically examining all possible amino acid substitutions on our model mRNA templates (**Figure 3**). Unlike Ψ, which was found to increase the error frequency by several near- and non-cognate aa-tRNAs, m1Ψ did not increase the observed rates of amino acid misincorporation. The increased miscoding by the ribosome on a Ψ-modified UAC codon is similar to that recently reported by Eyler et al. with a Ψ-modified UUU codon (Eyler et al., 2019), suggesting that this effect is not sequence-context specific. However, we note that the increase in the error frequencies that we observed is relatively modest and not likely to contribute to aberrant-protein production. Indeed, LC-MS/MS analysis of SARS-CoV-2 spike protein produced from mRNAs containing Ψ and m1Ψ exhibited no detectable increase in miscoded protein in human cell culture, and only a modest increase in a wheat germ system (**Figure 4B, Supplementary Figure 4B, Supplementary Figure 5A**). Together, our observations indicate that m1Ψ maintains the fidelity of protein synthesis while Ψ can marginally decrease the accuracy of the ribosome depending on the conditions.

Interestingly, this distinction between Ψ and m1Ψ appears to be due to inherent differences between the two nucleotides and their base-pairing properties during duplex-RNA formation. Similar to other reports (Kierzek et al., 2014), Ψ was found to stabilize all tested mismatches, especially those involving uridine:pyrimidine base pairs, as assessed by UV-melt curve analysis (**Figure 5, Supplementary Figure 6**). Furthermore, the modification even stabilized duplexes

involving mismatches with its neighbor. By contrast, m1Ψ destabilized all tested mismatched duplexes.

This dissimilarity between the two modified bases in their ability to mispair during duplex RNA formation has ramifications beyond codon-anticodon interactions during protein synthesis. For example, it appears that only Ψ increases dNMP misincorporation by the reverse transcriptases M-MLV and AMV (**Figure 6A**). What is the structural basis for these differences between Ψ and m1Ψ? While our data do not directly address this question, others have proposed models rationalizing the ability of Ψ to stabilize duplex RNA (Davis, 1995; Deb et al., 2019; Hudson et al., 2013; Kierzek et al., 2014). A new imino proton becomes available when uridine is isomerized to Ψ – C5 of uridine is replaced with N1 of Ψ -- which gives Ψ two hydrogen-bond donors at N1 and N3. This means that Ψ is capable of forming equivalent hydrogen bond interactions with adenosine, for example, regardless of whether it adopts a typical *anti* conformation or the atypical *syn* conformation (**Figure 7**). Indeed, a Ψ:U mismatch can form two distinct structures with different hydrogen-bonding interactions (Kierzek et al., 2014). On the other hand, the introduction of a methyl group to N1 of m1Ψ disrupts the ability of N1 to donate a hydrogen bond, limiting the types of pairings that m1Ψ can form with other bases (**Figure 7**). Furthermore, better base stacking by Ψ has been suggested to play a role in its ability to stabilize RNA duplexes (Davis, 1995; Deb et al., 2019; Hudson et al., 2013; Kierzek et al., 2014) and as such, it is likely that m1Ψ is incapable of equivalent stacking interactions. Even so, the lack of a noticeable effect by m1Ψ on decoding and the superior in vivo characteristics of m1Ψ-modified mRNAs support usage of this modification in mRNA-based therapeutics.

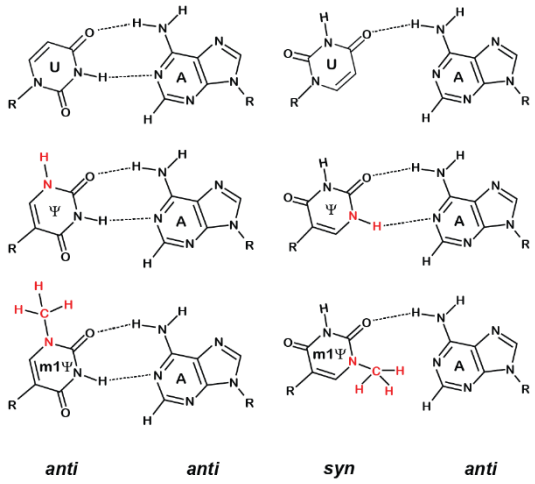

Figure 7: Ψ can form additional base pairing interactions with adenosine while m1Ψ cannot
U-A, Ψ-A, and m1Ψ-A base pairs shown in either the anti-anti (left) or syn-anti (right) conformation.

Limitations of the Study

Here we utilized a multidisciplinary approach to study the effects of the mRNA modification N1-methylpseudouridine on the decoding process by the ribosome, as well as on cDNA synthesis by reverse transcriptases. However, our approach does have some limitations. For instance, although the use of the bacterial reconstituted system allowed us to systematically examine how mRNA modifications alter the tRNA selection by the ribosome, our observations may not be completely reflective of occurrences during translation in eukaryotes. In addition, the task of detecting miscoded peptides by mass spectrometry is a difficult one. We focused our analysis to those miscoded peptides detected with high confidence to investigate how the modifications affect translational fidelity in a clinically relevant manner. As such, we may have missed other miscoded peptides due to complexities with peak assignment for low-frequency events. Although such rare events would have minimal impact on application of the modification in therapeutics, more extended characterization of these events may shed insights on how the modification impacts local RNA structure on the ribosome.

Acknowledgements

We thank the lab of Dr. Roberto Galletto for their assistance in obtaining the UV-melt data. We thank the Alvin J. Siteman Cancer Center at Washington University School of Medicine and Barnes-Jewish Hospital in St. Louis, MO. and the Institute of Clinical and Translational Sciences (ICTS) at Washington University in St. Louis, for the use of the Genome Technology Access Center, which provided sequencing services. The Siteman Cancer Center is supported in part by an NCI Cancer Center Support Grant #P30 CA091842 and the ICTS is funded by the National Institutes of Health's NCATS Clinical and Translational Science Award (CTSA) program grant #UL1 TR002345. This work was supported by a grant from the National Institutes of Health to H.S.Z. (R01GM141474).

Author Contributions

K.Q.K., B.D.B., S.C.T., C.J., C.J., J.Z., L.L.Ψ, S.D., and H.S.Z. carried out the experimental work. K.Q.K. and H.S.Z. conceived the work. K.Q.K., B.D.B., R.D.V. and H.S.Z. wrote the manuscript. H.S.Z. supervised the work.

Data and code availability

The mass spectrometry data are available in the ProteomeXchange database under accession number PXD029291. The reverse transcriptase sequencing data is available at GEO under accession number GSE186464. Both are publicly available as of the date of publication and accession numbers are listed in the key resources table. Source data and original western blots and phosphorimages have been deposited at Mendeley at https://dx.doi.org/10.17632/9jv472yv2c.1.

Experimental Model And Subject Details

Cell culture conditions

Flp-In T-REx 293 cells (Thermo Fischer) were cultured using standard protocols in Dulbecco's modified Eagle's medium (DMEM) (Gibco) and supplemented with 10% heat-inactivated FBS (Gibco), 1 × Penicillin-Streptomycin-Glutamine (Gibco) and 1 × MEM Non-Essential Amino Acids (Gibco). Cells were tested for mycoplasma contamination using the Universal Mycoplasma Detection Kit (ATCC) every 6 months.

Method Details

Purification of *E. coli* ribosomes and translation factors

70S tight-couple ribosomes were purified from Escherichia coli MRE600 (ATCC29417) as described (Moazed and Noller, 1986). Translation factors were purified as previously described (Zaher and Green, 2009).

mRNAs used for assays

Unmodified control mRNA (5' CAGAGGAGGUAAAAAA AUG UAC UUG UACAAA 3'; coding sequence underlined) was purchased from Millipore Sigma. Modified mRNAs containing Ψ (5' CAGAGGAGGUAAAAAA AUG ΨAC UUG UACAAA 3') and m1Ψ (5' CAGAGGAGGUAAAAAA AUG m1ΨAC UUG UACAAA 3') were purchased from Dharmacon and GeneLink, respectively.

Validation of RNA modifications by liquid chromatography-mass spectrometry/mass spectrometry

Free adenosine, guanosine, and cytosine standards were purchased from Acros Organics and uridine was purchased from Tokyo Chemical Industry. To generate Ψ and m1Ψ standards, 50

nmol of UTP (NEB), YTP (ApexBio), and m1ΨTP (ApexBio) were diluted to a final volume of 25 μL in 100 mM Tris pH 7.5 buffer and incubated with 10 U of calf intestinal alkaline phosphatase (CIP; NEB) at 37°C for 4 hours. For analysis of the synthetic RNA, 1 nmol of synthetic RNA was digested by nuclease P1 (Millipore Sigma, 10 Units) at 50 °C for 150 minutes. Afterwards, Tris pH 7.5 was added to a final concentration of 100 mM to adjust the pH and 10 U of CIP was added. The reaction was incubated at 37 °C for an additional 90 minutes to dephosphorylate the nucleotide 5′-monophosophates. For all reactions treated with CIP, the resulting nucleosides were filtered using a 0.22 μm pore size syringe filter. To run each sample, 10 μL was loaded onto a Zorbax Eclipse Plus C18 column (2.1 × 50 mm, 1.8 micron) paired with an Agilent 6490 QQQ triple-quadrupole LC mass spectrometer. Runs were analyzed using multiple-reaction monitoring in positive-ion mode. The transitions used were: 268.1→136 (A), 244.1→112 (C), 284.2→152 (G), 245.1→113 (U), 245.1→125 (Ψ), 259.1→139 (m1Ψ).

Charging of tRNAs

f-[^{35}S]-Met-tRNA^{fMet} was prepared as previously described (Walker and Fredrick, 2008). The remaining tRNAs were aminoacylated by incubating 150 μM total RNA mix (Roche) with 0.4 mM of the appropriate amino acid, ~5 μM tRNA synthetase, and 2 mM ATP in charging buffer (100 mM K-HEPES pH 7.6, 20 mM $MgCl_2$, 10 mM KCl, and 1 mM DTT) at 37°C for 30 minutes. Aminoacylated tRNAs were then purified by phenol/chloroform extraction, ethanol precipitated, and resuspended in aa-tRNA buffer (20 mM KOAc pH 5.2 and 1 mM DTT).

Formation of ribosome initiation complexes

Initiation complexes (IC) were prepared as previously described (Pierson et al., 2016). Briefly, 2 μM 70S ribosomes, 3 μM of each IF1, IF2, IF3, [^{35}S]-fMet-tRNA^{fMet}, 2 mM GTP, and 6 μM of mRNA was incubated in 1 × polymix buffer (Jelenc and Kurland, 1979) (95 mM KCl, 5 mM

NH_4Cl, 5 mM $Mg(OAc)_2$, 0.5 mM $CaCl_2$, 8 mM putrescine, 1 mM spermidine, 10 mM K_2HPO_4 pH 7.5, 1 mM DTT) at 37°C for 30 minutes. Initiation complexes were then isolated via centrifugation over sucrose cushion (composed of 1.1 M sucrose, 20 mM Tris-HCl pH 7.5, 500 mM NH_4Cl, 0.5 mM EDTA, and 10 mM $MgCl_2$) for 2 hr at 287,000 × g at 4°C. Resultant pellets were resuspended in 1 × polymix buffer and stored at -80°C. The radioactivity of the resuspended pellet was compared to input radioactivity in order to determine the concentration of the prepared IC.

Kinetics of peptidyl transfer

To prepare ternary complexes, EF-Tu, and GTP were incubated for 15 minutes at 37°C. aa-tRNA was added to the mixture, and the resulting ternary complex was incubated for an additional 15 minutes. The final concentration of EF-Tu, GTP, and aa-tRNA was 30 μM, 2 mM, and ~5 μM, respectively. Kinetics of peptidyl transfer was performed by mixing equivalent volume of IC (1 μM) and TC at 37°C; either manually or using an RQF-3 quench flow instrument, depending on how fast the reaction was. The reaction was stopped at different time points using KOH to a final concentration of 500 mM. Dipeptide products were separated on cellulose TLC plates by electrophoresis in pyridine acetate at pH 2.8 (Youngman et al., 2004). The TLC plates were exposed to a phosphor screen overnight and the screens were imaged using a GE Typhoon scanner. All reactions were done in triplicate.

fMet release assay

Peptide release assays were performed in polymix buffer at 37°C. Equal volumes of initiation complexes and methylated release factor (either RF1 or RF2) (Pierson et al., 2016) were mixed to a final concentration of 0.5 μM and 10 μM, respectively. The reaction was stopped by adding twice the volume of the reaction of 50 mM sodium acetate pH 5.0 containing 40 mM EDTA at

varying time points. Released f-[^{35}S]-Met was separated from f-[^{35}S]-Met-tRNA^{fMet} by electrophoretic TLC and imaged via phosphorimaging as above. All reactions were done in triplicate.

In vitro transcription of Pfizer spike protein mRNA

The sequence corresponding to the complete BNT162b2 mRNA Covid-19 vaccine (Pfizer) was modified to encode a SARS-CoV-2 spike protein with an N-terminal His tag and a C-terminal FLAG tag. The rest of the CDS sequence, the 5'-UTR, 3'-UTR, and the polyA sequence remained unchanged (**Table S1**). A plasmid containing the entire sequence under a T7 promoter was synthesized by GenScript and the sequence was verified using Sanger sequencing. The DNA template for in vitro transcription was generated by PCR amplification using primers described in **Table S1**. Capped mRNAs were generated using the MEGAscript T7 Kit (Thermo Fisher Scientific) according to manufacturer's instructions, except that GTP concentration was reduced from 7.5 mM to 1.5 mM and cap analogue 3´-O-Me-m7G(5')ppp(5')G (NEB) was added to a final concertation of 6 mM. To generate Ψ and m1Ψ-modified mRNAs, UTP was substituted with YTP or m1ΨTP, respectively. Following transcription, mRNAs were purified using the LiAC method per manufacturer's instructions, and their integrity assessed using denaturing formaldehyde agarose electrophoresis (Sambrook and Russell, 2006).

Expression and purification of spike protein in HEK 293 cells

90% confluent cells were washed with 1 × PBS, harvested, and resuspended in 1 × PBS at a density of ~2 × 10^7 cells/mL. 5 mg of RNA or 4 mg of pCDNA5-EGFP was mixed with 100 mL of cells. Electroporation was carried out using a Neon Transfection System (Thermo Fisher Scientific) as per manufacturer's instructions. Following electroporation, cells were allowed to

recover in 1 mL DMEM media with 10% FBS without antibiotics for 30 minutes at 37°C, before plating them on a 10 cm dish and incubating an additional 24 hours at 37°C. Media was then removed and cells were collected in 10 mL conical tubes, washed with PBS, and lysed in 1 mL of FLAG-IP buffer (50 mM HEPES pH 7.5, 0.3 M KCl, 10% glycerol, 0.5% Triton, 1 mM EDTA, 0.5 mM DTT and supplemented with protease inhibitor from Gold Biotechnology). 20 mL was used for western-blot analysis and the rest was flash frozen in liquid nitrogen. For purification, the lysate was thawed on ice and applied to 100 µL of anti-FLAG magnetic beads (Millipore Sigma). The beads were washed 5 times with FLAG-IP buffer without detergent and stored at -80°C prior to on-bead trypsin digest. All reactions were done in triplicate.

On-bead digestion and LC-MS/MS analysis of spike protein produced in HEK 293 cells

Beads were reduced with 10 mM TCEP and alkylated with 25 mM Iodoacetamide, followed by digestion with trypsin at 37°C overnight. The digest was separated from the beads using a magnetic stand and acidified with 1% TFA before being cleaned up with C18 tip. The extracted peptides were dried down and each sample was resuspended in 10 µL 5% ACN/0.1% FA. 5 µL was analyzed by LC-MS using a Dionex RSLCnano HPLC coupled to a Orbitrap Fusion Lumos mass spectrometer (Thermo Fisher Scientific) using a 2-hour gradient. Peptides were resolved using a 75 µm × 50 cm PepMap C18 column (Thermo Fisher Scientific).

Peptides were eluted at 300 nL/min from a 75 µm x 50 cm PepMap C18 column (Thermo Fisher Scientific) using the following gradient: time = 0–4 min, 2% B isocratic; 4–8 min, 2–10% B; 8–83 min, 10–25% B; 83–97 min, 25–50% B; 97–105 min, 50–98% B. Mobile phase A consisted of 0.1% formic acid and mobile phase B consisted of 0.1% formic acid in acetonitrile. The instrument was operated in data-dependent acquisition mode in which each MS1 scan was

followed by higher-energy collisional dissociation (HCD) of as many precursor ions in a 2 second cycle (top speed method). The mass range for the MS1 done using the FTMS was 365 to 1800 m/z with resolving power set to 60,000 @ 400 m/z and the automatic gain control (AGC) target set to 1,000,000 ions with a maximum fill time of 100 ms. The selected precursors were fragmented in the ion trap using an isolation window of 1.5 m/z, an AGC target value of 10,000 ions, a maximum fill time of 100 ms, a normalized collision energy of 35, and activation time of 30 ms. Dynamic exclusion was performed with a repeat count of 1, exclusion duration of 30 s, and a minimum MS ion count for triggering MS/MS set to 5000 counts.

Identification of amino acid substitutions in the HEK 293 dataset

Two strategies were utilized to identify possible miscoded peptides. In the first approach, raw MS files were searched using the MASCOT search engine (version 2.5) against the Pfizer spike protein sequence using an error-tolerant search allowing for all amino acid substitutions. Mascot search parameters included Trypsin/P specificity, up to 2 missed cleavages, a fragment ion mass tolerance of 0.60 Da and a parent ion tolerance of 10 ppm, and variable modifications of carbamidomethyl cysteine and oxidized methionine. In the second approach, raw MS files were searched against an in silico generated SARS-CoV-2 spike protein library consisting of every possible single substitution protein product arising from a miscoding event at each uridine in the sequence. Searches against the computationally generated library with the Mascot search engine were launched in Proteome Discoverer (version 2.4) using the same parameters as the first approach. The sequences of candidate miscoded peptides identified from both methods, as determined by greater than 90% peptide probability in Scaffold (version 4.8.2) with Mascot Ion Score > 15, were concatenated to a mock sequence for a final confirmation search. The final search was performed using the MASCOT search engine launched in Proteome Discoverer

against the Human reference proteome (Uniprot.org, downloaded 05/2019) modified to include the mock sequence and the wild-type Pfizer spike protein sequence. Mascot results of the final search were loaded into Skyline-daily (University of Washington, version 20) to check proper peak picking for each peptide of interest. Each peak was manually inspected for good fragment ion coverage and elution times in line with the MS/MS identification time of the peptide. The sum of the top 3 isotopes were then exported for each wild-type and miscoded peptide for further analysis.

Dual-luciferase reporter assays in HEK 293 cells

Dual-luciferase reporter mRNAs were transcribed in vitro using the same method as for the spike protein mRNA. The AAA codon coding for K529 was mutated to AAU using site-directed mutagenesis. RNAs were electroporated into HEK 293 cells using a similar method as for the spike protein mRNA, except cells were cultured in 6-well plates instead of dishes and RNA amounts were scaled down accordingly. After recovery, cells were lysed using passive lysis buffer (Promega) and luminescence was measured using the Dual-Luciferase Reporter Assay System (Promega) on a Tecan plate reader equipped with an automated injection system. All reactions were done in triplicate.

In vitro translation of spike protein using wheat germ extracts

Wheat-germ extracts were purchased from Promega and used per manufacturer's instructions. For ^{35}S-incorporation assays, translation reactions (10 μL volume) were initiated in the presence of 6 mCi of EasyTag™ L-[35S]-Methionine (Perkin Elmer). Reactions were stopped by adding an equivalent volume of HU buffer (8 M Urea, 5% SDS, 200 mM Tris pH 6.8, 100 mM DTT). Protein products were resolved using 8% SDS PAGE and transferred to a PVDF membrane using a semi-dry transfer apparatus (Bio-Rad). Protein products were visualized using

phosphorimaging as described earlier. The PVDF membrane was then subjected to immunoblotting using anti-FLAG (Millipore Sigma) and anti-Renilla luciferase (Millipore Sigma) antibodies.

For spike protein purification from wheat-germ extracts, the reaction volume was increased to 400 µL and unlabeled methionine was used. Following incubation, the reaction was diluted to 5 mL in FLAG-IP buffer and incubated with 50 µL of prewashed anti-FLAG Agarose beads (Millipore Sigma) for 3 hours at 4°C. Beads were washed 4 times with FLAG-IP buffer in spin columns. Bound proteins were eluted using HU buffer and resolved on 8% SDS PAGE. The bands corresponding to the size of spike protein were cut and subjected to in-gel trypsin digestion. All reactions were done in duplicate.

In-gel digestion and LC-MS/MS analysis of spike protein produced in wheat germ extracts

Coomassie-stained gel bands containing the spike protein were excised and cut into smaller pieces. Gel slices were destained twice with 25 mM ammonium bicarbonate in 50% acetonitrile for 30 minutes at 37°C. Gel slices were then reduced with 50 mM DTT in 50 mM ammonium bicarbonate at 60°C for 10 minutes, followed by alkylation with 200 mM chloroacetamide in 50 mM ammonium bicarbonate in the dark at room temperature for 1 hour. Gel slices were washed twice with 25 mM ammonium bicarbonate in 50% acetonitrile for 30 minutes at 37°C and then dehydrated with 100% acetonitrile for 10 minutes at room temperature. Excess solvent was removed by speed-vacuum. After dehydration, gel slices were rehydrated in a solution of 0.01 mg/ml trypsin in 100 mM ammonium bicarbonate and digested for 16 hours at 37°C. Digested peptides were extracted using a 50% acetonitrile, 0.1% trifluoracetic acid solution by incubation at 37°C for 10 minutes. The extraction process was repeated two additional times and the three extractions were pooled with the digest solution. Samples were dried completely in a speed-

vacuum and resuspended in ~0.1-1% trifluoroacetic acid to achieve a pH of ~3. Samples were then concentrated and desalted using OMIX C18 pipette tips (Agilent) and eluted with a 0.1% acetic acid, 75% acetonitrile solution.

Prepared peptides were analyzed with a Q-Exactive Plus mass spectrometer (Thermo Fisher Scientific) after reversed-phase nano-HPLC separation with a 25-cm analytical C18 resin column (Acclaim PepMap RSLC; Thermo Fisher Scientific) and a 5 to 95% acetonitrile step gradient in 0.1% formic acid (FA) at a flow rate of 250 nL/min for 70 min. The mass spectrometer was operated in the data-dependent mode to automatically switch between full-scan MS and MS/MS acquisition. Data-dependent acquisitions were obtained using Xcalibur 4.0 software in positive-ion mode. MS1 spectra were measured at a resolution of 70,000 with an automatic gain control of 1 × 106, a maximum ion time of 40 msec, and a mass range of 300-1,800 m/z. Up to 12 MS2 scans, with a charge state of 2 to 4, were triggered at a resolution of 17,500, an automatic gain control of 5 × 105 with a maximum ion time of 120 msec, a 1.6-m/z isolation window, and a normalized collision energy of 28. MS1 scans that triggered MS2 scans were dynamically excluded for 30 sec.

Identification of amino acid substitutions in the wheat germ extract dataset

The resulting MS data sets were searched against an artificially generated SARS-COV-2 spike protein database, consisting of every possible single substitution product arising from a miscoding event at each uridine in the sequence, using Proteome Discoverer (version 2.5.0.400; Thermo Fisher Scientific) and a list of common protein contaminants. Peptides were assigned by SEQUEST HT, allowing a maximum of two missed tryptic cleavages, a minimum peptide length of 6, a precursor mass tolerance of 10 ppm, and fragment mass tolerances of 0.02 Da. Carbamidomethylation of Cys and oxidation of Met were specified as static and dynamic

modifications, respectively. Only peptides where both the wild-type peptide and the substitution product were detected were further analyzed.

Duplex-RNA melting analysis

A Varian Cary-100 spectrophotometer with a Peltier-controlled cuvette holder was used to monitor the change in absorbance at a wavelength of 260 nm. RNAs were first annealed in a reaction containing equal molarities of each RNA, calculated from optical density measurements and absorbance values at 260 nm, with the goal of having a final absorbance value for the annealed RNA of about 0.5-0.6 at room temperature. RNAs were heated in water to 80°C for 5 minutes to denature. They were then cooled to room temperature and buffer was added to a final concentration of 50 mM Tris-HCl, 100 mM NaCl, 10 mM $MgCl_2$ pH 7.9. Annealed RNAs were then incubated for 3 minutes at the starting temperature of 40°C in the Varian Cary-100 spectrophotometer. Following incubation, the temperature ramp was set to 1°C/min and absorbance values were measured in 0.2°C increments until the final temperature of 96°C was reached. All assays were done in triplicate.

Primer-Extension Assays

50 nmol of primer was 5'-end labeled using ~70 mCi [γ-^{32}P] ATP (6000 Ci/mmol) and T4 polynucleotide kinase (PNK) in a total reaction volume of 10 μL. The reaction was incubated at 37°C for 30 minutes, and then at 65°C for 15 minutes to inactivate PNK before diluting to a final volume of 50 μL. Radiolabeled primer and synthetic RNA, at ~70 nM and ~4 uM, respectively, were reverse transcribed with Promega M-MLV according to manufacturer instructions, using the radiolabeled primer and only providing a single deoxy nucleotide triphosphate (either adenosine, guanosine, cytosine, or thymidine), no dNTPs, or all four dNTPs. Samples were

separated by urea denaturing polyacrylamide gel electrophoresis and imaged on a GE Typhoon scanner. All reactions were done in duplicate.

cDNA library generation for high-throughput sequencing

We used a short-RNA cloning protocol similar to the one used for ribosome profiling (Ingolia et al., 2009). Briefly, ~100 pmole of the synthetic mRNAs used in our reconstituted translation reactions (unmodified, pseudouridine-containing, and N1-methylpseudouridine-containing) were ligated to 150 pmole of short adenylated DNA oligonucleotide, 5′rAppCTGTAGGCACCATCAAT/3ddC/3′, at their 3′ end using truncated T4 RNA ligase 2 (NEB) in a total volume of 10 μL. The ligated products were purified using denaturing urea PAGE and subjected to reverse transcription using M-MLV (Promega) or AMV (Promega) enzymes and RS-1 primer (/5Phos/AGATCGGAAGAGCGTCGTGTAGGGAAAGAGT GTAGATCTCGGTGGTCGC/iSp18/CACTCA/iSp18/TTCAGACGTGTGCTCTTCCGATCTA TTGATGGTGCCTACAG). Following PAGE purification, cDNA products were circularized using CircLigase kit (Epicentre). Pilot PCR was then used to determine the optimal numbers of cycles required to amplify the cDNA. Following PCR amplification with unique barcoded primers, the DNA libraries were purified using native PAGE and then analyzed for length and purity using Agilent Bioanalyzer.

Sequencing and bioinformatic analysis

Prepared cDNAs were sequenced as paired 75-nt NextSeq runs at the Genome Technology Access Center (GTAC) of Washington University in St. Louis. Samples were demultiplexed based on their 6-nt barcode and checked for initial quality using FastQC (Andrews et al., 2010). Overhangs from each paired end set were removed, such that only consensus sequence between each mate pair remained, and then merged to form a single consensus read using NGmerge

(Gaspar, 2018). Stitched reads were processed with Cutadapt (Martin, 2011) to remove the 17-nt linker sequence and any reads not containing the linker sequence were discarded. Reads were mapped to the unmodified control RNA sequence using BBMap (Bushnell and Work, 2014) in local mode with "very slow" settings. Mapped sam files were sorted, converted to the bam format, and indexed using Samtools. Reads were analyzed using deepSNV (Gerstung et al., 2014), with only mapped reads having high mapping quality (MAPQ >= 20 out of 41) and high-quality bases (Q >= 30) counted. Error rates for the nucleotides surrounding the modification (A T G X A C, where X is the modified nucleotide) were analyzed. Deletions were ignored as they appeared to be an artifact of sequencing; deletions were completely absent when mapping quality filter was set to >=25.

Quantification And Statistical Analysis

Quantification of RNA modifications

The presence of modified nucleosides in the synthetic RNAs was checked by comparing retention times and nucleoside to base ion mass transitions to those of the standards. The nucleoside composition of each synthetic RNA was calculated using the diode array detector (DAD) signal intensities as follows: the integrated peak area of each nucleoside in the synthetic RNA (A, U, C, and G) was compared to the peak area of one of the other nucleosides in the synthetic RNA, and then normalized to the corresponding ratio of areas in the standards (eg. $\frac{\frac{\mathrm{A}_{synth}}{\mathrm{U}_{synth}}}{\frac{\mathrm{A}_{standard}}{\mathrm{U}_{standard}}}$). The normalized value was then multiplied by the reference count (A: 15, U: 6, C: 3, G: 7) to generate a count value. The process was repeated for the other two nucleoside comparisons and the average of the three counts was used as the final count for each nucleoside.

Pseudouridine co-eluted with cytidine, which is reflected in the loss of a U and a gain of a C for the ΨAC mRNA.

Analysis of peptidyl transfer kinetics and fMet release assays

Imaged phosphor screens were quantified using Image Lab (Bio-Rad). Fractional radioactivity corresponding to the dipeptides were plotted against time, and observed rates and endpoints were determined using a one-phase association equation in Prism (GraphPad). Differences in observed rates and endpoints were tested for statistical significance using an unpaired t test in Prism.

Quantification of spike protein in HEK 293 cells

Spike protein abundances for on-bead digestion were calculated using the label-free quantitation values for detected wild-type spike protein. Western blot quantification was done by normalizing the FLAG signal to actin signal using ImageQuant (Cytiva). Differences in normalized signal were tested for statistical significance by one-way ANOVA in Prism (GraphPad).

Quantification of amino acid substitutions in the HEK 293 dataset

Relative abundance was calculated by comparing the label-free quantitation value of each miscoded peptide to the value of the parent, faithful peptide, as determined by manual peak picking in Skyline. Only those peptides where both the wild-type and the miscoded species were detected were quantified.

Analysis of dual-luciferase reporter assays in HEK 293 cells

Firefly luminescence values were normalized to corresponding in-frame, unaltered Renilla luminescence values. Differences between normalized values were tested for statistical significance using an unpaired t test in Prism (GraphPad).

Quantification of amino acid substitutions in the wheat germ extract dataset

Relative abundance was calculated by comparing the label-free quantitation value of each miscoded peptide to the value of the parent, faithful peptide. In the event only one of the technical replicate values for a peptide was missing, quantitation values were log2 transformed and the missing values imputed using a maximum likelihood-based method from the MSnbase R package (Gatto and Lilley, 2012; Gatto et al., 2021).

Duplex-RNA melting point determination

To determine the melting point, absorbance values were first normalized to the initial absorbance value. The first derivative of the data was calculated and fit to a Gaussian function to find the peak, which corresponds to the melting point of the duplex, using Prism (GraphPad). Differences in melting point were tested for statistical significance using an unpaired t-test in Prism (GraphPad).

References

1. Adachi, H., and Yu, Y.T. (2020). Pseudouridine-mediated stop codon readthrough in s. cerevisiae is sequence context–independent. Rna *26*, 1247–1256.
2. Akira, S., Uematsu, S., and Takeuchi, O. (2006). Pathogen recognition and innate immunity. Cell *124*, 783–801.
3. Anderson, B.R., Muramatsu, H., Nallagatla, S.R., Bevilacqua, P.C., Sansing, L.H., Weissman, D., and Karikó, K. (2010). Incorporation of pseudouridine into mRNA enhances translation by diminishing PKR activation. Nucleic Acids Res. *38*, 5884–5892.
4. Andrews, S., Krueger, F., Segonds-Pichon, A., Biggins, L., Krueger, C., and Wingett, S. (2010). FastQC.
5. Andries, O., Mc Cafferty, S., De Smedt, S.C., Weiss, R., Sanders, N.N., and Kitada, T. (2015). N1-methylpseudouridine-incorporated mRNA outperforms pseudouridine-incorporated mRNA by providing enhanced protein expression and reduced immunogenicity in mammalian cell lines and mice. J. Control. Release *217*, 337–344.
6. Baden, L.R., El Sahly, H.M., Essink, B., Kotloff, K., Frey, S., Novak, R., Diemert, D., Spector, S.A., Rouphael, N., Creech, C.B., et al. (2021). Efficacy and Safety of the mRNA-1273 SARS-CoV-2 Vaccine. N. Engl. J. Med. *384*, 403–416.
7. Baronti, L., Karlsson, H., Marušič, M., and Petzold, K. (2018). A guide to large-scale RNA sample preparation. Anal. Bioanal. Chem. *410*, 3239–3252.
8. Bushnell, B., and Work, R. (2014). BBMap : A Fast, Accurate, Splice-Aware Aligner. 3–5.
9. Damase, T.R., Sukhovershin, R., Boada, C., Taraballi, F., Pettigrew, R.I., and Cooke, J.P. (2021). The Limitless Future of RNA Therapeutics. Front. Bioeng. Biotechnol. *9*, 1–24.
10. Davis, D.R. (1995). Stabilization of RNA stacking by pseudouridine. Nucleic Acids Res. *23*,

5020–5026.

11. Deb, I., Popenda, Ł., Sarzyńska, J., Małgowska, M., Lahiri, A., Gdaniec, Z., and Kierzek, R. (2019). Computational and NMR studies of RNA duplexes with an internal pseudouridine-adenosine base pair. Sci. Rep. *9*, 1–13.
12. Dennis, P.P., and Bremer, H. (1974). Differential rate of ribosomal protein synthesis in Escherichia coli B/r. J. Mol. Biol. *84*, 407–422.
13. Eyler, D.E., Franco, M.K., Batool, Z., Wu, M.Z., Dubuke, M.L., Dobosz-Bartoszek, M., Jones, J.D., Polikanov, Y.S., Roy, B., and Koutmou, K.S. (2019). Pseudouridinylation of mRNA coding sequences alters translation. Proc. Natl. Acad. Sci. U. S. A. *116*, 23068–23074.
14. Fernández, I.S., Ng, C.L., Kelley, A.C., Wu, G., Yu, Y.T., and Ramakrishnan, V. (2013). Unusual base pairing during the decoding of a stop codon by the ribosome. Nature *500*, 107–110.
15. Freund, I., Eigenbrod, T., Helm, M., and Dalpke, A.H. (2019). RNA modifications modulate activation of innate toll-like receptors. Genes (Basel). *10*.
16. Gaspar, J.M. (2018). NGmerge: merging paired-end reads via novel empirically-derived models of sequencing errors. BMC Bioinformatics *19*, 536.
17. Gatto, L., and Lilley, K.S. (2012). MSnbase-an R/Bioconductor package for isobaric tagged mass spectrometry data visualization, processing and quantitation. Bioinformatics *28*, 288–289.
18. Gatto, L., Gibb, S., and Rainer, J. (2021). MSnbase, Efficient and Elegant R-Based Processing and Visualization of Raw Mass Spectrometry Data. J. Proteome Res. *20*, 1063–1069.

19. Gerstung, M., Papaemmanuil, E., and Campbell, P.J. (2014). Subclonal variant calling with multiple samples and prior knowledge. Bioinformatics *30*, 1198–1204.

20. Guan, S., and Rosenecker, J. (2017). Nanotechnologies in delivery of mRNA therapeutics using nonviral vector-based delivery systems. Gene Ther. *24*, 133–143.

21. Van Hoecke, L., and Roose, K. (2019). How mRNA therapeutics are entering the monoclonal antibody field. J. Transl. Med. *17*, 1–14.

22. Hoernes, T.P., Clementi, N., Faserl, K., Glasner, H., Breuker, K., Lindner, H., Hüttenhofer, A., and Erlacher, M.D. (2016). Nucleotide modifications within bacterial messenger RNAs regulate their translation and are able to rewire the genetic code. Nucleic Acids Res. *44*, 852–862.

23. Hoernes, T.P., Heimdörfer, D., Köstner, D., Faserl, K., Nußbaumer, F., Plangger, R., Kreutz, C., Lindner, H., and Erlacher, M.D. (2019). Eukaryotic translation elongation is modulated by single natural nucleotide derivatives in the coding sequences of mRNAs. Genes (Basel). *10*, 1–12.

24. Hudson, G.A., Bloomingdale, R.J., and Znosko, B.M. (2013). Thermodynamic contribution and nearest-neighbor parameters of pseudouridine-adenosine base pairs in oligoribonucleotides. Rna *19*, 1474–1482.

25. Ingolia, N.T., Ghaemmaghami, S., Newman, J.R.S., and Weissman, J.S. (2009). Genome-wide analysis in vivo of translation with nucleotide resolution using ribosome profiling. Science (80-.). *324*, 218–223.

26. Jelenc, P.C., and Kurland, C.G. (1979). Nucleoside triphosphate regeneration decreases the frequency of translation errors. Proc. Natl. Acad. Sci. U. S. A. *76*, 3174–3178.

27. Jeong, D.-E., McCoy, M., Artiles, K., Ilbay, O., Fire, A., Nadeau, K., Park, H., Betts, B.,

Boyd, S., Hoh, R., et al. (2021). Assemblies-of-putative-SARS-CoV2-spike-encoding-mRNA-sequences-for-vaccines-BNT-162b2-and-mRNA-1273.

28. Jirikowski, G.F., Sanna, P.P., Maciejewski-Lenoir, D., Bloom, F.E., F., J.G., Paolo, S. Pietro, Dominique, M.-L., and E., B.F. (1992). Reversal of Diabetes Insipidus in Brattleboro Rats: Intrahypothalamic Injection of Vasopressin mRNA. Science *255*, 996–998.
29. Kaczmarek, J.C., Kowalski, P.S., and Anderson, D.G. (2017). Advances in the delivery of RNA therapeutics: from concept to clinical reality. Genome Med. *9*, 60.
30. Karijolich, J., and Yu, Y.T. (2011). Converting nonsense codons into sense codons by targeted pseudouridylation. Nature *474*, 395–399.
31. Karikó, K., Ni, H., Capodici, J., Lamphier, M., and Weissman, D. (2004). mRNA Is an Endogenous Ligand for Toll-like Receptor 3. J. Biol. Chem. *279*, 12542–12550.
32. Karikó, K., Buckstein, M., Ni, H., and Weissman, D. (2005). Suppression of RNA recognition by Toll-like receptors: The impact of nucleoside modification and the evolutionary origin of RNA. Immunity *23*, 165–175.
33. Karikó, K., Muramatsu, H., Welsh, F.A., Ludwig, J., Kato, H., Akira, S., and Weissman, D. (2008). Incorporation of pseudouridine into mRNA yields superior nonimmunogenic vector with increased translational capacity and biological stability. Mol. Ther. *16*, 1833–1840.
34. Karikó, K., Muramatsu, H., Ludwig, J., and Weissman, D. (2011). Generating the optimal mRNA for therapy: HPLC purification eliminates immune activation and improves translation of nucleoside-modified, protein-encoding mRNA. Nucleic Acids Res. *39*, 1–10.
35. Keedy, H.E., Thomas, E.N., and Zaher, H.S. (2018). Decoding on the ribosome depends on the structure of the mRNA phosphodiester backbone. Proc. Natl. Acad. Sci. U. S. A. *115*, E6731–E6740.

36. Kierzek, E., Malgowska, M., Lisowiec, J., Turner, D.H., Gdaniec, Z., and Kierzek, R. (2014). The contribution of pseudouridine to stabilities and structure of RNAs. Nucleic Acids Res. *42*, 3492–3501.

37. Kormann, M.S.D., Hasenpusch, G., Aneja, M.K., Nica, G., Flemmer, A.W., Herber-Jonat, S., Huppmann, M., Mays, L.E., Illenyi, M., Schams, A., et al. (2011). Expression of therapeutic proteins after delivery of chemically modified mRNA in mice. Nat. Biotechnol. *29*, 154–159.

38. Kramer, E.B., and Farabaugh, P.J. (2007). The frequency of translational misreading errors in E. coli is largely determined by tRNA competition. Rna *13*, 87–96.

39. Martin, M. (2011). Cutadapt removes adapter sequences from high-throughput sequencing reads. EMBnet.Journal *17*, 10.

40. Mauger, D.M., Joseph Cabral, B., Presnyak, V., Su, S. V., Reid, D.W., Goodman, B., Link, K., Khatwani, N., Reynders, J., Moore, M.J., et al. (2019). mRNA structure regulates protein expression through changes in functional half-life. Proc. Natl. Acad. Sci. U. S. A. *116*, 24075–24083.

41. Nir, R., Hoernes, T.P., Muramatsu, H., Faserl, K., Karikó, K., Erlacher, M.D., Sas-Chen, A., and Schwartz, S. (2022). A systematic dissection of determinants and consequences of snoRNA-guided pseudouridylation of human mRNA. Nucleic Acids Res. *50*, 4900–4916.

42. Ou, X., Liu, Y., Lei, X., Li, P., Mi, D., Ren, L., Guo, L., Guo, R., Chen, T., Hu, J., et al. (2020). Characterization of spike glycoprotein of SARS-CoV-2 on virus entry and its immune cross-reactivity with SARS-CoV. Nat. Commun. *11*.

43. Parr, C.J.C., Wada, S., Kotake, K., Kameda, S., Matsuura, S., Sakashita, S., Park, S., Sugiyama, H., Kuang, Y., and Saito, H. (2020). N 1-Methylpseudouridine substitution enhances the performance of synthetic mRNA switches in cells. Nucleic Acids Res. *48*, E35.

44. Pierson, W.E., Hoffer, E.D., Keedy, H.E., Simms, C.L., Dunham, C.M., and Zaher, H.S. (2016). Uniformity of Peptide Release Is Maintained by Methylation of Release Factors. Cell Rep. *17*, 11–18.

45. Polack, F.P., Thomas, S.J., Kitchin, N., Absalon, J., Gurtman, A., Lockhart, S., Perez, J.L., Pérez Marc, G., Moreira, E.D., Zerbini, C., et al. (2020). Safety and Efficacy of the BNT162b2 mRNA Covid-19 Vaccine. N. Engl. J. Med. *383*, 2603–2615.

46. Potapov, V., Fu, X., Dai, N., Corrêa, I.R., Tanner, N.A., and Ong, J.L. (2018). Base modifications affecting RNA polymerase and reverse transcriptase fidelity. Nucleic Acids Res. *46*, 5753–5763.

47. Riba, A., Nanni, N. Di, Mittal, N., Arhné, E., Schmidt, A., and Zavolan, M. (2019). Protein synthesis rates and ribosome occupancies reveal determinants of translation elongation rates. Proc. Natl. Acad. Sci. U. S. A. *116*, 15023–15032.

48. Sahin, U., Karikó, K., and Türeci, Ö. (2014). MRNA-based therapeutics-developing a new class of drugs. Nat. Rev. Drug Discov. *13*, 759–780.

49. Sambrook, J., and Russell, D.W. (2006). Separation of RNA According to Size: Electrophoresis of RNA through Agarose Gels Containing Formaldehyde. Cold Spring Harb. Protoc. *2006*, pdb.prot4050.

50. Simms, C.L., Hudson, B.H., Mosior, J.W., Rangwala, A.S., and Zaher, H.S. (2014). An Active Role for the Ribosome in Determining the Fate of Oxidized mRNA. Cell Rep. *9*, 1256–1264.

51. Svidritskiy, E., Madireddy, R., and Korostelev, A.A. (2016). Structural Basis for Translation Termination on a Pseudouridylated Stop Codon. J. Mol. Biol. *428*, 2228–2236.

52. Svitkin, Y. V., Cheng, Y.M., Chakraborty, T., Presnyak, V., John, M., and Sonenberg, N.

(2017). N1-methyl-pseudouridine in mRNA enhances translation through eIF2α-dependent and independent mechanisms by increasing ribosome density. Nucleic Acids Res. *45*, 6023–6036.

53. Vogel, U., and Jensen, K.F. (1994). The RNA chain elongation rate in Escherichia coli depends on the growth rate. J. Bacteriol. *176*, 2807–2813.

54. Walker, S.E., and Fredrick, K. (2008). Preparation and evaluation of acylated tRNAs. Methods *44*, 81–86.

55. Watanabe, Y., Allen, J.D., Wrapp, D., McLellan, J.S., and Crispin, M. (2020). Site-specific glycan analysis of the SARS-CoV-2 spike. Science (80-.). *369*, 330–333.

56. Weissman, D., Ni, H., Scales, D., Dude, A., Capodici, J., McGibney, K., Abdool, A., Isaacs, S.N., Cannon, G., and Karikó, K. (2000). HIV Gag mRNA Transfection of Dendritic Cells (DC) Delivers Encoded Antigen to MHC Class I and II Molecules, Causes DC Maturation, and Induces a Potent Human In Vitro Primary Immune Response. J. Immunol. *165*, 4710–4717.

57. Wolff, J.A., Malone, R.W., Williams, P., Chong, W., Acsadi, G., Jani, A., and Felgner, P.L. (1990). Direct gene transfer into mouse muscle in vivo. Science *247*, 1465–1468.

58. Young, R., and Bremer, H. (1976). Polypeptide-chain-elongation rate in Escherichia coli B/r as a function of growth rate. Biochem. J. *160*, 185–194.

59. Youngman, E.M., Brunelle, J.L., Kochaniak, A.B., and Green, R. (2004). The active site of the ribosome is composed of two layers of conserved nucleotides with distinct roles in peptide bond formation and peptide release. Cell *117*, 589–599.

60. Zaher, H.S., and Green, R. (2010). Hyperaccurate and Error-Prone Ribosomes Exploit Distinct Mechanisms during tRNA Selection. Mol. Cell *39*, 110–120.

61. Zhang, J., Ieong, K.W., Mellenius, H., and Ehrenberg, M. (2016). Proofreading neutralizes potential error hotspots in genetic code translation by transfer RNAs. Rna *22*, 896–904.

Supplementary Figures and Tables

Supplementary Table 1: Plasmids and primers used for in vitro transcription of spike protein and dual-luciferase reporter RNAs

Plasmid and primers used to make the DNA template for in vitro transcription of spike protein mRNA

Plasmid/Primer Name	Notes	Sequence
>2_pfizer-spike_pUC57	Italicized is the T7 promoter, underlined is the template for the in vitro transcription, bloded is the start and stop codos.	TCGCGCGTTTCGGTGATGACGGTGAAAACCTCTGACACATGCAGCTCCCGGAGACGGTCACAGCTTGTCTGTAAGCGGATGCCGGGAGCAGACAA GCCCGTCAGGGCGCGTCAGCGGGTGTTGGCGGGTGTCGGGGCTGGCTTAACTATGCGGCATCAGAGCAGATTGTACTGAGAGTGCACCATATGCG GTGTGAAATACCGCACAGATGCGTAAGGAGAAAATACCGCATCAGGCGCCATTCGCCATTCAGGCTGCGCAACTGTTGGGAAGGGCGATCGGTGC GGGCCTCTTCGCTATTACGCCAGCTGGCGAAAGGGGGATGTGCTGCAAGGCGATTAAGTTGGGTAACGCCAGGGTTTTCCCAGTCACGACGTTGTA AAACGACGGCCAGTGAATTCGAGCTCGGTACCTCGCGAATGCATCTAGAT*TAATACGACTCACTATA* GAGAATAAACTAGTATTCTTCTGGTCCCCA CAGACTCAGAGAGAACCCGCCACC**ATG**CATCACCATCACCATCACTTCGTGTTCCTGGTGCTGCTGCCTCTGGTGTCCAGCCAGTGTGTGAACCTGA CCACCAGAACACAGCTGCCTCCAGCCTACACCAACAGCTTTACCAGAGGCGTGTACTACCCCGACAAGGTGTTCAGATCCAGCGTGCTGCACTCTAC CCAGGACCTGTTCCTGCCTTTCTTCAGCAACGTGACCTGGTTCCACGCCATCCACGTGTCCGGCACCAATGGCACCAAGAGATTCGACAACCCCGTG CTGCCCTTCAACGACGGGGTGTACTTTGCCAGCACCGAGAAGTCCAACATCATCAGAGGCTGGATCTTCGGCACCACACTGGACAGCAAGACCCAG AGCCTGCTGATCGTGAACAACGCCACCAACGTGGTCATCAAAGTGTGCGAGTTCCAGTTCTGCAACGACCCCTTCCTGGGCGTCTACTACCACAAGA ACAACAAGAGCTGGATGGAAAGCGAGTTCCGGGTGTACAGCAGCGCCAACAACTGCACCTTCGAGTACGTGTCCCAGCCTTTCCTGATGGACCTGG AAGGCAAGCAGGGCAACTTCAAGAACCTGCGCGAGTTCGTGTTTAAGAACATCGACGGCTACTTCAAGATCTACAGCAAGCACACCCCTATCAACCT CGTGCGGGATCTGCCTCAGGGCTTCTCTGCTCTGGAACCCCTGGTGGATCTGCCCATCGGCATCAACATCACCCGGTTTCAGACACTGCTGGCCCT GCACAGAAGCTACCTGACACCTGGCGATAGCAGCAGCGGATGGACAGCTGGTGCCGCCGCTTACTATGTGGGCTACCTGCAGCCTAGAACCTTCCT GCTGAAGTACAACGAGAACGGCACCATCACCGACGCCGTGGATTGTGCTCTGGATCCTCTGAGCGAGACAAAGTGCACCCTGAAGTCCTTCACCGT GGAAAAGGGCATCTACCAGACCAGCAACTTCCGGGTGCAGCCCACCGAATCCATCGTGCGGTTCCCCAATATCACCAATCTGTGCCCCTTCGGCGA GGTGTTCAATGCCACCAGATTCGCCTCTGTGTACGCCTGGAACCGGAAGCGGATCAGCAATTGCGTGGCCGACTACTCCGTGCTGTACAACTCCGC CAGCTTCAGCACCTTCAAGTGCTACGGCGTGTCCCCTACCAAGCTGAACGACCTGTGCTTCACAAACGTGTACGCCGACAGCTTCGTGATCCGGGG AGATGAAGTGCGGCAGATTGCCCCTGGACAGACAGGCAAGATCGCCGACTACAACTACAAGCTGCCCGACGACTTCACCGGCTGTGTGATTGCCTG GAACAGCAACAACCTGGACTCCAAAGTCGGCGGCAACTACAATTACCTGTACCGGCTGTTCCGGAAGTCCAATCTGAAGCCTTCGAGCGGGACAT CTCCACCGAGATCTATCAGGCCGGCAGCACCCCTTGTAACGGCGTGGAAGGCTTCAACTGCTACTTCCCACTGCAGTCCTACGGCTTTCAGCCCAC AATGGCGTGGGCTATCAGCCCTACAGAGTGGTGGTGCTGAGCTTCGAACTGCTGCATGCCCCTGCCACAGTGTGCGGCCCTAAGAAAGCACCAAT CTCGTGAAGAACAAATGCGTGAACTTCAACTTCAACGGCCTGACCGGCACCGGCGTGCTGACAGAGAGCAACAAGAAGTTCCTGCCATTCCAGCAG TTTGGCCGGGATATCGCCGATACCACAGACGCCGTTAGAGATCCCCAGACACTGGAAATCCTGGACATCACCCCTTGCAGCTTCGGCGGAGTGTCT GTGATCACCCCTGGCACCAACACCAGCAATCAGGTGGCAGTGCTGTACCAGGACGTGAACTGTACCGAAGTGCCCGTGGCCATTCACGCCGATCAG CTGACACCTACATGGCGGGTGTACTCCACCGGCAGCAATGTGTTTCAGACCAGAGCCGGCTGTCGATCGGAGCCGAGCACGTGAACAATAGCTAC GAGTGCGACATCCCCATCGGCGCTGGAATCTGCGCCAGCTACCAGACACAGACAAACAGCCCTCGGAGAGCCAGAAGCGTGGCCAGCCAGAGCAT CATTGCCTACACAATGTCTCTGGGCGCCGAGAACAGCGTGGCCTACTCCAACAACTCTATCGCTATCCCCACCAACTTCACCATCAGCGTGACCACA GAGATCCTGCCTGTGTCCATGACCAAGACCAGCGTGGACTGCACCATGTACATCTGCGGCGATTCCACCGAGTGCTCCAACCTGCTGCTGCAGTAC GGCAGCTTCTGCACCCAGCTGAATAGAGCCCTGACAGGGATCGCCGTGGAACAGGACAAGAACACCCAAGAGGTGTTCGCCCAAGTGAAGCAGAT CTACAAGACCCCTCCTATCAAGGACTTCGGCGGCTTCAATTTCAGCCAGATTCTGCCCGATCCTAGCAAGCCCAGCAAGCGGAGCTTCATCGAGGAC CTGCTGTTCAACAAAGTGACACTGGCCGACGCCGGCTTCATCAAGCAGTATGGCGATTGTCTGGGGCGACATTGCCGCCAGGGATCTGATTTGCGCC CAGAAGTTTAACGGACTGACAGTGCTGCCTCCTCTGCTGACCGATGAGATGATCGCCCAGTACACATCTGCCCTGCTGGCCGGCACAATCACAAGC GGCTGGACATTTGGAGCAGGCGCCGCTCTGCAGATCCCCTTGCATGCAGATGGCCTACCGGTTCAACGGCATCGGAGTGACCCAGAATGTGCTG TACGAGAACCAGAAGCTGATCGCCAACCAGTTCAACAGCGCCATCGGCAAGATCCAGGACAGCCTGAGCAGCACAGCAAGCGCCCTGGGAAAGCT GCAGGACGTGGTCAACCAGAATGCCCAGGCACTGAACACCCTGGTCAAGCAGCTGTCCTCCAACTTCGGCGCCATCAGCTCTGTGCTGAACGATAT CCTGAGCAGACTGGACCCTCCTGAGGCCGAGGTGCAGATCGACAGACTGATCACAGGCAGACTGCAGAGCCTCCAGACATACGTGACCCAGCAGC TGATCAGAGCCGCCGAGATTAGAGCCTCTGCCAATCTGGCCGCCACCAAGATGTCTGAGTGTGTGCTGGGCCAGAGCAAGAGAGTGGACTTTTGCG GCAAGGGCTACCACCTGATGAGCTTCCCTCAGTCTGCCCCTCACGGCGTGGTGTTTCTGCACGTGACATATGTGCCCGCTCAAGAGAAGAATTTCAC CACCGCTCCAGCCATCTGCCACGACGGCAAAGCCCACTTTCCTAGAGAAGGCGTGTTCGTGTCCAACGGCACCCATTGGTTCGTGACACAGCGGAA CTTCTACGAGCCCCAGATCATCACCACCGACAACACCTTCGTGTCTGGCAACTGCGACGTCGTGATCGGCATTGTGAACAATACCGTGTACGACCCT CTGCAGCCGAGCTGGACAGCTTCAAAGAGGAACTGGACAAGTACTTTAAGAACCACACAAGCCCCGACGTGGACCTGGGCGATATCAGCGGAAT CAATGCCAGCGTCGTGAACATCCAGAAAGAGATCGACCGGCTGAACGAGGTGGCCAAGAATCTGAACGAGAGCCTGATCGACCTGCAAGAACTGG GGAAGTACGAGCAGTACATCAAGTGGCCCTGGTACATCTGGCTGGGCTTTATCGCCGGACTGATTGCCATCGTGATGGTCACAATCATGCTGTGTT GCATGACAGCTGCTGTAGCTGCCTGAAGGGCTGTTGTAGCTGTGGCAGCTGCTGCAAGTTCGACGAGGACGATTCTGAGCCCGTGCTGAAGGGC GTGAAACTGCACTACACAGGGGGAGGCGGGGGTGGAGATTACAAGGACGACGATGACAAG**TGA**TGACTCGAGCTGGTACTGCATGCACGCAATGC TAGCTGCCCTTTCCCGTCCTGGGTACCCCGAGTCTCCCCCGACCTCGGGTCCCAGGTATGCTCCCACCTCCACCTGCCCCACTCACCACCTCTGCT AGTTCCAGACACCTCCCAAGCACGCAGCAATGCAGCTCAAAACGCTTAGCCTAGCCACACCCCCACGGGAAACAGCAGTGATTAACCTTTAGCAATA AACGAAAGTTTAACTAAGCTATACTAACCCCAGGGTTGGTCAATTTCGTGCCAGCCACACCCTGGAGCTAGCAAAAAAAAAAAAAAAAAAAAAAA AAAAAGCATATCACTAAAAAAAAAAAAAAAAAAAAAAAAAAAAAAAAAAAAAAAAAAAAAAAAAAAAAAAAAAAAAAAAAAAAAAAAAAAAAA GCCCGTCGACTGCAGAGGCCTGCATGCAAGCTTGGCGTAATCATGGTCATAGCTGTTTCCTGTGTGAAATTGTTATCCGCTCACAATTCCACACAAC ATACGAGCCGGAAGCATAAAGTGTAAAGCCTGGGGTGCCTAATGAGTGAGCTAACTCACATTAATTGCGTTGCGCTCACTGCCCGCTTTCCAGTCG GGAAACCTGTCGTGCCAGCTGCATTAATGAATCGGCCAACGCGCGGGGAGAGGCGGTTTGCGTATTGGGCGCTCTTCCGCTTCCTCGCTCACTGAC TCGCTGCGCTCGGTCGTTCGGCTGCGGCGAGCGGTATCAGCTCACTCAAAGGCGGTAATACGGTTATCCACAGAATCAGGGGATAACGCAGGAAA GAACATGTGAGCAAAAGGCCAGCAAAAGGCCAGGAACCGTAAAAAGGCCGCGTTGCTGGCGTTTTTCCATAGGCTCCGCCCCCCTGACGAGCATCA CAAAAATCGACGCTCAAGTCAGAGGTGGCGAAACCCGACAGGACTATAAAGATACCAGGCGTTTCCCCCTGGAAGCTCCCTCGTGCGCTCTCCTGT TCCGACCCTGCCGCTTACCGGATACCTGTCCGCCTTTCTCCCTTCGGGAAGCGTGGCGCTTTCTCATAGCTCACGCTGTAGGTATCTCAGTTCGGTG TAGGTCGTTCGCTCCAAGCTGGGCTGTGTGCACGAACCCCCCGTTCAGCCCGACCGCTGCGCCTTATCCGGTAACTATCGTCTTGAGTCCAACCCG GTAAGACACGACTTATCGCCACTGGCAGCAGCCACTGGTAACAGGATTAGCAGAGCGAGGTATGTAGGCGGTGCTACAGAGTTCTTGAAGTGGTG GCCTAACTACGGCTACACTAGAAGAACAGTATTTGGTATCTGCGCTCTGCTGAAGCCAGTTACCTTCGGAAAAAGAGTTGGTAGCTCTTGATCCGGC AAACAAACCACCGCTGGTAGCGGTGGTTTTTTTGTTTGCAAGCAGCAGATTACGCGCAGAAAAAAAGGATCTCAAGAAGATCCTTTGATCTTTTCTA CGGGGTCTGACGCTCAGTGGAACGAAAACTCACGTTAAGGGATTTTGGTCATGAGATTATCAAAAAGGATCTTCACCTAGATCCTTTTAAATTAAAA ATGAAGTTTTAAATCAATCTAAAGTATATATGAGTAAACTTGGTCTGACAGTTACCAATGCTTAATCAGTGAGGCACCTATCTCAGCGATCTGTCTATT TCGTTCATCCATAGTTGCCTGACTCCCCGTCGTGTAGATAACTACGATACGGGAGGGCTTACCATCTGGCCCCAGTGCTGCAATGATACCGCGAGAC CCACGCTCACCGGCTCCAGATTTATCAGCAATAAACCAGCCAGCCGGAAGGGCCGAGCGCAGAAGTGGTCCTGCAACTTTATCCGCCTCCATCCAG TCTATTAATTGTTGCCGGGAAGCTAGAGTAAGTAGTTCGCCAGTTAATAGTTTGCGCAACGTTGTTGCCATTGCTACAGGCATCGTGGTGTCACGCT CGTCGTTTGGTATGGCTTCATTCAGCTCCGGTTCCCAACGATCAAGGCGAGTTACATGATCCCCCATGTTGTGCAAAAAAGCGGTTAGCTCCTTCGG TCCTCCGATCGTTGTCAGAAGTAAGTTGGCCGCAGTGTTATCACTCATGGTTATGGCAGCACTGCATAATTCTCTTACTGTCATGCCATCCGTAAGAT GCTTTTCTGTGACTGGTGAGTACTCAACCAAGTCATTCTGAGAATAGTGTATGCGGCGACCGAGTTGCTCTTGCCCGGCGTCAATACGGGATAATAC CGCGCCACATAGCAGAACTTTAAAAGTGCTCATCATTGGAAAACGTTCTTCGGGGCGAAAACTCTCAAGGATCTTACCGCTGTTGAGATCCAGTTCG ATGTAACCCACTCGTGCACCCAACTGATCTTCAGCATCTTTTACTTTCACCAGCGTTTCTGGGTGAGCAAAAACAGGAAGGCAAAATGCCGCAAAAA AGGGAATAAGGGCGACACGGAAATGTTGAATACTCATACTCTTCCTTTTTCAATATTATTGAAGCATTTATCAGGGTTATTGTCTCATGAGCGGATAC ATATTTGAATGTATTTAGAAAAATAAACAAATAGGGGTTCCGCGCACATTTCCCCGAAAAGTGCCACCTGACGTCTAAGAAACCATTATTATCATGAC ATTAACCTATAAAAATAGGCGTATCACGAGGCCCTTTCGTC
Pfizer-1-F	Forward primer	TAA TAC GAC TCA CTA TAG AGA ATA AAC TAG TAT TCT TCT GGT CC
Pfizer-2-R	Reverse primer	TTT TTT TTT TTT TTT TTT TTT TTT TTT TTT TTT TTT TTT TTT TTT TTT TTT TTT TTT TTT TTT TAG TCA TAT GCT TTT TTT TTT

Plasmid and primers used for dual-luciferase reporters

Plasmid/Primer Name	Notes	Sequence
RL-FL sequence		TAATACGACTCACTATAGGAAGTAATTATCTACTTTTTACAACAAATATACCTCGAGCAAGGATCCATGACTTCGAAAGTTTATGATCCAGAACAAAGGAAACGGATGATAACTGG TCCGCAGTGGTGGGCCAGATGTAAACAAATGAATGTTCTTGATTCATTTATTAATTATTATGATTCAGAAAAACATGCAGAAAATGCTGTTATTTTTTTACATGGTAACGCGGCCT CTTCTTATTTATGGCGACATGTTGTGCCACATATTGAGCCAGTAGCGCGGTGTATTATACCAGACCTTATTGGTATGGGCAAATCAGGCAAATCTGGTAATGGTTCTTATAGGTTA CTTGATCATTACAAATATCTTACTGCATGGTTTGAACTTCTTAATTTACCAAAGAAGATCATTTTTGTCGGCCATGATTGGGGTGCTTGTTTGGCATTTCATTATAGCTATGAGCAT CAAGATAAGATCAAAGCAATAGTTCACGCTGAAAGTGTAGTAGATGTGATTGAATCATGGGATGAATGGCCTGATATTGAAGAAGATATTGCGTTGATCAAATCTGAAGAAGGA GAAAAAATGGTTTTGGAGAATAACTTCTTCGTGGAAACCATGTTGCCATCAAAAATCATGAGAAAGTTAGAACCAGAAGAATTTGCAGCATATCTTGAACCATTCAAAGAGAAAG GTGAAGTTCGTCGTCCAACATTATCATGGCCTCGTGAAATCCCGTTAGTAAAAGGTGGTAAACCTGACGTTGTACAAATTGTTAGGAATTATAATGCTTATCTACGTGCAAGTGAT GATTTACCAAAAATGTTTATTGAATCGGACCCAGGATTCTTTTCCAATGCTATTGTTGAAGGTGCCAAGAAGTTTCCTAATACTGAATTTGTCAAAGTAAAAGGTCTTCATTTTTCG CAAGAAGATGCACCTGATGAAATGGGAAAATATATCAAATCGTTCGTTGAGCGAGTTCTCAAAAATGAACAAATGTCGACgtgcgatcaaacgttcGGATCCTTCAACTTCCCTGAGC TCGAAGACGCCAAAAACATAAAGAAAGGCCCGGCGCCATTCTATCCTCTAGAGGATGGAACCGCTGGAGAGCAACTGCATAAGGCTATGAAGAGATACGCCCTGGTTCCTGGA ACAATTGCTTTTACAGATGCACATATCGAGGTGAACATCACGTACGCGGAATACTTCGAAATGTCCGTTCGGTTGGCAGAAGCTATGAAACGATATGGGCTGAATACAAATCACA GAATCGTCGTATGCAGTGAAAACTCTCTTCAATTCTTTATGCCGGTGTTGGGCGCGTTATTTATCGGAGTTGCAGTTGCGCCCGCGAACGACATTTATAATGAACGTGAATTGCT CAACAGTATGAACATTTCGCAGCCTACCGTAGTGTTTGTTTCCAAAAAGGGGTTGCAAAAAATTTTGAACGTGCAAAAAAATTACCAATAATCCAGAAAATTATTATCATGGATT CTAAAACGGATTACCAGGGATTTCAGTCGATGTACACGTTCGTCACATCTCATCTACCTCCCGGTTTTAATGAATACGATTTTGTACCAGAGTCCTTTGATCGTGACAAAACAATT GCACTGATAATGAATTCCTCTGGATCTACTGGGTTACCTAAGGGTGTGGCCCTTCCGCATAGAACTGCCTGCGTCAGATTCTCGCATGCCAGAGATCCTATTTTTGGCAATCAAA TCATTCCGGATACTGCGATTTTAAGTGTTGTTCCATTCCATCACGGTTTTGGAATGTTTACTACACTCGGATATTTGATATGTGGATTTCGAGTCGTCTTAATGTATAGATTTGAAG AAGAGCTGTTTTTACGATCCCTTCAGGATTACAAAATTCAAAGTGCGTTGCTAGTACCAACCCTATTTTCATTCTTCGCCAAAAGCACTCTGATTGACAAATACGATTTATCTAATT TACACGAAATTGCTTCTGGGGGCGCACCTCTTTCGAAAGAAGTCGGGGAAGCGGTTGCAAAACGCTTCCATCTTCCAGGGATACGACAAGGATATGGGCTCACTGAGACTACAT CAGCTATTCTGATTACACCCGAGGGGGATGATAAACCGGGCGCGGTCGGTAAAGTTGTTCCATTTTTTGAAGCGAAGGTTGTGGATCTGGATACCGGGAAAACGCTGGGCGTTA ATCAGAGAGGCGAATTATGTGTCAGAGGACCTATGATTATGTCCGGTTATGTAAACAATCCGGAAGCGACCAACGCCTTGATTGACAAGGATGGATGGCTACATTCTGGAGACA TAGCTTACTGGGACGAAGACGAACACTTCTTCATAGTTGACCGCTTGAAGTCTTTAATTAAATACAAAGGATATCAGGTGGCCCCCGCTGAATTGGAATCGATATTGTTACAACA CCCCAACATCTTCGACGCGGGCGTGGCAGGTCTTCCCGACGATGACGCCGGTGAACTTCCCGCCGCCGTTGTTGTTTTGGAGCACGGAAAGACGATGACGGAAAAAGAGATCG TGGATTACGTCGCCAGTCAAGTAACAACCGCGAAAAAGTTGCGCGGAGGAGTTGTGTTTGTGGACGAAGTACCGAAAGGTCTTACCGGAAAACTCGACGCAAGAAAAATCAGA GAGATCCTCATAAAGGCCAAGAAGGGCGGAAAGTCCAAATTGTAAcacgtgtaattctagagcggccgcctgcagctcgaggcatgcAAGCTTttcgtggccgaggaaaaaaaaaaaaaaaaaaaa aaaaaaaaaaaaaaaaaaaaa
RL-FL-IVT-F		TAATACGACTCACTATAGGAAGTAATTATCTACTTTTTACAAC
RL-FL-IVT-R		TTTTTTTTTTTTTTTTTTTTTTTTTTTTTTTTTTTTTTTTTTTTCCTCGGCCACGAAAAG
RL-FL-AAU-F	Used for site-directed mutagenesis	GAAAGGTCTTACCGGAAATCTCGACGCAAGAAAAATC
RL-FL-AAU-R	Used for site-directed mutagenesis	GATTTTTCTTGCGTCGAGATTTCCGGTAAGACCTTTC

Supplementary Table 2: Detected peptides and proteins from mass spectrometry analysis of spike protein translated in HEK293 cells

WT/Miscoded	start pos	miscoded pos	mod(+/-Da)	Peptide Sequence	Uridine1 Total Area	Uridine2 Total Area	Uridine3 Total Area	PseudoU 1 Total Area	PseudoU 2 Total Area	PseudoU 3 Total Area	N1MpU1 Total Area	N1MpU2 Total Area	N1MpU3 Total Area	U1 PSMs	U2 PSMs	U3 PSMs	pU1 PSMs	pU2 PSMs	pU3 PSMs	N1MpU1 PSMs	N1MpU2 PSMs	N1MpU3 PSMs
WT	28			TQLPPAYTNSFTR	5111413248	6.21E+09	6.85E+09	7.15E+09	1.16E+10	9.36E+08	1.56E+10	4.65E+09	1.29E+10	8	8	8	8	17	9	8	9	9
Miscoded		28	Thr->Gln (+27)	QQLPPAYTNSFTR	394159	1752822	505958	746879	1964578	1448460	#N/A	#N/A	2655780		2	1		3	2			2
WT	364			ISNCVADYSVLYNSASFSTFK	92833328	3.23E+08	1.01E+08	1.85E+08	3.61E+08	4.12E+08	5.37E+08	21464868	6.1E+08	1	2			2	2	2		2
Miscoded		265	Ser->Trp (+99), Carbam	IWNC[+57]VADYSVLYNSASFSTFK	#N/A	6107288	#N/A	#N/A	5855660	#N/A	#N/A	#N/A	#N/A		1			1				
WT	641			VYSTGSNVFQTR	4076289024	5.68E+09	4.91E+09	5.86E+08	8.36E+09	3.46E+08	1.08E+10	3.2E+09	8.06E+09	4	6	4	4	2	5	5	4	5
Miscoded		648	Val->Gln (+29)	VYSTGSNQFQTR	#N/A	1874790	#N/A	#N/A	#N/A	#N/A	#N/A	#N/A	#N/A		1							
Miscoded		641	Val->Asn (+15)	NYSTGSNVFQTR	757306	2449997	438867	#N/A	1751995	#N/A	1722801	#N/A	1239415	1	1	1		1		1		1
Miscoded		641	Val->Gln (+29)	QYSTGSNVFQTR	#N/A	2909977	#N/A	#N/A	#N/A	#N/A	#N/A	#N/A	#N/A	1	1							
Miscoded		647	Asn->Met (+17)	VYSTGSMVFQTR	#N/A	#N/A	#N/A	#N/A	#N/A	#N/A	2026308	#N/A	1104621		1					1		1
Miscoded		643	Ser->Asn (+27)	VYNTGSNVFQTR	#N/A	#N/A	4703006	3092209	#N/A	3020282	914994	1894476	1380627			1	1		1	1	1	1
		649	Phe->Tyr (+16)	VYSTGSNVYQTR	695100	1240939	1795088	#N/A	491336	#N/A	1449157	#N/A	433786	2	2	1		1		1		2
WT	772			ALTGIAVEQDKNTQEVFAQVK	4286196224	5.38E+09	3.8E+09	5.3E+09	7.95E+09	7.3E+09	1.37E+10	3.58E+09	4.5E+09	3	3	3	3	5	3	3	3	3
Miscoded		774	Thr->Gln (+27)	ALQGIAVEQDKNTQEVFAQVK	#N/A	#N/A	#N/A	#N/A	#N/A	2368856	#N/A	948525	#N/A						1		1	
WT	1035			MSECVLGQSK	137131232	4.01E+08	88575712	26194446	4.07E+08	2.51E+08	8.05E+08	56396584	8.28E+08	4	5	1	1		3	3	1	2
Miscoded		1038	Cys->Ala (-32)	MSEAVLGQSK	23587668	719827	4910791	4025282	1340976	2968574	11167276	0	1611967						1			
WT	1276			LHYTGGGGGGDYKDDDDK	246828848	3.64E+08	2.21E+08	66794480	3.45E+08	#N/A	4.54E+08	6.35E+08	2.09E+08	2	4	4		2		3	3	1
Miscoded		1279	Thr->Gln (+27)	LHYQGGGGGGDYKDDDDK	763553	1702247	1027370	#N/A	2960340	#N/A	#N/A	#N/A	#N/A	1	1	1		2			1	
Miscoded		1277	His->Tyr (+26)	LYYTGGGGGGDYKDDDDK	9386236	22234428	10168410	#N/A	6149055	#N/A	10059328	#N/A	#N/A	1	1	1		2				
Miscoded		1280	Gly->Thr (+44)	LHYTTGGGGGDYKDDDDK	#N/A	#N/A	#N/A	#N/A	#N/A	#N/A	850220	#N/A	#N/A							1		

Supplementary Table 3: Detected peptides from mass spectrometry analysis of spike protein translated in wheat germ extracts

Run 1						
Annotated Sequence	U 1	U 2	Y 1	Y 2	m1Y 1	m1Y 2
[K].NHTSPDVDLGDISGINASVVNIQK.[E]	2265548	1046176	495120	874983	99819.91	116807.2
[K].NHTSPDVDLGDNSGINASVVNIQK.[E]	91344.52	19346.64	106579.4	147582.3	5402.667	12076.07
[R].EGVFVSNGTHWFVTQR.[N]	608709.1	500142.3	127890.9	150647.4	30588.48	25203.51
[R].EGVFVSNGTHWYVTQR.[N]	75718.56	74079.53	12351.57	21427.81		4407.491
[R].FNGIGVTQNVLYENQK.[LR]	615332.4	605486	731412.9	732740.8	299235.3	329331.3
[R].FNGNGVTQNVLYENQK.[L]	629687.2	580421.8	856896.6	905827.1	272839	319685
[R].GWIFGTTLDSK.[T]	4484531	3132869	4342448	5204075	1313567	1259466
[R].GWIYGTTLDSK.[T]	828257.1	692208.5	1266458	1261737	457852.8	471013.1
Run 2						
Annotated Sequence	U 1	U 2	Y 1	Y 2	m1Y 1	m1Y 2
[K].NHTSPDVDLGDISGINASVVNIQK.[E]	21.11143	19.99669	18.91742	19.7389	16.60704	16.83377
[K].NHTSPDVDLGDNSGINASVVNIQK.[E]	16.47903	14.2398	16.70157	17.17116	12.39946	13.55986
[K].QLSSNFGAISSVLNDILSR.[L]	24.83635	25.22681	23.51341	23.24052	22.40879	21.4724
[K].QLSSNFGANSSVLNDILSR.[L]	13.35848	12.98946	19.69888	20.17968	12.5853	10.91692
[K].QPSSNFGAISSVLNDILSR.[L]	20.60835	21.23375	18.20489	18.36813	18.27657	19.71893
[R].ALTGIAVEQDKNTQEVFAQVK.[Q]	22.16007	22.14807	21.26343	21.49413	19.23774	19.33111
[R].ALTGNAVEQDKNTQEVFAQVK.[Q]	17.23393	17.09685	16.48925	16.21164	14.25727	14.64518
[R].EGVFVSNGTHWFVTQR.[N]	19.21539	18.93198	16.96455	17.20082	14.9007	14.62134
[R].EGVFVSNGTHWYVTQR.[N]	16.20836	16.17679	13.59241	14.3872	11.59045	12.10574
[R].FDNPVLPFNDGVYFASTEK.[S]	20.36203	21.03543	22.47498	22.17419	20.5183	18.36706
[R].FDNPVQPFNDGVYFASTEK.[S]	13.4852	13.78113	13.32399	10.95337	12.25024	11.39026
[R].FNGIGVTQNVLYENQK.[LR]	19.23101	19.20773	19.48033	19.48294	18.19092	18.32918
[R].FNGNGVTQNVLYENQK.[L]	19.26428	19.14674	19.70876	19.78888	18.05769	18.28629
[R].GWIFGTTLDSK.[T]	22.09653	21.57905	22.05008	22.31121	20.32506	20.26438
[R].GWIYGTTLDSK.[T]	19.65972	19.40085	20.27237	20.26698	18.80452	18.84541
[R].LQSLQTYVTQQLIR.[A]	24.59433	23.4835	23.91811	24.02758	22.30471	19.61663
[R].LQSLQTYVTQQQIR.[A]	15.30937	14.02631	14.86936	15.19954	7.875572	12.63309
[R].SYLTPGDSSSGWTAGAAAYYVGYLQPR.[T]	19.9906	20.93866	18.35758	17.52533	9.976832	10.66112
[R].SYQTPGDSSSGWTAGAAAYYVGYLQPR.[T]	13.62988	13.18276	12.77572	12.15665	7.907696	8.400159

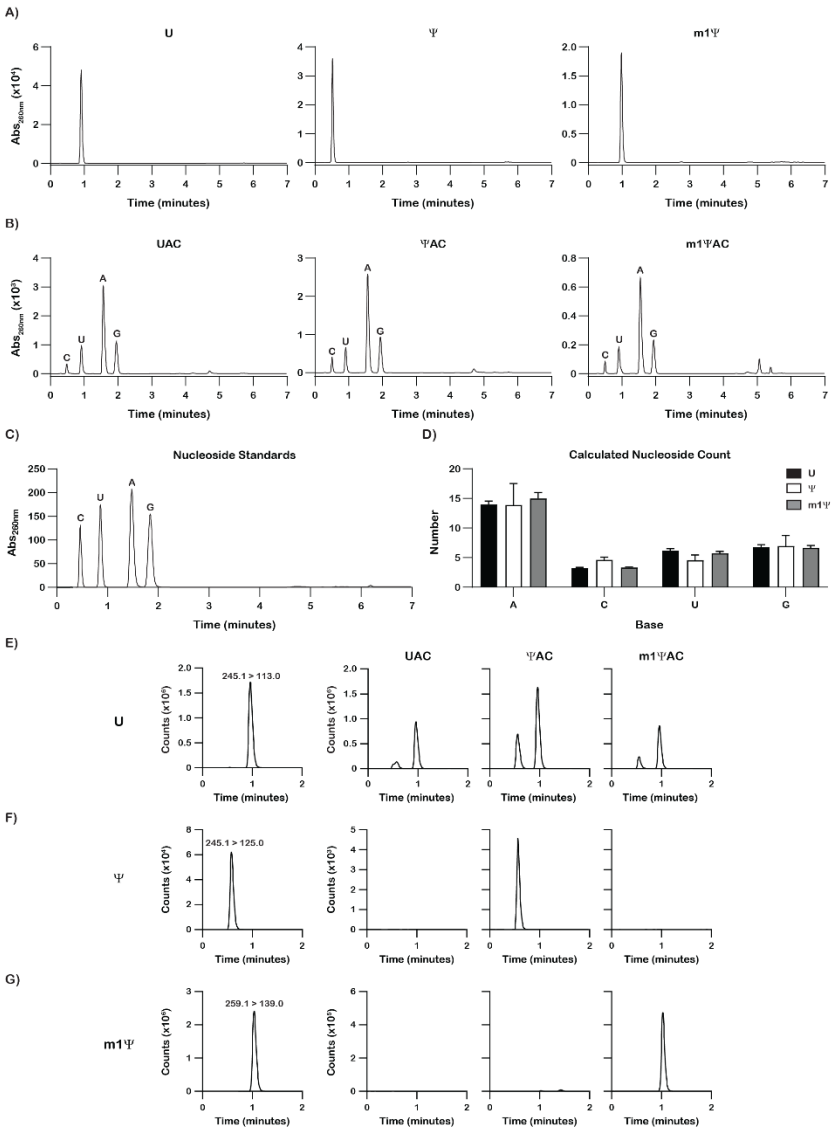

Supplementary Figure 1: LC-MS/MS validation of synthetic model RNAs.
A) Diode array detector chromatograms of peaks detected at 260 nm for uridine, pseudouridine, and N1-methylpseudouridine standards. **B)** Diode array detector chromatograms of peaks detected at 260 nm for the UAC, ΨAC, and m1ΨAC model mRNAs. The identity of each peak is labeled, as confirmed by comparison to canonical nucleoside standards. **C)** Diode array detector chromatogram of peaks detected at 260 nm for the four canonical ribonucleosides. An equimolar amount of cytidine, uridine, adenosine, and guanosine were run as standards. **D)** Plot showing the calculated number of each nucleoside in each model mRNA. Plotted are the average of the three calculated counts with error bars representing the standard deviation around the mean. Pseudouridine co-eluted with cytidine, which is reflected in the loss of a U and a gain of a C for the ΨAC mRNA. **E)** On the left is a plot of the mass spectrometry counts for the uridine standard; the mass transition used to detect the ion product of the fragmentation reaction is denoted above the peak. On the right are plots of the mass spectrometry counts for the three model mRNAs at the given mass transition. **F)** On the left is a plot of the mass spectrometry counts for a pseudouridine standard; the mass transition used to detect the ion product of the fragmentation reaction is denoted above the peak. On the right are plots of the mass spectrometry counts for the three model mRNAs at the given mass transition. **G)** On the left is a plot of the mass spectrometry counts for the N1-methylpseudouridine standard; the mass transition used to detect the ion product of the fragmentation reaction is denoted above the peak. On the right are plots of the mass spectrometry counts for the three model mRNAs at the given mass transition.

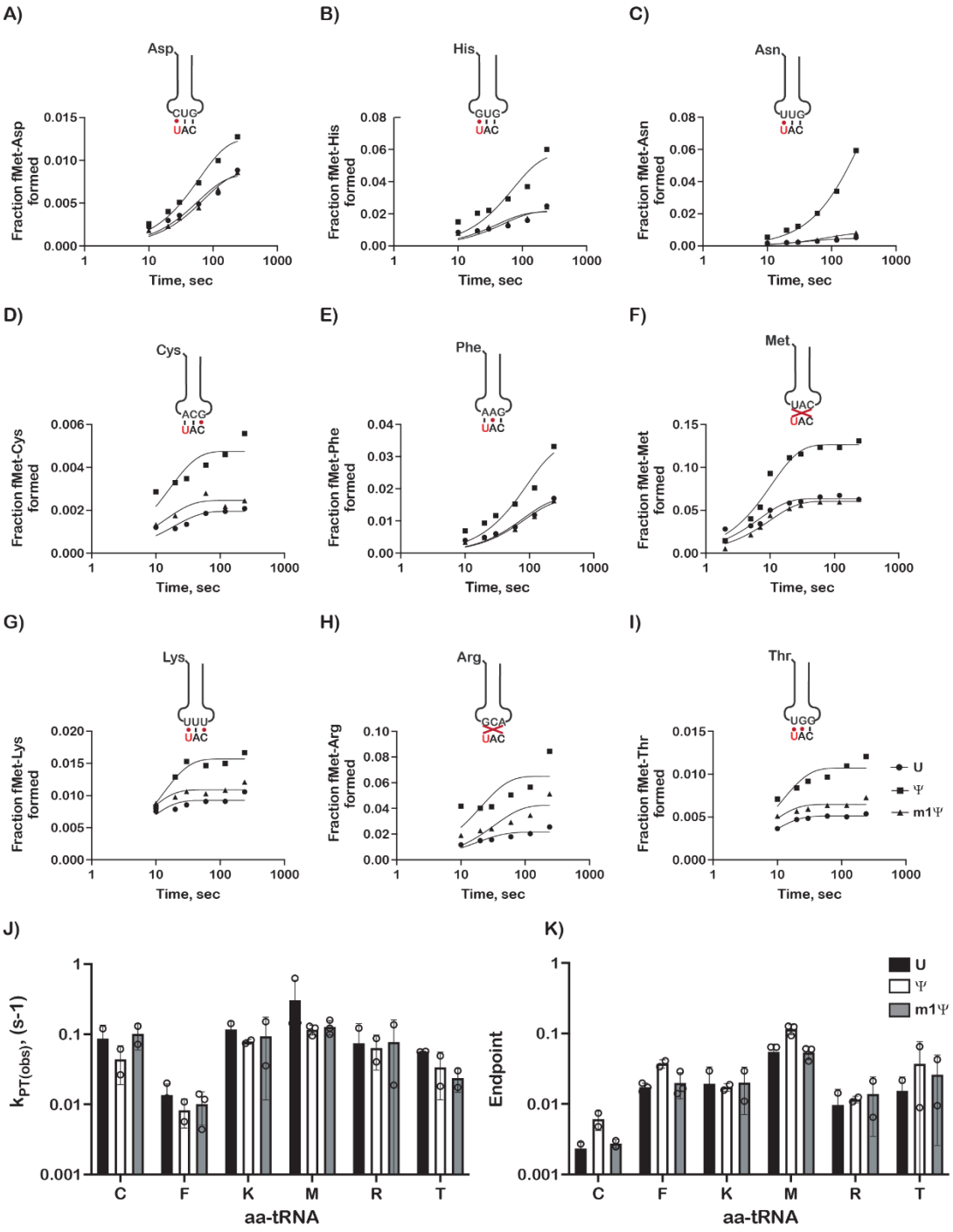

Supplementary Figure 2: Pseudouridine increases misincorporation of near and non-cognates while N1-methylpseudouridine does not.

A-I) Representative time courses of the indicated near and non- cognate tRNA ternary complexes and UAC, ΨAC, or Met-m1ΨAG initiation complexes. The codon (UAC; modification in red), near cognate tRNA, and the mismatch (red dot) are indicated. All reactions were conducted at least in duplicates. J-K) Bar graph showing the measured observed rates of peptide-bond formation and reaction end points, respectively, in the presence of 1 μM initiation complex and 2.5 μM denoted ternary complex. Plotted are the average values with error bars representing the standard deviation around the mean.

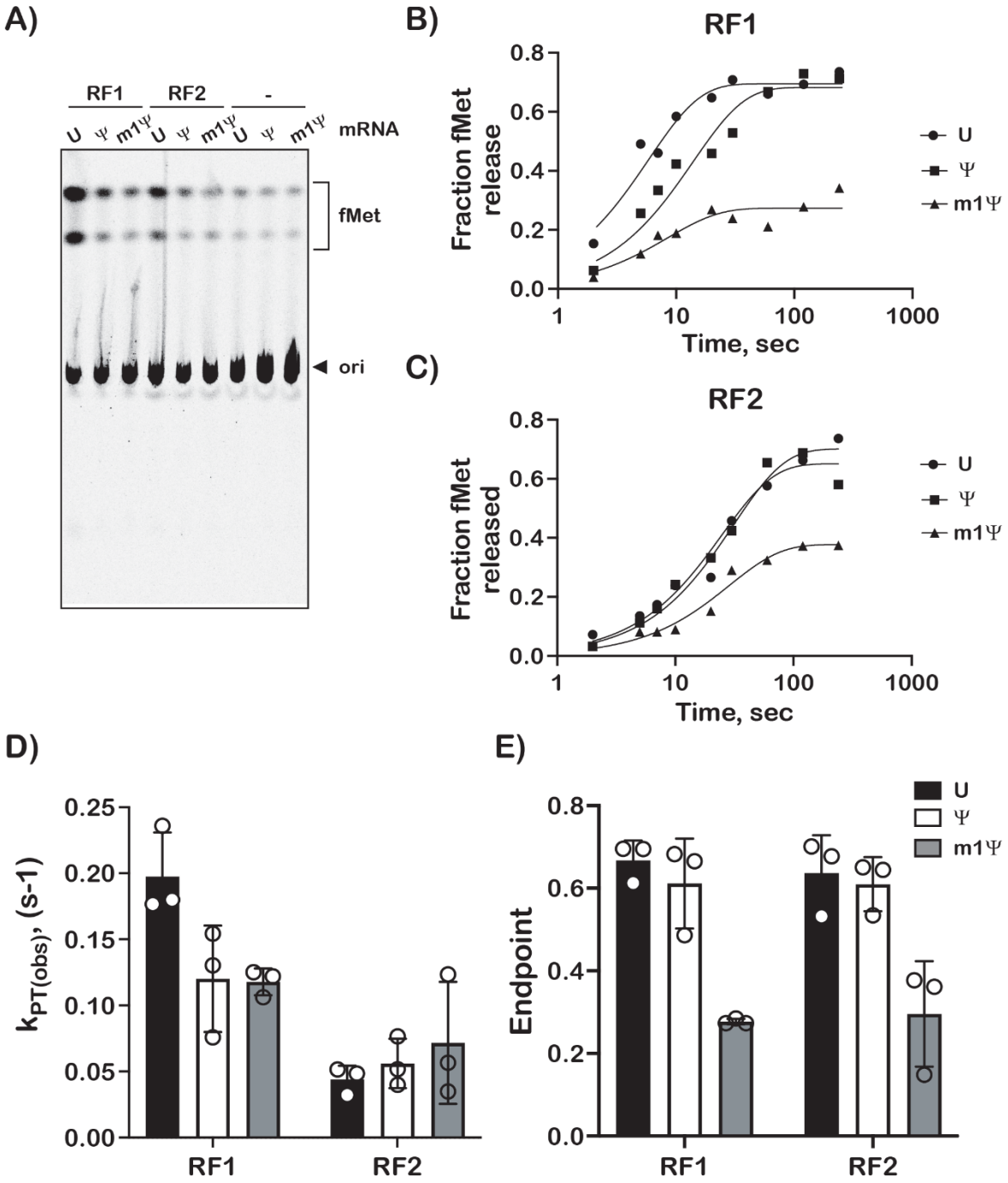

Supplementary Figure 3: The presence of N1-methylpseudouridine in mRNA increases the accuracy of stopcodon recognition by release factors.

A) A representative phosphorimage of an electrophoretic TLC showing peptide release on near-stop codon UAC, ΨAC, and m1ΨAC in the presence and absence of RF1 and RF2. All reactions were conducted in at least duplicates. **B-C)** Kinetics of fMet peptide release on an unmodified and modified codon; UAC codon (circles), ΨAC (squares), m1ΨAC (Triangles) in the presence of RF1 (B) and RF2 (C). Representative time courses are shown. **D-E)** Bar graph showing the measured observed rates of peptide-bond formation and reaction end points, respectively, in the presence of 1 μM initiation complex and 2.5 μM denoted ternary complex. Plotted are the average values determined from three independent time courses with error bars representing the standard deviation around the mean.

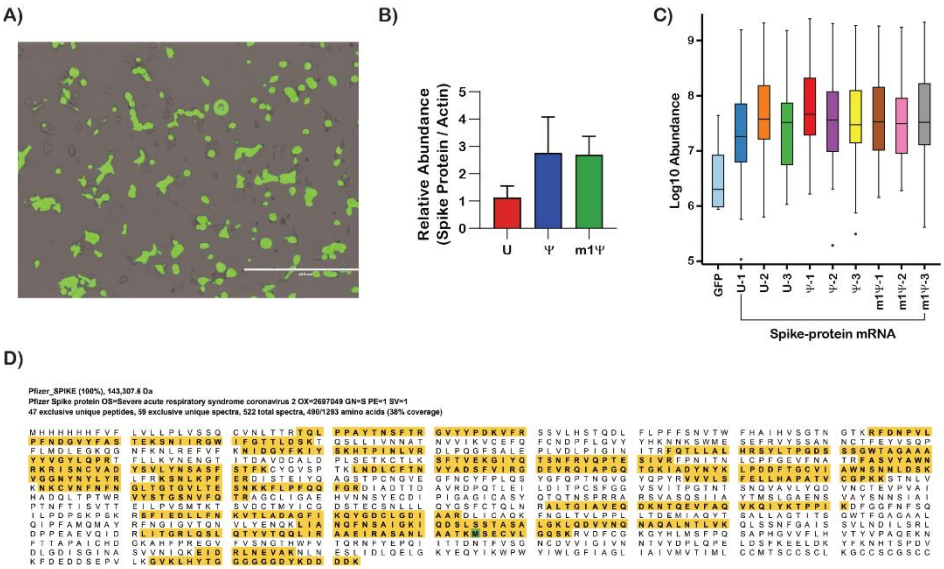

Supplementary Figure 4: Amino acid substitution products from HEK 293 cells can be detected by mass spectrometry

A) Microscope image of HEK 293 cells transfected with EGFP. A white scale bar is included for reference and represents a distance of 400 μm. **B)** Relative abundances of spike protein translated from mRNAs containing the denoted modification, as quantified from the immunoblot. **C)** Normalized abundance of peptides from each sample matching the wild-type spike protein sequence, as determined by label-free quantitation from LC-MS/MS analysis. **D)** Coverage of the spike protein resulting from on-bead digestion and MS/MS analysis. Amino-acids matched to a MS/MS spectrum are highlighted in yellow while amino-acids highlighted in green denote a post-translational modification (ie. Oxidation).

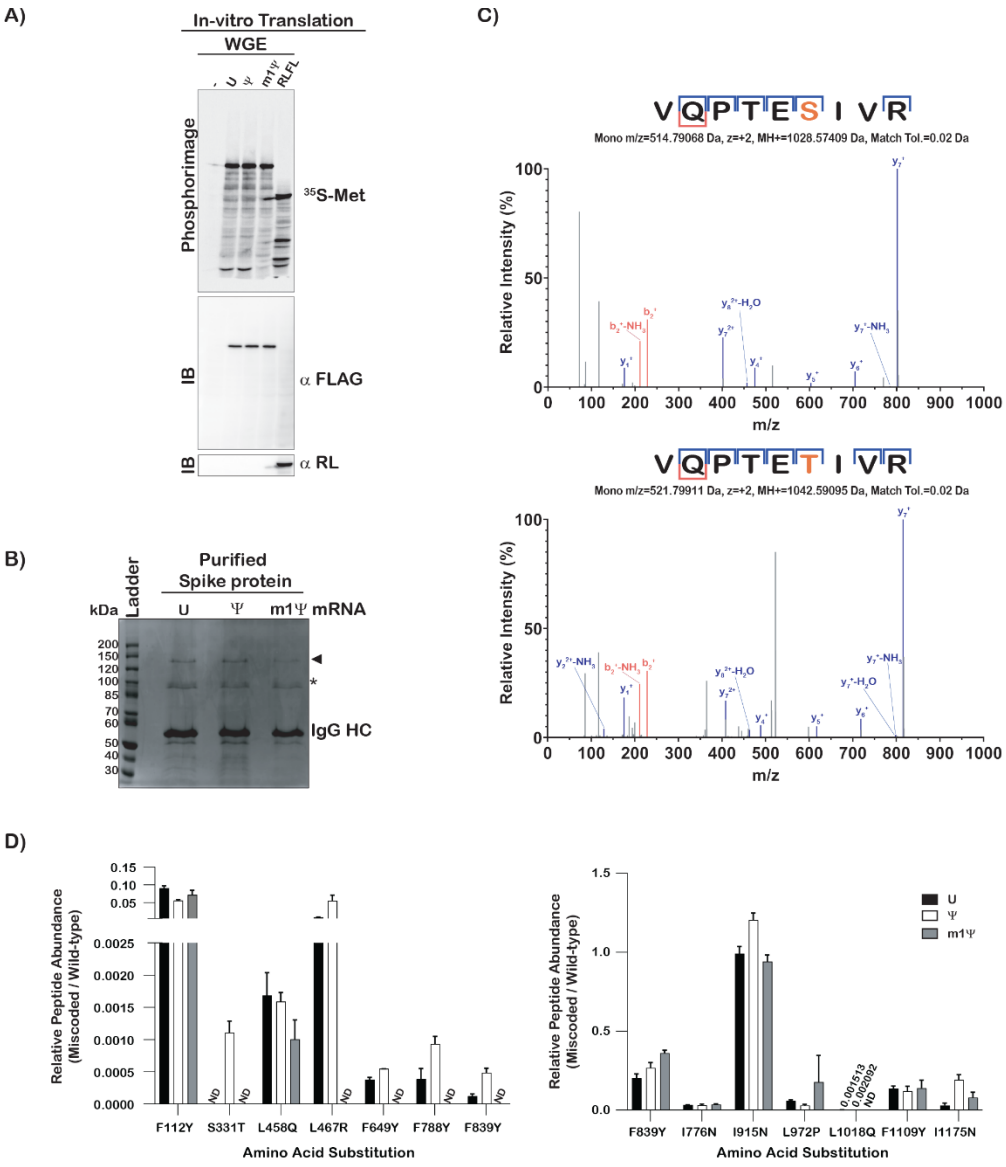

Supplementary Figure 5: Unlike Ψ-containing SARS-CoV-2 spike protein mRNA, m1Ψ-containing spike protein mRNA does not increase amino-acid misincorporation frequency during translation in wheatgerm extracts.

A) At top is a phosphorimage of a PVDF membrane with protein products transferred from the SDS-polyacrylamide gel used to resolve them from the indicated cell-free translation reactions in the presence of the depicted mRNA constructs. In-vitro protein synthesis was monitored through the addition of [35S]-Methionine to the reactions. At bottom are immunoblotting analysis of the same PVDF membrane with the indicated antibodies. **B)** Image of a Coomassie-stained SDS-polyacrylamide gel used to assess the purity of FLAGimmunoprecipitated spike proteins produced from translation reactions containing the indicated modification. **C)** Fragmentation spectra of a wild-type sequence peptide and its substituent miscoded product. b and y ions are denoted in red and blue, respectively, while the substituted amino acid is denoted in orange. The difference in the m/z for the y4, y5, y6, y7, and y8 peaks between the wild-type peptide (top) and miscoded product (bottom) corresponds to a serine to threonine substitution. The nominal mass difference between serine and threonine is 14 Da. **D)** Plots showing the relative peptide abundance of each detected wild-type peptide and its substituent miscoded product. Plotted are the means from technical replicates with error bars representing the standard deviation around the mean. The plot on the left displays the results of the first biological replicate mass spectrometry run, while the plot on the right displays the results of the second run. ND denotes the miscoded product was not detected in either technical replicate.

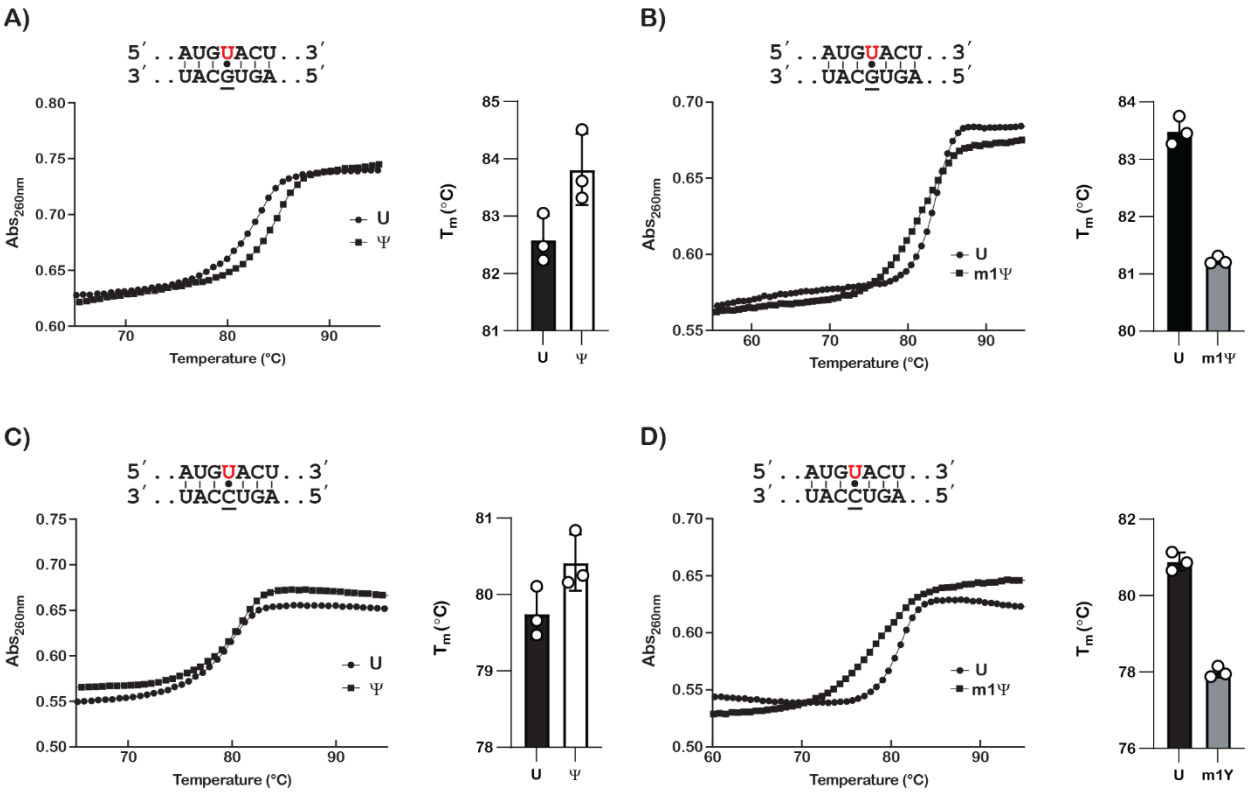

Supplementary Figure 6: Pseudouridine stabilizes formation of mismatched RNA duplexes whereas N1-methylpseudouridine does not.

A-D) Scatterplots showing the change in absorbance at 254 nm as a function of temperature for the indicated duplexes, with an accompanying bar graph showing the determined melting temperature for the same duplexes. Plotted are the means of the calculated melting temperature from three replicate experiments, with the error bars representing the standard deviation around the mean. A, C) correspond to duplexes containing Ψ while B, D) correspond to duplexes containing m1Ψ.

Chapter 4

Alkylative damage of mRNA leads to ribosome stalling and rescue by trans translation in bacteria

Erica N Thomas, Kyusik Q Kim, Emily P McHugh, Thomas Marcinkiewicz, and Hani S Zaher

This chapter is currently published in Elife as Erica N Thomas, Kyusik Q Kim, Emily P McHugh, Thomas Marcinkiewicz, and Hani S Zaher (2020). Alkylative damage of mRNA leads to ribosome stalling and rescue by trans translation in bacteria

Abstract

Similar to DNA replication, translation of the genetic code by the ribosome is hypothesized to be exceptionally sensitive to small chemical changes to its template mRNA. Here we show that addition of common alkylating agents to growing cultures of *E. coli* leads to accumulation of several adducts within RNA, including N(1)-methyladenosine (m^1A). As expected, the introduction of m^1A to model mRNAs was found to reduce the rate of peptide-bond formation by three orders of magnitude in a well-defined *in vitro* system. These observations suggest that alkylative stress is likely to stall translation *in vivo* and necessitates activation of ribosome-rescue pathways. Indeed, the addition of alkylation agents was found to robustly activate the transfer-messenger RNA system, even when transcription was inhibited. Our findings suggest that bacteria carefully monitor the chemical integrity of their mRNA and they evolved rescue pathways to cope with its effect on translation.

Introduction

Nucleic acids are consistently experiencing damage from numerous endogenous and exogenous insults, including reactive-oxygen species, ultraviolet radiation, and alkylating agents (1–3). In particular, the oxygen and nitrogen atoms of nucleobases are readily modified by alkylating agents. RNA is more susceptible to chemical insults than DNA, in part due to its exposed Watson-Crick (WC) hydrogen-bonding interface (4, 5). Notably, the integrity of the WC face is paramount during codon recognition of the tRNA selection process, during which the three nucleotides of the codon base pair with those of the anticodon of the tRNA (6). Changes that disrupt the ability of the mRNA to properly base pair with the cognate tRNA are then highly likely to reduce translational speed and fidelity (7–12). To this end, several alkylative damage adducts have either been predicted or shown to be detrimental to the decoding process (8, 11, 12). For example, our group has previously shown that O6-methylguanosine (m^6G), which is highly mutagenic during DNA replication, interferes with the speed and accuracy of decoding when present in mRNA. Interestingly, the effect of m^6G on translation was found to depend on its position within the codon (8). These observations suggest that given the nature of the decoding process, during which three nucleotides are read simultaneously, modifications to the mRNA can have complex effects on tRNA selection that cannot be solely predicted by their effect on base pairing.

N1-methyladenosine (m^1A) is an interesting modification because it has been the focus of several recent studies as a potential regulatory modification on mRNA (13). However, a functional role for m^1A in RNA metabolism is not without controversy. Depending on the m^1A-seq technique used, m^1A has been found on as much as 20% of the transcriptome (14, 15), and as low as nine sites only (16). Still, regardless of the method used to map the modification, over half of the

identified m^1A adducts have been mapped to the coding region of transcripts, suggesting that modification is likely to affect ribosome function (14, 15). Notably, a specific regulatory role of this modification during translation has not been convincingly identified. On the contrary, studies generally support the hypothesis that m^1A exists primarily as a damage adduct that disrupts the decoding process (12). This idea is supported by studies conducted using *E. coli* translation extracts, for which the presence of m^1A at any of the three positions within the codon significantly decreased protein-synthesis yield (12). This effect on translation is not unexpected, considering the structure of m^1A; the addition of the methyl group to the N1 atom changes the hydrogen-bond donation and acceptance of the nucleobase. Furthermore, the modification introduces a resonance structure with a positive charge to the nucleobase. Consistent with these ideas, the presence of m^1A has been shown to cause local duplex melting in RNA (17), and hence would likely occur during codon recognition of tRNA selection.

No known methyltransferase that specifically adds m^1A to mRNA has been identified. Instead, m^1A and several other adducts have been hypothesized to primarily result from reactions between RNA and endogenous and exogenous chemicals (3). In yeast, for example, the addition of alkylating compounds was found to significantly increase the levels of m^1A within mRNA, among several other adducts (18). Interestingly, these compounds were also observed to activate eukaryotic-quality-control pathways known to be responsible for ribosome rescue, suggesting that alkylation stress causes ribosome stalling presumably due to its damaging effect on mRNA. These quality-control processes include the mRNA-surveillance pathway of no-go decay (NGD) and ribosome-quality-control (RQC) pathway responsible for the degradation of the associated incomplete nascent peptide (19). Briefly, in eukaryotes, ribosome stalling results in ribosome pileup and eventual collisions. Collided ribosomes are recognized by an E3 ligase (Hel2 in yeast

and ZNF598 in mammals), which adds K63-linked ubiquitin chains to ribosomal proteins (20–27). The ubiquitination is used as a signal to recruit downstream factors involved in mRNA degradation and ribosome splitting (20, 24). The dissociated large-ribosome subunit, still bound to the peptidyl tRNA, is recognized by another E3 ligase (Ltn1 in yeast and listerin in mammals), which adds K48-linked ubiquitin to the nascent peptide, acting as a signal for its degradation by the proteasome (28–31).

Bacteria appear to have evolved entirely distinct mechanisms to deal with stalled ribosomes. This distinction between the two domains of life has been hypothesized to be the result of the divergent mechanisms utilized to terminate protein synthesis and recycle the ribosome (19). In bacteria, at least four discrete rescue mechanisms have been identified. These include *trans* translation by the tmRNA as well as several other mechanisms that recruit alternative rescue factors (Arf proteins), which alone or in complex with release factors terminate protein synthesis in the absence of stop codons (32). Of these, the tmRNA system appears to be the most widely utilized and conserved rescue pathway (33). tmRNA or transfer-messenger RNA is a unique molecule in that it contains a transfer RNA segment, which is aminoacylated by Ala-tRNA synthetase; and a messenger mRNA segment, which is used to switch the mRNA template from the defective mRNA to the molecule itself, and hence the name *trans* translation (34, 35). Upon ribosome stalling, tmRNA binds the A site of the ribosome in a quaternary complex with elongation factor Tu (EFTu), its partner protein SmpB and GTP (36). Following peptidyl transfer to tmRNA, the original defective mRNA exits the ribosome, which then begins *trans* translation whereby the ribosome switches template to the mRNA part of tmRNA (35, 37). This mRNA encodes a peptide-degradation signal followed by a stop codon, ensuring that the incomplete

peptide is degraded by the ClpXP protease system following canonical termination and recycling of the ribosome (38).

We note that the tmRNA system has been extensively studied in the context of truncated mRNAs, which result from a myriad of conditions including ribosome stalling (35), but whether the process is also activated in response to chemical insults that modify RNA is unknown. Here we explored the impact of alkylation damage on translation and investigated its effect on tmRNA activity in *E. coli*. We first demonstrated that treating *E. coli* with common alkylating agents increases the levels of several potentially disruptive alkylative adducts, including m^1A. To quantify the effect of m^1A on decoding, we used a well-defined *in vitro* translation system to measure observed rates of peptide-bond formation in the absence and presence of the modification in mRNA. The modification reduced the rate of peptide-bond formation by almost three orders of magnitude. The decrease in peptide-bond formation was also accompanied by a reduction in the end point of the peptidyl-transfer reaction, suggesting that the modification affects the proofreading phase of tRNA selection. Highlighting the disruptive effect of m^1A on tRNA selection was the observation that aminoglycosides, which increase peptide-bond formation on mismatched-codon-anticodon interactions, had no effect on reactions with m^1A-programmed mRNAs. These findings suggest that alkylation stress, which increases the amount of disruptive adducts such as m^1A, causes widespread stalling in bacterial cells and activates rescue pathways. In complete agreement with these ideas, we documented robust activation of tmRNA in *E. coli* cells treated with alkylating agents, even when transcription was inhibited. Interestingly, DNA damage was also found to trigger tmRNA activation, but this activation was significantly suppressed when transcription was inhibited. Hence, alkylation stress is likely to significantly impact translation through its effect on mRNA and rescue pathways such as *trans* translation are

responsible for dealing with its consequences. Consistent with these proposals, *E. coli* strains lacking functional tmRNA were found to be sensitive to alkylating agents, and exhibited delayed recovery compared to wild-type (WT) cells. Collectively our data suggest chemical damage to mRNA is highly detrimental to cellular homeostasis, even in organisms where mRNA is highly transient.

Results

Treatment of *E. coli* with MMS or MNNG causes significant increases in alkylative damage of RNA

As an initial step to explore the impact of alkylative damage on translation in bacteria, we sought to establish methods that allowed us to robustly induce RNA alkylation in *E. coli.* We have recently shown that addition of methyl methanesulfonate (MMS) to growing yeast cultures leads to accumulation of alkylation adducts in RNA (18). As a result, we expected the compound to similarly modify RNA in bacteria. To ensure that any effect we observe on translation is a general response to RNA alkylation, we also chose to study the impact of methylnitronitrosoguanidine (MNNG) on RNA metabolism and translation. MMS and MNNG work through different nucleophilic-substitution mechanisms to alkylate nucleic acids. MMS alkylates its target through an SN_2-type mechanism, while MNNG reacts through an SN_1-type one (5); therefore, we expected to observe differences in the types and levels of adduct that each agent generated. To identify and determine the abundance of each modification, total RNA was isolated from mid-log growing *E. coli* cells that had been mock treated (DMSO) or treated with MMS (0.1 %) or MNNG (5 μg/mL) for 20 minutes. RNA was consequently digested to nucleotide monophosphates by incubating it with P1 nuclease. Nucleosides were generated by incubating the P1-reaction products with calf-intestinal phosphatase (CIP); and analyzed by liquid chromatography – mass spectrometry (LC-MS). We generated standard curves for each of the unmodified nucleosides, as well as for N1-methyladenosine (m^1A), N6-methyladenosine (m^6A), N1-methylguanosine (m^1G), O6-methylguanosine (m^6G), and N3-methylcytidine (m^3C) in order to directly quantify the modified nucleosides within each treatment (Supplementary Figure 1).

To confirm that our LC-MS methods are relatively accurate, we measured the ratio of m^6A/A levels in untreated cells, which has been estimated to be 0.3% in *E. coli* (39). In agreement with these earlier studies, we measure a ratio of 0.6% (Figure 1A). Also as expected, we did not detect an increase in m^6A levels after treatment with either alkylating agent (Figure 1A), as neither MMS nor MNNG alkylate the N6 position of adenosine (5). Additionally, MMS and MNNG have been shown to react with N1 of G, albeit it with reduced efficiency (5); but we did not observe significant increases in m^1G levels (Figure 1B). These observations can be rationalized by the fact that m^1G is a natural modification of *E. coli* tRNA and rRNA (40), which significantly increases the background levels of the modification. Indeed, the base level of m^1G is at least 200-fold higher than that of m^1A (Figure 1). Similarly, since m^7G is a natural modification in rRNA and tRNA (40), we observe no significant change to its levels upon MMS and MNNG additions (Figure 1C).

Contrary to m^6A and m^1G, we measured 10- to 200-fold increases in m^3C and m^1A relative levels in cells treated with MMS or MNNG (Figures 1D and 1E), and a more than tenfold increase in m^6G relative levels, but only in those treated with MNNG (Figure 1F). These findings are consistent with previous studies showing that the O6 position of guanosine is reactive with MNNG but not MMS, and that m^3C and m^1A are minor alkylative adducts in double-stranded DNA (41) but are substantially more reactive as nucleophiles in the absence of hydrogen bonding (42). This same increase in reactivity for N1 to G in single-stranded RNA is not observed because it is a secondary amine with an adjacent carbonyl group which is less reactive than N1 of A and N3 of C, both of which have the higher reactivity profiles of amidine groups (5).

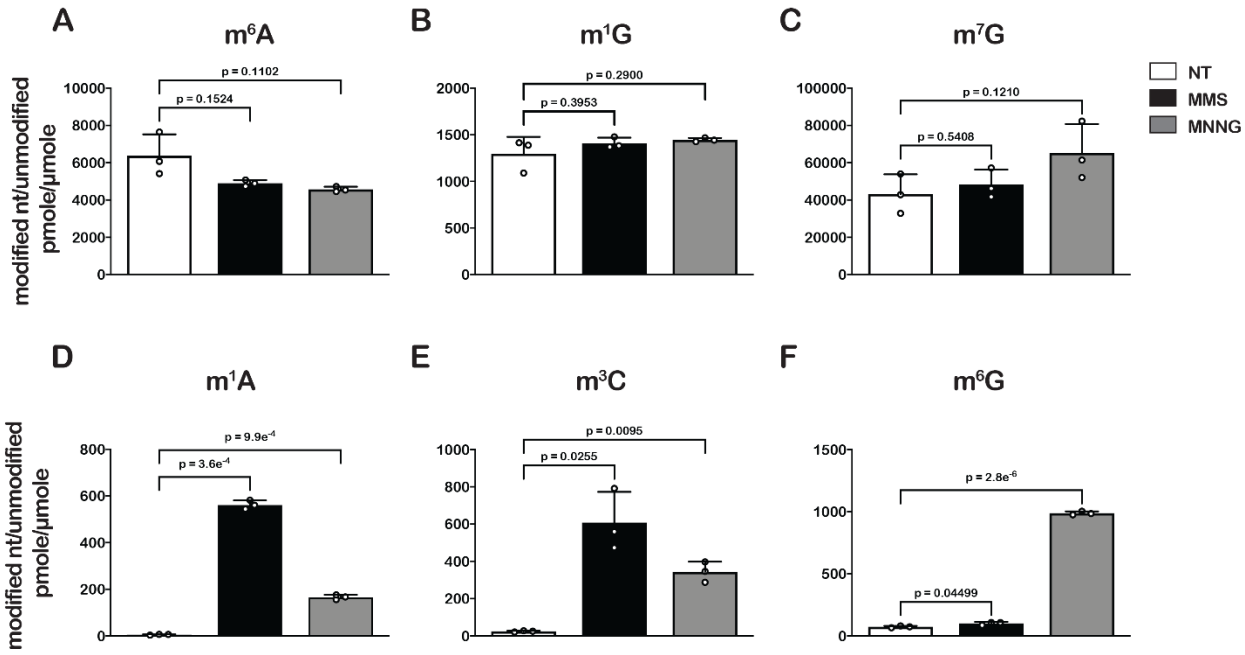

Figure 1: Treatment of *E. coli* with MMS and MNNG results in significant accumulation of alkylative-damage adducts in RNA

A-E) Bar graphs showing the amount of the indicated modified nucleotides relative to their unmodified parent in untreated (white bars), MMS-treated (black bars) and MNNG-treated (grey bars) cells. The values plotted are the averages of three biological repeats and the error bars represent standard deviations around the mean. Significant differences in mean, as denoted by $p < 0.05$, were determined by Welch's t-test.

N1-methyladenosine has drastic effects on peptide-bond formation *in vitro*

Having established a method of increasing the levels of alkylative adducts in *E. coli* mRNA, we next became interested in assessing the effects of some of these modifications on translation using a well-defined *in vitro* system (43). In particular, we focused on modifications whose levels significantly increase in the presence of alkylation stress and have been documented to disrupt base-pairing properties of the nucleobase. Therefore, m^1A and m^3C were obvious candidates as both satisfied these two requirements. Since m^3C phosphoramidite was not commercially available, we opted to study the effects of m^1A on translation in our system. Briefly, we generated ribosomal initiation complexes carrying f-[^{35}S]-Met-tRNA^{fMet} in the P site and displaying either an unmodified GAA codon, or an m^1A adduct at the second position ($G^{m1}AA$) in the A site (Figure 2B). The GAA codon is decoded by its cognate Glu-tRNA^{Glu}.

Both complexes were reacted with Glu-tRNA^{Glu}•EFTu•GTP ternary complex, and the formation of f-[^{35}S]-Met-Glu dipeptide was followed as a function of time by taking aliquots at the appropriate times and quenching the reaction with potassium hydroxide, which hydrolyzes the peptide away from the tRNA. The resulting dipeptide was resolved from unreacted fMet using an electrophoretic thin-layer chromatography (TLC) system (44). The relative amount of dipeptide was quantified using phosphorimaging and fitted to a single-exponential to determine the observed rate of peptide-bond formation. As expected, m^{1}A was found to severely inhibit peptide-bond formation. The observed rate of 0.15 s^{-1} for the G^{m1}AA complex was measured to be more than 250-fold slower relative to the observed rate of 58 s^{-1} for the unmodified GAA complex. Furthermore, the end point of the m^{1}A reaction, which reports on the efficiency of proofreading (45), was found to be ~tenfold lower relative to the unmodified one (Figure 2C). These results demonstrate that m^{1}A is highly detrimental to the tRNA selection process and is highly likely to stall ribosomes *in vivo*.

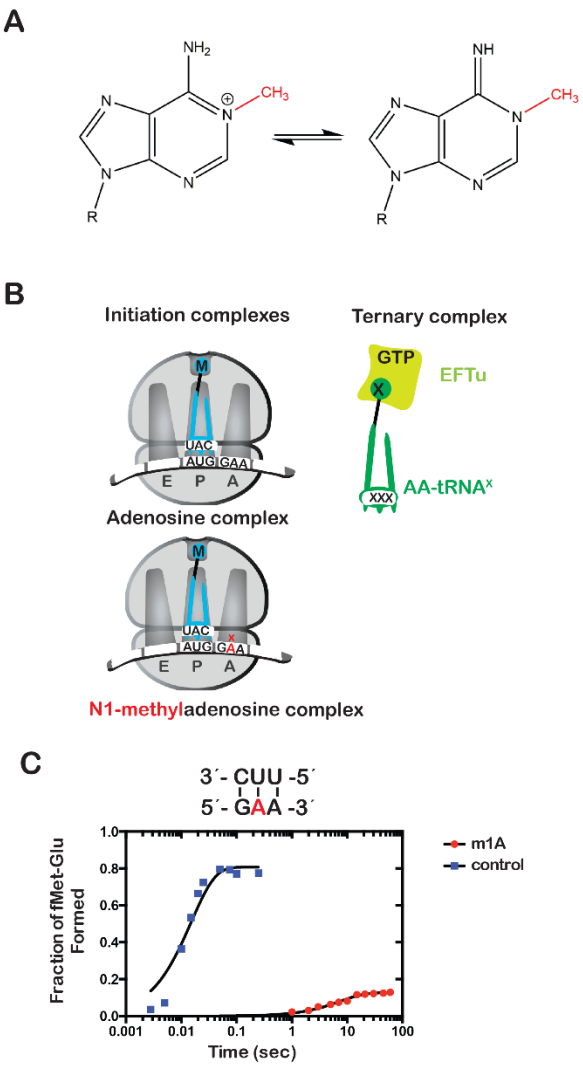

Figure 2: N(1)-methyladenosine (m^1A) in mRNA significantly decreases the rate and endpoint of peptide-bond formation *in vitro*
A) Chemical structure of m^1A. The N1-methyl group is highlighted in red, and the resonance structure of the molecule is represented. **B)** Schematic representation of adenosine and m^1A initiation complexes encoding for the dipeptide Met-Glu. Both complexes contain the initiator fMet-$tRNA^{fMet}$ in the P site; the A complex displays a GAA codon, while the m^1A complex displays a $G^{m1}AA$ codon in the A site. **C)** Representative time-courses of peptide-bond-formation reactions between initiation complexes programmed with unmodified mRNA (blue) or an m^1A-modified one (red) m^1A, and Glu-$tRNA^{Glu}$ ternary complex.

Next, we wondered whether the m^1A:U base pair between the codon and the anticodon of the tRNA is recognized by the ribosome as a simple mismatch or is more disruptive than that. During tRNA selection, aa-tRNAs that have only one mismatch between their anticodon and the A-site codon are termed near-cognate (46). Although the ribosome efficiently discriminates

against incorporation of near-cognate aa-tRNAs, the addition of certain aminoglycosides alters the selection process and allows for their misincorporation (47). For instance, paromomycin binds the decoding center of the ribosome, which leads to local conformational changes that lower the energy barrier required to shift the ribosome into a "closed" conformation (48, 49). This conformation typically occurs in the presence of cognate aa-tRNAs and is a prerequisite for their accommodation into the active site of the ribosome for peptidyl transfer to take place (49). In contrast, addition of aminoglycosides to reactions containing non-cognate aa-tRNAs, which harbor more than one mismatch between their anticodon and the A-site codon, has little to no effect on peptide-bond formation (47, 50). As a result, the effect of aminoglycosides on peptidyl transfer can be used as a diagnostic for the sort of interactions taking place in the decoding center and how modifications alter them. For instance, we recently showed that addition of paromomycin and streptomycin de-represses the effects of the oxidative adduct 8-oxoguanosine (8-oxoG) on peptide-bond formation (9). These findings suggest that the ribosome recognizes this modification as a simple mismatch when paired with its partner nucleotide. Interestingly and in contrast to 8-oxoG, in the presence of m^1A we found the addition of paromomycin to have little to no effect on the observed rate of peptide-bond formation. In particular we measured observed rates of 0.15 s^{-1} and 0.2 s^{-1} in the absence and presence of antibiotic, respectively (Figure 3). Additionally, the endpoints of the very same reactions were 0.10 and 0.11, respectively. These findings suggest that not only is m^1A unable to base pair with U in the decoding center, but that the modification significantly distorts the codon-anticodon helix. This distortion results in the aa-tRNA, that is otherwise cognate, to be recognized as a non-cognate one by the ribosome.

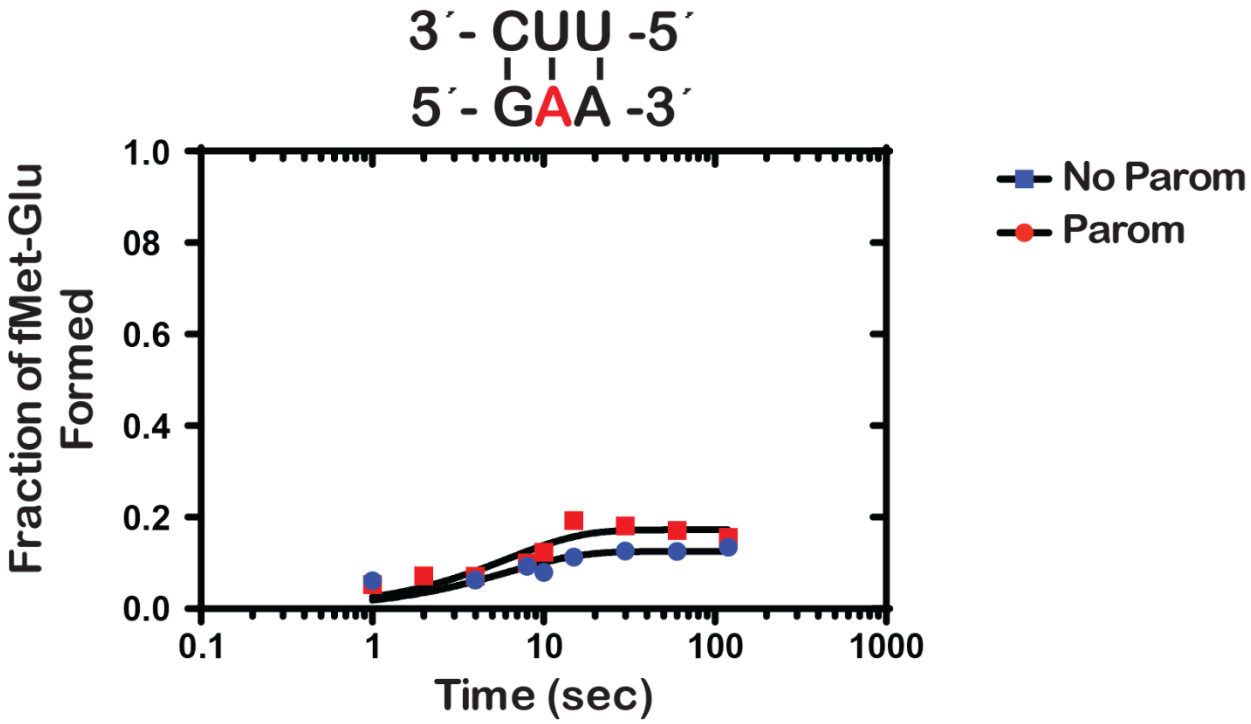

Figure 3: Paromomycin does not rescue the effect of m^{1}A on peptide-bond formation
Representative time-courses of peptide-bond-formation reactions between initiation complexes programmed with m^{1}A mRNA and Glu-tRNA^{Glu} ternary complexes in the absence (blue) and presence (red) of paromomycin.

To provide further insights into how an m^{1}A modification within the codon changes the base-pairing properties of the nucleotide, we investigated how it alters miscoding in the presence of all near- and non-cognate tRNAs. We performed an aa-tRNA-reactivity survey, in which we reacted the previously described unmodified- and m^{1}A-containing-initiation complexes (Figure 2) with all 20 possible aa-tRNA isoacceptors for two minutes (Figure 4). As anticipated, for the codon containing the unmodified adenosine, we observed no significant dipeptide accumulation except in the presence of the cognate Glu-tRNA^{Glu} ternary complex (Figure 4). For the codon containing m^{1}A, no significant dipeptide accumulation occurred in the presence of any aa-tRNA. These findings strongly suggest that the modification inhibits base pairing altogether and does not alter the base-pairing preference of the nucleotide.

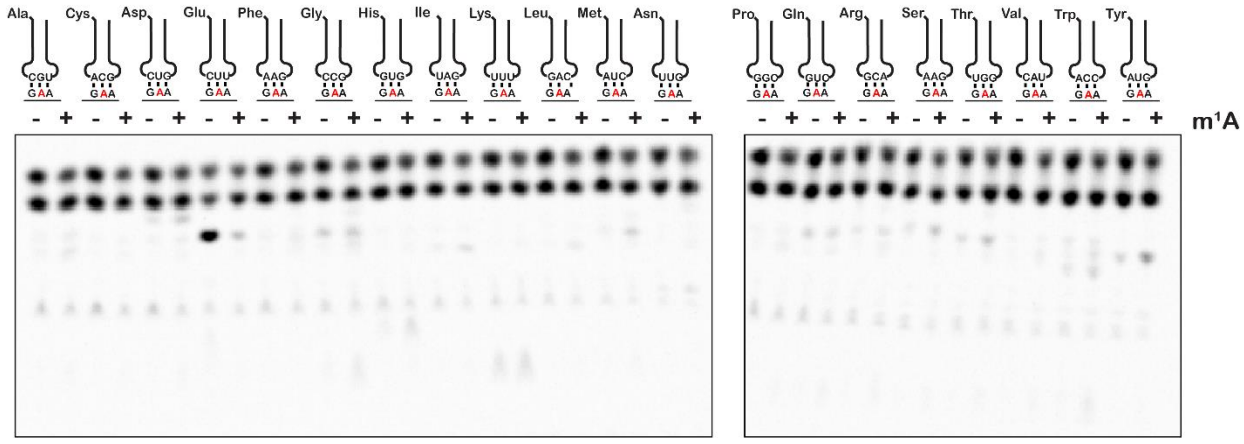

Figure 4: m[1]A does not alter the reactivity of ribosomes with near-cognate and non-cognate aa-tRNA
Phosphorimager scan of electrophoretic TLCs used to follow dipeptide-formation reactions between unmodified and m[1]A-modified complexes with all canonical aa-tRNA ternary complexes.

Alkylative damage of RNA increases tmRNA activity *in vivo*

Our mass-spectrometry analysis indicated that addition of MMS and MNNG to *E. coli* significantly increases the levels of several modified nucleotides, including m[1]A (Figure 1), which we showed to have drastic effects on peptide-bond formation (Figure 2). As a result, we predicted the addition of these compounds to stall translation *in vivo* and to activate rescue pathways such as *trans* translation by tmRNA. As mentioned earlier, tmRNA encodes a peptide-degradation sequence, which ensures incomplete nascent peptides are c-terminally tagged for rapid degradation by cellular proteases. The mRNA sequence encoding this tag can be modified without significantly affecting the *trans* translation activity of tmRNA. In particular, substituting the sequence for one that encodes a His-tag has been successfully used to identify tmRNA targets (51). We took advantage of this tmRNA variant to assess its relative activity in response to alkylation stress by probing with anti-His antibody. Consistent with our proposal that alkylation stress activates the tmRNA system, we observed 2 to 3-fold increases in His_6-tagging levels upon the addition of MMS and MNNG to *E. coli* expressing tmRNA-His_6 (Figures 5A and 5B). As expected, this increase in tmRNA activity was accompanied by activation of the

adaptive response as judged by the accumulation of Ada protein, the principal mediator of the process in response to alkylation damage (52–54). We also observe activation of the SOS response as evaluated by the accumulation of its principal mediator RecA (55) It is worth noting that at this concentration of MMS and duration of treatment, we observe little to no effect on cellular viability as assessed by spot assays (Supplementary Figure 2A and 2B). Altogether our data suggest that alkylation stress stalls translation in bacteria and activates *trans* translation by tmRNA.

Under normal conditions, His-tagged products resulting from tmRNA activation are targeted for degradation by the ClpAP, ClpXP, and Lon proteases, presumably because they are incomplete peptides that are likely to misfold. Indeed, previous reports have shown the deletion of *DclpP*, *clpX*, and *lon* genes to result in increased accumulation of His-tagged products (56). These observations suggest that the amount of His-tagging that we detect in the presence of MMS and MNNG is likely an underestimate of the tmRNA-activation levels. To obtain a more accurate measure of *trans* translation in response to alkylation stress, we treated *E. coli* null mutants of *clpP*, *clpX*, and *lon* with MMS and MNNG. As expected, the levels of His-tagging triggered by addition of the alkylation compounds increased by more than twofold in the absence of the proteases (Supplementary Figure 3). In agreement with previous studies that suggested Ada to be subject to proteolysis (57), in *clpP*, *clpX*, and *lon* cells, the factor was observed to accumulate even in the absence of alkylation stress.

As has been noted in a previous study, the His-tagging patterns between each of the samples appear almost identical (56). This was a surprising observation, as we expected the alkylative damage to be randomly located throughout the transcriptome, thereby resulting in a more uniform streak of his-tagging or banding patterns that varied from sample to sample. A

plausible explanation for this banding pattern is that the antibody we used displays preference for certain peptide sequences. We tested this idea by probing with antibodies from three different manufacturers and compared the observed pattern. Interestingly, each antibody displayed a unique pattern, with some recognizing only a small subset of potential peptides (Supplementary Figure 4). Thus, the observed consistent His-tagging pattern is likely due to an artifact of the His antibodies rather than a particular subset of proteins that are preferentially His-tagged at certain locations.

The accumulation of His-tagged peptide products suggests that alkylative damage of RNA is stalling ribosomes *in vivo* and activating tmRNA. However, the alkylative damage from MMS and MNNG damages DNA as well as RNA (5). This is supported by the increase in RecA that we observe upon treatment with alkylating agents, which is a protein that is essential for the maintenance and repair of DNA (58) (Figure 5A). Therefore, it is also possible that the resulting increase in His-tagging was primarily due to the production of truncated transcripts that are produced by stalled RNA polymerase on damaged DNA. As most of these truncated transcripts lack a stop codon, they represent the classical targets of tmRNA (35). To ensure that the observed His-tagging was due to RNA damage rather than truncated RNA produced from damaged DNA, we pre-treated cells with rifampicin approximately forty seconds before treating with damaging agents. Rifampicin is an inhibitor of RNA polymerase initiation; therefore, the pretreatment with rifampicin halts transcriptional initiation and allows us to separate the effects of DNA damage from RNA damage (59). In addition to MMS and MNNG, we also treated cells with ciprofloxacin and mitomycin C. Ciprofloxacin is an antibiotic that inhibits the ligation activity of DNA gyrase and topoisomerase IV but not the cleavage activity, thereby causing the topoisomerases to create double stranded breaks in DNA (60). Mitomycin C causes intra- and

inter-strand DNA crosslinks that can block the activities of DNA polymerase and RNA polymerase (61). We predicted that these two agents, which specifically cause DNA damage, would produce truncated transcripts and result in His-tagging by tmRNA. For these two drugs, however, the pretreatment with rifampicin is expected to inhibit the accumulation of His-tagged products. In agreement with our model, pretreatment with rifampicin only slightly decreased the amount of His-tagging induced by MMS and MNNG (10-20%) (Figure 5C), suggesting that the majority of the observed tmRNA activity is due to direct damage to the mRNA. In contrast, the same rifampicin pretreatment combined with ciprofloxacin treatment decreased the amount of His-tagging by almost twofold. Interestingly, for the mitomycin C treatment we did not observe any His-tagging even though we could infer that significant DNA damage had occurred as assessed by the increase in RecA levels (Supplementary Figure 5). Regardless of this last observation, we conclude that while truncated transcripts produced from damaged DNA do activate tmRNA, the predominate trigger of tmRNA activation in MMS- and MNNG- treated samples is alkylative damage of RNA.

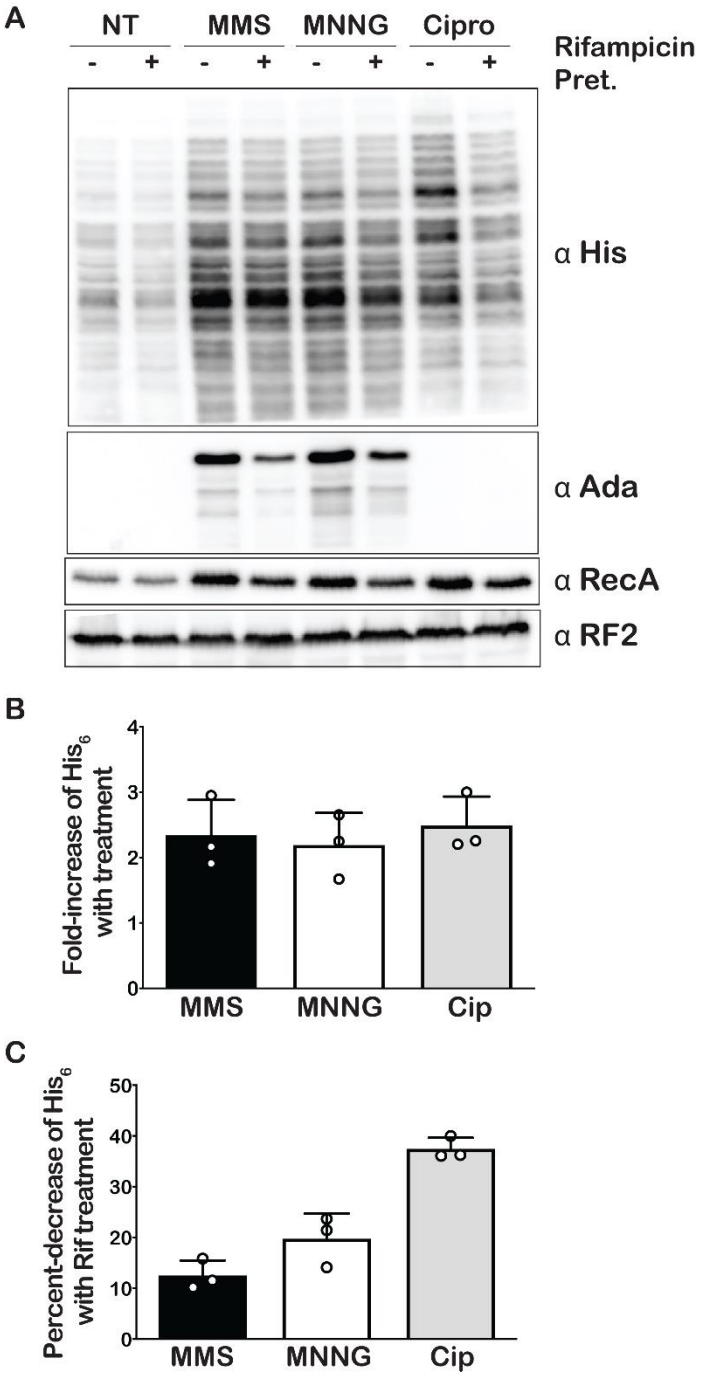

Figure 5: Alkylative stress activates *trans* translation in *E. coli* in a transcription-independent manner. Western-blot analyses of total protein isolated from an *E. coli* strain expressing tmRNA-His_6. Cells were either untreated or treated with MMS, MNNG, or ciprofloxacin. Additionally, for each condition, cells were either mock pretreated or received a rifampicin pretreatment. Blots were probed with the indicated antibodies.Bar graph showing the relative change in His signal (tmRNA activity) as a result of the addition of each of the indicated compound.Bar graph used to depict the fold-decrease of His_6 levels upon pre-treatment with rifampicin for each of the indicated treatments. In all cases, the initial His signal was normalized to that corresponding to RF2 levels before it was used to calculate the relative change. Three independent experiments were used to obtain the bar graphs, with the mean values plotted and the error bars representing the standard deviation around the mean.

Addition of MMS-treated mRNA to *E. coli* extracts results in *trans* translation

To add further support for our model that mRNA modification by alkylation agents activates tmRNA, we prepared S30 extracts from the protease-deficient *E. coli* strain that harbors His-tagged tmRNA and assessed the translation of chemically damaged mRNAs in a cell-free system. We amplified the *prmc* gene, added a FLAG tag to its N-terminus and used it as a template for *in vitro* transcription (Figure 6A). The resulting mRNA was either mock treated or treated with 0.5% MMS, which did not alter its integrity as assessed by denaturing agarose electrophoresis (Figure 6B). ^{35}S labeling and western-blotting analysis (using anti-FLAG antibody) revealed that both mRNA species were translated efficiently in our extract, with the MMS-treated mRNA yielding slightly less full-length product. These observations suggest that modification by MMS results in stalling on this mRNA (Figure 6C). Notably, probing with anti-His antibody revealed that tmRNA is significantly activated in reactions containing damaged mRNA (Figure 6C). The observation that tmRNA tagging occurs on modified mRNA in a system where transcription is not occurring provides important support for our model that *trans* translation responds to ribosome stalling on damaged mRNA.

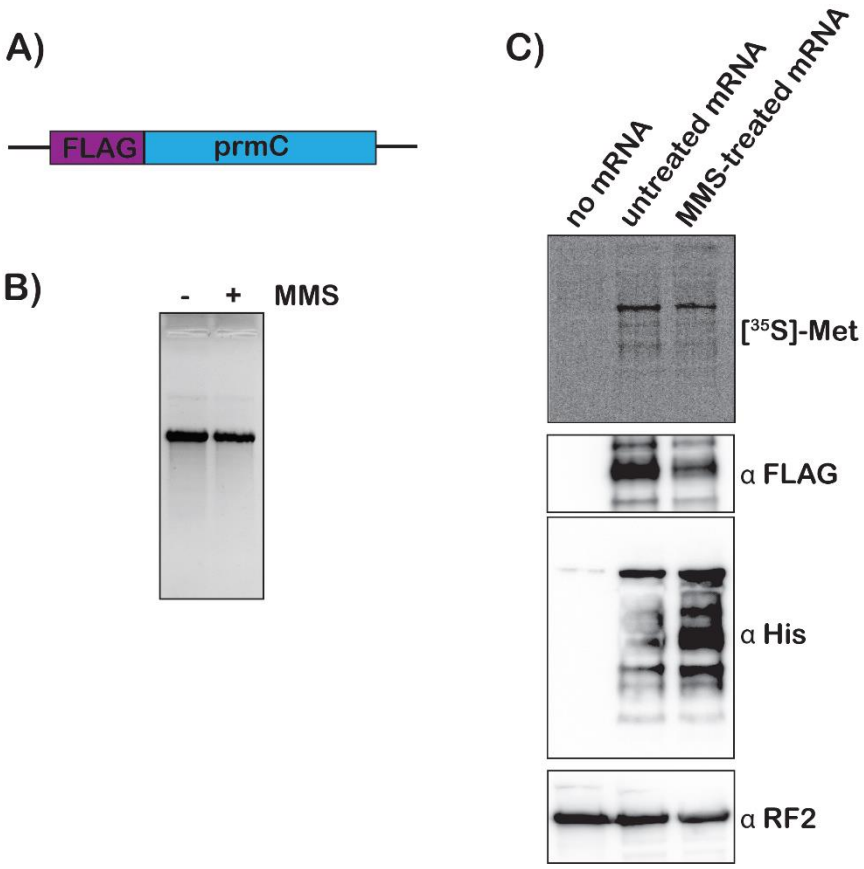

Figure 6: Translation of MMS-treated mRNA results in tmRNA tagging in an S30 extract.
A) Schematic of the mRNA used in the *in vitro* translation assays. **B)** Fluorescence image of EtBr-stained gel used to visualize the mock-treated and MMS-treated RNAs. **C)** Top shows a phosphor-imager scan of a PVDF-transfer membrane of a Bis-Tricine gel used to separate products from the *in-vitro*-translation reactions containing the indicated mRNAs. Bottom is western-blotting analyses of the same membranes with the indicated antibodies. Shown is a representative of two assays.

Deletion of the *ssrA* gene leads to stabilization of m^1A-modified mRNAs

Previous studies indicated that in addition to *trans* translation, tmRNA plays a role in the degradation of its target mRNAs. In particular, the molecule facilitates the recruitment of RNase R, which initiates nonstop mRNA decay (62). To this end, deletion of the *ssrA* gene results in the accumulation of nonstop mRNAs. As our findings suggest that ribosomes stalled on modified mRNAs engage the *trans*-translation machinery, we hypothesized that tmRNA is also likely to play a role in the degradation of chemically damaged mRNAs. We note that analogous studies by

our group conducted in yeast took advantage of the polyA tail of mRNAs in eukaryotes in order to purify them prior to modification analysis by LC-MS (18). Unfortunately, owing to the lack of a similar feature in bacterial mRNAs, a similar strategy for *E. coli* cannot be used. Nonetheless, we were able to use an indirect approach to qualitatively assess the levels of m^1A modification in mRNAs. In this approach, total RNA is resolved on denaturing agarose gels, transferred to nitrocellulose and probed with antibodies specific to the nucleoside of interest (63). In our hands, antibodies raised against m^1A did not produce a signal even with positive standards. In contrast, we were able to obtain a robust signal with an anti m^6A antibody (Supplementary Figure 8A). Since m^1A can readily isomerize to m^6A through Dimroth rearrangement by base treatment (64), immunoblotting of base-treated RNAs with this antibody can be used to assess the levels of m^1A. As expected, and in agreement with our LC-MS analysis (Figure 1), without base treatment immunoblotting with m^6A antibody showed that MMS addition to cells leads to a slight decrease in the signal, suggesting that the treatment does not alter the levels of this modification significantly. In contrast, base treatment of the gel prior to transfer revealed that treating cells with MMS causes a significant increase in the signal for RNA species that co-migrated between rRNA and tRNA species, which we attribute to mRNA species having m^1A modification (Supplementary Figure 8B). More important was the observation that the MMS-induced signal was much higher in the *ΔssrA* cells (Supplementary Figure 8B). Our observations suggest that not only does tmRNA rescue ribosomes stalled on modified mRNAs, but that m^1A levels in mRNA increase in its absence.

The ability to rescue stalled ribosomes is important for cellular recovery after alkylative damage

Even though the ssrA gene that encodes tmRNA is highly conserved in bacteria, previous studies have shown that Δ*ssrA E. coli* strains show no appreciable growth phenotype under standard laboratory conditions but do exhibit delayed growth under certain stress conditions (65, 66). Since we observed that tmRNA is utilized to rescue ribosomes stalled due to damaged RNA, we hypothesized that the ability of cells to rescue stalled ribosomes is important for cellular recovery upon treatment with alkylating agents. To test this, we treated Δ*ssrA* and WT cells with either 0.5% MMS or 20 μg/mL MNNG, washed the cells to remove the alkylating agent, and allowed them to recover while monitoring growth. As expected, in the absence of any pretreatment, Δ*ssrA* and WT cells recover at approximately the same rate. However, after treatment with MMS or MNNG, Δ*ssrA* cells have an approximately 1.5-hour lag in their recovery compared to WT cells (Figure 7). To rule out cellular death as a cause for the observed lag, we treated both Δ*ssrA* and WT cells with 0.5% MMS for 20, 40, and 60 minutes, washed the cells to remove the alkylating agents, and performed spot assays to quantify cell death. We observe similar levels of cell death for Δ*ssrA* and WT cells, suggesting that the observed lag in recovery time is not due to a difference in the number of cells killed, but rather the ability of the cells to quickly recover after treatment with alkylating agents (Supplementary Figure 2C and 2D). Collectively, our findings suggest that cells employ *trans* translation to rescue ribosomes stalled on damaged mRNA to quickly recover from alkylation stress.

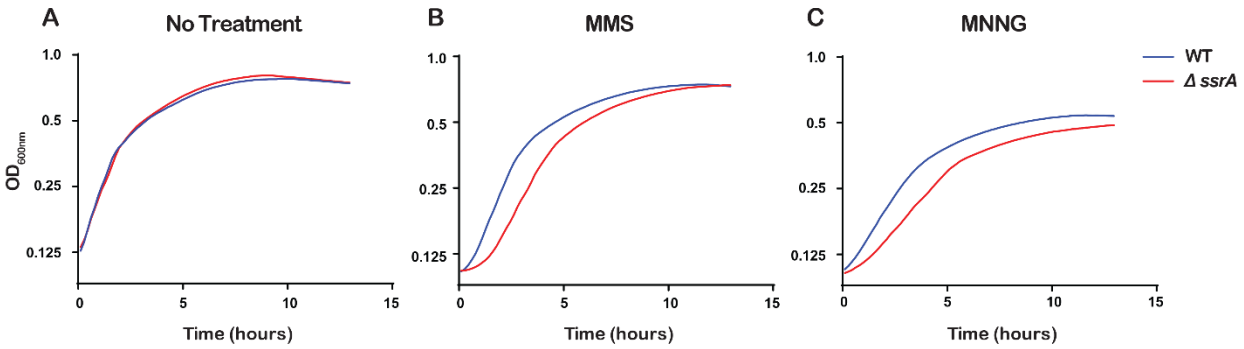

Figure 7: Ribosome rescue by tmRNA is important for cellular recovery after treatment with alkylating agents

A-C) Growth curves, as measured by change in OD_{600nm} as a function of time, for the indicated cells following a treatment with the denoted compound. Average of three replicate growth assays is plotted.

Discussion

Several recent reports have shown that mRNA can be enzymatically modified to regulate its function (67). Among these modifications, m^6A is arguably one of the most significant ones and appears to play important roles in the regulation of gene expression (68). Pseudouridine (Ψ), due to its high abundance in mRNA, has recently emerged as another potentially important modification. Interestingly, pseudouridine-modified (and derivatives of Ψ) mRNAs have been shown to be effective for biotechnological purposes as they are less immunogenic and produce significantly higher levels of functional proteins than their unmodified counterpart (69). Although much has been revealed about the role the so-called intentional modifications serve in regulating various aspects of mRNA metabolism, most chemical modifications of mRNA are disruptive damage adducts (2). Previous work had shown that several alkylative damage adducts, including m^1A and m^6G, drastically slow translation and increase miscoding *in vitro* (8, 12). However, little is known about how alkylative damage of mRNA elicits cellular responses *in vivo*, and especially in bacteria. Additionally, the quantitative effects of m^1A on the speed and accuracy of translation are not fully understood. Here, we used compounds that alkylate nucleic acids to introduce damage adducts to bacterial RNA and assessed cellular responses to potential defects to translation. A priori, we hypothesized that the main ribosome rescue system in bacteria, the *trans*-translation pathway, works to release ribosomes stalled on damaged mRNA. Indeed, we find that upon treatment of *E. coli* with alkylating agents, *trans*-translation activity significantly increased (Figure 5). Furthermore, we show that cells lacking tmRNA display prolonged recovery from alkylation stress relative to wild-type cells (Figure 7).

This response to alkylation-mediated changes to translation is likely to be general, as it was nearly identical regardless of the specific compound used to elicit the damage. We used two

alkylating agents, MMS and MNNG, which work through an SN_2- and SN_1-type nucleophilic substitution mechanism, respectively (5). Indeed, LC-MS analysis revealed that the addition of the compounds results in different signatures of RNA modification. For instance, addition of MNNG leads to more than tenfold increase in m^6G levels, whereas that of MMS leads to a modest < 1.5-fold increase for the same modification (Figure 1). This is consistent with studies showing that MNNG produces a greater percentage of O-methyl adducts (5).

Our group had previously utilized an *in vitro* reconstituted bacterial translation system to investigate the impact of m^6G on decoding (8); however, we had not analyzed the effects of m^1A. We hypothesized that the positively charged resonance structure of m^1A would disrupt its ability to base pair. During decoding on the ribosome, the first and second position of the codon-anticodon helix are closely monitored by rRNA nucleotides as well as ribosomal-protein amino acids, ensuring that only Watson-Crick base pairs are accepted (49, 70, 71). We chose to analyze m^1A in the second position of the codon rather than the first because we wanted to to avoid possibly altering the interaction between the initiator tRNA and the P-site codon. As expected, the modification severely inhibited tRNA selection by the ribosome as reflected by the three orders of magnitude drop in the observed rate of peptide-bond formation and the tenfold decrease in the endpoint of the reaction (Figure 2C). This is consistent with a previous study showing that m^1A in mRNA significantly decreased protein-synthesis yield in S30 extracts (12). Interestingly, while the observation that m^1A severely inhibits decoding is expected, our finding that the addition of paromomycin does not suppress this effect at all (Figure 3) is unanticipated. Since paromomycin allows the incorporation of near-cognate aa-tRNAs (47) (i.e. those that have one mismatch between their anticodon and the A-site codon), this observation suggests that the modification is so disruptive that it affects base-pairing between the neighboring nucleotides.

Consequently, all aa-tRNAs are recognized as non cognates, or as having more than one mismatch (Figure 4).

Having confirmed that m^1A-modified mRNAs are highly inhibitory to tRNA selection *in vitro*, we then sought to investigate how bacterial cells deal with alkylated RNA, which includes m^1A-modified ones, *in vivo*. We hypothesized that *trans* translation is likely to be activated in response to stalls caused by alkylation damage to mRNA. To add support for this hypothesis, we used *E. coli* strains harboring a modified *ssrA* gene (encoding tmRNA), for which the encoded ssrA-degradation tag is altered to one that codes for a His tag (72). In these strains, the addition of His tags, as evaluated by western-blotting analysis, can be used to assess tmRNA activation. In complete agreement with our model, we observe a significant increase in His-tagging and hence increased *trans*-translation activity upon cellular treatment with alkylating agents (Figure 5A). We also showed that this activity is independent of active transcription (Figure 5) and hence is likely to be initiated as a result of direct damage to mature mRNAs. Future experiments aimed at characterizing the identity of the tagged peptides, using mass-spectrometry approaches for example, are likely to reveal important insights into the specificity of tmRNA tagging as well as that of the antibody recognition of tagged products. Since MMS is known to modify A and C, at least in a way that affects their Watson-Crick-base pairing properties, we expect tagging to occur preferentially on codons enriched for these two nucleotides.

Notably, because bacterial mRNAs do not contain poly-A tails like their eukaryotic counterparts, it is difficult to purify mRNA away from rRNA and tRNA; therefore, we cannot be certain that the observed effects on translation are exclusively due to mRNA damage. However, there exist several compelling reasons to support the hypothesis that the tmRNA response is primarily due to mRNA damage. For one, *trans* translation has been studied almost exclusively

in the context of defective mRNAs. It is difficult to imagine how a defective ribosome would still be capable of performing peptidyl transfer only with tmRNA. Second, the folding of rRNA as well as its association with ribosomal proteins is thought to make it a poor target for alkylative damage (2). Specifically, the rRNA residues responsible for monitoring the base pairing in the decoding center are not exposed; therefore, it is unlikely that they are damaged by the agents at a high incidence (73). Additionally, tRNAs are susceptible to alkylative damage, but only 3 out of an average of 76 nucleotides directly participate in base pairing with the codon. This reduces the probability that damaged nucleotides in tRNA cause the observed ribosomal stalling. Furthermore, unless the P-site tRNA is damaged, tmRNA is unlikely to be able to sense defects to the tRNA pool. Finally, the CCA-adding enzyme in *E. coli* has been shown to discriminate against tRNA backbone damage (74); without CCA ends these tRNAs are not aminoacylated and cannot participate in peptidyl transfer.

Several studies have shown that bacteria lacking a functional *trans*-translation pathway do not recover as efficiently after cellular stress, including metabolic and oxidative stress (65, 66). We observe that alkylative stress also causes a delayed recovery period in cells lacking tmRNA, likely because they are unable to efficiency rescue stalled ribosomes and resume growth (Figure 7). The Δ*ssrA* cells are likely able to eventually resume growth after alkylative damage because of the existence of several alternative ribosome-rescue factors. One factor, known as alternative ribosome-rescue factor A (ArfA) works by recruiting RF2 to hydrolyze the peptidyl-tRNA and release the ribosome (75, 76). This factor acts as a backup for *trans*-translation, as its expression increases when tmRNA activity is limited (77, 78). Another factor that can release stalled ribosomes is ArfB, although it does not appear to function solely as a backup for tmRNA and its physiological function remains to be elucidated (79, 80). Regardless, these alternative

ribosome rescue factors in *E. coli* are likely responsible for the eventual recovery we observe, and future studies should be aimed at exploring their role in alkylation-stress response.

Experimental Procedures

Strains

Strains were either derivatives of *E. coli* MG1655 (F- lambda- ilvG- rfb-50 rph-1) or X90 (*ara*Δ(*lac-pro*) *nalA argE*(Am) *rif thi-1/*F*' lacI*^{q} *lac*$^{+}$ *pro*$^{+}$) (81). The following strains SM694 (X90, *ssrA::his*$_{6}$ *- kan*), SM876 (X90, *ssrA::his*$_{6}$ *- kan, clpPX-lon::cam*), and SM20 (X90, Δ*ssrA, cam*) were a gift from Dr. Sean Moore (72). The SKEC4 strain (MG1655, Δ*ssrA,* Δ*smpB, kan*) was a gift from Dr. Allen Buskirk. P1 transduction (82) was used to introduce kan^{R}-linked tmRNA-H_6 into MG1655.

Western analysis

To prepare total protein for Western blot analysis, *E. coli* were collected, washed with LB, and resuspended in 2 × SDS loading dye. The resuspension volume was adjusted to normalize for OD_{600nm} of the culture at the time of collection. Total protein was separated by SDS-PAGE and transferred to PVDF membrane in 1 × Transfer buffer (25 mM Tris, 192 mM glycine, 20% Methanol) in a wet apparatus. After transfer, the membrane was blocked for one hour in PBST (3.2 mM Na_2HPO_4, 0.5 mM KH_2PO_4, 1.3 mM KCl, 135 mM NaCl, 0.05% Tween 20, pH 7.4.) containing 5% w/v powdered milk. The membrane was then washed with PBST and incubated with primary antibody overnight at 4°C. The following dilutions of primary antibodies were used: 1:2500 anti-His (Abcam unless otherwise specified), 1:500 anti-Ada (Santa Cruz Biotechnologies), 1:10,000 anti-RecA (Abcam), and 1:1,000 anti-RF2 (purified as described in (83)). The blot was then washed three times for 5 minutes, and then incubated with the corresponding HRP-conjugated secondary antibody (1:10,000) (ThermoFisher) in PBST for one hour. After washing three times for 5 minutes, the membrane was treated with an HRP-reactive

chemiluminescent reagent (Pierce ECL Western Blotting Substrate). Quantity One software was utilized to quantify Western blots.

Treatment of *E. coli* with damaging agents

For all Western blot analyses, *E. coli* were treated with the following concentrations of damaging agents: 0.1% MMS (Sigma-Aldrich), 5 μg/mL MNNG (Tokyo Chemical Industry), 50 μg/mL ciprofloxacin (Sigma-Aldrich), or 6 μg/mL mitomycin C (Sigma-Aldrich). To determine the treatment time that generated significant tmRNA activity and Ada activation, MG1655 cells containing tmRNA-His_6 were grown from OD 0.05 to mid-log phase (OD 0.3-0.4) and treated with MMS for several timepoints. The resulting total protein was analyzed via western blot (Supplementary Figure 6). We observed significant tmRNA activity and Ada activation after a 20-minute treatment, which is the treatment time we utilized for the remaining samples analyzed via Western blot.

To determine the optimal length of time for rifampicin pre-treatments, we treated MG1655 cells containing tmRNA-His_6 with 6 ug/mL rifampicin for several timepoints followed by 20 min treatments with either MMS or ciprofloxacin. The resulting protein was analyzed via western blot (Supplementary Figure 7). We observed significant decreases in Ada activation in the MMS-treated samples and significant decreases in tmRNA activity and RecA activation in the ciprofloxacin-treated samples after 10 seconds of rifampicin pre-treatment. We utilized a 10 to 45-second rifampicin pre-treatment time for the remaining samples analyzed via western blot.

Quantification of nucleosides via liquid chromatography – mass spectrometry

Overnight cultures of MG1655 *E. coli* were diluted to OD_{600nm} 0.05 in LB and grown to an OD_{600nm} of 0.3-0.4 at 37°C before 20 min treatment with either 0.1% MMS or 5 μg/mL

MNNG. RNA was isolated using a hot phenol method as previously described (84). 10 μg of total RNA was digested by P1 nuclease (Sigma-Aldrich, 10 Units) at 50°C overnight. The pH was adjusted by adding Tris pH 7.5 to a final concentration of 100 mM before calf intestinal phosphatase (NEB) was added to a final concentration of 0.2 U/μL, and the reaction was further incubated for 1 hour at 37°C to convert 5'-monophosphates to nucleosides. The samples were diluted to 150 μL and filtered (0.22 μm pore size) before injecting 10 μL into an Agilent 1290 Infinity II UHPLC connected to an Agilent 6470 Triple Quadrupole mass spectrometer. Nucleosides were separated on a Zorbax Eclipse Plus C18 column (2.1 x 50 mm x 1.8 micron) and then analyzed using multiple-reaction monitoring in positive-ion mode. Calibration curves were generated with known concentrations of standards. Unmodified nucleosides were monitored by absorbance at 260 nm. Modified nucleosides were monitored by MRM. The retention times and mass transitions of each nucleoside are listed in Supplemental Table 1. Free unmodified A, G, and C standards were purchased from Acros Organics and U was purchased from Tokyo Chemical Industry. Free modified nucleosides m^7G, m^1G, and m^3C were purchased from Carbosynth, m^6G and m^6A were purchased from Berry's Associates, and m^1A was purchased from Cayman Chemical Company. Data was analyzed using Agilent qualitative analysis, Excel, and Graphpad Prism software.

Charging of Aminoacyl-tRNA

$[^{35}S]$-fMet-$tRNA^{fMet}$ was prepared as previously described (85). The tRNAs were aminoacylated by incubating total tRNA mix (Roche) at 150 μM with the appropriate amino acid (0.4 mM), tRNA synthetase (~5 μM) and ATP (2 mM) in charging buffer composed of 100 mM K-HEPES (pH 7.6), 20 mM $MgCl_2$, 10 mM KCl, 1 mM DTT. After a 30-minute incubation at

37°C, the aa-tRNAs were purified by phenol/chloroform extraction, ethanol precipitated, and resuspended in 20 mM KOAc (pH 5.2) and 1 mM DTT.

Formation of ribosome initiation complexes

Protocols were performed as previously described (86). All initiation complex (IC) formation and peptidyl transfer reactions were performed in 1 × polymix buffer (46), composed of [95 mM KCl, 5 mM NH_4Cl, 5 mM $Mg(OAc)_2$, 0.5 mM $CaCl_2$, 8 mM putrescine, 1 mM spermidine, 10 mM K_2HPO_4 (pH 7.5), 1 mM DTT]. In order to generate ICs, 70S ribosomes (2μM), IF1, IF2, IF3, [^{35}S]-fMet-tRNA^{fMet} (3μM each), mRNA (6 μM), and GTP (2 mM) were incubated in 1 × polymix buffer at 37°C for 30 min. The initiation complexes were purified from free tRNAs and initiation factors over a 500 μL sucrose cushion composed of 1.1 M sucrose, 20 mM Tris-HCl pH 7.5, 500 mM NH_4Cl, 0.5 mM EDTA, and 10 mM $MgCl_2$. The mixture was spun for 2 hours at 287,000 × g at 4°C, and the pellet was resuspended in 1 × polymix buffer and stored at -80°C. The fractional radioactivity that pelleted was used to determine the concentration of IC.

Modified mRNAs containing m^{1}A used in the IC formation reaction were purchased from The Midland Certified Reagent Company, and its sequence is as follows: C AGA GGA GGU AAA AAA AUG G(1-methyl-A)A UUG UAC AAA. The unmodified control mRNA was transcribed from a dsDNA template using T7 polymerase and purified via denaturing PAGE (88).

Kinetics of peptidyl transfer

In order to exchange bound GDP for GTP, EF-Tu (30 μM final) was initially incubated with GTP (2 mM final) in 1 × polymix buffer for 15 mins at 37°C. The mixture was then

incubated with aminacyl-tRNAs (~6 μM) for 15 mins at 37°C to form ternary complexes (TC). For reactions performed in the presence of paromomycin, 10 μg/mL final of the antibiotic were added to the mixtures. Kinetics assays were also performed using *trans*-translation quaternary complexes (QCs), which were formed by incubating Ala-tmRNA^{Ala} with SmpB, EF-Tu, and GTP in 1 × polymix for 15 mins at 37°C. The TC or QC mixture was then incubated with an equivalent volume of IC at 37°C either using an RQF-3 quench-flow instrument or by hand. KOH to a final concentration of 500 mM was used to stop reactions at different time points. Dipeptide products and free fMet were separated using cellulose TLC plates that were electrophoresed in pyridine-acetate at pH 2.8 (50). TLC plates were then exposed to a phosphor screen overnight, after which they were imaged using a Personal Molecular Imager (PMI) system. The images were quantified, and the fraction of dipeptide fMet at each time point was used to determine the rate of peptide bond formation using GraphPad Prism software.

S30 *in vitro* translation

Protocol for preparing S30 extract was adapted from (90). 2 L of SM876 were grown in YT medium (1.6% typtone, 1% yeast extract, 0.5% NaCl) at 37°C from an overnight culture. Cells were harvested at OD_{600nm} ~2 and washed in Buffer 1 (10 mM Tris/OAc pH 8.2, 60 mM KOAc, 14 mM $Mg(OAc)_2$, 1 mM DTT, 7 mM β-ME) and then Buffer 2 (Buffer 1 minus β-ME). The resulting pellet was weighed and resuspended in 1.3 mL buffer per 1 g of wet cell pellet. Cells were lysed by passing them through a French press three times. The resulting lysate was clarified twice by centrifugation at 30,000 × g for 30 minutes at 4°C. The supernatant was then transferred to a 15 mL conical tube and incubated with 0.15 × volume of preincubation buffer (300 mM Tris/OAc pH 7.6, 10 mM $Mg(OAc)_2$, 10 mM ATP, 80 mM phosphoenol pyruvate, 5 mM DTT, 40 μM of each amino acid, 8 U/ml pyruvate kinase) for 90 minutes at 37°C in the

dark. The lysate was dialyzed (mwco: 3,500 Da) overnight in Buffer 2 at 4°C and dialyzed again the next day for 1 hour in fresh buffer. Dialyzed lysate was centrifuged at 4,000 × g for 10 min at 4°C and the supernatant aliquoted and flash frozen in liquid nitrogen.

mRNAs templates for *in vitro* were generated by T7 RNA polymerase as previously described (88). mRNAs were subjected to two rounds of phenol chloroform extractions followed by ethanol precipitation. To complete the purification process, the transcripts were applied to P-30 gel filtration spin columns (Bio-Rad) to remove abortive short transcripts. MMS treatment of mRNA was conducted by incubating ~35 µg of RNA with 0.5% MMS in a total volume of 100 µL for 15 minutes followed by phenol/chloroform extraction and ethanol precipitation.

A typical 10 µL in vitro translation reaction contained the following: 3 µg of RNA, 1.2 µL Buffer 1, 2.4 µL S30 extract, 4 µL of S30 Premix Plus from the Promega S30 T7 High-Yield Protein Expression System kit and 2 µCi L-[^{35}S]-Methionine. Reactions were incubated at 37°C for 1 hour and samples were resolved using 15% Bis-Tris gels followed by transfer to PVDF membranes. Analysis was done by autoradiography on a Typhoon Phosphorimager and western blotting.

Analysis of mRNA modification by immunoblotting

50 mL of MG1655 and Δ*ssrA* MG1655 cells were grown to OD_{600nm} of 0.4. At this point a 10-mL aliquot was harvested, quickly centrifuged and the cell pellet flash frozen. To the remaining culture, 40 µL of MMS was added (final concentration 0.1%) and incubated for 15 more minutes. A 10-mL aliquot was collected as before. The rest of the cells were centrifuged, washed with fresh LB and allowed to recover for 10 minutes, at which point a third aliquot was removed. Total RNA was isolated from samples using the hot phenol method described above.

Samples were resolved using denaturing agarose gel electrophoresis. At this stage gels were either promptly transferred to nitrocellulose membrane in 10 × SSC buffer or incubated in buffer containing 50 mM NaOH, 1.5 M NaCl to convert m^1A to m^6A prior to transfer. Following transfer, samples were cross linked by UV treatment, blocked with milk in TBST (20 mM Tris-HCL pH 7.5, 150 mM NaCl, 0.1% Tween 20) prior to incubation with anti m^6A antibody (Synaptic Systems, product number 202 003).

Alkylative damage recovery assays

Overnight cultures of MG1655 and Δ*ssrA* MG1655 cells were diluted to OD_{600nm} 0.05 and grown to 0.3 – 0.4 at 37°C before treating with either 0.5% MMS or 20 μg/mL MNNG for 20 mins. The OD_{600nm} of the cells was recorded at the time of collection, and the samples were washed twice with LB and resuspended in an adjusted volume of LB. Cells were diluted to an OD_{600nm} of 0.005 at 100 μL final volume in a 96-well plate. Plates were shaken at 37°C for 20 hours in a BioTek Eon microtiter plate reader which measured the OD_{600nm} of each well every 10 mins.

Spot assays for viability analysis

X90 and SM20 E. coli were grown from OD_{600nm} 0.05 to OD 0.3 at 37°C before treating with either 0.1% or 0.5% MMS. At each time point, an aliquot of the culture was removed, washed with LB, and then serially diluted 1:10 eight times. 4 μL of each dilution were spotted on an LB plate. The plates were imaged, and colonies were counted using the Colony Counter plugin on ImageJ.

Acknowledgements

We thank Sean Moore for his gift of the tmRNA-His_6 strains, and Allen Buskirk for the tmRNA-deletion ones. We also thank Carrie Simms and members of the Zaher laboratory for useful discussions on earlier versions of this manuscript. This work was supported by a grant from the National Institutes of Health to HSZ (R01GM112641).

References

1. Wurtmann,E.J. and Wolin,S.L. (2009) RNA under attack: cellular handling of RNA damage. *Crit Rev Biochem Mol Biol*, **44**, 34–49.

2. Simms,C.L. and Zaher,H.S. (2016) Quality control of chemically damaged RNA. *Cell. Mol. Life Sci.*, 10.1007/s00018-016-2261-7.

3. Yan,L.L. and Zaher,H.S. (2019) How do cells cope with RNA damage and its consequences? *J. Biol. Chem.*, 10.1074/jbc.REV119.006513.

4. Hofer,T., Badouard,C., Bajak,E., Ravanat,J.L., Mattsson,Å. and Cotgreave,I.A. (2005) Hydrogen peroxide causes greater oxidation in cellular RNA than in DNA. *Biol. Chem.*, **386**, 333–337.

5. Wyatt,M.D. and Pittman,D.L. (2008) Methylating agents and DNA repair responses: methylated bases and sources of strand breaks. *Chem Res Toxicol*, **19**, 1580–1594.

6. Zaher,H.S. and Green,R. (2009) Fidelity at the Molecular Level: Lessons from Protein Synthesis. *Cell*, 10.1016/j.cell.2009.01.036.

7. Simms,C.L., Hudson,B.H., Mosior,J.W., Rangwala,A.S. and Zaher,H.S. (2014) An Active Role for the Ribosome in Determining the Fate of Oxidized mRNA. *Cell Rep.*, 10.1016/j.celrep.2014.10.042.

8. Hudson,B.H. and Zaher,H.S. (2015) O6-Methylguanosine leads to position-dependent effects on ribosome speed and fidelity. *RNA*, 10.1261/rna.052464.115.

9. Thomas,E.N., Simms,C.L., Keedy,H.E. and Zaher,H.S. (2019) Insights into the base-pairing preferences of 8-oxoguanosine on the ribosome. *Nucleic Acids Res.*, 10.1093/nar/gkz701.

10. Hoernes,T.P., Faserl,K., Juen,M.A., Kremser,J., Gasser,C., Fuchs,E., Shi,X., Siewert,A., Lindner,H., Kreutz,C., *et al.* (2018) Translation of non-standard codon nucleotides reveals minimal requirements for codon-anticodon interactions. *Nat. Commun.*, 10.1038/s41467-018-07321-8.

11. Hoernes,T.P., Clementi,N., Faserl,K., Glasner,H., Breuker,K., Lindner,H., Hüttenhofer,A. and Erlacher,M.D. (2016) Nucleotide modifications within bacterial messenger RNAs regulate their translation and are able to rewire the genetic code. *Nucleic Acids Res.*, 10.1093/nar/gkv1182.

12. You,C., Dai,X. and Wang,Y. (2017) Position-dependent effects of regioisomeric methylated adenine and guanine ribonucleosides on translation. *Nucleic Acids Res.*, **45**, 9059–9067.

13. Zhang,C. and Jia,G. (2018) Reversible RNA Modification N1-methyladenosine (m1A) in mRNA and tRNA. *Genomics, Proteomics Bioinforma.*, **16**, 155–161.

14. Dominissini,D., Nachtergaele,S., Moshitch-moshkovitz,S., Peer,E., Kol,N., Ben-haim,M.S., Dai,Q., Segni,A. Di, Clark,W.C., Zheng,G., *et al.* (2016) The dynamic N 1 -methyladenosine methylome in eukaryotic messenger RNA. *Nature*, **530**, 441–446.

15. Li,X., Xiong,X., Wang,K., Wang,L., Shu,X., Ma,S. and Yi,C. (2016) Transcriptome-wide mapping reveals reversible and dynamic N 1 -methyladenosine methylome. *Nat. Publ. Gr.*, **12**, 311–316.

16. Safra,M., Sas-chen,A., Nir,R., Winkler,R., Nachshon,A., Bar-yaacov,D., Erlacher,M., Rossmanith,W., Stern-ginossar,N. and Schwartz,S. (2017) The m1A landscape on cytosolic and mitochondrial mRNA at single-base resolution. *Nat. Publ. Gr.*, **551**, 251–255.

17. Zhou,H., Kimsey,I.J., Nikolova,E.N., Sathyamoorthy,B., Grazioli,G., Mcsally,J., Bai,T., Wunderlich,C.H., Kreutz,C., Andricioaei,I., *et al.* (2016) m 1 A and m 1 G disrupt A-RNA structure through the intrinsic instability of Hoogsteen base pairs. *Nat. Publ. Gr.*, **23**, 803–810.

18. Yan,L.L., Simms,C.L., McLoughlin,F., Vierstra,R.D. and Zaher,H.S. (2019) Oxidation and alkylation stresses activate ribosome-quality control. *Nat. Commun.*, 10.1038/s41467-019-13579-3.

19. Simms,C.L.C.L.L., Thomas,E.N.E.N. and Zaher,H.S.H.S. (2017) Ribosome-based quality control of mRNA and nascent peptides. *Wiley Interdiscip. Rev. RNA*, **8**.

20. Matsuo,Y., Ikeuchi,K., Saeki,Y., Iwasaki,S., Schmidt,C., Udagawa,T., Sato,F., Tsuchiya,H., Becker,T., Tanaka,K., *et al.* (2017) Ubiquitination of stalled ribosome triggers ribosome-associated quality control. *Nat Commun*, **8**, 159.

21. Simms,C.L., Yan,L.L. and Zaher,H.S. (2017) Ribosome Collision Is Critical for Quality Control during No-Go Decay. *Mol. Cell*, 10.1016/j.molcel.2017.08.019.

22. Saito,K., Horikawa,W. and Ito,K. (2015) Inhibiting K63 polyubiquitination abolishes no-go type stalled translation surveillance in Saccharomyces cerevisiae. *PLoS Genet*, **11**, e1005197.

23. Yan,L.L. and Zaher,H.S. (2019) Ubiquitin—a beacon for all during quality control on the ribosome. *EMBO J.*, 10.15252/embj.2019101633.

24. Ikeuchi,K., Tesina,P., Matsuo,Y., Sugiyama,T., Cheng,J., Saeki,Y., Tanaka,K., Becker,T., Beckmann,R. and Inada,T. (2019) Collided ribosomes form a unique structural interface to induce Hel2-driven quality control pathways. *EMBO J*, 10.15252/embj.2018100276.

25. Juszkiewicz,S. and Hegde,R.S. (2017) Initiation of Quality Control during Poly(A) Translation

Requires Site-Specific Ribosome Ubiquitination. *Mol Cell*, **65**, 743-750 e4.

26. Sundaramoorthy,E., Leonard,M., Mak,R., Liao,J., Fulzele,A. and Bennett,E.J. (2017) ZNF598 and RACK1 Regulate Mammalian Ribosome-Associated Quality Control Function by Mediating Regulatory 40S Ribosomal Ubiquitylation. *Mol Cell*, **65**, 751-760 e4.

27. Juszkiewicz,S., Chandrasekaran,V., Lin,Z., Kraatz,S., Ramakrishnan,V. and Hegde,R.S. (2018) ZNF598 Is a Quality Control Sensor of Collided Ribosomes. *Mol Cell*, 10.1016/j.molcel.2018.08.037.

28. Bengtson,M.H.H. and Joazeiro,C.A.P.A.P. (2010) Role of a ribosome-associated E3 ubiquitin ligase in protein quality control. *Nature*, **467**, 470–473.

29. Defenouillere,Q., Yao,Y., Mouaikel,J., Namane,A., Galopier,A., Decourty,L., Doyen,A., Malabat,C., Saveanu,C., Jacquier,A., *et al.* (2013) Cdc48-associated complex bound to 60S particles is required for the clearance of aberrant translation products. *Proc. Natl. Acad. Sci. U. S. A.*, **110**, 5046–5051.

30. Brandman,O., Stewart-Ornstein,J., Wong,D., Larson,A., Williams,C.C.C., Li,G.-W., Zhou,S., King,D., Shen,P.S.S., Weibezahn,J., *et al.* (2012) A Ribosome-Bound Quality Control Complex Triggers Degradation of Nascent Peptides and Signals Translation Stress. *Cell*, **151**, 1042–1054.

31. Lyumkis,D., Doamekpor,S.K., Bengtson,M.H., Lee,J.-W., Toro,T.B., Petroski,M.D., Lima,C.D., Potter,C.S., Carragher,B. and Joazeiro,C.A.P. (2013) Single-particle EM reveals extensive conformational variability of the Ltn1 E3 ligase. *Proc. Natl. Acad. Sci. U. S. A.*, **110**, 1702–1707.

32. Gagnon,M.G., Seetharaman,S. V, Bulkley,D. and Steitz,T.A. (2012) Structural Basis for the Rescue of Stalled Ribosomes: Structure of YaeJ Bound to the Ribosome. *Science (80-.).*, **335**, 1370–1372.

33. Keiler,K.C. (2015) Mechanisms of ribosome rescue in bacteria. *Nat. Rev. Microbiol.*, 10.1038/nrmicro3438.

34. Keiler,K.C., Waller,P.R.H. and Sauer,R.T. (1996) Role of a peptide tagging system in degradation of proteins synthesized from damaged messenger RNA. *Science (80-.).*, **271**, 990–993.

35. Moore,S.D. and Sauer,R.T. (2007) The tmRNA System for Translational Surveillance and Ribosome Rescue. *Annu. Rev. Biochem.*, **76**, 101–124.

36. Valle,M., Gillet,R., Kaur,S., Henne,A., Ramakrishnan,V. and Frank,J. (2003) Visualizing tmRNA Entry into a Stalled Ribosome. *Science (80-.).*, **300**, 127–130.

37. Gottesman,S., Roche,E., Zhou,Y.N. and Sauer,R.T. (1998) The ClpXP and ClpAP proteases degrade proteins with carboxy-terminal peptide tails added by the SsrA-tagging system. *Genes Dev.*, **12**, 1338–1347.

38. Keiler,K.C. and Sauer,R.T. (1996) Sequence determinants of C-terminal substrate recognition by the Tsp protease. *J. Biol. Chem.*, **271**, 2589–2593.

39. Deng,X., Chen,K., Luo,G., Weng,X., Ji,Q., Zhou,T. and He,C. (2015) Widespread occurrence of N 6 -methyladenosine in bacterial mRNA. **43**, 6557–6567.

40. Machnicka,M.A., Milanowska,K., Oglou,O.O., Purta,E., Kurkowska,M., Olchowik,A., Januszewski,W., Kalinowski,S., Dunin-Horkawicz,S., Rother,K.M., *et al.* (2013)

MODOMICS: A database of RNA modification pathways - 2013 update. *Nucleic Acids Res.*, **41**, 262–267.

41. Beranek,D.T. (1990) Distribution of methyl and ethyl adducts following alkylation with monofunctional alkylating agents. *Mutat. Res.*, **231**, 11–30.

42. Bodell,W.J. and Singer,B. (1979) Influence of hydrogen bonding in DNA and polynucleotides on reaction of nitrogens and oxygens toward ethylnitrosourea. *Biochemistry*, **18**, 2860–2863.

43. Zaher,H.S. and Green,R. (2009) Quality control by the ribosome following peptide bond formation. *Nature*, 10.1038/nature07582.

44. Youngman,E.M., Brunelle,J.L., Kochaniak,A.B. and Green,R. (2004) The active site of the ribosome is composed of two layers of conserved nucleotides with distinct roles in peptide bond formation and peptide release. *Cell*, **117**, 589–599.

45. Pape,T., Wintermeyer,W. and Rodnina,M. (1999) Induced fit in initial selection and proofreading of aminoacyl-tRNA on the ribosome. *Embo J.*, **18**, 3800–3807.

46. Gromadski,K.B. and Rodnina,M. V (2004) Kinetic determinants of high-fidelity tRNA discrimination on the ribosome. *Mol. Cell*, **13**, 191–200.

47. Pape,T., Wintermeyer,W. and Rodnina,M. V (2000) Conformational switch in the decoding region of 16S rRNA during aminoacyl-tRNA selection on the ribosome. *Nat. Struct. Biol.*, **7**, 104–107.

48. Fourmy,D., Recht,M.I., Blanchard,S.C. and Puglisi,J.D. (1996) Structure of the A site of Escherichia coli 16S ribosomal RNA complexed with an aminoglycoside antibiotic. *Science (80-.).*, 10.1126/science.274.5291.1367.

49. Ogle,J.M., Murphy IV,F. V., Tarry,M.J. and Ramakrishnan,V. (2002) Selection of tRNA by the ribosome requires a transition from an open to a closed form. *Cell*, **111**, 721–732.

50. Gromadski,K.B. and Rodnina,M. V (2004) Streptomycin interferes with conformational coupling between codon recognition and GTPase activation on the ribosome. *Nat. Struct. Mol. Biol.*, **11**, 316–322.

51. Roche,E.D. and Sauer,R.T. (2001) Identification of endogenous SsrA-tagged proteins reveals tagging at positions corresponding to stop codons. *J. Biol. Chem.*, **276**, 28509–28515.

52. Jeggot,P. (1979) Isolation and Characterization of Escherichia coli K-12 Mutants Unable to Induce the Adaptive Response to Simple Alkylating Agents. **139**, 783–791.

53. Sakumi,K. and Sekiguchi,M. (1989) Regulation of Expression of the ada Gene Controlling the Adaptive Response. *J. Mol. Biol.*

54. Uphoff,S., Lord,N.D., Okumus,B., Potvin-trottier,L., Sherratt,D.J. and Paulsson,J. (2016) Stochastic activation of a DNA damage response causes cell-to-cell mutation rate variation. **351**, 1094–1098.

55. Cox,M.M. (2007) Regulation of bacterial RecA protein function. *Crit. Rev. Biochem. Mol. Biol.*, 10.1080/10409230701260258.

56. Moore,S.D. and Sauer,R.T. (2005) Ribosome rescue: tmRNA tagging activity and capacity in Escherichia coli. *Mol. Microbiol.*, **58**, 456–466.

57. Sedgwick,B. (1989) In vitro proteolytic cleavage of the Escherichia coli ada protein by the ompT gene product. *J. Bacteriol.*, 10.1128/jb.171.4.2249-2251.1989.

58. Cox,M.M. (1991) The RecA protein as a recombinational repair system. **5**, 1295–1299.

59. Wehrli,W. Rifampin: mechanisms of action and resistance. *Rev. Infect. Dis.*, **5 Suppl 3**, S407-11.

60. LeBel,M. (1988) Ciprofloxacin: chemistry, mechanism of action, resistance, antimicrobial spectrum, pharmacokinetics, clinical trials, and adverse reactions. *Pharmacotherapy*, **8**, 3–33.

61. Verweij,J. and Pinedo,H.M. (1990) Mitomycin C: mechanism of action, usefulness and limitations. *Anticancer. Drugs*, **1**, 5–13.

62. Ge,Z., Mehta,P., Richards,J. and Karzai,A.W. (2010) Non-stop mRNA decay initiates at the ribosome. *Mol. Microbiol.*, 10.1111/j.1365-2958.2010.07396.x.

63. Meyer,K.D., Saletore,Y., Zumbo,P., Elemento,O., Mason,C.E. and Jaffrey,S.R. (2012) Comprehensive analysis of mRNA methylation reveals enrichment in 3' UTRs and near stop codons. *Cell*, **149**, 1635–1646.

64. Macon,J.B. and Wolfenden,R. (1968) 1-Methyladenosine. Dimroth Rearrangement and Reversible Reduction. *Biochemistry*, 10.1021/bi00850a021.

65. Nishikawa,K., Inokuchi,H., Kitabatake,M., Yokogawa,T. and Komine,Y. (2006) A tRNA-like structure is present in 10Sa RNA, a small stable RNA from Escherichia coli. *Proc. Natl. Acad. Sci.*, **91**, 9223–9227.

66. Wali Karzai,A., Susskind,M.M. and Sauer,R.T. (1999) SmpB, a unique RNA-binding protein essential for the peptide-tagging activity of SsrA (tmRNA). *EMBO J.*, **18**, 3793–3799.

67. Peer,E., Rechavi,G. and Dominissini,D. (2017) Epitranscriptomics : regulation of mRNA metabolism through modifications. *Curr. Opin. Chem. Biol.*, **41**, 93–98.

68. Xiao Wang1 Adrian Gomez1, Gary C. Hon2, Yanan Yue1, Dali Han1, Ye Fu1, Marc

Parisien3, Qing Dai1, Guifang Jia1, 4, Bing Ren2, Tao Pan3, and Chuan He1,Z.L. (2014) m6A-dependent regulation of messenger RNA stability. *Nature*, **505**, 1–20.

69. Karikó,K., Muramatsu,H., Welsh,F.A., Ludwig,J., Kato,H., Akira,S. and Weissman,D. (2008) Incorporation of pseudouridine into mRNA yields superior nonimmunogenic vector with increased translational capacity and biological stability. *Mol. Ther.*, **16**, 1833–40.

70. Wimberly,B.T., Brodersen,D.E., Clemons,W.M., Morgan-Warren,R.J., Carter,A.P., Vonrhein,C., Hartsch,T. and Ramakrishnan,V. (2000) Structure of the 30S ribosomal subunit. *Nature*, **407**, 327–339.

71. Carter,A.P., Brodersen,D.E., Morgan-warren,R.J., Hartsch,T., Wimberly,B.T. and Ramakrishnan,V. (2001) Crystal Structure of an Initiation Factor Bound to the 30S Ribosomal Subunit. *Science (80-.).*, **291**, 498–501.

72. Moore,S.D. and Sauer,R.T. (2005) Ribosome rescue: tmRNA tagging activity and capacity in Escherichia coli. *Mol. Microbiol.*, **58**, 456–466.

73. Clemons,W.M., May,J.L.C., Wimberly,B.T., McCutcheon,J.P., Capel,M.S. and Ramakrishnan,V. (1999) Structure of a bacterial 30S ribosomal subunit at 5.5 Å resolution. *Nature*, **400**, 833–840.

74. Hou,Y. (2010) Critical Review CCA Addition to tRNA : Implications for tRNA Quality Control. **62**, 251–260.

75. Shimizu,Y. (2012) ArfA Recruits RF2 into Stalled Ribosomes. *J. Mol. Biol.*, **423**, 624–631.

76. Chadani,Y., Ito,K., Kutsukake,K. and Abo,T. (2012) ArfA recruits release factor 2 to rescue stalled ribosomes by peptidyl-tRNA hydrolysis in Escherichia coli. **86**, 37–50.

77. Garza-sánchez,F., Schaub,R.E., Janssen,B.D. and Hayes,C.S. (2011) tmRNA regulates synthesis of the ArfA ribosome rescue factor. **80**, 1204–1219.

78. Chadani,Y., Matsumoto,E., Aso,H. and Wada,T. (2011) trans -translation-mediated tight regulation of the expression of the alternative ribosome-rescue factor ArfA in Escherichia coli.

79. Chadani,Y., Ono,K., Kutsukake,K. and Abo,T. (2011) Escherichia coli YaeJ protein mediates a novel ribosome-rescue pathway distinct from SsrA- and ArfA-mediated pathways. *Mol. Microbiol.*, **80**, 772–785.

80. Handa,Y., Inaho,N. and Nameki,N. (2011) YaeJ is a novel ribosome-associated protein in Escherichia coli that can hydrolyze peptidyl-tRNA on stalled ribosomes. *Nucleic Acids Res.*, **39**, 1739–1748.

81. Parsell,D.A. and Sauer,R.T. (1989) The Structural Stability of a Protein Is an Important Determinant of Its Proteolytic Susceptibility in. **264**, 7590–7595.

82. Thomason,L.C., Costantino,N. and Court,D.L. (2007) E. coli Genome Manipulation by P1 Transduction . In *Current Protocols in Molecular Biology*.

83. Zaher,H.S. and Green,R. (2011) A primary role for release factor 3 in quality control during translation elongation in Escherichia coli. *Cell*, 10.1016/j.cell.2011.08.045.

84. Simms,C.L., Yan,L.L., Zaher,H.S., Simms,C.L., Yan,L.L. and Zaher,H.S. (2017) Ribosome Collision Is Critical for Quality Control during No-Go Decay Article Ribosome Collision Is Critical for Quality Control during No-Go Decay. *Mol. Cell*, **68**, 361-373.e5.

85. Walker,S.E. and Fredrick,K. (2008) Preparation and evaluation of acylated tRNAs. *Methods*, **377**, 364–377.

86. Pierson,W.E., Hoffer,E.D., Keedy,H.E., Simms,C.L., Dunham,C.M. and Zaher,H.S. (2016) Uniformity of Peptide Release Is Maintained by Methylation of Release Factors. *Cell Rep.*, 10.1016/j.celrep.2016.08.085.

87. Jelenc,P.C. (1979) Nucleoside triphosphate regeneration decreases the frequency of. *Proc. Natl. Acad. Sci. U. S. A.*, **76**, 3174–3178.

88. Zaher,H.S. and Unrau,P.J. (2004) T7 RNA polymerase mediates fast promoter-independent extension of unstable nucleic acid complexes. *Biochemistry*, 10.1021/bi0497300.

89. Youngman,E.M., Brunelle,J.L., Kochaniak,A.B. and Green,R. (2004) The active site of the ribosome is composed of two layers of conserved nucleotides with distinct roles in peptide bond formation and peptide release. *Cell*, **117**, 589–99.

90. Kigawa,T., Yabuki,T., Matsuda,N., Matsuda,T., Nakajima,R., Tanaka,A. and Yokoyama,S. (2004) Preparation of Escherichia coli cell extract for highly productive cell-free protein expression. *J Struct Funct Genomics*, **5**, 63–68.

Supplementary Figures and Tables

Supplementary Table 1: Mass transitions, retention times, and collision energies for nucleoside standards

Nucleoside	Precursor mass, *m/z*	Product ion, *m/z*	Retention time, minute	Collision Energy, V
A	268.1	136	1.92	18
C	244.1	112	0.48	14
G	284.2	152	2.4	16
U	245.2	152.1	1	14
m^1A	282.2	150.1	0.9	16
m^6A	282	150	4.08	16
m^3C	258.2	126	0.8	8
m^7G	298.2	166	1.5	10
m^1G	298	166	4.623	10
m^6G	298	166	4.84	10

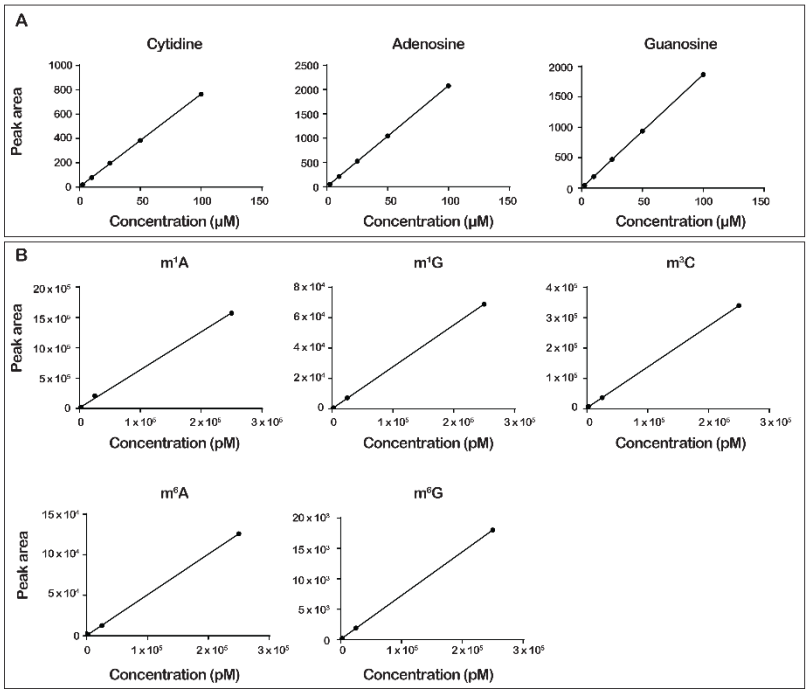

Supplementary Figure 1: LC-MS calibration curves for modified and unmodified nucleosides
A) The integrated peak area for absorbance at 260 nm for each indicated unmodified nucleotide plotted against its concentration. **B)** The integrated peak area for cps intensity plotted against concentrations of modified nucleoside standards. For all plots in **A** and **B**, the data were fit to linear-regression lines forced to have zero x and y intercepts. Retention times and mass transitions shown in supplementary table 1, which were determined empirically, were used to identify the peak for each nucleotide.

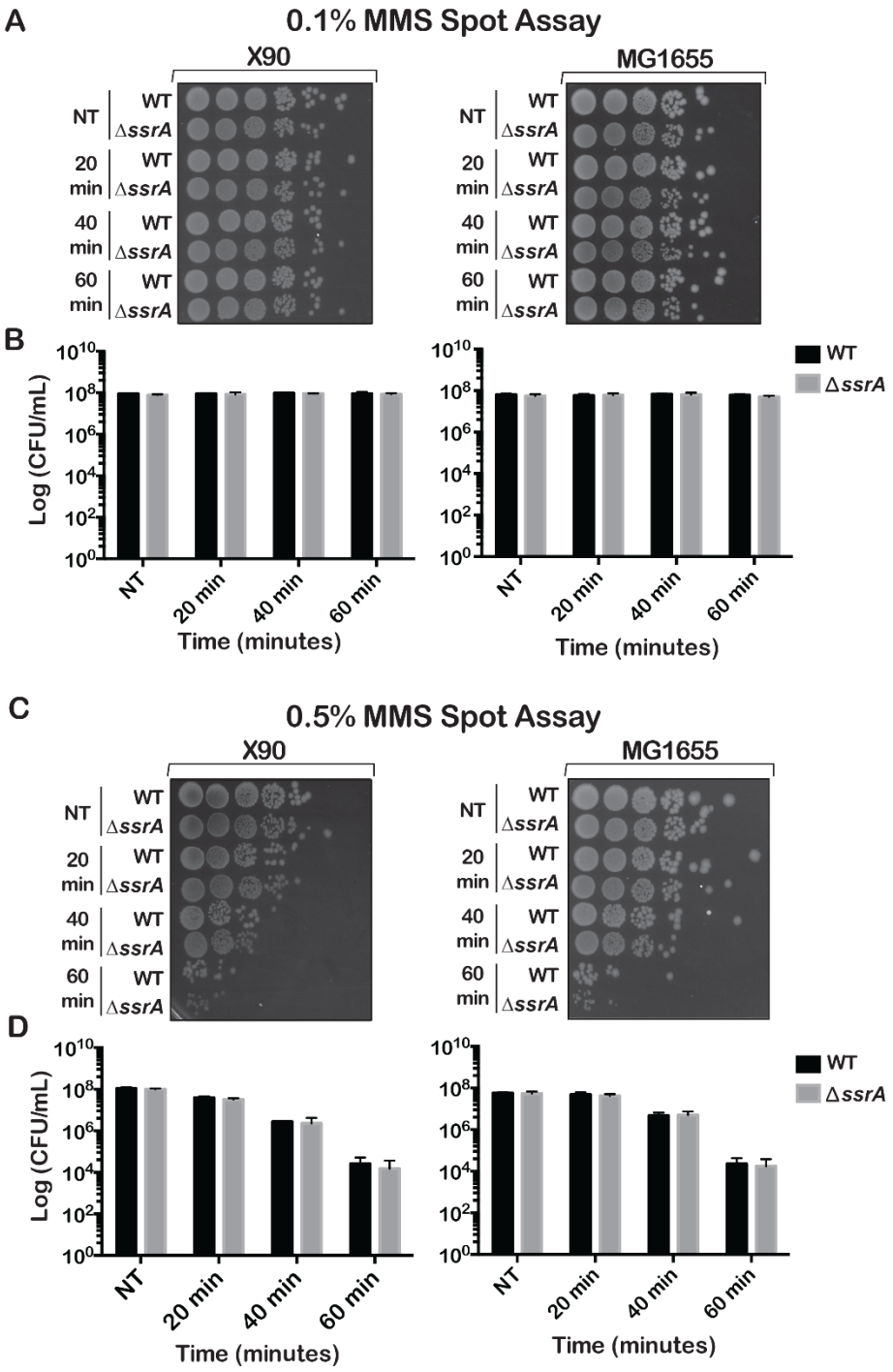

Supplementary Figure 2: WT and Δ*ssrA E. coli* exhibit similar survival phenotypes after treatment with MMS

A) Spot assay of WT and Δ*ssrA* cells either after a mock treatment or treatment with 0.1% MMS for the indicated amount of time. **B)** Quantification of colony forming units in (**A**) performed in triplicates. **C)** Spot assay of WT and Δ*ssrA* cells either after no treatment or treatment with 0.5% MMS for the indicated amount of time. **D)** Quantification of colony forming units in (C) performed in at least duplicates. In all cases the data plotted is the average of three experiments and the error bars represent standard deviations from the mean.

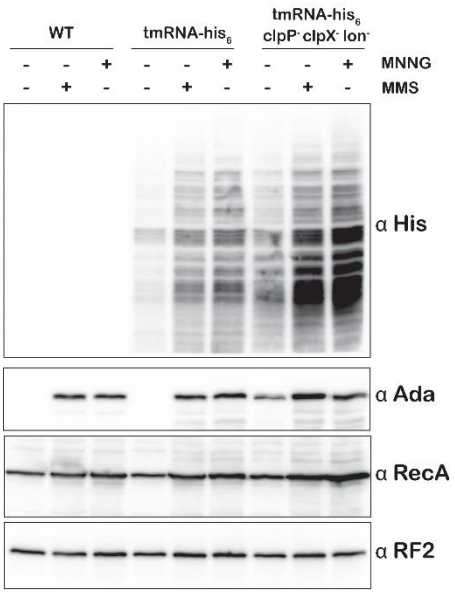

Supplementary Figure 3: Deletion of ClpAP, ClpXP, and Lon proteases results in further accumulation of tmRNA-induced His_6 tagging of peptides upon alkylative stress
Western-blot analysis collected from the indicated *E. coli* strains grown in the absence or presence of the denoted compounds. Blots were probed with the depicted antibodies.

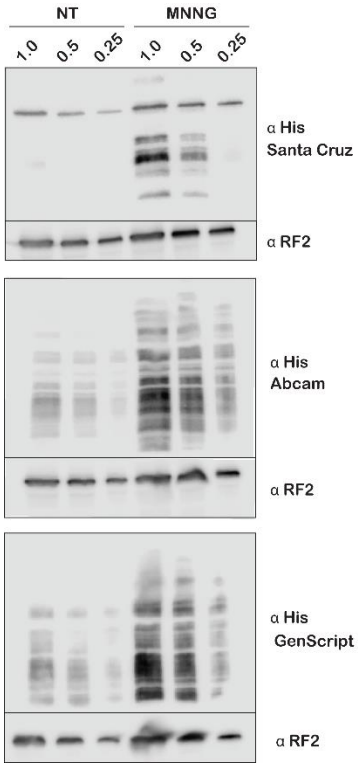

Supplementary 4: Different His antibodies display unique banding patterns on western blots
Western blots of total protein isolated from *E. coli* expressing tmRNA-His_6 in the absence or presence of MNNG. For each of the two treatments, lysates were serially diluted by 2 and 4-fold before being resolved by SDS-PAGE next to their undiluted sample. Following transfer, the blots were probed with one of three different anti-His antibodies (Santa Cruz Biotechnology, Abcam, or GenScript). a-RF2 was used as a loading control.

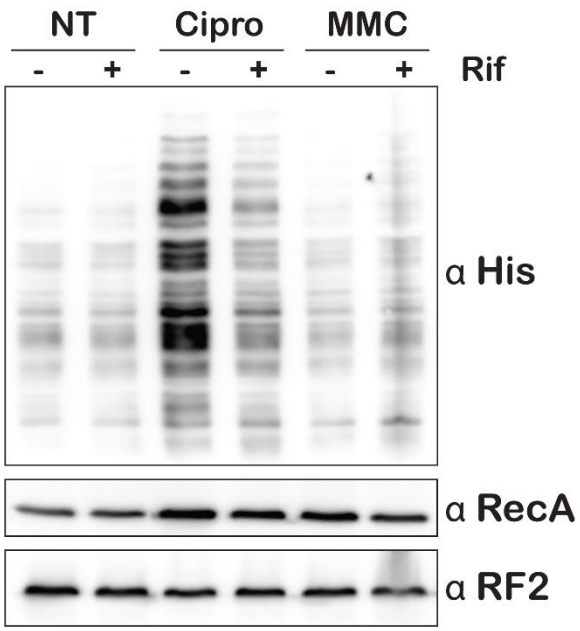

Supplementary Figure 5: Ciprofloxacin, but not mitomycin C, increases His_6 tagging by tmRNA
Western-blot analysis of total protein collected from *E. coli* expressing tmRNA-His_6. Cells were either untreated or treated with ciprofloxacin (cipro) or mitomycin C (MMC). Additionally, cells either received (+) or did not receive (-) a pre-treatment with rifampicin before treatment with the indicated damaging agent. The blot was probed with the indicated antibodies.

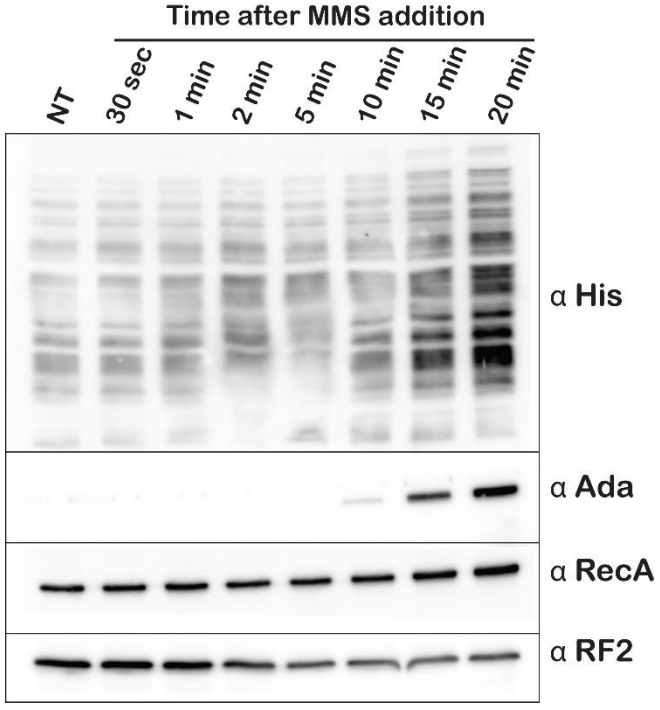

Supplementary Figure 6: Optimal His_6 tagging and activation of Ada and RecA levels are achieved after 20 minutes of MMS treatment
Western-blot analysis of total protein collected from *E. coli* expressing tmRNA-His_6. Cells were either untreated or treated with MMS for the indicated lengths of time. The blot was probed with anti His, Ada, RecA, and RF2 antibodies.

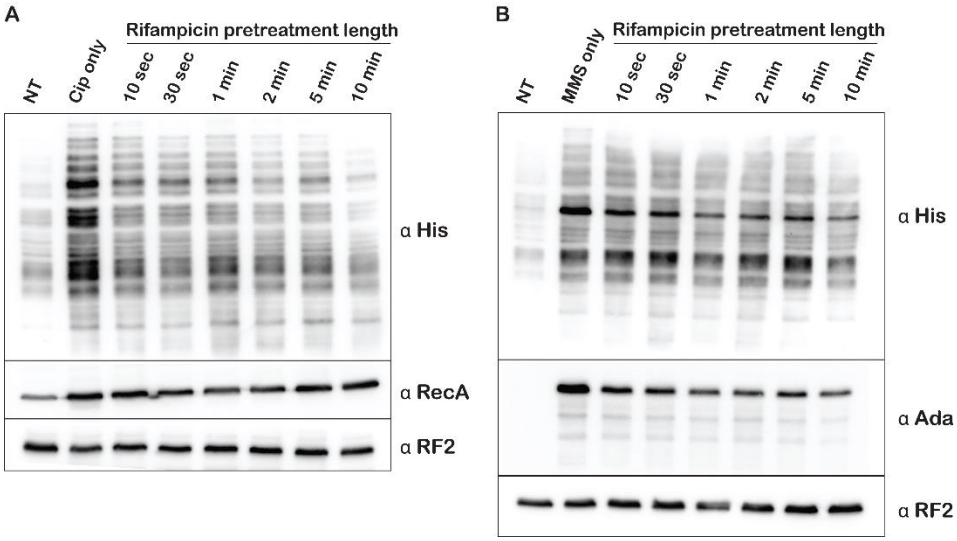

Supplementary Figure 7: Significant transcriptional runoff is achieved after 10 seconds of rifampicin treatment

Western-blot analysis used to follow the effect of rifampicin pretreatment on ciprofloxacin (Cipro)- (**A**) and MMS-induced (**B**) activation of His tagging by tmRNA. Times on top of the blots indicate the amount of time cells were incubated in the presence of rifampicin before ciprofloxacin and MMS were added. The blots were probed with the depicted antibodies.

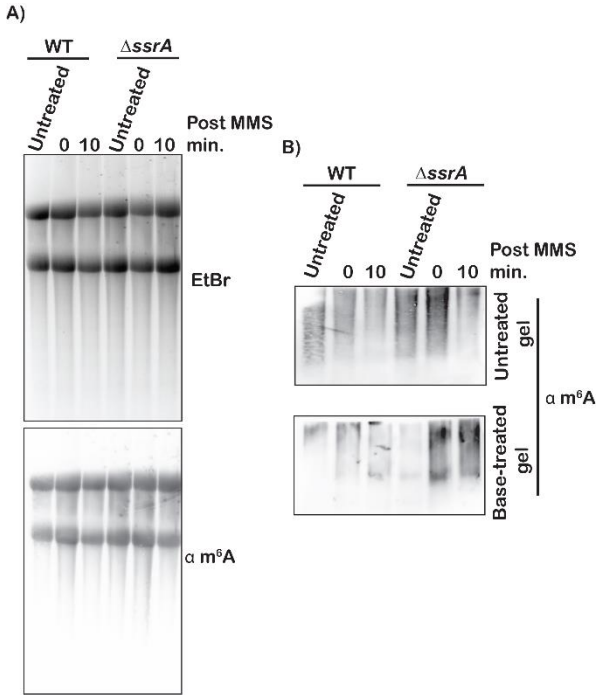

Supplementary Figure 8: Deletion of *ssrA* gene results in decreased decay of m^{1}A-modified mRNA

A) Top: fluorescence image of a denaturing agarose gel used to separate total RNA isolated from the indicated cells under the denoted conditions. Bottom: immunoblot analysis of the same samples using m^{6}A antibody. **B)** m^{6}A-immunoblot analysis of the indicated RNA samples. Top blot shows analysis of samples that were transferred directly following electrophoresis. Bottom blot shows analysis of the same samples except that the agarose gel was soaked in an alkaline buffer (50 mM NaOH, 1.5 M NaCl) prior to transfer.

Chapter 5

Interactions between the mRNA and Rps3/uS3 at the entry tunnel of the ribosomal small subunit are important for no-go decay

Carrie L Simms, Kyusik Q Kim, Liewei L Yan, Jessica Qiu, and Hani S Zaher

This chapter is currently published in PLoS Genetics as Carrie L Simms, Kyusik Q Kim, Liewei L Yan, Jessica Qiu, and Hani S Zaher (2018). Interactions between the mRNA and Rps3/uS3 at the entry tunnel of the ribosomal small subunit are important for no-go decay

Abstract

No-go Decay (NGD) is a process that has evolved to deal with stalled ribosomes resulting from structural blocks or aberrant mRNAs. The process is distinguished by an endonucleolytic cleavage prior to degradation of the transcript. While many of the details of the pathway have been described, the identity of the endonuclease remains unknown. Here we identify residues of the small subunit ribosomal protein Rps3 that are important for NGD by affecting the cleavage reaction. Mutation of residues within the ribosomal entry tunnel that contact the incoming mRNA leads to significantly reduced accumulation of cleavage products, independent of the type of stall sequence, and renders cells sensitive to damaging agents thought to trigger NGD. These phenotypes are distinct from those seen in combination with other NGD factors, suggesting a separate role for Rps3 in NGD. Conversely, ribosomal proteins ubiquitination is not affected by *rps3* mutations, indicating that upstream ribosome quality control (RQC) events are not dependent on these residues. Together, these results suggest that Rps3 is important for quality control on the ribosome and strongly supports the notion that the ribosome itself plays a central role in the endonucleolytic cleavage reaction during NGD.

Introduction

The elongation phase of translation is an imperfect process, during which the ribosome moves with irregular speed along the mRNA template (1). By and large the elongation speed is determined by sequence and structural features of the coding sequence. For instance, the identity of the A-site codon is known to have a drastic effect on the rate of protein synthesis depending on the availability of its partner tRNA and the nature of the codon-anticodon base-pairing interaction (2, 3). Furthermore, the chemical characteristics of the locally-encoded amino acids have been shown to regulate the rate of protein synthesis based on the manner they interact with the exit tunnel of the ribosome (4). mRNAs are also known to harbor local secondary structures that can slow down the ribosome as it unwinds them (5, 6). Regardless of the underlying mechanism, the fluctuating rate of protein synthesis along an mRNA molecule appears to serve important biological functions such as promoting appropriate co-translational protein folding and ensuring that the encoded protein is targeted to the correct destination in the cell (7-12).

In contrast to this "programmed" regulation of ribosome traffic, the ribosome often encounters unwanted obstacles that severely hinder its progression and in some cases stall protein synthesis all together (13, 14). Most of these impediments are typically associated with defects in the mRNA, including stable secondary structures, stretches of rare and inhibitory codons, as well as truncations and chemical damage (3, 15-17), (18). Because multiple ribosomes are typically translating a single mRNA at any given point, one stalled ribosome is likely to impede the progression of multiple upstream ribosomes. As a result, if left unresolved, these stalling events have the potential to severely reduce cellular fitness. Notably, the stalling of the ribosome itself is not such a detriment to the cell as is the loss of valuable ribosomes from the translating net pool (13, 14). In eukaryotes, the evolutionary solution to this predicament was

No-Go Decay (NGD) (15) as a means to dissociate stalled ribosomes (19-21). It is thought that over time, this mechanism was expanded on to include mRNA surveillance to dispose of the aberrant mRNA. In particular, the mRNA undergoes an endonucleolytic cleavage upstream of the stall site. The resulting deadenylated 5'-end and uncapped 3'-end pieces are then rapidly degraded by the exosome and Xrn1, respectively (3, 15-17).

Initial studies on NGD in yeast focused on the two factors Dom34 (Pelota in mammals) and Hbs1 (15, 22, 23). These factors are homologs of the termination factors eRF1 and eRF3, respectively. Early reports of NGD hinted at a role for the factors in mediating the endonucleolytic cleavage of the mRNA near the stalled ribosome (15, 24). However, later studies by the same group and others showed the cleavage to take place in the absence of the factors (22) leaving the question of the role of the factors in the process unanswered. Interestingly prior to the discovery of NGD, genetics studies suggested that Dom34 and Hbs1 are important in maintaining ribosome homeostasis of the cell (25). To this end, both factors become essential or near-essential when ribosomes are depleted either by knocking down certain ribosomal proteins or under conditions when ribosomes are sequestered (25-27). These observations are consistent with biochemical studies using a yeast translation reconstituted system, which showed the factors to be responsible for dissociating ribosomes into their respective subunits (18). This splitting activity of Dom34-Hbs1 was also found to be much more efficient in the presence of Rli1 (ABCE1 in mammals) (20, 21). *In vivo* data also supported this model for the role of the three factors in dissociating ribosomes (16). Hence, this rescuing/recycling activity of these factors rationalizes the effect of their deletion on ribosome availability, especially under stress conditions.

In addition to ribosome rescue and degradation of the aberrant RNA, NGD is closely linked to a newly discovered protein-quality-control process termed ribosome quality control (RQC). This process is responsible for degrading the incomplete nascent protein resulting from stalled translation (28-34). RQC proceeds after the splitting action of Dom34-Hbs1-Rli1, which results in a peptidyl-tRNA-associated large-ribosome subunit. This atypical form of the 60S subunit is recognized by the E3 ligase Ltn1 (Listerin in mammals) alongside Rqc2 (formerly Tae2) (30, 33, 35). Ltn1 ligates ubiquitin chains to the nascent peptide as it is attached to the tRNA on the large subunit. The ubiquitinated nascent peptide is then extracted and delivered to the proteasome for degradation through the action of Rqc2 and Cdc48 (and its adaptor proteins Ufd1 and Npl4). Two additional factors, the ribosome-associated Asc1 and the E3 ligase Hel2 (Rack1 and Znf598 in mammals, respectively), also appear to be important for proper RQC function. Both factors are important for ribosomal protein ubiquitination and appear to play a role during stalling (36, 37). In particular, deletion of either factor results in increased readthrough of stall sequences (38, 39). How regulatory ribosomal protein ubiquitination interconnects with RQC and NGD is currently poorly understood.

Even though the consequences of ribosome stalling in eukaryotes was initially described in the context of its impact on mRNA steady state levels (15), as detailed above we know far more about its entanglement with ribosome rescue and quality control of the associated nascent peptide. More specifically, degradation of the mRNA is initiated by endonucleolytic cleavage, but the identity of the endonuclease remains elusive. This in turn has precluded further critical mechanistic dissections of NGD. Some of these outstanding important questions are: 1) How does the endonuclease recognize stalled ribosomes? 2) Is it associated with the ribosome? 3) Does it have a specificity for certain mRNAs 4) How is its function activated? 5) Can NGD be

used to regulate gene expression? Work from our group recently provided some clues about the cleavage reaction. Using reporters and genetic manipulation of yeast we showed that the physical act of ribosome collision is important for initiating the process of RNA degradation and ribosome rescue during no-go decay (NGD) (40). High-resolution mapping of the cleavage products also provided some important clues about the potential role of the ribosome in the reaction. Namely, cleavage appears to take place well upstream of the lead stalled ribosome with the closest most prominent one being ~45 nt upstream of the stall site. As ribosomes are likely to be stacked on the mRNA, this suggested the possibility that the cleavage is taking place inside the ribosome (18, 41). Multiple regions of the ribosome make intimate contact with the mRNA. Most noteworthy among these is the mRNA entry tunnel, which encompasses residues of the ribosomal proteins Rps3/uS3 and Rps2/uS5 (42). In eukaryotes additional contacts are made by helices 18 and 14 of the 18S rRNA, whereas in bacteria these contacts are carried out by Rps4/uS4 (orthologous to Rps9 in yeast and humans) (42-44). In the entry tunnel, Rps3's contacts with the mRNA stand out because they appear to be almost universally conserved and form an integral part of the helicase domain of the ribosome (42). Furthermore, the protein has been implicated in translation initiation during the rearrangement of the small subunit that allows for the opening of the ribosomal mRNA binding channel and subsequent scanning of the mRNA (45) as well as start-codon selection (46).

Here we show the entry tunnel of the ribosome to play an important role during NGD. Mutation of the residues of *RPS3* that form part of the entry tunnel, which have also been implicated in the helicase activity of the ribosome, were found to significantly reduce the accumulation of cleavage products. This effect on cleavage efficiency to a large extent was independent of the identity of the stall site. Combining these mutations with factors involved in

other aspects of NGD revealed that the entry tunnel is also likely to be important in ribosome rescue. Our findings provide new insights into how quality control mechanisms evolved to integrate into fundamental biological machines.

Results

Mutation of the entry-tunnel residues of *RPS3* inhibit cleavage of NGD reporters

To address a potential role for Rps3 in the cleavage reaction, we introduced a number of mutations to the protein and assessed their effect on cleavage of stalling reporters. Our choice of residues for the mutations was motivated by three criteria: they had to be conserved, made intimate contacts with the mRNA and have basic or acidic side chains (Figure 1A and 1B). This led us to Arg116 (R116) and Arg117 (R117). In addition to these, we also analyzed two residues that have been suggested to be important for Rps3's extra-ribosomal activity in DNA repair (47-51), Asp154 (D154) and Lys200 (K200). Mutation of these residues abolishes the 8-oxoguanosine glycoslase and AP/endonuclease activities of the protein (51). The variant-yeast strains were generated by introducing mutations to the chromosomal copy of *RPS3* (see Methods) in different backgrounds of deletions and mutations. All in all, we generated the following mutants: Arg116 and Arg117 were substituted by Ala residues (R116A/R117A), Asp154 was substituted by an Ala residue (D154A), Lys200 was substituted by an Asn residue (K200N) and finally we generated a double mutant D154A/K200N. Of these the R116A/R117A mutation was notable as the side chain of these residues are projected into the entry tunnel of the ribosome and make electrostatic interactions with the mRNA (Figure 1B).

Next, we assessed the effect of these mutations on the cleavage of NGD substrates. We initially used an NGD reporter, which harbors a stable stem loop in the *PGK1* coding sequence and was originally designed by Parker and colleagues. The stem loop presents a robust obstacle for the ribosome and is subject to an endonucleolytic cleavage as evidenced by the accumulation of 5' and 3' fragments when the exosome and Xrn1 are inactivated, respectively (15). Indeed, similar to what was observed by us and others (15, 16, 40), in the *ski2Δ* strain- which is defective

for 3'-5' mRNA degradation- northern analysis of cells expressing PGK1-SL revealed substantial accumulation of 5'-fragments (Figure 1C). The D154A and K200N mutations in *RPS3*, which have been suggested to be important for an AP endonuclease activity (51), had no observable effect on the cleavage efficiency and appear to play no role in NGD. In contrast, the R116A/R117A mutations appear to reduce the accumulation of cleavage fragments and increased heterogeneity among these products (Figure 1C). Interestingly, the mutations also appear to affect the steady-state levels of endogenous PGK1 transcript (Figure 1C). Regardless, these observations suggest that residues of Rps3 that interact with the mRNA in the entry tunnel are important during NGD.

The effects of the R116A/R117A mutations on the cleavage reaction were further studied in the context of other deletions that alter different aspects of NGD. Namely, we introduced these mutations into *dom34Δ* and *xrn1Δ* strains in addition to the wild-type parent strain. As expected, expression of the PGK1-SL in these strains does not result in the accumulation of 5'-fragments and the R116A/R117A mutations have no effect. As a control, these fragments were seen in the *ski2Δ* background and the *rps3* mutations significantly reduced their levels (Figure 1D). Production of the 3'-fragments, as expected, was seen in the absence of *XRN1* and their levels diminished in the presence of the *RPS3* mutations, albeit to a lower extent than that seen for the 5' fragments (Figure 1E). These latter observations suggested that the R116A/R117A mutations do not completely inhibit cleavage and that they may affect other aspects of NGD.

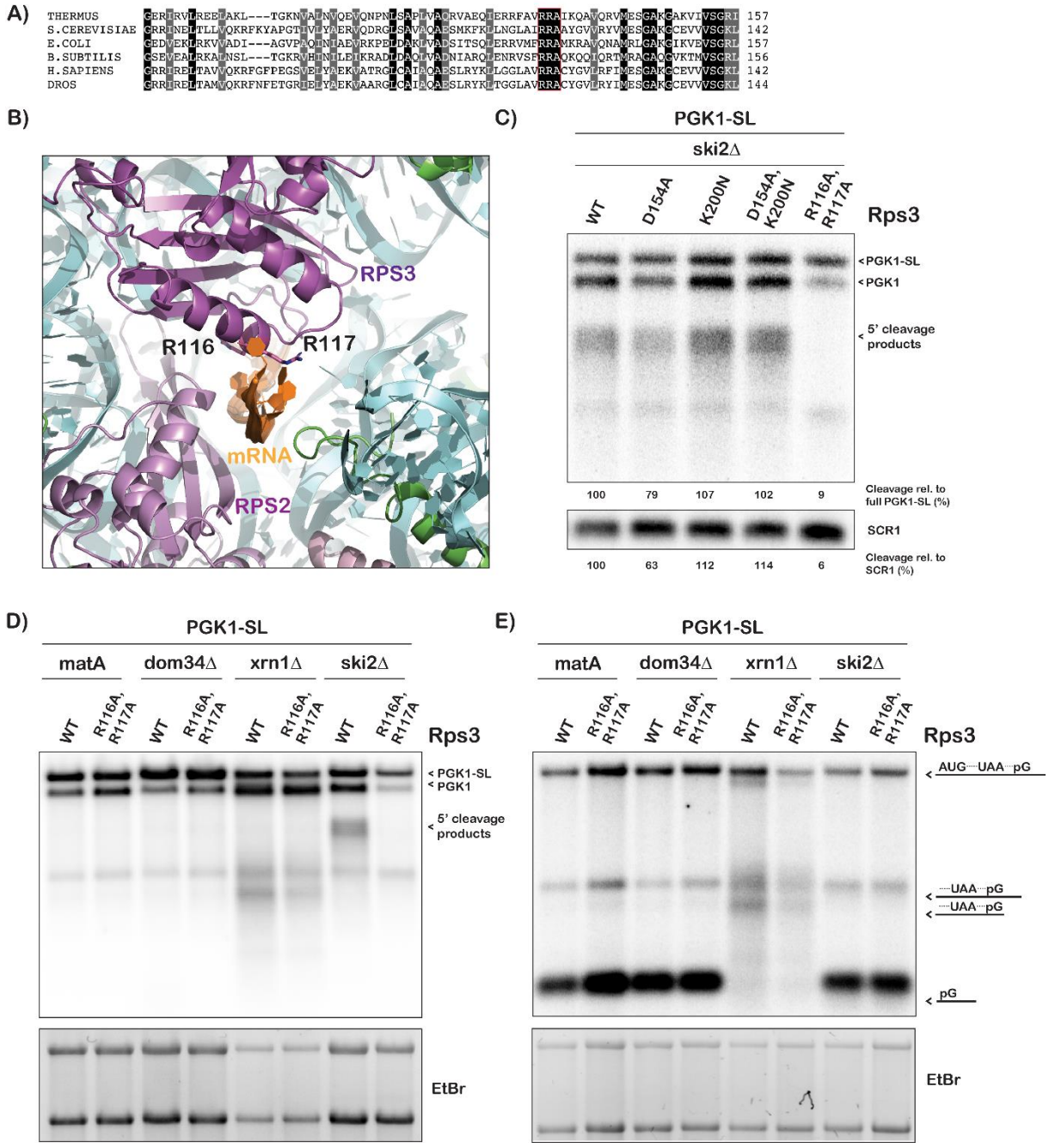

Figure 1: Conserved residues in *RPS3* that affect the endonucleolytic cleavage reaction.
A) Alignment of partial Rps3 sequences from bacteria species, yeast, Drosophila, and human, with conserved residues highlighted including yeast R116 and R117, shown boxed in red. **B)** Structure of the entry tunnel of the ribosome, with position of Rps3 residues R116 and R117 shown (PDB ID 5AJ0). **C)** Northern analysis of 5' fragments derived from a PGK1-stem loop (SL) reporter in *ski2Δ* strains harboring mutations in *RPS3*. Cleavage efficiency is significantly reduced in the R116A/R117A mutant. Products were quantified relative to full length PGK1-SL (top band) or to SCR1 (bottom panel). **D)** Northern analysis of 5' fragments accumulation from PGK1-SL in the indicated strains with either wild type or mutant *RPS3*. Corresponding ethidium-bromide stained agarose gel (bottom panel). **E)** Northern analysis of 3' fragments accumulation from PGK-SL in the indicated strains with wild type or mutant *RPS3*. The fragments are labeled as in (Chen et al. 2010). Corresponding ethidium-bromide stained agarose gel (bottom panel).

The R116A/R117A mutations affect the stability of an NGD reporter mRNA

To provide further support for a role for the entry tunnel residues of Rps3 during NGD, we next examined the effect of the mutations on the stability of the PGK1-SL mRNA. Our reporters are expressed under the control of the GAL1 promoter, and as a result transcriptional-shutoff by shifting cells to glucose-containing media was used to measure the decay rate of the reporter mRNAs. As a control, we initially measured the decay rate of a non-NGD reporter (PGK1), which does not harbor any stalling sequence. The mutations were found to have little effect on the decay rate of the PGK1 mRNA reporter (Figure 2A); we measured half-lives of 28 ± 1.9 and 26 ± 4.4 minutes in the WT and the RPS3-mutant stains, respectively. As expected, the PGK1-SL mRNA decays with a faster rate relative to its PGK1 parent (Figure 2B). Its half-life of 4.7 ± 0.2 minutes is similar to previously published reports (15). Here the RPS3 mutations result in a moderate but reproducible increase in reporter half-life to 6.0 ± 1.3 minutes, suggesting greater stabilization of the PGK1-SL mRNA (Figure 2B). Hence, these findings add additional support for the entry tunnel of the ribosome playing a role in mRNA-surveillance during NGD, whereby loss of interactions with the mRNA leads to stabilization of mRNAs harboring stalls.

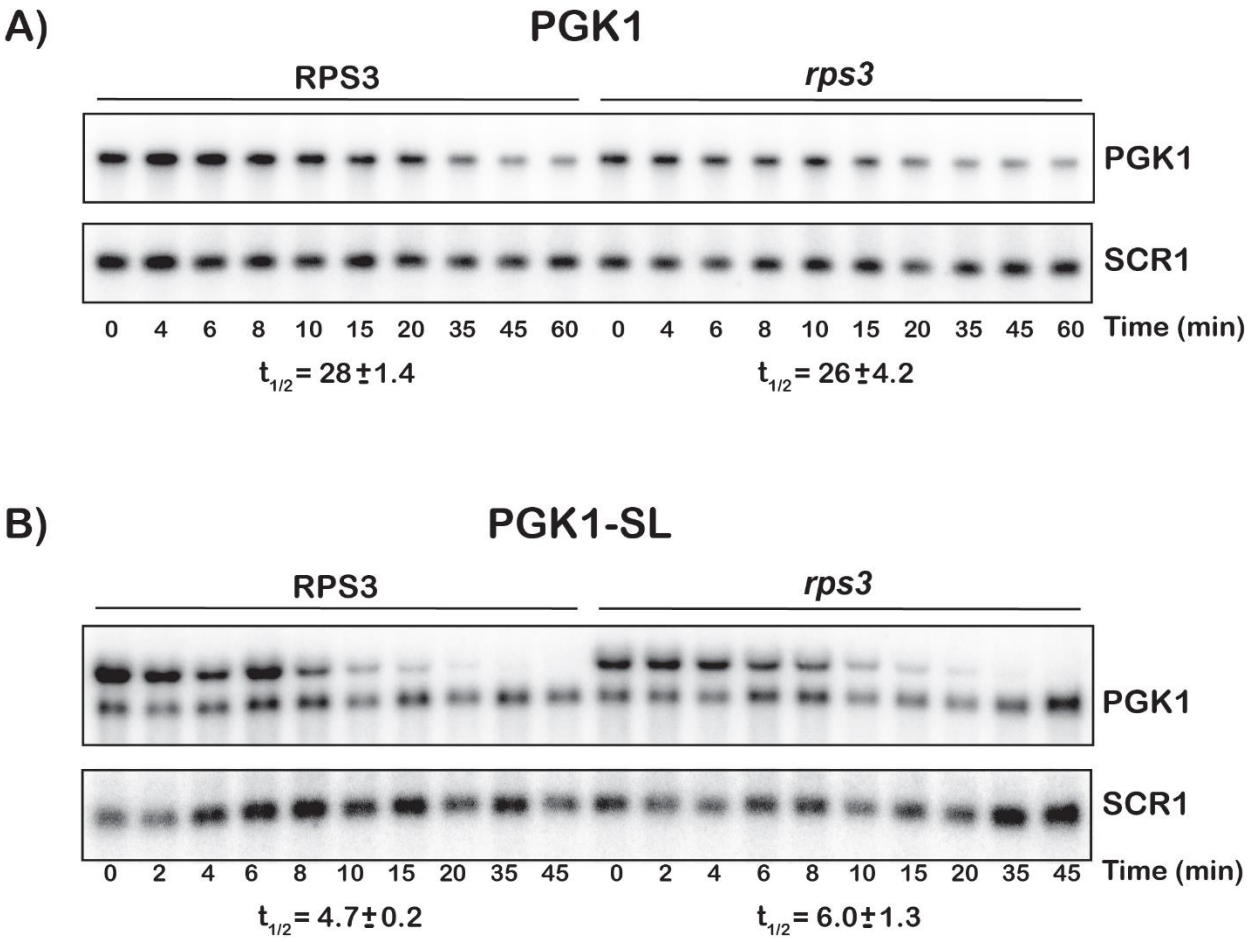

Figure 2: Mutations in *RPS3* stabilize a PGK1-SL NGD reporter.
A) Northern analysis of time course measuring decay of a control PGK1 reporter (top panel) with blot re-probed for control RNA *SCR1* (bottom panel). No substantial difference in half-lives was observed between wild type and mutant *RPS3*. **B)** In the presence of R116A/R117A mutations, the turnover of the PGK-SL stem loop reporter is reduced by about one third. Half-lives reported below each panel are an average ± SD.

The effect of R116A/R117A mutations on the cleavage reaction is independent of the stalling sequence

So far, our analysis has focused on one type of stall - a stable RNA secondary structure in the form of a stem loop. Since the mutations under investigation here are important for the helicase function of the ribosome, any effect we saw on the cleavage reaction could be explained by defects in the unwinding activity of the ribosome and not in NGD. To rule out this potential explanation, we used two other reporters that had 12 stretches of the inhibitory arginine CGA or

lysine AAA codons. Both are known to efficiently block translation and are not predicted to form secondary structures (3, 15, 23). These new reporters were introduced to wild-type or mutant RPS3 yeast strains in the ski2Δ background. As expected, the CGA and AAA reporters accumulated 5'-fragments in the wild-type RPS3 strain, whereas the control UUU reporter did not (Figure 3). Similar to what we observed for the SL reporter, the R116A/R117A mutations significantly reduced the 5'-fragments levels for the CGA and AAA reporters, suggesting that the entry tunnel residues affect the accumulation of cleavage fragments independent of the type of stall (Figure 3). Interestingly, however, unlike the SL reporter, for which we observe an almost complete loss of cleavage products when RPS3 was mutated, cleavage fragments resulting from the CGA and AAA reporters were still visible but instead were heterogeneous in nature (Figure 3). This also made it difficult to perform any meaningful quantification. This is likely due to cleavage fragments produced by inefficient initial cleavage reactions, which lead to ribosome queuing upstream of the lead stalled ribosome.

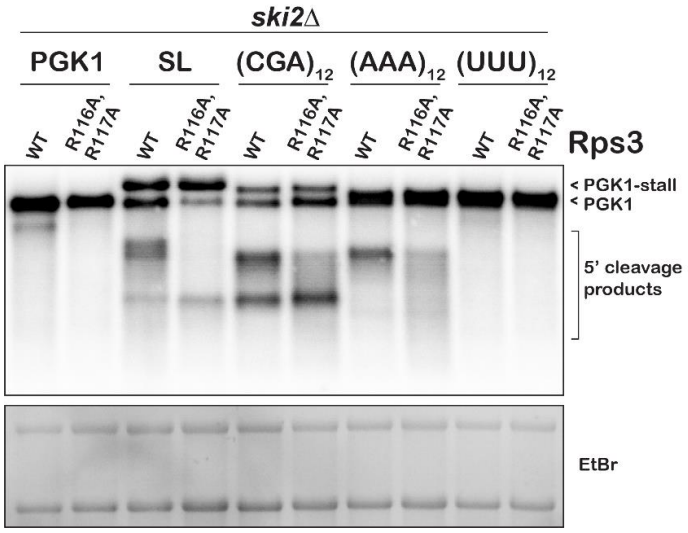

Figure 3: Mutations in *RPS3* affect cleavage efficiency independent of stall sequence.
Northern analysis of 5' fragments accumulation from *ski2Δ* strains, with and without mutations in *RPS3*, carrying different stalling reporters. PGK1 contains a PGK1 mRNA without any additional sequence; SL contains a stem loop at position 1040 of PGK1; $(CGA)_{12}$, $(AAA)_{12}$, and $(UUU)_{12}$ indicate the corresponding codons were inserted at position 950 of PGK1. Corresponding ethidium-bromide stained agarose gel is shown (bottom panel).

Ski7, a component of the exosome in yeast, has been implicated in non-stop decay (NSD) (52-54); given the similarities between NSD and NGD, the mutations in RPS3 could potentially affect the function of Ski7. To address this possibility, we deleted SKI7 from the wild-type, dom34Δ and ski2Δ stains in the absence and presence of the RPS3 mutations and assessed its effect on NGD efficiency from the SL reporter. We observed no significant changes to the accumulation of the 5'-fragments due to the SKI7 deletion suggesting that the entry tunnel residues do not affect the function of the factor (Supplementary Figure 1).

As mentioned earlier, in addition to Rps3, the mRNA entry tunnel of the small subunit also encompasses conserved residues of the ribosomal protein Rps2 (42, 55). Namely the side-chain of Glu120 of the yeast protein protrudes into the entry tunnel and is likely to interact with the mRNA downstream of the A site (Supplementary Figure 1). Consequently, we determined whether this residue contributes to NGD or not. We mutated Glu120 to Ala in the ski2Δ strain and evaluated its effect on NGD cleavage efficiency. In contrast to the RPS3 mutations, the RPS2 mutation had no noticeable effect on the cleavage reaction; we observed comparable levels of 5'-fragments accumulation from the SL reporters in the RPS2 wild-type and mutant strains (Supplementary Figure 1). It thus appears that the changes to NGD we observe in the presence of the RPS3 mutations are the result of Rps3-dependent effects, and likely not from general alterations to the mRNA-entry tunnel.

Dom34 and Asc1 modify the effects of the R116A/R117A mutation

Initial reports of NGD suggested that Dom34 plays a role in the cleavage reaction due to the loss of the cleavage products accumulation when the factor is deleted (15, 24). Later studies, however, showed that the protein together with Hbs1 and ABCE1 dissociates stalled ribosomes

(19). In its absence ribosomes pile up on the mRNA leading to multiple cleavage events upstream of the lead stalled ribosome, which run as a long smear on a gel that appears to result in loss of cleavage efficiency (16). Furthermore, overexpression of certain ribosomal proteins restored cleavage in the absence of *DOM34*, suggesting that the protein is involved in maintaining ribosome homeostasis (22). To gain further insights into the role of the entry-tunnel residues in ribosome rescue, we deleted *DOM34* from our *RPS3*-mutant strains and assessed its effect on the accumulation of 5'-fragments from the PGK1-SL reporter. As had been seen by others, deletion of *DOM34* appeared to result in a loss of cleavage (16). Interestingly the same deletion in the presence of the R116A/R117A mutations appears to restore cleavage with one caveat; the fragments are much more heterogeneous relative to those observed under normal conditions (Figure 4A). In particular, the products were observed to form a long smear on agarose gels. It seems that, under conditions where ribosome rescue is inhibited, mutation of the entry tunnel residues leads to a spreading of cleavage events well upstream of the stall site.

To provide further support for this notion, we examined the effect of mutations in *ASC1* on cleavage in conjunction with the *RPS3* mutations. Asc1 is a ribosome-associated protein that has been implicated in multiple aspects of ribosome quality control processes including NGD (38, 56-58). For instance, cryoEM structures of a Dom34-Hbs1-bound ribosome revealed the factor to interact with Dom34 suggesting that it is critical for NGD (59, 60). In addition, recent data from the Inada group showed that the factor is important for sequential endonucleolytic cleavage during non-stop decay (NSD) in the absence of *DOM34* (58). Instead of deleting *ASC1*- which harbors a snoRNA gene in its intron- from our *rps3* strains, we opted to introduce the R38D/K40E mutations into the chromosomal copy of the gene. These mutations are known to affect the association of the factor with the ribosome and phenocopy its deletion in NGD (61).

Similar to the effect we saw in the *dom34Δ* background, the *ASC1* mutations resulted in the accumulation of heterogeneous 5'-fragments from the PGK1-SL NGD substrate in the presence of the R116A/R117A mutations (Figure 4B). To verify that the effect on NGD we observe with the *RPS3* mutants are not due to decreased association of Asc1 with the ribosome, we carried out polysome analysis and used western analysis to look at the binding of Asc1 to ribosomes. As can be seen in Figure 4C, ribosomal occupancy by wild-type Asc1 is not significantly altered by the mutations in *RPS3*; similar to the wild-type, the protein was found to primarily associate with the polysomes in the presence of the *RPS3* mutation (top panels). As a control, the R38D/K40E mutant was observed in the light fractions of the sucrose gradient, that is not ribosome-associated, regardless of *RPS3* status (bottom panels). We should note, though, Asc1 participates in a multitude of processes on the ribosome including translation of short ORFs, stall clearance and ribosomal protein ubiquitination (37, 38, 56-58, 62). As a result, any interpretation of its consequence on NGD is likely to be complicated by the larger context of its effect on ribosome function.

How inhibition of ribosome rescue either by deletion of *DOM34* or mutation of *ASC1* restores cleavage efficiency to entry-tunnel mutants, albeit with a distinct signature of heterogeneous product accumulation, is difficult to interpret. One plausible explanation is that the R116A/R117A mutations inhibit the accumulation of cleavage fragments and under normal conditions ribosome rescue is fast enough to dissociate stalled ribosomes, which results in the observed disappearance of cleavage products. When rescue slows down due to reduced cleavage kinetics, ribosomes accumulate on the mRNA, initiating cleavage further upstream of the stall sequence.

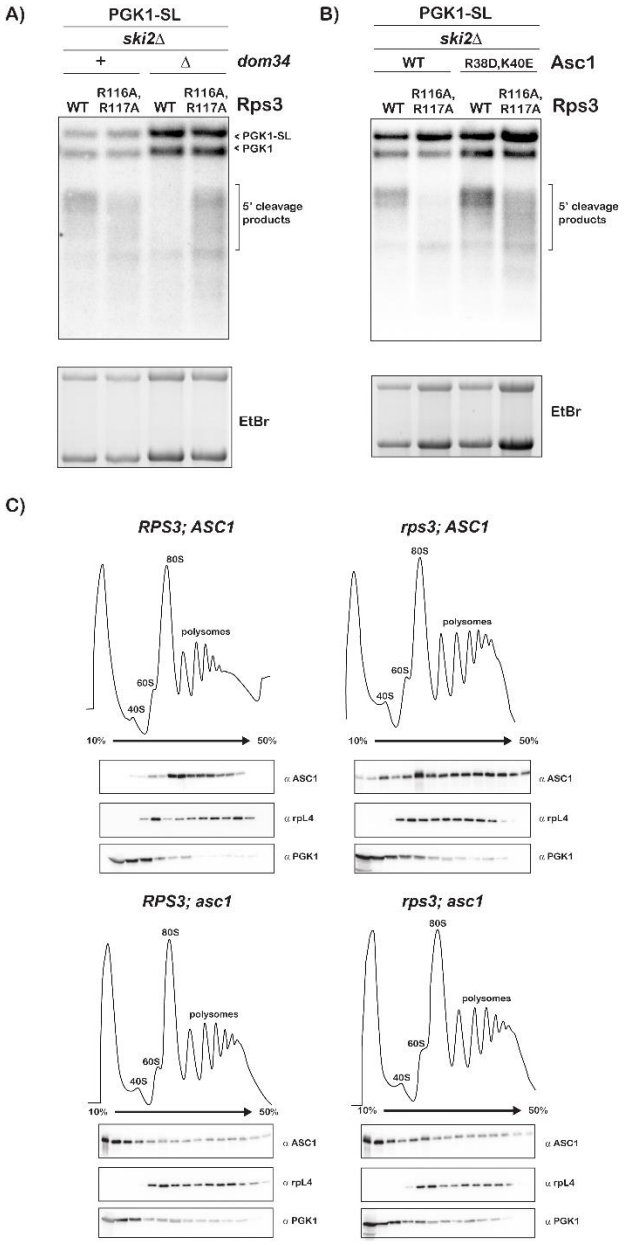

Figure 4: Assessing the effect of Dom34 and Asc1 modification on the cleavage reactions in the presence of the *RPS3* mutations.

A) Northern analysis of 5' fragments produced from the PGK1-SL reporter in cells with *DOM34* deleted and *rps3* R116A/R117A mutations. Cleavage efficiency is restored in the *dom34Δ*; *rps3* R116A, R117A cells relative to the *dom34Δ* alone cells, however the products appear smeared compared to those from the *rps3* mutant cells, indicating increased heterogeneous cleavage. **B)** Northern analysis of 5' fragments generated by cells with the *asc1* R38D/K40E and *rps3* R116A/R117A mutations. Mutations in *asc1* restore cleavage in a *rps3* mutant strain, but also lead to greater heterogeneous cleavage. In both A and B, bottom panels show the corresponding ethidium-bromide stained agarose gel. **C)** Polysome profiles of cells from the indicated strains. Shown below in each panel are western analyses across the polysome fractions of: Asc1 (top panels), Rpl4 (middle panels) and Pgk1 (bottom panels). As expected the wild type Asc1 protein's interaction with the ribosome is not affected by the *RPS3* mutations (top two panels). As expected, Asc1 R38D/K40E resides predominantly in the light fractions, unbound by the ribosome (bottom two panels). Rpl4 and Pgk1 are included as controls and remain unchanged in the presence of the *rps3* mutations. Blots shown represent three biological replicate experiments.

High-throughput sequencing of the 5'-fragments reveals spreading of cleavage events in the presence of the *RPS3* mutations

Our Northern analysis of the NGD-cleavage products suggested that the R116A/R117A mutations affect cleavage fragments accumulation and result in ribosome queueing upstream of the stall site. This pile-up of ribosomes, in turn, results in cleavage reactions even farther upstream leading to diffusion of the NGD intermediates. We provided further support for these ideas by conducting high-throughput sequencing to map the 3'-end of the 5'-NGD fragments. Briefly, total RNA was isolated from strains harboring either the *RPS3* mutants, *dom34Δ*, or *ASC1* mutants in the *ski2Δ* background, each expressing one of the three NGD reporters- SL, $(CGA)_{12}$ and $(AAA)_{12}$. An adenylated DNA oligonucleotide was ligated to the 3'-end of the RNA samples, which was used to prime reverse transcription. The resulting cDNA was then amplified using a PGK1-specific 5'-primer and subjected to high-throughput sequencing using the Illumina Hiseq 2500 platform (GEO accession: GSE117652). Similar to what we have reported earlier (40), for otherwise wild-type cells, the 5'-fragments resulting from the PGK1-SL reporter mapped well upstream of the stall in all strains regardless of the mutational background (Figure 5). However, mapping of the fragments from the R116A/R117A mutant cells revealed extensive spreading of the cleavage events (Figure 5B). More specifically, whereas in the wild-type *RPS3* background we observe one predominant peak near the ~150-nt upstream mark, in the *rps3* mutant background, no predominant peak was observed (Figure 5B). Instead, fragments mapped throughout a 500-nt region upstream of the stall site and multiple peaks were observed with a near 30-nt periodicity. Interestingly, in the *dom34Δ* and the *asc1* cells, the fragments displayed distinct mapping patterns relative to the wild-type and *rps3* cells as well as to each other. Similar to what was observed for the *rps3* mutant cells, in the *dom34Δ* cells the

predominant peak at ~150-nt is lost, but here the distance between the peaks increased significantly to 40-60 nt (Figure 5C). This is consistent with the role of Dom34 in rescuing ribosomes that run to the end of the transcript following endonucleolytic cleavage on NGD reporters. Since multiple ribosomes appear to be required for efficient cleavage, the reaction would be expected to occur every ~45-nt- with the lead ribosome protecting 15-nt, while the one behind protects 30-nt. In clear distinction to both the *rps3* and the *dom34Δ* cells, mapping of the 5'-fragments from the SL reporter was not as diffuse in the *asc1* mutant cells. Instead, only one additional predominant peak (relative to the wild-type cells) was observed at ~250 nt upstream (Figure 5D). Differences in cleavage patterns from the WT, *rps3* and *dom34Δ* cells were also evident for 5'-fragments obtained from the $(CGA)_{12}$ reporter, and to a lesser extent for $(AAA)_{12}$ reporter (Supplementary Figure 2). We note that for both the $(CGA)_{12}$ and $(AAA)_{12}$ reporters, fewer reads were mapped in the *rps3* cells, presumably due to decreased cleavage efficiency. These differences between the R116A/R117A mutant, and the *DOM34* and *ASC1* mutants suggest that the entry tunnel of Rps3 affects different aspects of NGD relative to these factors. It is also consistent with our model that these residues are important for the endonuclease function.

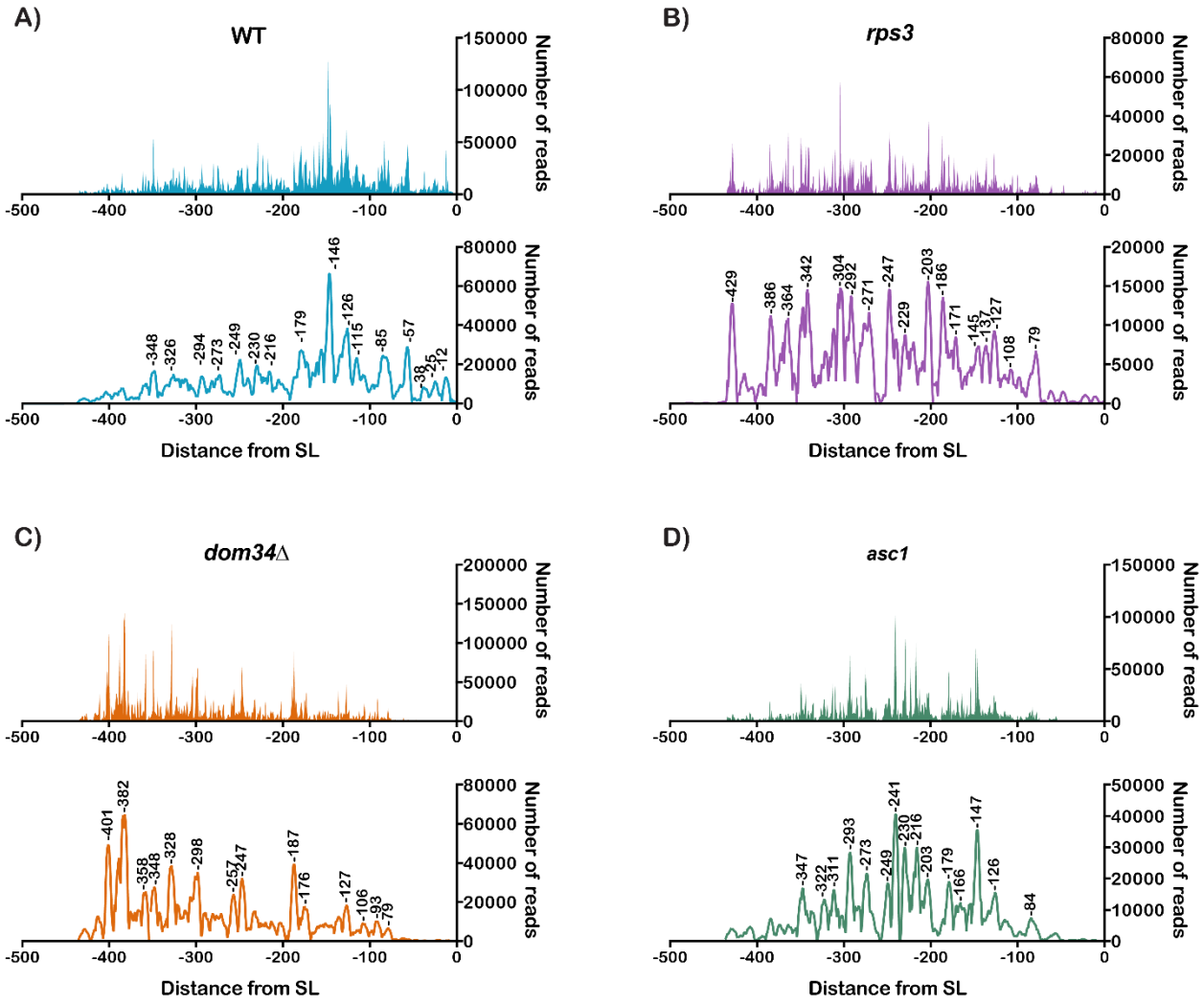

Figure 5: Large scale sequencing reveals changes in cleavage patterns in the presence of *RPS3* mutations. Plot of sequencing reads of 3' RACE products from the indicated strains, each expressing PGK1-SL. All strains are in a *ski2Δ* background. Each point represents a single read, mapped relative to the stall site and the bottom plot in each panel denotes smoothed data, produced using a 5-point quadratic polynomial. Peaks with values at the 75th quartile or above are labelled as position relative to the stall sequence. (**A-B**) Compared to wild type (**A**), *RPS3* mutations (**B**) result in highly heterogeneous cleavage without a predominant peak. (**C-D**) Deletion of *DOM34* (**C**) or mutations in *ASC1* (**D**) each produce greater heterogeneity of cleavage products with distinct patterns compared to each other and to wild type. Data in panel A is adapted from Simms et al (62).

Polysome analysis reveals that the *RPS3* mutations do not affect ribosome homeostasis

Recently we showed that ribosome collision appears to play an important role in initiating NGD during stalling (17). In particular, decreasing ribosome concentration, and hence ribosome density per mRNA, by deleting certain ribosomal protein paralogues was found to reduce cleavage of NGD targets (40). As a result, we wondered whether the mutations of the

entry tunnel residues had similar effects on ribosome density. To address this potential explanation, we compared the polysome profile of the *rps3* cells to the wild-type ones. Our analysis revealed that the mutations in *RPS3* had little effect on ribosome density (Figure 6). The ratio of polysomes to monosomes in the mutant is largely similar to that observed in the wild-type background. In contrast, similar analysis of the *dom34Δ* cells- as has been seen before (27)- revealed elevated levels of 80S monosomes relative to polysomes (Figure 6). The finding that the *RPS3* mutations do not seem to affect ribosome density has two immediate ramifications: 1) the observed inhibition of NGD in the presence of these mutations does not result from changes to ribosome collisions; 2) consistent with our mapping analysis, the mutations are not likely affecting the function of Dom34.

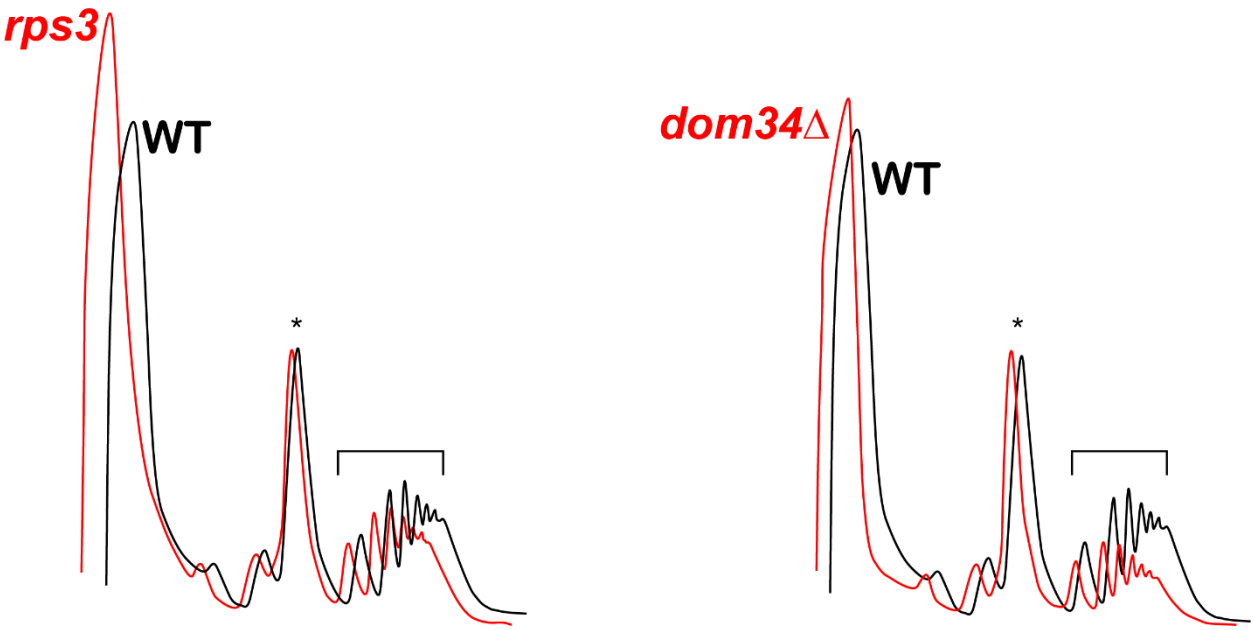

Figure 6: Mutations in Rps3 do not affect global ribosome density
Polysome profiles from wild type cells (black) and either *rps3* or *dom34Δ* mutant cells (red). The ratio of peak height for polysomes (bracket) to monosomes (asterisk) in *rps3* cells is similar to wild type (left) while this ratio is substantially lower in *dom34Δ* cells (right).

Stalling-induced ubiquitination of ribosomal proteins is unchanged in the presence of the R116A/R117A mutations

As discussed earlier, ubiquitination of ribosomal proteins by Hel2 (Znf598 in humans) has recently been recognized as an important feature of ribosome stalling. This modification promotes stalling on inhibitory codons as deletion of *HEL2* results in significant bypassing of stalls by the ribosome (36-38, 63, 64). Relevant to our studies is the observation that Rps3 is one of the targets for Hel2-mediated ubiquitination on K212, but it is currently unclear if its modification is important for stalling (64). Nevertheless, if the entry tunnel mutations somehow affect Hel2 function, this could in principle explain their effect on NGD. As a result, we set out to assess stalling-induced ribosomal protein ubiquitination in the presence of R116A/R117A mutations. We took advantage of our previous observation that the addition of cycloheximide to an intermediary concentration, whereby ribosome collisions presumably occur at a global level, results in robust ribosomal protein ubiquitination (62). We added cycloheximide to a final concentration of 2 μg/mL to wild-type, *rps3* R116A/R117A, *dom34Δ* and double mutant cells; and isolated ribosomes. Ubiquitination patterns of ribosomal proteins resulting from cycloheximide addition, as assessed by western-blotting, was nearly identical among all strains (Figure 7). However, we noted that deletion of *DOM34* had a discernible effect on the ubiquitination levels suggesting that Dom34 might affect Hel2 function (Figure 7). The *rps3* mutations on their own, however, had no observable effect on the efficiency of ribosomal proteins ubiquitination. Hence, it is very unlikely that the effect of the entry-tunnel mutations on NGD are due to differences in ribosomal protein ubiquitination during stalling.

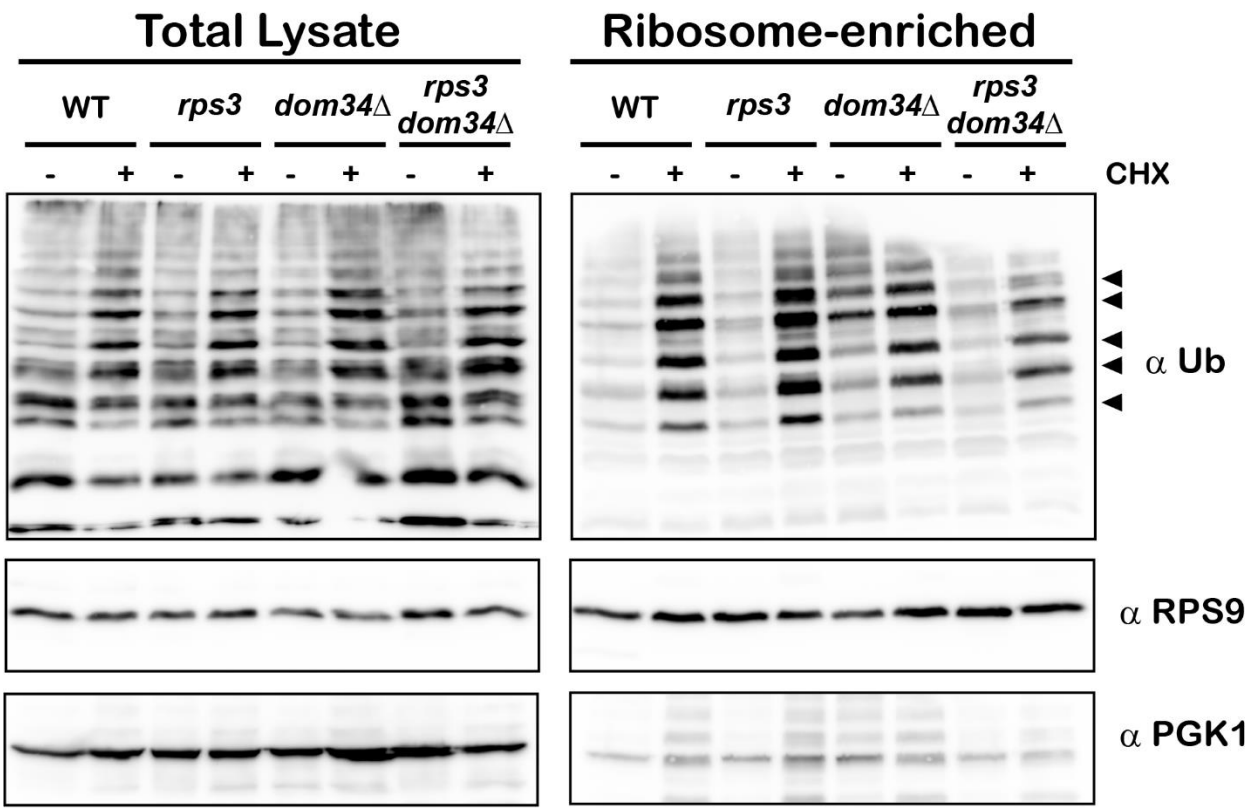

Figure 7: Ubiquitination of ribosomal proteins upon stalling is not affected by *rps3* mutations.
Western blot of total cell lysate (left) or ribosome-enriched lysates (right) from the indicated strains. Cells were treated with cycloheximide at 2 μg/mL to induce ribosome stalling. Ubiquitination patterns were essentially the same in cells with *rps3* R116A/R117A compared to those with wild type Rps3. Top panel shows blot for anti-ubiquitin; middle and bottom panels are blotted for Rps9 and Pgk1, respectively, as controls.

RPS3 mutations render cells sensitive to cycloheximide and RNA-damaging agents

We reasoned that if the entry-tunnel residues of Rps3 are affecting NGD, then mutating them should result in increased sensitivity to cycloheximide especially at intermediate concentrations, at which ribosome collisions will occur and hence NGD is triggered. Growth of the *rps3* strain was compared to the wild-type one in the presence of varying concentrations of cycloheximide (Figure 8A and 8B). To distinguish between effects on the growth rate versus lag time, we determined the first derivative of the growth curve to measure the instantaneous growth rate. The maxima of the resulting curves report on the maximal growth rate, whereas the distance between the maxima reports on the lag. As expected, the mutations had no effect on the growth

rate or lag period in the absence of the drug and at very low and high concentrations (Supplementary Figure 3). In contrast and in agreement with our model, the addition of cycloheximide at intermediate concentrations (0.02-0.32 μg/mL) significantly increased the lag period for the R116A/R117A mutant. This effect was most noticeable at the 0.16 μg/mL concentration, for which we observed a lag-time difference between the wild-type and the mutant cells of more than 4 hours (Supplementary Figure 3). Our data suggests that the entry-tunnel residues are important for dealing with intermittent collision events, and likely the ensuing process of ribosome rescue.

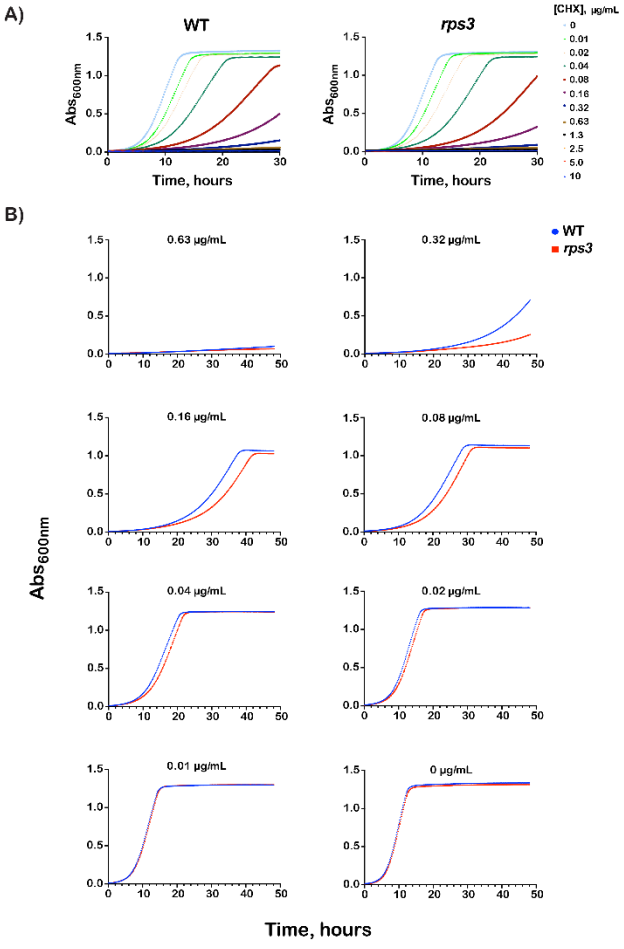

Fig 8: *RPS3* mutations result in increased sensitivity to cycloheximide.
A) Plot of OD_{600} over time of wild type or *rps3* mutant cells grown in the presence of cycloheximide at the indicated concentrations. **B)** Individual plots from (**A**) showing data at the specified cycloheximide concentration. *rps3* mutations affect growth at intermediate concentrations of cycloheximide.

Previous work from our lab revealed that RNA oxidation strongly stalls translation *in vitro* (17). In particular, the introduction of a single 8-oxoguanosine adduct to the mRNA reduced the rate of peptide-bond formation by almost three orders of magnitude in a bacterial reconstituted system and prevented the formation of full-length protein products in wheat-germ and rabbit-reticulocyte extracts. We also provided evidence that showed oxidized mRNA is subject to NGD. Because our *rps3* mutations appear to affect NGD, they should also in principle result in increased sensitivity to agents that react with RNA to produce adducts such as 8-oxoguanosine. We used the chemical 4-Nitroquinoline 1-oxide (4NQO), a UV mimetic and known to produce reactive oxygen species, to introduce 8-oxoguanosine into RNA (65) in living yeast. Wild-type and *rps3*-mutant cells were grown to mid-logarithmic before being challenged with 5 μg/mL of 4NQO for 30 minutes. Cells were washed with fresh media, diluted and their growth monitored. In the absence of any drugs, the *rps3* mutant displayed a growth rate nearly identical to that of the wild-type (6.6 ±0.23 versus 6.3 ±0.07 hours). After incubation with 4NQO, the mutant displayed a notable lag in its growth of 1.4 hours (10.4 ±0.18 versus 9.0±0.79) (Figure 9A and 9B) We note that although the effects we saw are modest, they are reproducible and suggest that mutations of the entry-tunnel residues render cells sensitive to damaging agents. These effects are also reminiscent of the effects that we and others have documented for *dom34Δ* and *xrn1Δ* strains (17). These findings together with the observation that mutations in *RPS3* result in increased sensitivity towards cycloheximide provide further support for a role for the factor in NGD.

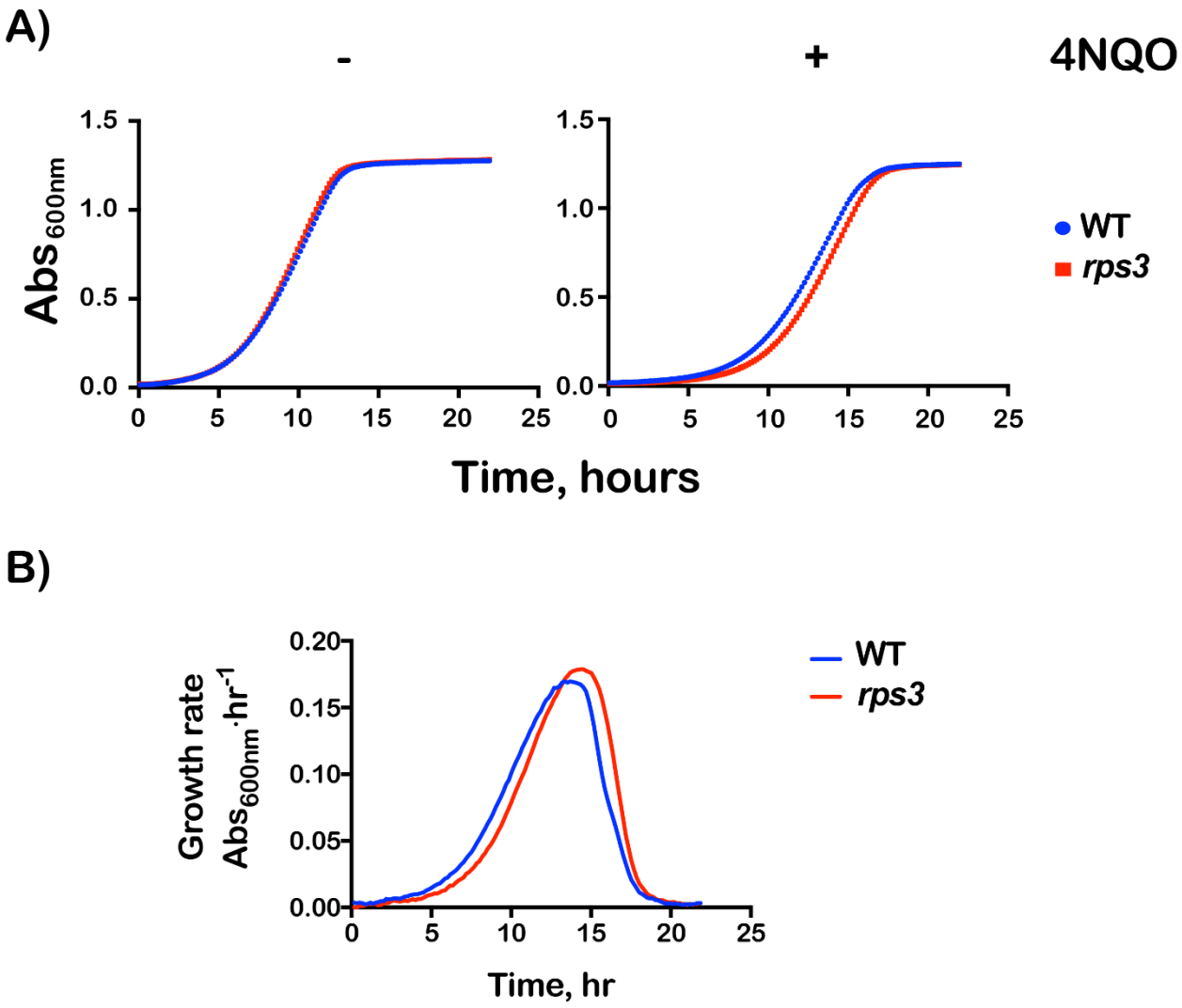

Fig 10: Mutations in Rps3 render cells sensitive to 4-NQO.
A) Plot of OD_{600} over time for wild type (blue) and rps3 cells (red) in the absence or presence of 4-nitroquinoline oxide. **B)** Instantaneous growth rate plot for samples in (**A**) treated with 4-NQO indicates increased lag time of recovery from the drug for the *rps3* mutant. Data was collected in technical duplicates from three biological replicates.

Discussion

NGD is a conserved eukaryotic process that responds to stalled ribosomes (14). The process is characterized by an endonucleolytic cleavage of the aberrant mRNA upstream of the lead ribosome (15). The identity of the culprit endonuclease remains unknown. As a result, there is a critical gap in our understanding of some of the mechanistic details of the process. Nonetheless, multiple studies have provided important hints about the enzyme. For instance, mapping experiments suggested that the endonuclease is ribosome-associated (40, 41). In particular, cleavage takes place in frame with the ribosome and is phased by ~30 nt, the mRNA-length protected by the ribosome. Furthermore, the reaction appears to likely take place between stacked ribosomes (40). All of these studies hinted at a role for the ribosome itself in activating or recruiting the endonuclease. Here we provided further evidence for this notion. More specifically, we find the entry tunnel of the ribosomal protein Rps3 to be important for the cleavage reaction. Mutation of the key-entry-tunnel residues Arg116 and Arg117 were found to drastically affect the outcome of the cleavage event; we observe a significant reduction in the accumulation of 5'-fragments from a number of NGD reporters when these residues are mutated to Ala. Consistent with these findings, although subtle, the half-life of the SL reporter increases in the presence of the mutations suggesting that these mutations may stabilize NGD reporters. Mapping of the cleavage products also revealed spreading of the cleavage reaction in the presence of the mutations. We note that Rps3 is known to interact with two key NGD factors: Dom34 and ribosome-associated Asc1 (60, 66). Although deletion or mutation of these factors affects the cleavage pattern in the *rps3* background, as evidenced by northern analysis, the effect of the mutations on NGD do not appear to phenocopy those observed in the *dom34Δ* and *asc1* strains, which is apparent in the high-throughput mapping data. Furthermore, the mutations do

not alter Asc1 occupancy on the ribosome. Collectively our data suggests that the entry-tunnel region of Rps3, and hence the ribosome, has a function in NGD upon stalling. In agreement with this proposal, mutations of this region render cells sensitive to intermediate concentrations of cycloheximide and the nucleic-acid damaging agent 4NQO; both stall the ribosome and likely trigger NGD.

Apart from the decoding center nucleotides, the Arg116 and Arg117 residues of the entry tunnel of the ribosome come closest to the mRNA. Indeed, some of the first studies on this region showed it to be important for unwinding the mRNA and make up part of the helicase domain of the ribosome (42). While our data do not show the residues to be required for cleavage to take place –we still observe accumulation of NGD fragments in the presence of the mutations– they clearly affect the pattern of the cleavage reaction. It is feasible that the electrostatic interaction between the side chains and the phosphodiester backbone of the mRNA is important for locking the mRNA in place for the endonuclease to carry out its cleavage reaction. When these residues are mutated to Ala residues, the mRNA is more dynamic and its accessibility to the enzyme's active site is severely affected. Alternatively, these residues might be important for recruiting or activating the endonuclease and as a result, changing their identities inhibits the cleavage reaction, although it is not clear how residues buried deep in the ribosome could be used efficiently to recruit exogenous protein factors. Instead, we favor a model whereby the endonuclease is intimately associated with the ribosome and it is activated upon stalling. In agreement with this, previous work has indicated that during non-stop decay, when the ribosome runs to the end of an mRNA, the endonucleolytic cleavage takes place near the exit tunnel of the ribosome (16, 41, 67) as evidenced partly by the accumulation of 15-18 nt fragments. Similarly, during a novel form of mRNA degradation termed ribothrypsis, it was suggested that an

endonucleolytic cleavage event takes place near the exit tunnel (68). Interestingly, recent structural data from human cells has revealed the position of multiple ribosomal proteins and associated factors at collided di-ribosomes – events that trigger NGD (69). It appears that this higher order structure brings an entry- and exit-tunnel face of adjacent ribosomes in close proximity, which could potentially allow for interactions between otherwise distally positioned components. These include RACK1/Asc1 on the stalled ribosome with uS3, eS10, and uS10 on the collided ribosome, as well as eS26 and eS28 facing uS4 and rRNA helix 16 on the stalled and collided ribosomes, respectively. It will be exciting to see how modifications to these factors may affect endonuclease activity.

In an endonuclease-independent consequence, the residues and their interaction with the mRNA could play a role in recruiting Dom34 and Hbs1 to the ribosome. Biochemical and structural studies have suggested that Hbs1 is recruited to a ribosome with little to no mRNA downstream of the A site (20, 21, 66, 70). The N-terminal of Hbs1 binds in the RNA entry tunnel, interacting with Rps3 (66). It was hypothesized that Hbs1 cannot bind in the presence of mRNA in the entry tunnel (19, 20, 60, 66). Additional recent structural studies also revealed a potential role for Dom34 in sensing the mRNA channel, whereby it uses a unique β-loop to protrude into the mRNA channel to sense its absence (60). Together these two mechanisms ensure that ribosome dissociation only occurs when the ribosome reaches the end of the mRNA, such as during NSD or on the behind ribosomes following cleavage during NGD. It is possible that the mutations in the entry tunnel of Rps3 make the mRNA more dynamic, preventing a clash with Dom34 and Hbs1. In turn, this allows the factors to bind and dissociate the ribosomes before cleavage could take place. In agreement with this model, deletion of *DOM34* in the presence of the *rps3* mutations restores cleavage efficiency, and with increased heterogeneity, as

expected, due to widespread ribosome queueing. This model, however, does not explain why the cleavage patterns in the double mutant do not look similar to those observed in the *dom34Δ* mutant. Therefore, the effects of the *rps3* mutations appear to be more complex and they are likely to alter different aspects of NGD including the cleavage and the dissociation reactions. In contrast, the mutations do not appear to affect the RQC pathway, as we observe comparable ribosomal protein ubiquitination patterning and efficiency upon inducing ribosome collisions regardless of the status of Rps3.

Perhaps not surprising given its proximity to the mRNA, Rps3 plays a number of roles on the ribosome during translation. It has been shown to be important for providing the helicase activity to the ribosome; in bacteria Rps3/uS3, together with Rps4/uS4 and Rps5/uS5, encircle the incoming mRNA within the entry tunnel. When Arg131 and Arg132 in bacteria (corresponding to Arg116 and Arg117 in yeast) were mutated to Alanine, the efficiency of unwinding an RNA duplex by the ribosome was reduced (42). Residues of Rps4 were also shown to contribute to helicase activity, but the process overall is coupled to and dependent on movements during translocation (71). Rps3 is known to interact with other ribosomal proteins, including ribosome-bound Asc1/RACK1 (60, 66). In addition to its aforementioned role in NGD, Asc1 is known to be involved in preventing readthrough of inhibitory codons and reading-frame maintenance (72). In eukaryotes, the C-terminal tail of Rps3 lies further inside the mRNA channel, proximal to Asc1 (43). It is tempting to speculate that conformational changes that involve Rps3 could be communicated to Asc1, which then may initiate additional steps in NGD. However, the convergence of phenotypes among Rps3, Asc1 and Dom34 highlight the potential for redundancy or simply subtle differences of function between these and related factors. This is also evident during non-functional 18S rRNA decay (NRD), where both Asc1 and Rps3 have

recently been identified as players in the pathway (73). The post-translationally modified C-terminal tail of Rps3 is required for 18S NRD and, as Asc1 can collaborate with either Dom34 or Hbs1, it was suggested that multiple overlapping pathways function to deal with damaged rRNA. At another step in the translation cycle, Rps3 also contributes to stabilizing the incoming mRNA during initiation. Again, yeast residues Arg116 and Arg117 were shown to promote binding of the mRNA to eIF3 dependent pre-initiation complexes (PICs) and in particular, when the exit channel is empty, they were absolutely required (46). This demonstrates the diverse functionality of Rps3 that is likely due in part to its position at the entry tunnel where it interacts with and can survey incoming transcripts.

Collectively our findings provide further evidence for the central role of the ribosome in mRNA-surveillance pathways beyond just recognizing the aberrant mRNA and initiating the downstream events. The observation that mutations deep into the ribosome lead to dramatic changes to NGD bolsters arguments by us and others that the endonuclease is likely to be an integral part of the machine. This in turn could explain why it has been difficult to identify the endonuclease. It would be interesting to examine how quality control mechanisms evolved to integrate into fundamental biological machines. Further delineation of the details of this mechanism will also contribute to the understanding of how cells identify and degrade defective biological molecules. Finally, similar to NMD, NGD is likely to have been coopted to regulate gene expression. Indeed, recent reports have shown conditional deletion of Pelota (the human orthologue of Dom34) results in abnormal cellular differentiation (74). The identification of the endonuclease is more than likely to provide further and important appreciation of the pervasiveness of this mode of gene regulation through NGD.

Methods

Yeast strains and plasmids

Cells were grown at 30°C in YPD or in defined media when expressing reporter plasmids. Yeast strains were made using standard PCR-based disruption techniques in the background BY4741 (*MATa* (*his3Δ1 leu2Δ0 met15Δ0 ura3Δ0*). SKI7 knockout strains were generated with a LEU2 cassette, amplified using oligos complementary to the insertion site.

RPS3 mutant strains were constructed by first cloning a fragment encoding RPS3-HIS3-rpS3 3'UTR, generated by fusion PCR, into the BamHI/XhoI sites in pPROEX-HTb. Point mutations in RPS3 were introduced by site directed mutagenesis and a cassette encoding the entire region was PCR amplified and used to transform the target yeast strains. RPS2 (E120A) strains were made using the same method and ASC1 (R38D, K40E) strains were made similarly, except using BamHI/XbaI sites in pET28a. HIS3 and LEU2 coding regions were amplified from plasmids pFAGa-6xGLY-FLAG-HIS3 and pAG415 (75) respectively.

Plasmids encoding the PGK1 gene or PGK1-SL under control of the GAL1 promoter were obtained from R. Parker (15). PGK1-$(CGA)_{12}$, PGK1-$(AAA)_{12}$ and PGK1-$(UUU)_{12}$ were made by annealing complementary oligos and ligating them to XbaI digested PGK1 plasmid (40).

Northern blotting

Culture was grown overnight in a defined media (-Ura) with glucose. Cells were washed twice in media containing 2% Raffinose and 2% galactose, diluted to OD 0.1 in the same media and grown to an OD of 0.5-0.8 to permit expression of the gal-driven reporters. RNA was isolated using hot phenol extraction followed by two sets of chloroform extraction and ethanol

precipitation. 2 μg of total RNA was resolved on 1.2% formaldehyde agarose gel, followed by transfer to positively-charged nylon membrane (GE Lifesciences) using a vacuum blotter (Biorad). Next, nucleic acids were UV cross-linked to the membrane and baked at 80°C for 15 minutes. Membranes were then pre-hybridized in Rapid-Hyb buffer (GE Lifesciences) for 30 minutes in a hybridization oven. Radiolabeled DNA probe, which was labeled using polynucleotide kinase and [γ-^{32}P]ATP, was added to the buffer and incubated overnight. Membranes were washed with nonstringent buffer (2 × SSC, 0.1% SDS) three times, in some cases followed by three washes in stringent buffer (0.2 × SSC, 0.1% SDS), all at hybridization temperature. Membranes were exposed to a phosphorimager screen and analyzed using a Biorad Personal Molecular Imager. All Northern analyses were performed using at least three biological replicates. Representative images are shown.

RNA half-life measurements

Cells expressing PGK1-SL were grown overnight in defined media (-Ura) plus glucose. Cultures were then washed in -Ura media, resuspended at OD 0.1 in 50 mL -Ura plus galactose, and grown for 18-20 hours to allow expression of the reporter plasmid. Cells were collected at OD 0.5-0.6, washed once and resuspended in 11 mL pre-warmed -Ura media. A 1 mL aliquot was saved for the t_0 timepoint and 1 mL 40% glucose added to the remainder. Cells were incubated at 30°C while shaking and aliquots taken at the indicated timepoints. For each sample, cells were pelleted, media was removed, and tubes were frozen on dry ice. RNA was isolated using a hot phenol method followed by two rounds of chloroform extraction and ethanol precipitation. 2 μg of total RNA for each sample was analyzed by Northern blot.

Polysomes analysis

Yeast cultures were grown to mid-log phase before addition of cycloheximide to a final concentration of 100 μg/mL. The culture was chilled by adding an equal volume of ice and centrifuged at 4°C. Cells were then resuspended in polysome lysis buffer (20 mM Tris pH 7.5, 140 mM KCl, 5 mM $MgCl_2$, 0.5 mM DTT, 1% Triton-100, 100 μg/mL cycloheximide, 200 μg/mL heparin), washed once and lysed with glass beads using a FastPrep (MP Biomedical). Supernatant from cleared lysate corresponding to 1 mg of total RNA was layered over a 10-50% sucrose gradient and centrifuged at 37,000 rpm for 160 min in an SW41Ti (Beckman) swinging bucket rotor. Gradients were fractionated using a Brandel tube-piercing system combined with continuous absorbance reading at A_{254} nm. Proteins were precipitated by the addition of TCA to 10% after a twofold dilution with water, and resuspended in HU buffer (8 M Urea, 5% SDS, 200 mM Tris pH 6.8, 100 mM DTT).

Western blotting

Proteins were resolved on 15% SDS PAGE gels and transferred to PVDF membranes using a semi-dry transfer apparatus (BioRad). The membranes were blocked with milk in PBST for ~ 30 minutes at room temperature followed by incubation with primary antibody overnight at 4°C. After washing with PBST, the membrane was incubated with the appropriate HRP-conjugated secondary antibody for ~ 1hr at room temperature before washing 3-4 × with PBST. Detection was carried out on a GE ImageQuant LAS 4000 using the Pierce SuperSignal West Pico Chemiluminescent Substrate. The following antibodies were used: mouse anti-PGK1[22C5D8] (ab113687) and rabbit anti-rpS9 (ab117861) from Abcam; rabbit anti-ASC1 was a gift from Wendy Gilbert (Yale University) (61); mouse anti-rpL4 was a gift from Heather

True (Washington University in St. Louis); goat anti-mouse IgG HRP (31430) and goat anti-rabbit IgG HRP (31460) from Thermo Scientific.

High throughput sequencing

Total RNA from the indicated strains was ligated to a short adenylated DNA oligonucleotide, 5'rAppCTGTAGGCACCATCAAT/3ddC/ 3', at its 3' end using truncated T4 RNA ligase 2 (NEB). For each sample, total RNA from at least two biological replicates was included. Reverse transcription using a primer complementary to the adaptor was performed, and then cDNA was amplified with a 5'-primer that annealed at position 585 of PGK1. Primers were designed for the Illumina HiSeq platform and samples were column purified to remove primers before sequencing.

Single-read HiSeq 2500 sequencing was performed by the Genome TechnologyAccess Center (GTAC) at Washington University. Raw data was analyzed for quality using the Fastx toolkit (http://hannonlab.cshl.edu/fastx_toolkit/index.html), trimmed using cutadapt (76) and aligned to our reference reporter sequence using NovoAlign (http://www.novocraft.com/). Sequencing results are available at GEO (accession #GSE117652).

Growth curves and sensitivity assays

Sensitivity assays were conducted essentially as described (74). Yeast cells were grown to mid-log-phase (OD_{600} of 0.5-0.7), collected, washed and resuspended in YPD to a final density of OD 0.8. 5 μl of the cell suspension was added to 195 μl of YPD with CHX at various concentrations, from 0-10 μg/mL. All samples were prepared in biological triplicates as well as technical duplicates in 96-well polystyrene microplates. The plate was incubated at 30°C with shaking on a microplate scanning spectrophotometer (Biotek). Cell density was monitored every

10 min over 24-48 h at 600nm. To assay sensitivity to 4NQO, after growing cells to mid-log (OD 0.5-0.7) cultures were treated with and without 5 μg/mL 4QNO for 30 minutes. Cells were collected, washed and adjusted to OD 0.8. Samples were plated and growth monitored as above.

Acknowledgments

The authors are grateful to Wendy Gilbert and Heather True for providing the Asc1 and Rpl4 antibodies. We thank Roy Parker for the PGK1 and PGK1-SL reporter plasmids. The authors also wish to thank Nima Mosammaparast and members of the Zaher laboratory for comments on earlier versions of the manuscript. This work was supported by the National Institutes of Health (NIH R01GM112641 to HSZ).

References

1. Richter JD & Coller J (2015) Pausing on Polyribosomes: Make Way for Elongation in Translational Control. *Cell* 163(2):292-300.

2. Novoa EM & Ribas de Pouplana L (2012) Speeding with control: codon usage, tRNAs, and ribosomes. *Trends Genet* 28(11):574-581.

3. Letzring DP, Dean KM, & Grayhack EJ (2010) Control of translation efficiency in yeast by codon-anticodon interactions. *RNA* 16(12):2516-2528.

4. Lu J & Deutsch C (2008) Electrostatics in the Ribosomal Tunnel Modulate Chain Elongation Rates. *Journal of Molecular Biology* 384(1):73-86.

5. Pop C, *et al.* (2014) Causal signals between codon bias, mRNA structure, and the efficiency of translation and elongation. *Mol Syst Biol* 10:770.

6. Faure G, Ogurtsov AY, Shabalina SA, & Koonin EV (2016) Role of mRNA structure in the control of protein folding. *Nucleic Acids Res* 44(22):10898-10911.

7. Chaney JL & Clark PL (2015) Roles for Synonymous Codon Usage in Protein Biogenesis. *Annual review of biophysics* 44:143-166.

8. Kim SJ, *et al.* (2015) Protein folding. Translational tuning optimizes nascent protein folding in cells. *Science* 348(6233):444-448.

9. Shalgi R, *et al.* (2013) Widespread Regulation of Translation by Elongation Pausing in Heat Shock. *Molecular Cell* 49(3):439-452.

10. Liu B, Han Ψ, & Qian S-B (2013) Cotranslational Response to Proteotoxic Stress by Elongation Pausing of Ribosomes. *Molecular Cell* 49(3):453-463.

11. Fredrick K & Ibba M (2010) How the sequence of a gene can tune its translation. *Cell* 141(2):227-229.

12. Rodnina MV & Wintermeyer W (2016) Protein Elongation, Co-translational Folding and Targeting. *J Mol Biol* 428(10 Pt B):2165-2185.

13. Brandman O & Hegde RS (2016) Ribosome-associated protein quality control. *Nat Struct Mol Biol* 23(1):7-15.

14. Simms CL, Thomas EN, & Zaher HS (2016) Ribosome-based quality control of mRNA and nascent peptides. *Wiley Interdiscip Rev RNA*.

15. Doma MK & Parker R (2006) Endonucleolytic cleavage of eukaryotic mRNAs with stalls in translation elongation. *Nature* 440(7083):561-564.

16. Tsuboi T, *et al.* (2012) Dom34:hbs1 plays a general role in quality-control systems by dissociation of a stalled ribosome at the 3' end of aberrant mRNA. *Mol Cell* 46(4):518-529.

17. Simms CL, Hudson BH, Mosior JW, Rangwala AS, & Zaher HS (2014) An active role for the ribosome in determining the fate of oxidized mRNA. *Cell reports* 9(4):1256-1264.

18. Simms CL & Zaher HS (2016) Quality control of chemically damaged RNA. *Cellular and molecular life sciences : CMLS* 73(19):3639-3653.

19. Shoemaker CJ, Eyler DE, & Green R (2010) Dom34:Hbs1 promotes subunit dissociation and peptidyl-tRNA drop-off to initiate no-go decay. *Science* 330(6002):369-372.

20. Pisareva VP, Skabkin MA, Hellen CU, Pestova TV, & Pisarev AV (2011) Dissociation by Pelota, Hbs1 and ABCE1 of mammalian vacant 80S ribosomes and stalled elongation complexes. *The EMBO journal* 30(9):1804-1817.

21. Shoemaker CJ & Green R (2011) Kinetic analysis reveals the ordered coupling of translation termination and ribosome recycling in yeast. *Proc Natl Acad Sci U S A* 108(51):E1392-1398.

22. Passos DO, *et al.* (2009) Analysis of Dom34 and its function in no-go decay. *Molecular biology of the cell* 20(13):3025-3032.

23. Chen L, *et al.* (2010) Structure of the Dom34-Hbs1 complex and implications for no-go decay. *Nat Struct Mol Biol* 17(10):1233-1240.

24. Lee HH, *et al.* (2007) Structural and functional insights into Dom34, a key component of no-go mRNA decay. *Mol Cell* 27(6):938-950.

25. Davis L & Engebrecht J (1998) Yeast dom34 mutants are defective in multiple developmental pathways and exhibit decreased levels of polyribosomes. *Genetics* 149(1):45-56.

26. Bhattacharya A, McIntosh KB, Willis IM, & Warner JR (2010) Why Dom34 stimulates growth of cells with defects of 40S ribosomal subunit biosynthesis. *Molecular and cellular biology* 30(23):5562-5571.

27. van den Elzen AM, Schuller A, Green R, & Seraphin B (2014) Dom34-Hbs1 mediated dissociation of inactive 80S ribosomes promotes restart of translation after stress. *The EMBO journal* 33(3):265-276.

28. Chiabudini M, Conz C, Reckmann F, & Rospert S (2012) Ribosome-Associated Complex and Ssb Are Required for Translational Repression Induced by Polylysine Segments within Nascent Chains. *Molecular and cellular biology* 32(23):4769-4779.

29. Defenouillere Q, *et al.* (2013) Cdc48-associated complex bound to 60S particles is required for the clearance of aberrant translation products. *Proceedings of the National Academy of Sciences of the United States of America* 110(13):5046-5051.

30. Shao S, von der Malsburg K, & Hegde RS (2013) Listerin-Dependent Nascent Protein Ubiquitination Relies on Ribosome Subunit Dissociation. *Molecular Cell* 50(5):637-648.

31. Verma R, Oania RS, Kolawa NJ, & Deshaies RJ (2013) Cdc48/p97 promotes degradation of aberrant nascent polypeptides bound to the ribosome. *Elife* 2.

32. Shao S & Hegde RS (2014) Reconstitution of a Minimal Ribosome-Associated Ubiquitination Pathway with Purified Factors. *Molecular Cell* 55(6):880-890.

33. Shao S, Brown A, Santhanam B, & Hegde RS (2015) Structure and Assembly Pathway of the Ribosome Quality Control Complex. *Molecular Cell* 57(3):433-444.

34. Shen PS, *et al.* (2015) Rqc2p and 60S ribosomal subunits mediate mRNA-independent elongation of nascent chains. *Science* 347(6217):75-78.

35. Bengtson MH & Joazeiro CAP (2010) Role of a ribosome-associated E3 ubiquitin ligase in protein quality control. *Nature* 467(7314):470-473.

36. Juszkiewicz S & Hegde RS (2017) Initiation of Quality Control during Poly(A) Translation Requires Site-Specific Ribosome Ubiquitination. *Mol Cell* 65(4):743-750 e744.

37. Sundaramoorthy E, *et al.* (2017) ZNF598 and RACK1 Regulate Mammalian Ribosome-Associated Quality Control Function by Mediating Regulatory 40S Ribosomal Ubiquitylation. *Mol Cell* 65(4):751-760 e754.

38. Letzring DP, Wolf AS, Brule CE, & Grayhack EJ (2013) Translation of CGA codon repeats in yeast involves quality control components and ribosomal protein L1. *Rna* 19(9):1208-1217.

39. Saito K, Horikawa W, & Ito K (2015) Inhibiting K63 polyubiquitination abolishes no-go type stalled translation surveillance in Saccharomyces cerevisiae. *PLoS Genet* 11(4):e1005197.

40. Simms CL, Yan LL, & Zaher HS (2017) Ribosome Collision Is Critical for Quality Control during No-Go Decay. *Mol Cell* 68(2):361-373 e365.

41. Guydosh NR & Green R (2017) Translation of poly(A) tails leads to precise mRNA cleavage. *RNA* 23(5):749-761.

42. Takyar S, Hickerson RP, & Noller HF (2005) mRNA helicase activity of the ribosome. *Cell* 120(1):49-58.

43. Ben-Shem A, *et al.* (2011) The structure of the eukaryotic ribosome at 3.0 A resolution. *Science* 334(6062):1524-1529.

44. Jenner L, *et al.* (2012) Crystal structure of the 80S yeast ribosome. *Curr Opin Struct Biol* 22(6):759-767.

45. Graifer D, Malygin A, Zharkov DO, & Karpova G (2014) Eukaryotic ribosomal protein S3: A constituent of translational machinery and an extraribosomal player in various cellular processes. *Biochimie* 99:8-18.

46. Dong J, *et al.* (2017) Rps3/uS3 promotes mRNA binding at the 40S ribosome entry channel and stabilizes preinitiation complexes at start codons. *Proc Natl Acad Sci U S A* 114(11):E2126-E2135.

47. Wilson DM, 3rd, Deutsch WA, & Kelley MR (1993) Cloning of the Drosophila ribosomal protein S3: another multifunctional ribosomal protein with AP endonuclease DNA repair activity. *Nucleic Acids Res* 21(10):2516.

48. Wilson DM, 3rd, Deutsch WA, & Kelley MR (1994) Drosophila ribosomal protein S3 contains an activity that cleaves DNA at apurinic/apyrimidinic sites. *The Journal of biological chemistry* 269(41):25359-25364.

49. Deutsch WA, Yacoub A, Jaruga P, Zastawny TH, & Dizdaroglu M (1997) Characterization and mechanism of action of Drosophila ribosomal protein S3 DNA glycosylase activity for the removal of oxidatively damaged DNA bases. *The Journal of biological chemistry* 272(52):32857-32860.

50. Sandigursky M, Yacoub A, Kelley MR, Deutsch WA, & Franklin WA (1997) The Drosophila ribosomal protein S3 contains a DNA deoxyribophosphodiesterase (dRpase) activity. *The Journal of biological chemistry* 272(28):17480-17484.

51. Seong KM, *et al.* (2012) Yeast ribosomal protein S3 possesses a beta-lyase activity on damaged DNA. *FEBS Lett* 586(4):356-361.

52. Frischmeyer PA, *et al.* (2002) An mRNA surveillance mechanism that eliminates transcripts lacking termination codons. *Science* 295(5563):2258-2261.

53. van Hoof A, Frischmeyer PA, Dietz HC, & Parker R (2002) Exosome-mediated recognition and degradation of mRNAs lacking a termination codon. *Science* 295(5563):2262-2264.

54. Klauer AA & van Hoof A (2012) Degradation of mRNAs that lack a stop codon: a decade of nonstop progress. *Wiley Interdiscip Rev RNA* 3(5):649-660.

55. Ben-Shem A, Jenner L, Yusupova G, & Yusupov M (2010) Crystal structure of the eukaryotic ribosome. *Science* 330(6008):1203-1209.

56. Sitron CS, Park JH, & Brandman O (2017) Asc1, Hel2, and Slh1 couple translation arrest to nascent chain degradation. *RNA*.

57. Matsuda R, Ikeuchi K, Nomura S, & Inada T (2014) Protein quality control systems associated with no-go and nonstop mRNA surveillance in yeast. *Genes to Cells* 19(1):1-12.

58. Ikeuchi K & Inada T (2016) Ribosome-associated Asc1/RACK1 is required for endonucleolytic cleavage induced by stalled ribosome at the 3' end of nonstop mRNA. *Scientific reports* 6:28234.

59. Becker T, *et al.* (2012) Structural basis of highly conserved ribosome recycling in eukaryotes and archaea. *Nature* 482(7386):501-U221.

60. Hilal T, *et al.* (2016) Structural insights into ribosomal rescue by Dom34 and Hbs1 at near-atomic resolution. *Nat Commun* 7:13521.

61. Coyle SM, Gilbert WV, & Doudna JA (2009) Direct link between RACK1 function and localization at the ribosome in vivo. *Molecular and cellular biology* 29(6):1626-1634.

62. Thompson MK, Rojas-Duran MF, Gangaramani P, & Gilbert WV (2016) The ribosomal protein Asc1/RACK1 is required for efficient translation of short mRNAs. *Elife* 5.

63. Garzia A, *et al.* (2017) The E3 ubiquitin ligase and RNA-binding protein ZNF598 orchestrates ribosome quality control of premature polyadenylated mRNAs. *Nat Commun* 8:16056.

64. Matsuo Ψ, *et al.* (2017) Ubiquitination of stalled ribosome triggers ribosome-associated quality control. *Nat Commun* 8(1):159.

65. Tada M & Kohda K (1993) Identification of N4-(guanosin-7-yl)-4-aminoquinoline 1-oxide and its possible role in guanine C8 adduction. *Nucleic acids symposium series* (29):25-26.

66. Becker T, *et al.* (2011) Structure of the no-go mRNA decay complex Dom34-Hbs1 bound to a stalled 80S ribosome. *Nature Structural & Molecular Biology* 18(6):715-U116.

67. Arribere JA & Fire AZ (2018) Nonsense mRNA suppression via nonstop decay. *Elife* 7.

68. Ibrahim F, Maragkakis M, Alexiou P, & Mourelatos Z (2018) Ribothrypsis, a novel process of canonical mRNA decay, mediates ribosome-phased mRNA endonucleolysis. *Nat Struct Mol Biol* 25(4):302-310.

69. Juszkiewicz S, *et al.* (2018) ZNF598 Is a Quality Control Sensor of Collided Ribosomes. *Mol Cell*.

70. Pisarev AV, *et al.* (2010) The Role of ABCE1 in Eukaryotic Posttermination Ribosomal Recycling. *Molecular Cell* 37(2):196-210.

71. Qu X, *et al.* (2011) The ribosome uses two active mechanisms to unwind messenger RNA during translation. *Nature* 475(7354):118-121.

72. Wolf AS & Grayhack EJ (2015) Asc1, homolog of human RACK1, prevents frameshifting in yeast by ribosomes stalled at CGA codon repeats. *RNA* 21(5):935-945.

73. Limoncelli KA, Merrikh CN, & Moore MJ (2017) ASC1 and RPS3: new actors in 18S nonfunctional rRNA decay. *RNA* 23(12):1946-1960.

74. Liakath-Ali K, *et al.* (2018) An evolutionarily conserved ribosome-rescue pathway maintains epidermal homeostasis. *Nature* 556(7701):376-380.

75. Alberti S, Gitler AD, & Lindquist S (2007) A suite of Gateway cloning vectors for high-throughput genetic analysis in Saccharomyces cerevisiae. *Yeast* 24(10):913-919.

76. Martin M (2011) Cutadapt removes adapter sequences from high-throughput sequencing reads. *EMBnet.journal* 17(1):10-12.

Supplementary Figures and Tables

Supplementary Table 1: List of yeast strains

Strain	Genotype	Source
BY4741 (matA)	MATa (his3Δ1 leu2Δ0 met15Δ0 ura3Δ0)	Dharmacon
DOM34Δ	BY4741; dom34::KanMX	Dharmacon
XRN1Δ	BY4741; xrn1::KanMX	Dharmacon
SKI2Δ	BY4741; ski2::KanMX	Dharmacon
matA; RPS3	BY4741; rps3-HIS3	This work
DOM34Δ; RPS3	BY4741; dom34::KanMX; rps3-HIS3	This work
XRN1Δ; RPS3	BY4741; xrn1::KanMX; rps3-HIS3	This work
SKI2Δ; RPS3	BY4741; ski2::KanMX; rps3-HIS3	This work
matA; RPS3(R116A,R117A)	BY4741; rps3 (R116A, R117A)-HIS3	This work
DOM34Δ; RPS3(R116A,R117A)	BY4741; dom34::KanMX; rps3 (R116A, R117A)-HIS3	This work
XRN1Δ; RPS3(R116A,R117A)	BY4741; xrn1::KanMX; rps3 (R116A, R117A)-HIS3	This work
SKI2Δ; RPS3(R116A,R117A)	BY4741; ski2::KanMX; rps3 (R116A, R117A)-HIS3	This work
SKI2Δ; RPS3(D154A)	BY4741; ski2::KanMX; rps3 (D154A)-HIS3	This work
SKI2Δ; RPS3(K200N)	BY4741; ski2::KanMX; rps3 (K200N)-HIS3	This work
SKI2Δ; RPS3(D154A,K200N)	BY4741; ski2::KanMX; rps3 (D154A, K200N)-HIS3	This work
DOM34Δ; SKI2Δ; RPS3	BY4741; dom34::KanMX; ski2::KanMX; rps3-HIS3	This work
DOM34Δ; SKI2Δ; RPS3(R116A,R117A)	BY4741; dom34::KanMX; ski2::KanMX; rps3 (R116A, R117A)-HIS3	This work
matA; RPS3; ASC1	BY4741; rps3-HIS3; asc1-LEU2	This work
matA; RPS3(R116A,R117A); ASC1	BY4741; rps3 (R116A, R117A)-HIS3; asc1-LEU2	This work
matA; RPS3; ASC1(R38D,K40E)	BY4741; rps3-HIS3; asc1 (R38D, K40E)-LEU2	This work
matA; RPS3(R116A,R117A); ASC1(R38D,K40E)	BY4741; rps3 (R116A, R117A)-HIS3; asc1 (R38D, K40E)-LEU2	This work

SKI2Δ; RPS3; ASC1	BY4741; ski2::KanMX; rps3-HIS3; asc1-LEU2	This work
SKI2Δ; RPS3(R116A,R117A); ASC1	BY4741; ski2::KanMX; rps3 (R116A, R117A)-HIS3; asc1-LEU2	This work
SKI2Δ; RPS3; ASC1(R38D,K40E)	BY4741; ski2::KanMX; rps3-HIS3; asc1 (R38D, K40E)-LEU2	This work
SKI2Δ; RPS3(R116A,R117A); ASC1(R38D,K40E)	BY4741; ski2::KanMX; rps3 (R116A, R117A)-HIS3; asc1 (R38D, K40E)-LEU2	This work
SKI2Δ; RPS3; RPS2	BY4741; ski2::KanMX; rps3-HIS3; rps2-LEU2	This work
SKI2Δ; RPS3(R116A,R117A); RPS2	BY4741; ski2::KanMX; rps3 (R116A, R117A)-HIS3; rps2-LEU2	This work
SKI2Δ; RPS3; RPS2(E120A)	BY4741; ski2::KanMX; rps3-HIS3; rps2 (E120A)-LEU2	This work
SKI2Δ; RPS3(R116A,R117A); RPS2(E120A)	BY4741; ski2::KanMX; rps3(R116A, R117A)-HIS3; rps2 (E120A)-LEU2	This work
matA; RPS3; SKI7Δ	BY4741; rps3-HIS3; ski7::LEU2	This work
matA; RPS3(R116A,R117A); SKI7Δ	BY4741; rps3 (R116A, R117A)-HIS3; ski7::LEU2	This work
SKI2Δ; RPS3; SKI7Δ	BY4741; ski2::KanMX; rps3-HIS3; ski7::LEU2	This work
SKI2Δ; RPS3(R116A,R117A); SKI7Δ	BY4741; ski2::KanMX; rps3 (R116, R117A)-HIS3; ski7::LEU2	This work
DOM34Δ; RPS3; SKI7Δ	BY4741; dom34::KanMX; rps3-HIS3; ski7::LEU2	This work
DOM34Δ; RPS3(R116A,R117A); SKI7Δ	BY4741; dom34::KanMX; rps3 (R116A, R117A)-HIS3; ski7::LEU2	This work

Supplementary Table 2: List of DNA Oligos

Oligo	Purpose	Sequence
PGK-HS-RT3	HiSeq - amplify 5'fragments from RT reaction	AAT GAT ACG GCG ACC ACC GAG ATC TAC ACT CTT TCC CTA CAC GAC GCT CTT CCG ATC TAT TGA TGG TGC CTA CAG
HS-F2	HiSeq	CAA GCA GAA GAC GGC ATA CGA GAT ACT GAT GTG ACT GGA GTT CAG ACG TGT GCT CTT CCG ATC TGG TAA GGC TTT GGA GAA CCC A

HS-F3	HiSeq	CAA GCA GAA GAC GGC ATA CGA GAT ATG CTG GTG ACT GGA GTT CAG ACG TGT GCT CTT CCG ATC TGG TAA GGC TTT GGA GAA CCC A
HS-F4	HiSeq	CAA GCA GAA GAC GGC ATA CGA GAT ACG TCG GTG ACT GGA GTT CAG ACG TGT GCT CTT CCG ATC TGG TAA GGC TTT GGA GAA CCC A
HS-F5	HiSeq	CAA GCA GAA GAC GGC ATA CGA GAT AGC TGC GTG ACT GGA GTT CAG ACG TGT GCT CTT CCG ATC TGG TAA GGC TTT GGA GAA CCC A
HS-F6	HiSeq	CAA GCA GAA GAC GGC ATA CGA GAT ATC GTA GTG ACT GGA GTT CAG ACG TGT GCT CTT CCG ATC TGG TAA GGC TTT GGA GAA CCC A
HS-F7	HiSeq	CAA GCA GAA GAC GGC ATA CGA GAT TGG TCA GTG ACT GGA GTT CAG ACG TGT GCT CTT CCG ATC TGG TAA GGC TTT GGA GAA CCC A
HS-F8	HiSeq	CAA GCA GAA GAC GGC ATA CGA GAT CAC TGT GTG ACT GGA GTT CAG ACG TGT GCT CTT CCG ATC TGG TAA GGC TTT GGA GAA CCC A
HS-F9	HiSeq	CAA GCA GAA GAC GGC ATA CGA GAT ATT GGC GTG ACT GGA GTT CAG ACG TGT GCT CTT CCG ATC TGG TAA GGC TTT GGA GAA CCC A
HS-F10	HiSeq	CAA GCA GAA GAC GGC ATA CGA GAT GAT CTG GTG ACT GGA GTT CAG ACG TGT GCT CTT CCG ATC TGG TAA GGC TTT GGA GAA CCC A
HS-F11	HiSeq	CAA GCA GAA GAC GGC ATA CGA GAT TCA AGT GTG ACT GGA GTT CAG ACG TGT GCT CTT CCG ATC TGG TAA GGC TTT GGA GAA CCC A
5PGK probe	northern blotting	AAC TGG AGC CAA AGA GTA TTT TTC GTT TCT TTC ACC GTT TGG TCT ACC CAA GTG AGA AGC
oRP121 probe	northern blotting	AAT TCC CCC CCC CCC CCC CCC CA
SCR1 probe	northern blotting	GTC TAG CCG CGA GGA AGG
PGK-CGA12-F	cloning	CTAGA CGA CGA CGA CGA CGA CGA CGA CGA CGA CGA CGA T
PGK-CGA12-R	cloning	CTAGA TCG TCG TCG TCG TCG TCG TCG TCG TCG TCG TCG T

PGK-AAA12-F	cloning	CTAGA CGC AAA AAA AAA AAA AAA AAA AAA AAA AAA AAA AAA AAA T
PGK-AAA12-R	cloning	CTAGA TTT TTT TTT TTT TTT TTT TTT TTT TTT TTT TTT TTT GCG T
SKI7::Leu-2-F	knockout cassette	CGA GGA GGT GGT CTT CGA AAC TTA CAG TAC CAC CTG ACG TTA ACT GTG GGA ATA CTC AGG
SKI7::Leu-2-F-1	knockout cassette	GAT TGG AGG TAT AAA CCT AGA GAC CCT TCT ACA ATA CAC GTA CGA GGA GGT GGT CTT CGA
SKI7::Leu-2-Rk	knockout cassette	TAA GTA TGA ATG CCT AGT ATA ATT TCT TAG TTG TAG GAT TGA CTT AAA CTC CAT CAA ATG
SKI7::Leu-2-R-1	knockout cassette	CAA CTT ATT ACT ATT CAT TTT ATA TAT TAA ACA ATA AGT ATG AAT GCC TAG TAT AAT TTC
Rps3-F (BamHI)	cloning	ACT GAG TTC GGA TCC GTC GCT TTA ATC TCT AAG AA
Rps3-R (XhoI)	cloning	CAA ATC TGG CTC GAG CTA AGC TTC AAC TGG TTC AGC TTG AGC T
Rps3-UTR-5':	cloning	GCT GAA CCA GTT GAA GCT TAG
Rps3-UTR-3':	cloning	CCT AGC GGA TCT GCC GGA GAA AGA TGA ACT GCT ACT CAC T
Rps3-UTR-His-5'	cloning	AGT GAG TAG CAG TTC ATC TTT CTC CGG CAG ATC CGC TAG G
Rps3-UTR-His-3'	cloning	AAC TCA TTC ATA TCC GAG AAA TCG TCC TGT AAG CTG GAA TTC GAG CTC GTT TAA ACT GGA
Rps3-UTR-His-3'-2	cloning	TAC AGG CGG CGT ATA CAA GTG GTG AAA ACG ATA GCG AAC TCA TTC ATA TCC GAG AAA TCG
R116117A-F	site-directed mutagenesis	GTT GAA CGG TTT GGC TAT CGC TGC TGC TGC TTA CGG TGT CGT CAG
R116117A-R	site-directed mutagenesis	CTG ACG ACA CCG TAA GCA GCA GCA GCG ATA GCC AAA CCG TTC AAC

Rps2-F (BamHI)	cloning	ACTGAGTTCGGATCCATGTCTGCTCCAGAAGCTCA
Rps2-R (XhoI)	cloning	GCTAATGACCTCGAGCTCCACCTCCGGTTGAAAAG
Rps2-E120A-F	site-directed mutagenesis	GTATCAAGACCGCCAAGGCAGTTGCTGGTGCCATCAG
Rps2-E120A-R	site-directed mutagenesis	GTATCAAGACCGCCAAGGCAGTTGCTGGTGCCATCAG
ASC1-F(XbaI)	cloning	CAA TAT TTA CTC TAG ATG CAC CAT TCT ACG
ASC1-R(BamHI)	cloning	GAT CAA CTG GAT CCT TCA ATT GCA CAG TC
ASC1-R38D-K40E-F	site-directed mutagenesis	CCT ATT GTT GTC CGC TTC CGA CGA CGA GAC TTT GAT CTC CTG GAA G
ASC1-R38D-K40E-R	site-directed mutagenesis	CTT CCA GGA GAT CAA AGT CTC GTC GTC GGA AGC GGA CAA CAA TAG G

Supplementary Table 3: Data for RNA Turnover Experiments

Data for half-life of PGK reporter (volumes norm to SCR1 control)				
	Rep#1		**Rep#2**	
Timepoint	RPS3	R116A/ R117A	RPS3	R116A/ R117A
4	2.015604	1.806837	1.505228	1.325566
6	2.415159	1.699051	1.520285	1.282251
8	1.94398	1.341875	1.380346	1.125901
10	2.00311	1.385055	1.246843	1.049667
15	1.376298	1.089653	1.109483	0.8451478
20	1.655102	1.229939	0.932001	0.5940057
30	1.159702	0.7400237	0.687046	0.5433328
45	0.80576	0.6894254	0.521908	0.3971944
60	0.662216	0.5930871	0.417094	0.396566
Half-life	29.37	29.46	26.72	23.24

Data for half-life of PGK-SL reporter (volumes norm to SCR1 control)						
	Rep#1		**Rep#2**		**Rep#3**	
Timepoint	RPS3	R116A/ R117A	RPS3	R116A/ R117A	RPS3	R116A/ R117A
0	0.3633651	0.3406607			3.140675	1.771899
2	0.3558836	0.3368302	2.251609	1.742165	2.982754	2.062591
4	0.2259869	0.2693999	2.070131	1.535391	1.546552	2.138491
6		0.1886632	1.719454	1.232219	1.875425	1.05953
8	0.1300156	0.1370354	1.193768	0.8918103	0.8642106	0.8444306
10	0.0831964	0.1004652	0.917871	0.7323559	0.5701541	0.6077968
15	0.0620343	0.078545	0.683499	0.569866	0.2207081	0.266305
20	0.0389782	0.04778258	0.533104	0.5056936	0.108911	0.1560542
30	0.03871754	0.03567653	0.828736	0.3872215	0.0568324	0.04669998
45	0.02060939	0.02693141	0.432809	0.3267397	0.049591	0.02600133
Half-life	4.78	5.76	4.45	4.8	4.85	7.37

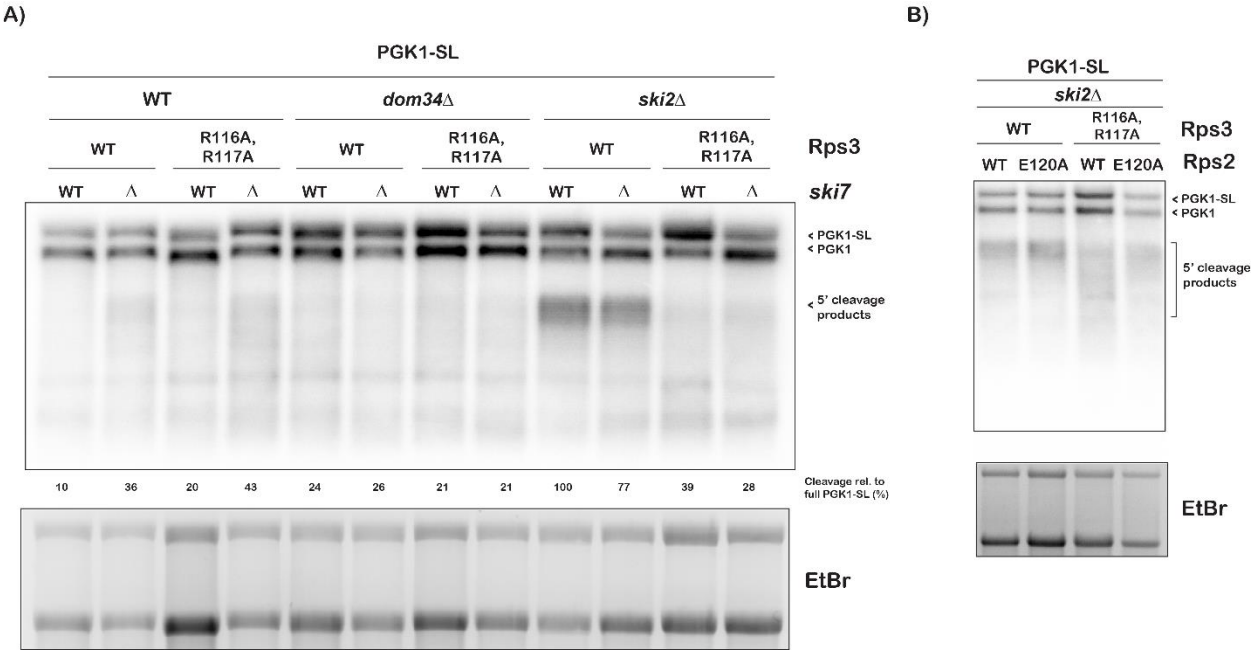

Supplementary Figure 1: Deletion of SKI7 or mutations in RPS2 do not modify the effect of RPS3 mutation on cleavage.

A) Northern analysis of 5' fragments generated in the indicated strains, each with and without ski7Δ and mutations in RPS3. Deletion of SKI7 does not affect the cleavage reaction when paired with rps3 mutations. **B)** Northern analysis of 5' fragments accumulation from cells with and without mutations in RPS3 and RPS2. In both A and B, bottom panels are the corresponding ethidium-bromide stained agarose gels.

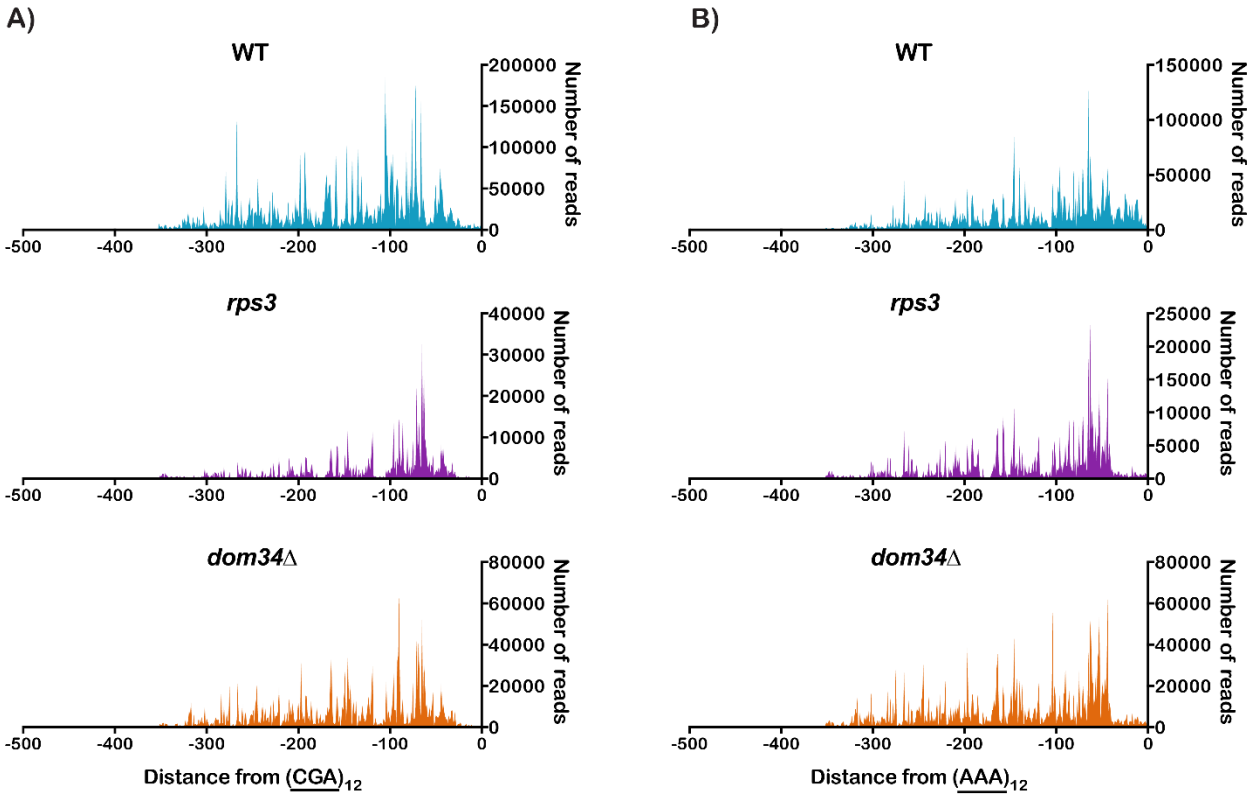

Supplementary Figure 2: Large-scale sequencing of (CGA)12 and (AAA)12 reporters.
Plots of sequencing reads from the indicated strains expressing either a (CGA)12 reporter (A) or a (AAA)12 reporter (B). Each point represents a single read, mapped relative to the distance upstream of the stall site. Top panels are from wild type cells, middle panels from rps3 R116A/R117A and bottom panels are from dom34Δ cells. In all cases, strains are in a ski2Δ background and data from wild type panels is adapted from Simms et al [62].

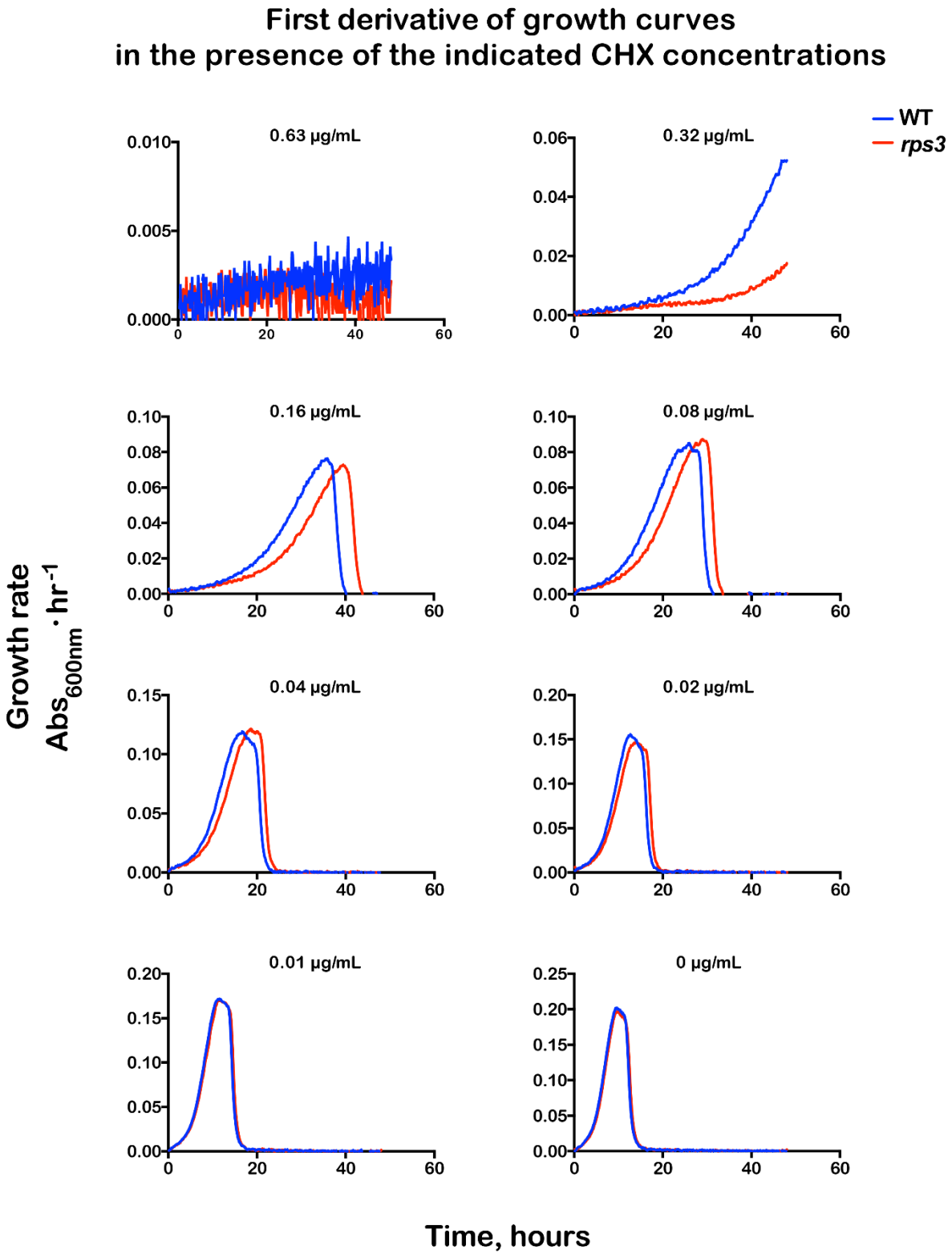

Supplementary Figure 3: Instantaneous growth rates in the presence of cycloheximide.
First derivative of growth curves from Fig 9B, with wild type cells shown in blue and rps3 R116A/R117A cells shown in red. Cells were grown at the indicated cycloheximide concentrations–intermediate concentrations result in increased lag time as indicated by shift between the maximas. Data was collected in technical duplicate from three biological replicates.

Chapter 6

Mbf1 acts in conjunction with Gcn4 to activate the Integrated Stress Response

Kyusik Q Kim, Miguel Pacheco, Victor Lasehinde, Elesa McDonald, Nanjaraj Urs, Liewei L Yan, Rachel Green, and Hani S Zaher

Abstract

Mounting evidence suggests that eukaryotes monitor collisions between ribosomes in order to select the appropriate response pathway. Elevated collision frequency leads to activation of the eIF2α kinase Gcn2, resulting in phosphorylation of eIF2α, selective translation of key response genes such as Gcn4 in yeast, and triggering of the integrated stress response (ISR). Interestingly, it was previously shown that transcription of Gcn4 targets required an additional factor, Mbf1, as a coactivator to bridge interactions with TATA binding protein (Spt15 in yeast). Following studies on Mbf1 found that it binds collided ribosomes in order to maintain reading frame. The observation that ribosome collisions are central to the activity of both factors suggests that activation of the ISR may be more complex than previously thought, requiring both production of Gcn4 and stimulation of its function by Mbf1. Here we show that Mbf1is required for transcription of Gcn4 target genes responsive to MMS stress. We find that Mbf1 is not required for translation of *GCN4* but appears to play a role in its stability. However, this does not appear to be its primary role, as stabilization of Gcn4 levels did not rescue ISR activation in the absence of Mbf1. Induction of Gcn4 in an eIF2α phosphorylation-independent manner suggests that activation of Gcn2 is necessary for Mbf1 to function as a coactivator. Accordingly, we find that ribosome binding is also necessary for Mbf1 coactivation function, as strains complemented with a mutant Mbf1 unable to bind the ribosome phenocopy the deletion strain in their inability to activate the ISR. The mechanism by which this occurs is known. The mutant protein only exhibits slight differences in localization and its recruitment to Gcn4 targets remains unaffected. Furthermore, reconstitution of the mutant factor with Gcn4 and Spt15 in vitro shows it is still capable of binding both factors. Regardless, our data suggest that yeast tightly regulates activation of the ISR, only enacting the pathway when multiple signals confirm its necessity.

Introduction

Cells devote a tremendous amount of energy to synthesizing proteins (Buttgereit and Brand, 1995; Russell and Cook, 1995). As the ultimate expression of the genetic information encoded in DNA, proteins are the molecules that enable cells to respond to their environment, grow, and divide. Under normal conditions, cells enact genetic programs that produce proteins for typical cellular functioning and maintenance. However, under stress conditions, cells must quickly switch programs into producing response factors that will allow for restoration of homeostasis. In eukaryotes, this genetic program is a conserved stress response pathway known as the integrated stress response (ISR) (Costa-Mattioli and Walter, 2020; Hinnebusch, 2005; Pakos-Zebrucka et al., 2016). Activation of the ISR begins with kinases that monitor distinct stresses, of which mammals have four: GCN2, PERK, HRI, and PKR, while the budding yeast *Saccharomyces cerevisiae* has just one, Gcn2 (Donnelly et al., 2013; Pakos-Zebrucka et al., 2016; Wek, 2018). Upon detection of their respective stress, the kinases phosphorylate the α subunit of the translation initiation factor eIF2, resulting in repression of global translation initiation and selective translation of stress response genes, particularly key transcription factors such as ATF4 in mammals or Gcn4 in yeast (Dever et al., 1992; Natarajan et al., 2001; Pakos-Zebrucka et al., 2016).

Given its conservation and importance in triggering the ISR, much attention has focused on understanding how Gcn2 is activated. In the classical model, Gcn2 is thought to be activated by deacylated tRNAs based on work interrogating its histidyl-tRNA synthetase-like domain, which can bind uncharged tRNAs in vitro and in which mutations that inhibit binding also eliminate Gcn2 activation (Dong et al., 2000; Wek et al., 1995; Zhu et al., 1996). However, deacylated tRNAs alone were insufficient to activate Gcn2 in vitro (Dong et al., 2000). Instead,

Gcn2 activity in vivo requires the presence of two additional coactivators, Gcn2 and Gcn20 (Garcia-Barrio, 2000; Marton et al., 1997, 1993; Sattlegger and Hinnebusch, 2005).

Recent evidence has pointed to a ribosome-collision centric model of activation, as several conditions that would not be expected to increase deacylated tRNA levels result in activation of the ISR (Hughes et al., 2000; Natarajan et al., 2001; Yan and Zaher, 2021). Support for such a model began with a key study by Ishimura and Nagy et al., which reported elevated stalling and GCN2-mediated eIF2α phosphorylation, without a concordant increase in deacylated tRNA levels, in neurons of mice deficient in $tRNA^{Arg}_{UCU}$ and the ribosome recycling factor GTPBP2 (Ishimura et al., 2016). Further support came experiments which reconstituted GCN2-mediated phosphorylation of eIF2α in vitro and found that ribosomes, in particular the ribosomal P-stalk, activated the kinase far more robustly than deacylated tRNAs (Inglis et al., 2019). Complementary results from a different group validated these observations, showing that P-stalks from wild-type ribosomes, but not mutant P-stalks, were competent in activation of Gcn2 (Harding et al., 2019). Meanwhile, studies using agents that stall the ribosome found that addition of the agents only at concentrations that promote collisions was able to promote eIF2α phosphorylation (Wu et al., 2020; Yan and Zaher, 2021). Indeed, it even appears that Gcn1 preferentially binds to collided ribosomes (Lee et al., 2015; Pochopien et al., 2021; Sattlegger and Hinnebusch, 2005).

Taken together, these observations suggest that the ISR is triggered by ribosome collision-mediated activation of Gcn2 and resulting translation of Gcn4. However, to add more complexity to the activation mechanism, a previous study reported that Gcn4-mediated transcription of its targets requires the factor Mbf1 as a coactivator to recruit TATA binding protein (TBP) (Takemaru et al., 1998). Initially isolated in *Bombyx mori* as the coactivator of the

transcription factor fushi tarazu (FTZ-F1) (Li et al., 1994), Mbf1 factors and their role as coactivators via binding to transcription factors and recruiting TBP is broadly conserved (Jaimes-Miranda and Chávez Montes, 2020, 2020; Kabe et al., 1999; Li et al., 1994; Liu et al., 2007, 2003; Marrero Coto et al., 2011; Takemaru et al., 1998, 1997; Tsuda et al., 2004; Wang et al., 2017; Zanetti, 2003). In addition, Mbf1 factors have already been shown to play a role during stress in plants (Jaimes-Miranda and Chávez Montes, 2020), while the human homolog, EDF1, has been implicated in responding to ribosome collisions (Juszkiewicz et al., 2020; Sinha et al., 2020).

While it was known that Mbf1 likely associated with ribosomes, due to its role as a frame maintenance factor (Wang et al., 2018), it was not immediately clear how the activities of Gcn2 and Mbf1 might be coordinated. Recent Cryo-EM studies have revealed that Mbf1 also binds to collided ribosomes (Pochopien et al., 2021; Sinha et al., 2020), providing a mechanism linking the two factors. The presence of two factors that independently monitor ribosome collisions suggests that ISR activation may be even more tightly regulated than previously thought. While the mechanisms that enable translation of Gcn4 have been widely characterized (Hinnebusch, 2005), the role of Mbf1 as an integral part of the ISR has yet to be fully elucidated.

Here we test the model of Mbf1 as a coactivator of Gcn4 and investigate its role in activation of the ISR. Transcriptomic analysis of *mbf1*Δ cells shows that Mbf1 is necessary for induction of the Gcn4 regulon, and for Gcn4 targets during MMS stress more generally, as those genes that exhibited impaired expression were similarly impaired in *gcn2*Δ and *gcn4*Δ strains. Immunoblot analysis revealed that loss of Mbf1 leads to decreased accumulation of Gcn4 in response to MMS stress. The observed decrease did not appear to be due to changes in de-repression of *GCN4* translation, as *GCN4-lacZ* reporters showed no difference between wild-

type and *mbf1Δ* cells treated with MMS or 3-AT. Instead, the decrease appears to be the result of defects in stability, as deletion of Gcn4 degradation factors largely rescued Gcn4 levels. However, stabilization of Gcn4 failed to rescue activation of the ISR, as judged by expression of the Gcn4 target gene *ARG1*, indicating that the primary role of Mbf1 is as a coactivator of Gcn4. Phosphorylation of eIF2α, or conditions that lead to Gcn2 activation, appears to be necessary for Mbf1 coactivation function, as induction of Gcn4 in an eIF2α-independent manner, via a plasmid borne-Gcn4 under the control of a copper-responsive promoter, was not sufficient to induce *ARG1* expression. Contact with the ribosome also appears to be necessary, as complementation of the *mbf1*Δ strain with an R89G mutant Mbf1, which does not comigrate with polysomes upon treatment with MMS, did not rescue *ARG1* induction. The mechanism for regulation of Mbf1 function does not appear to be through control of its localization. Visualization of Mbf1-mCherry and Mbf1 R89G-mCherry reporters by fluorescence microscopy showed that Mbf1 is distributed throughout the cell, and that treatment with MMS did not alter localization of the reporter with wild-type Mbf1. In addition, the R89G mutation does not impair Mbf1 recruitment to Gcn4 targets, nor does it disrupt binding to Gcn4 or Spt15, based on CHIP-qPCR results and gel shift assays. Overall, our findings have elucidated important details about a second regulatory mechanism cells utilize to ensure that the ISR is only activated when necessary.

Results

Mbf1 is necessary for induction of Gcn4 target genes

In Takemaru et al., the authors proposed a model where Mbf1 serves as a transcriptional coactivator by binding to the basic-leucine zipper (bZIP) domain of Gcn4 and recruiting TATA binding protein (Spt15) to Gcn4 targets (Figure 1A) (Takemaru et al., 1998). If this model is correct, we would expect *mbf1*Δ strains to be defective in induction of the Gcn4 regulon under conditions that activate the ISR. However, as RNA microarray technology had not yet been established, the authors were unable to perform transcriptome-wide testing of their model.

To establish if Mbf1 is necessary for induction of the Gcn4 regulon, we grew wild-type and *mbf1*Δ strains and subjected them to treatment with 0.1% methyl methanesulfonate (MMS) for one hour. As controls, we also grew *gcn4*Δ and *gcn2*Δ cells and subjected them to the same conditions. Our group and others have previously shown that treatment with MMS at this concentration and time frame is sufficient to robustly activate the ISR (Lee et al., 2007; Natarajan et al., 2001; Yan and Zaher, 2021). For verification of induction, we used quantitative reverse-transcription PCR (qRT-PCR) to measure expression of a Gcn4 target gene, *ARG1*, in relation to a control gene, *TAF10*. As expected, treatment induced an over 30-fold increase in *ARG1* expression in wild-type cells (Figure 1B). By contrast, the response in *gcn4*Δ and *gcn2*Δ cells was significantly impaired, with an only 3 and 1.3-fold increase, respectively. *mbf1*Δ cells were similarly defective in their response at a 4-fold increase, recapitulating the previously reported findings with *HIS3* (Takemaru et al., 1998).

Confident that the Gcn4 regulon was induced in our cells, we conducted transcriptomic analysis by RNA-seq. Resultant reads were checked for quality, analyzed using fastp (Chen et

al., 2018) to remove adapter contamination, and mapped using Salmon (Patro et al., 2017) to the SGD R64-3-1 transcriptome with 200 bases upstream and downstream of the CDSes included. Quantification results were then imported into DESeq2 (Love et al., 2014) using tximport (Soneson et al., 2016) and checked for clustering by principal component analysis. As expected, untreated and MMS treated samples clustered apart from one another, while replicates clustered together (Figure 1C). Interestingly, both treated and untreated *gcn4*Δ samples segregated into distinct clusters, although this could be attributable to the fewer mapped reads in the other samples as a result of lower-than-expected poly(A) enrichment (data not shown).

We proceeded with differential gene analysis by comparing the effect of MMS treatment in each genotype to the effect in wild type, normalizing for differences due to genotype. We plotted the differential expression results, paying attention to those genes annotated as part of the Gcn4 regulon (Figure 1D). As expected, the majority of the genes in the regulon exhibited impaired expression (Log_2 fold change < 0) in the *gcn4*Δ and *gcn2*Δ strains, at 70 and 76%, respectively. Similar impairment was observed in the *mbf1*Δ strain, at 69%, validating the necessity of Mbf1 in induction of the Gcn4 regulon.

To investigate if Mbf1 is more generally required for induction of Gcn4 targets, we expanded the analysis to encompass all MMS-responsive genes – those genes with at least two-fold induction and adjusted p-value ≤ 0.05 in the wild-type in response to MMS. 1124 genes fit this category, in agreement with previous findings (Jelinsky and Samson, 1999), confirming that our RNA-seq analysis was successful in capturing the entirety of the MMS-induced response. A comparison of genes that exhibited any impairment in expression (Relaxed dataset; Log_2 fold change < 0, adjusted p-value ≤ 0.05) showed statistically significant overlaps in impaired genes shared between the three genotypes (Figure 1E). Here, the overlapping set was larger than the set

unique to each genotype, suggesting that Mbf1 is required for their induction. However, few genes were uniquely impaired in the *mbf1*Δ strain compared to the *gcn2*Δ or *gcn4*Δ strain, indicating a requirement for intact ISR signaling in the response to MMS. Overlaps also remained statistically significant even with a more stringent classification of impaired genes (Stringent dataset; Log2 fold change ≤ -1, adjusted p-value ≤ 0.05), further supporting that Mbf1 is required for induction of these genes. Of note was the observation that the set of impaired genes in the *mbf1*Δ strain overlapped more closely with the *gcn2*Δ set than the *gcn4*Δ set, although understanding the functional relevancy of this finding will require further analysis.

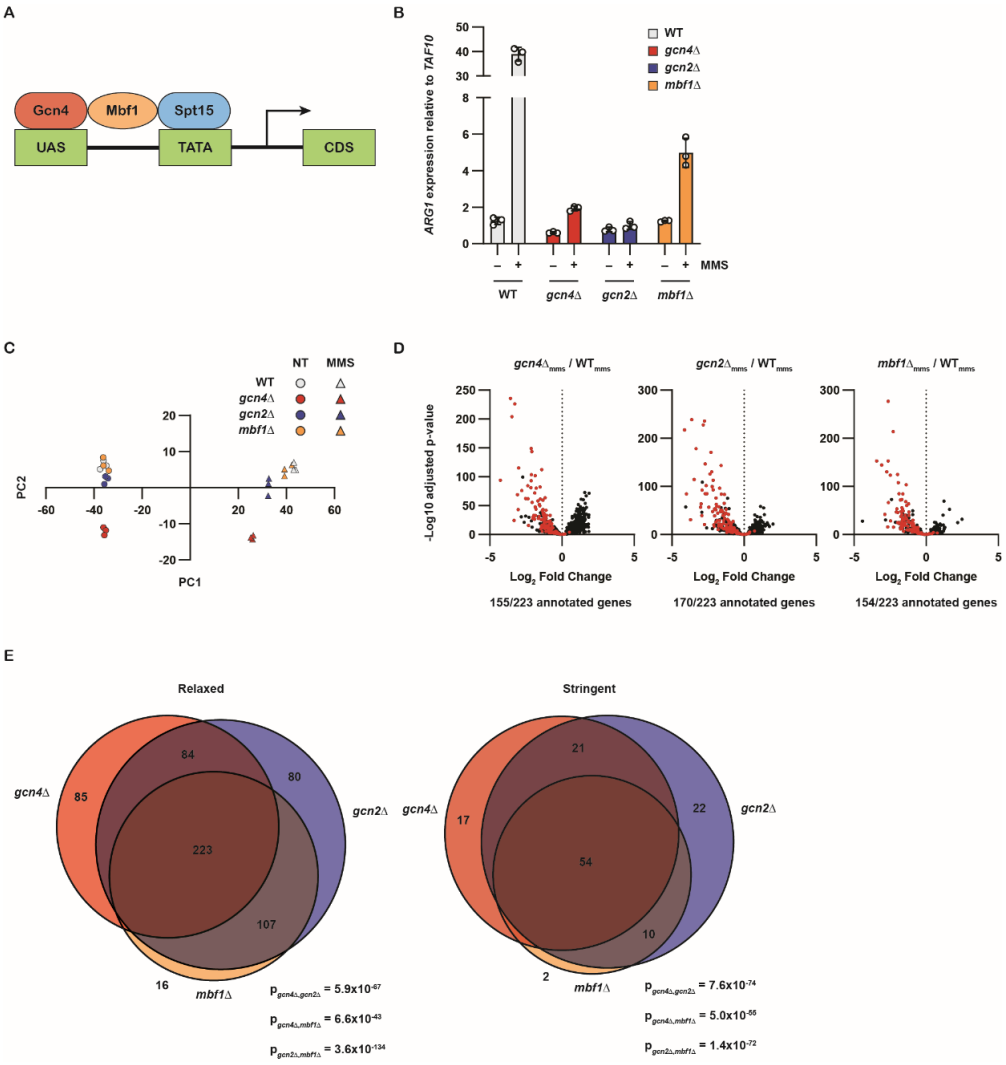

Figure 1: *mbf1*Δ strains exhibit similar defects in response to MMS as *gcn4*Δ and *gcn2*Δ strains
A) Schematic of proposed model for Mbf1 activity as a transcriptional coactivator of Gcn4. Upon induction, Gcn4 binds to upstream activating elements (UAS) of target genes (coding sequence; CDS) to drive their transcription. Mbf1 binds to the basic-leucine zipper domain of Gcn4 and recruits TATA binding protein (Spt15). **B)** *ARG1* expression, relative to *TAF10* expression, as measured by qRT-PCR, for the indicated strains and conditions. Cells were grown in YPD medium to OD_{600} ~0.6 before treatment with 0.1% MMS for one hour. Shown are the results of three biological replicates. **C)** PCA plot of variance stabilized transformed counts of genes as determined by RNA-seq analysis of cells from B. **D)** Volcano plots of the response to MMS in the indicated genotype compared to response in wild-type, normalized for genotype differences. Plotted are the Log_2 fold differences in expression against the $-Log_{10}$ transformed significance of that finding adjusted for multiple testing (adjusted p-value). Genes belonging to the Gcn4 regulon are marked in red. The number of regulon genes with impaired expression (Log_2 fold change < 0, adjusted p-value ≤ 0.05) are denoted below each plot. Differential expression was determined using the Salmon-DESeq2 pipeline. **E)** Proportional Venn diagrams displaying the number of genes with impaired response to MMS treatment for the indicated genotypes. Overlaps denote the genes shared by the respective genotypes. For the relaxed set (left), any genes with Log_2 fold change < 0 and adjusted p-value ≤ 0.05 were denoted as having an impaired response. For the stringent set (right), only genes with Log_2 fold change ≤ -1 and adjusted p-value ≤ 0.05 were denoted as such. MMS-responsive genes (1124 genes) were those with a Log_2 fold change ≥ 1 and adjusted p-value ≤ 0.05 in the wild-type as a result of treatment. p-values indicate the significance of the overlap as determined by one-tailed Fisher's exact test.

Gcn4 stability is decreased in the absence of Mbf1

While Takemaru et al. reported no difference in Gcn4 levels in *mbf1*Δ cells when treated with the histidine starvation inducer 3-aminotriazole (3-AT) (Hinnebusch, 1984; Takemaru et al., 1998), we wanted to ensure the case was the same for treatment with MMS. To enable tracking of Gcn4 levels, we introduced a 3xFLAG tag into the native *GCN4* locus. We tested if we could observe Gcn4 accumulation by treating cells with various compounds known to induce eIF2α phosphorylation. Immunoblots of whole cell extracts revealed significantly increased phospho-eIF2α and Gcn4 levels in cells treated with MMS, as expected (Figure 2A). Treatment with 4-nitroquinoline 1-oxide (4-NQO) or rapamycin also increased levels of phospho-eIF2α and Gcn4. 4-NQO has been shown to induce eIF2α phosphorylation, likely through oxidative damage to RNA (Yan et al., 2019; Yan and Zaher, 2021), while rapamycin has been shown to activate Gcn2 and de-repress *GCN4* translation (Cherkasova and Hinnebusch, 2003; Kubota et al., 2003). Treatment with hydroxyurea (HU), on the other hand, did not lead to significant increases in phospho-eIF2α or Gcn4 levels. While previous reports have shown that treatment with HU can induce eIF2α phosphorylation and upregulation of Gcn4 target genes (Cherkasova and Hinnebusch, 2003; Hughes et al., 2000), the duration of our treatment may not be sufficient for induction, which has also been noted (Cherkasova and Hinnebusch, 2003).

In contrast with Takemaru et al., we observed significantly lower Gcn4 and phospho-eIF2α levels in *mbf1*Δ cells treated with MMS, compared to wild-type cells under the same conditions, suggesting that Mbf1 plays a role in regulation of Gcn4 levels during MMS stress (Figure 2A). As GCN4 is translationally regulated by a unique mechanism dependent on eIF2α-phosphorylation, we entertained the possibility that Mbf1 is necessary for de-repression of *GCN4* translation via regulation of phospho-eIF2α levels. Briefly, *GCN4* translation is typically

repressed by the four upstream open reading frames (uORFs) in its 5'UTR. Ribosomes initiate on uORF1, and some small ribosomal subunits (SSUs) are able to remain attached and continue scanning even after termination on the uORF. Under normal conditions, remaining SSUs are able to initiate again on one of the downstream ORFs in a mechanism known as reinitiation. Reinitiation and termination on the other uORFs then results in the remaining ribosomes dissociating from the transcript, preventing production of Gcn4. Under stress conditions, phosphorylation of eIF2α removes this repression by enabling remaining SSUs to scan past the downstream uORFs and translate the main ORF (for complete review see (Hinnebusch, 2005)).

To test if differences in Gcn4 levels were due to altered translation of *GCN4*, we transformed *GCN4-lacZ* reporters (Hinnebusch, 1985) into our cells. We treated cells with MMS, as well as 3-AT to serve as a positive control (Hinnebusch, 1984). β-galactosidase activity of treated cells, normalized to activity in untreated cells, was not significantly different between the two strains treated with either compound (Figure 2B), indicating that *GCN4* translational de-repression remained intact in *mbf1*Δ cells. In addition to regulation of *GCN4* at the translational level, Gcn4 is also regulated post-translationally via rapid degradation by the proteasome. To test if differences in Gcn4 levels were due to increased turnover, we conducted cycloheximide chase experiments with wild-type and *mbf1*Δ cells. Immunoblots of whole cell extracts revealed that Gcn4 degradation appeared to occur more rapidly in *mbf1*Δ strains (Figure 2C, D), suggestive of a role for Mbf1 in stabilization of Gcn4.

Under normal conditions, Gcn4 is highly unstable, with an estimated half-life of approximately 5 minutes (Kornitzer et al., 1994). Degradation is mediated by the SCF^{Cdc4} complex, which ubiquitinates Gcn4 in response to phosphorylation of the Gcn4 threonine 165 residue by the cyclin-dependent kinases Pho85 and Srb10 (Chi et al., 2001; Kornitzer et al.,

1994; Meimoun et al., 2000). Pho85-mediated phosphorylation of Gcn4 is dependent on the presence of the cyclin Pcl5 (Shemer et al., 2002). Deletion of *PCL5* or *PHO85* in both the wild-type and *mbf1*Δ background significantly stabilized levels of Gcn4 (Figure 2E, F). Even so, stabilization failed to rescue *ARG1* induction in either double deletion mutant (Figure 2G), suggesting that the primary role of Mbf1 in induction of Gcn4 targets is coactivation rather than stabilization of Gcn4.

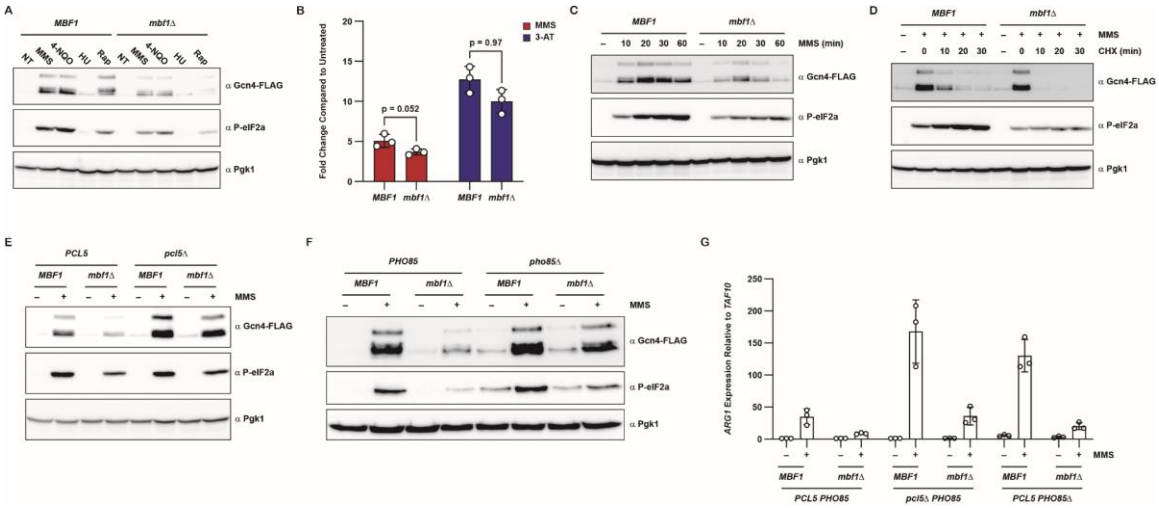

Figure 2: Loss of Mbf1 does not affect de-repression of *GCN4* translation but significantly inhibits Gcn4 stability

For immunoblots, whole cell extracts were collected using an alkaline hydrolysis and trichloroacetic acid precipitation method unless otherwise noted. **A)** Immunoblot of whole cell extracts for the indicated strains treated with the indicated compounds. Cells were grown in YPD medium to OD_{600} 0.6-0.8 before treatment. HU denotes treatment with hydroxyurea, while Rap denotes treatment with rapamycin. Treatment conditions were as follows: 0.1% MMS for 30 minutes, 5 ug/mL 4-NQO for 30 minutes, 1 µg/mL rapamycin for 30 minutes, and 100 mM hydroxyurea for one hour. Shown is a representative blot of triplicates. **B)** β-galactosidase assay of whole cell extracts from wild-type and *mbf1*Δ strains. Cells were grown in synthetic complete medium minus uracil and histidine to OD_{600} 0.7 before treatment with 0.1% MMS for 30 minutes. Whole cell extracts were collected by zymolyase treatment and lysis in Promega passive lysis buffer. Lysates were cleared by centrifugation and supernatants were incubated with ONPG for 2 hours before the addition of Na_2CO_3. Fold changes were calculated by normalizing the $Abs_{420\,nm} - 1.75 \times Abs_{550\,nm}$ of the treated samples to the same in the untreated samples. Shown are the results of three biological replicates. **C)** Immunoblot of whole cell extracts for the indicated strains treated with 0.1% MMS for the indicated time in minutes. Cells were grown in YPD medium to OD_{600} ~0.6 before treatment. Shown is a representative blot of triplicates. **D)** Immunoblot of whole cell extracts for the indicated strains incubated with cycloheximide (CHX) for the indicated time after treatment with 0.1% MMS for 30 minutes. Cells were grown in YPD medium to OD_{600} ~0.6 before treatment. Shown is a representative blot of triplicates. **E-G)** Cells were grown in YPD medium to OD_{600} 0.6-0.8 before treatment with 0.1% MMS for 30 minutes. **E, F)** Immunoblot of whole cell extracts for the indicated strains and conditions. Shown are representative blots of triplicates. **G)** *ARG1* expression relative to *TAF10* expression, as measured by qRT-PCR, for the indicated strains and conditions. Shown are the results of three biological replicates.

Gcn4 and Mbf1 alone are insufficient to induce the Gcn4 regulon in the absence of eIF2α phosphorylation

If Mbf1 is able to bind Gcn4 and recruit TBP by default, then induction of Gcn4, regardless of eIF2α phosphorylation status, should result in induction of the regulon. In order to increase levels of Gcn4 in an eIF2α-phosphorylation-independent manner, we introduced a plasmid harboring *GCN4-FLAG* under the control of a copper-inducible promoter (CUP) into our FLAG-tagged Gcn4 strain from above. Addition of copper led to accumulation of Gcn4 without a concomitant increase in eIF2α phosphorylation, as seen by immunoblot (Figure 3A). Gcn4 also appeared to accumulate to similar levels as seen with MMS treatment. However, the increase in Gcn4 levels did not induce *ARG1* expression in the absence of eIF2α phosphorylation (Figure 3B), suggesting that conditions that activate Gcn2 are necessary for Mbf1 coactivation function.

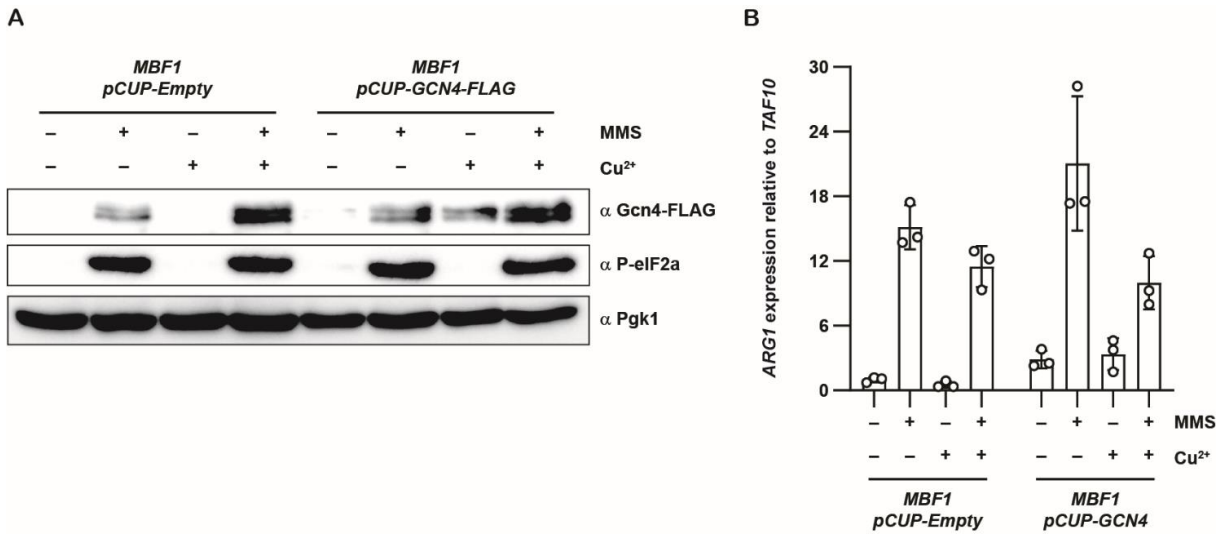

Figure 3: Accumulation of Gcn4 alone is insufficient to induce its regulon
A) Immunoblot of whole cell extracts for the indicated conditions. Whole cell extracts were collected using an alkaline hydrolysis and trichloroacetic acid precipitation method. Cells were grown in synthetic complete medium minus uracil to OD_{600} ~0.4. Cultures were then split in half and 100 uM Cu^{2+} added to one of them. After two hours, both cultures were treated with 0.1% MMS for 30 minutes. Shown is a representative blot of triplicates. **B)** *ARG1* expression relative to *TAF10* expression, as measured by qRT-PCR, for cells grown in the same conditions as A). Shown are the results of three biological replicates.

Ribosome binding is necessary for Mbf1 coactivation function

Several recent reports have implicated ribosome collisions in the activation of Gcn2 (Pochopien et al., 2021b; Wu et al., 2020; Yan and Zaher, 2021). As Mbf1 is known to also bind collided ribosomes (Pochopien et al., 2021b; Sinha et al., 2020), we asked if ribosome binding was necessary for Mbf1 coactivation function. A previous screen for increased frameshifting mutants isolated an Mbf1 mutant with an arginine to glycine mutation (R89G) (Wang et al., 2018). The residue is in the helix-turn-helix domain of Mbf1 and participates in various contacts with the 40S subunit of the collided ribosome (Pochopien et al., 2021; Sinha et al., 2020; Wang et al., 2018), implying that mutation of the residue disrupts these interactions.

To assess if R89G mutants are able to bind the ribosome we complemented our Gcn4-tagged *mbf1*Δ strain with wild-type Mbf1, or the R89G mutant, bearing a N-terminal HA tag. To validate our complemented strains and ensure that addition of the HA tag did not interfere with Mbf1 function, we transformed our complemented strains, along with the isogenic parent strains, with a frameshifting reporter comprised of a Firefly luciferase in the +1 frame downstream of Renilla luciferase with four in-frame CGA codons inserted between the two (Simms et al., 2019). Luciferase assays showed that complementation with the wild-type Mbf1 restored frameshifting back to wild-type levels (Figure 4A), indicating that the addition of the HA tag did not disrupt the ability of Mbf1 to bind the ribosome. On the other hand, complementation with the R89G mutant resulted in frameshifting comparable with the deletion strain, as expected.

Next, we harvested whole cell extracts for polysome profiling analysis by grinding using a mortar and pestle and centrifugation over sucrose gradients. Resultant traces showed that complementation with the mutant did not have any apparent effects on polysomes, in either normal conditions or MMS treatment (Figure 4B). However, immunoblots of collected fractions

revealed that the R89G mutation abrogated Mbf1 binding to the collided ribosome, as the mutant Mbf1 did not comigrate with polysomes upon treatment with MMS.

If ribosome binding is necessary for Mbf1 coactivation function, then we would expect the R89G mutant to phenocopy the deletion strain in impairment of *ARG1* induction. Indeed, complementation with the wild-type Mbf1 rescued *ARG1* induction, while complementation with the R89G mutant did not (Figure 4C), confirming the necessity of ribosome contact in this process. Observed differences in *ARG1* induction were not due to differences in *MBF1* expression, which remained the same between the two complemented strains and their isogenic parents (Figure 4D). Interestingly, complementation with the R89G mutant was even more detrimental to *ARG1* expression than the absence of the protein, impairing induction by an additional 2-fold. Cells complemented with the mutant also exhibited defects in accumulation of Gcn4, similar to the deletion strain (Figure 4E). The mechanism by which this occurs is unclear but may reflect feedback from Mbf1 or the ribosome on Gcn2-mediated ISR signaling.

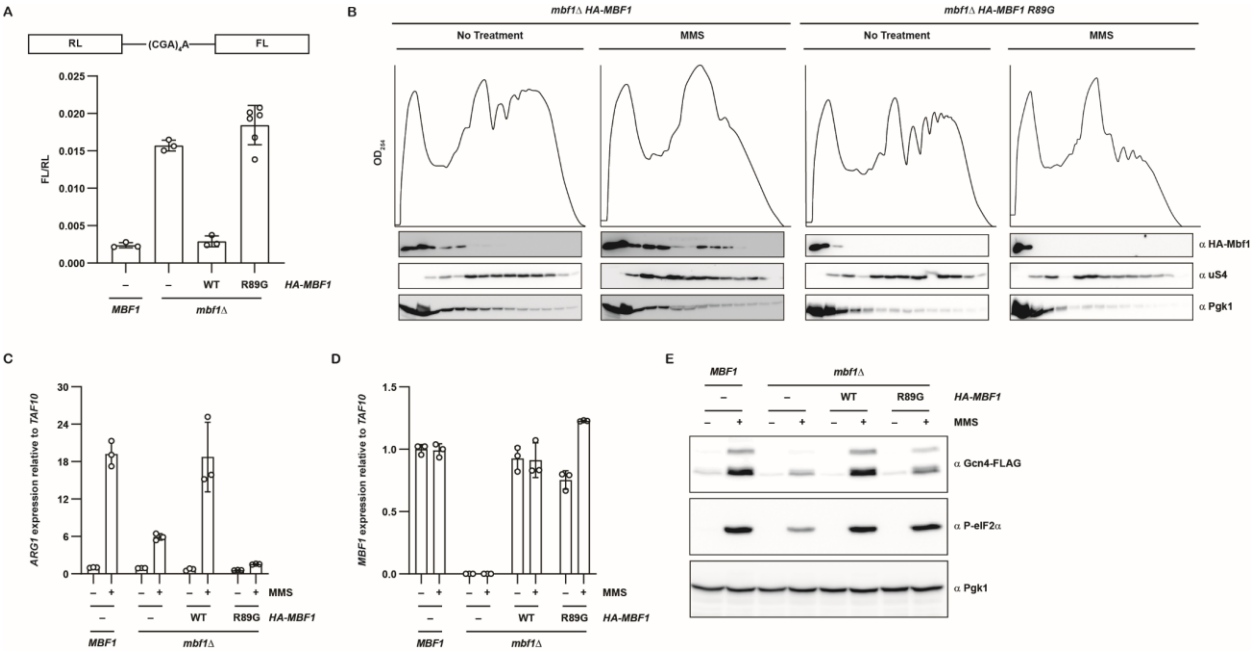

Figure 4: Mbf1 R89G mutants phenocopy deletion mutants in their inability to respond to MMS stress
A) Firefly luciferase (FL) activity normalized to Renilla luciferase (RL) activity for the indicated strains. Cells were transformed with a reporter construct (shown above) where Firefly luciferase (FL) is in the +1 frame downstream of Renilla luciferase (RL), with four in-frame CGA codons inserted between the two. Cells were grown in synthetic complete medium minus uracil and histidine and supplemented with additional adenine to OD_{600} ~0.8, and whole cell extracts were generated by zymolyase treatment and lysis in Promega passive lysis buffer. Lysates were cleared by centrifugation and luminescence measured in supernatants via automated injection on a plate reader. Shown are the results of three biological replicates. **B-E)** cells were grown in YPD medium supplemented with adenine to OD_{600} ~0.8 before treatment with 0.1% MMS for 30 minutes. **B)** Polysome profiles and corresponding immunoblots of collected fractions of whole cell extracts from cells complemented with either HA-tagged wild-type Mbf1 or an R89G mutant. After treatment with MMS, cells were collected by rapid vacuum filtration and flash frozen using liquid nitrogen. Frozen cell pellets were ground with mortar and pestle and reconstituted in polysome lysis buffer. For polysome profile traces, absorbance readings were taken continuously at OD_{254}. Simultaneously, output was collected in 14 equivalent fractions, and proteins precipitated by the addition of trichloroacetic acid. Shown are representative blots of triplicates. **C, D)** *ARG1* and *MBF1* expression relative to *TAF10* expression, as measured by qRT-PCR, for the indicated strains and conditions. Shown are the results of three biological replicates. **E)** Immunoblot of whole cell extracts for the indicated strains and conditions. Whole cell extracts were collected using an alkaline hydrolysis and trichloroacetic acid precipitation method. Shown is a representative blot of triplicates.

Mbf1 is distributed throughout the cell

Previous reports on EDF1 localization in human umbilical vein endothelial cells reported the factor to be distributed throughout the cell, but become primarily localized to the nucleus upon treatment with either 12-O-tetradecanoylphorbol-13-acetate or forskolin (Mariotti et al., 2004, 2000). This raised the possibility that Mbf1 function in yeast might be controlled via

localization, where the factor resides primarily in the cytoplasm under normal conditions, but upon detecting and binding collided ribosomes, becomes localized to the nucleus. If this model is correct, then we should see an increase in nucleus-localized Mbf1 during MMS treatment.

To track Mbf1 localization, we tagged Mbf1, as well as the R89G mutant, with a C-terminal mCherry at the native locus in the wild-type background. Immunoblots of whole cell extracts confirmed expression of the reporter, with no apparent differences in protein levels between the two strains (Figure 5A). As with our HA-tagged strains, we assessed frameshifting levels to check if ribosome binding was disrupted by the addition of mCherry. Luciferase assays verified that the tagged Mbf1 was still able to bind the ribosome, as cells with Mbf1-mCherry showed frameshifting levels similar to wild-type levels (Figure 5B). Meanwhile, cells with Mbf1 R89G-mCherry exhibited frameshifting levels similar to the deletion strain, indicating that the tagged mutant retained the binding defect. Measurement of *ARG1* expression revealed that Mbf1-mCherry was also competent in its coactivation function, with minimal effects on induction in response to MMS (Figure 5C). Likewise, *ARG1* induction remained impaired in cells with Mbf1 R89G-mCherry.

We then fixed our cells with paraformaldehyde, incubating them briefly with DAPI to stain the nucleus, and visualized them using fluorescence microscopy. Commensurate with reports on EDF1 (Mariotti et al., 2004, 2000), Mbf1-mCherry was present in both the nucleus and the cytoplasm in untreated cells (Figure 5D). The same was also seen for the Mbf1 R89G-mCherry. However, in contrast to EDF1 (Mariotti et al., 2004, 2000), treatment with MMS did not appear to significantly alter Mbf1 localization. To analyze our images in an objective manner, we used an automated processing method to compare mCherry intensity in the nucleus to the intensity across the entire cell, which yielded over 200 nuclei – whole cell pairs for each

group. Determined cellular and nuclear areas in the processed output were largely consistent across groups and in line with the scale of the cells, suggesting that our analysis was successful in isolating mCherry and DAPI signal from background fluorescence (Figure 5E). Further analysis confirmed that normalized nuclear mCherry intensity was not altered by treatment with MMS in cells with Mbf1-mCherry. By contrast, there was a slight decrease in normalized nuclear intensity in cells with Mbf1 R89G-mCherry. However, we note that the average cell sizes, but not the average nuclear area, determined for these cells were significantly smaller, which may signify an issue with the visualization or automated processing of this set of images.

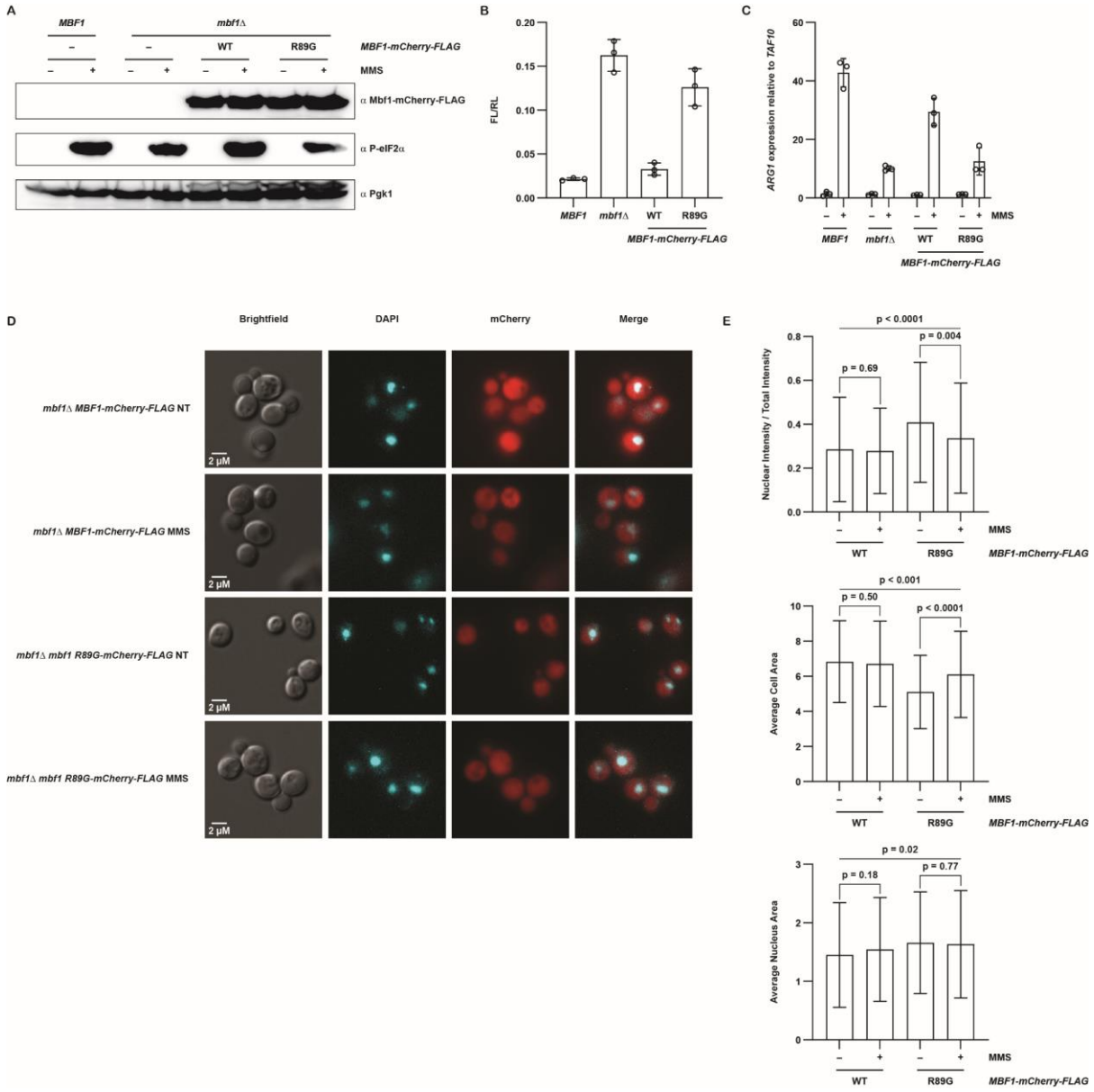

Figure 5: Mbf1 is distributed throughout the cell

A-D) Cells were grown in YPD medium supplemented to OD_{600} 0.6-0.8 before treatment with 0.1% MMS for 30 minutes. **A)** Immunoblot of whole cell extracts for the indicated conditions. Shown is a representative blot of triplicates. **B)** Firefly luciferase (FL) activity normalized to Renilla luciferase (RL) activity for the indicated strains. Cells were transformed with the same frameshifting reporter from before. Shown are the results of three biological replicates. **C)** *ARG1* expression relative to *TAF10* expression, as measured by qRT-PCR, for the indicated strains and conditions. Shown are the results of three biological replicates. **D)** Fluorescence microscopy images of cells fixed using paraformaldehyde and incubated with DAPI before visualization. Scale bar is included for reference. **E)** Results of automated image analysis by FIJI. For intensity ratios, mCherry signal in the nucleus was normalized to the mCherry signal of the corresponding whole cell. Whole cell area was determined by automatic thresholding of mCherry signal while nuclear area was determined by thresholding based on DAPI signal. The p-value above the top bar was determined by one-way ANOVA across all groups. The other two p-values were determined by unpaired t-test between conditions for each strain. Statistical analysis was done in GraphPad Prism. Over 200 nuclei – cell pairs were analyzed for each group.

Ribosome binding is not necessary for Mbf1 recruitment to Gcn4 targets

To investigate the mechanism by which ribosome binding regulates Mbf1 function, we isolated nucleoprotein complexes from our HA-tagged complementation strains and the isogenic untagged parent, both untreated and subjected to MMS treatment. Quantitative PCR (qPCR) with primers for the *ARG1* and *ARG4* promoter regions revealed enrichment in DNA isolated from the tagged strains compared to DNA from the untagged parent, indicating successful isolation of HA-Mbf1 bound targets (Figure 6A). Enrichment was observed in DNA from both strains under either treatment condition, suggesting that ribosome binding is not required for Mbf1 recruitment to Gcn4 targets, although the noisiness of the data makes it difficult to draw firm conclusions. As a control, we also measured amplification using primers for the *TAF10* CDS. We observed no enrichment for any of the samples, as expected.

While Mbf1 recruitment may not be altered by the R89G mutation, we considered the possibility that the mutation may also preclude Mbf1 from binding to Gcn4 or Spt15. To test if this was the case, we purified recombinant Mbf1, Mbf1 R89G, Gcn4, and Spt15 expressed in *E. coli*. We then reconstituted various combinations of the three proteins with radiolabeled oligonucleotides encompassing the Gcn4-binding region of the *ARG4* promoter and separated the complexes by electrophoresis on a native TBE gel (Figure 6B). As expected, a supershift was observed for incubation with Gcn4 alone, but not for incubation with Mbf1 or Spt15 alone, commensurate with the role of Mbf1 as a coactivator and its necessity in recruiting Spt15. Accordingly, no additional shift was observed for incubation with Gcn4 and Spt15 without Mbf1. Incubation with either wild-type Mbf1 or the R89G mutant, in conjunction with Gcn4 or both Gcn4 and Spt15, was sufficient in inducing additional shifts, suggesting that the R89G mutation does not impair the ability of Mbf1 to bind Gcn4 or Spt15.

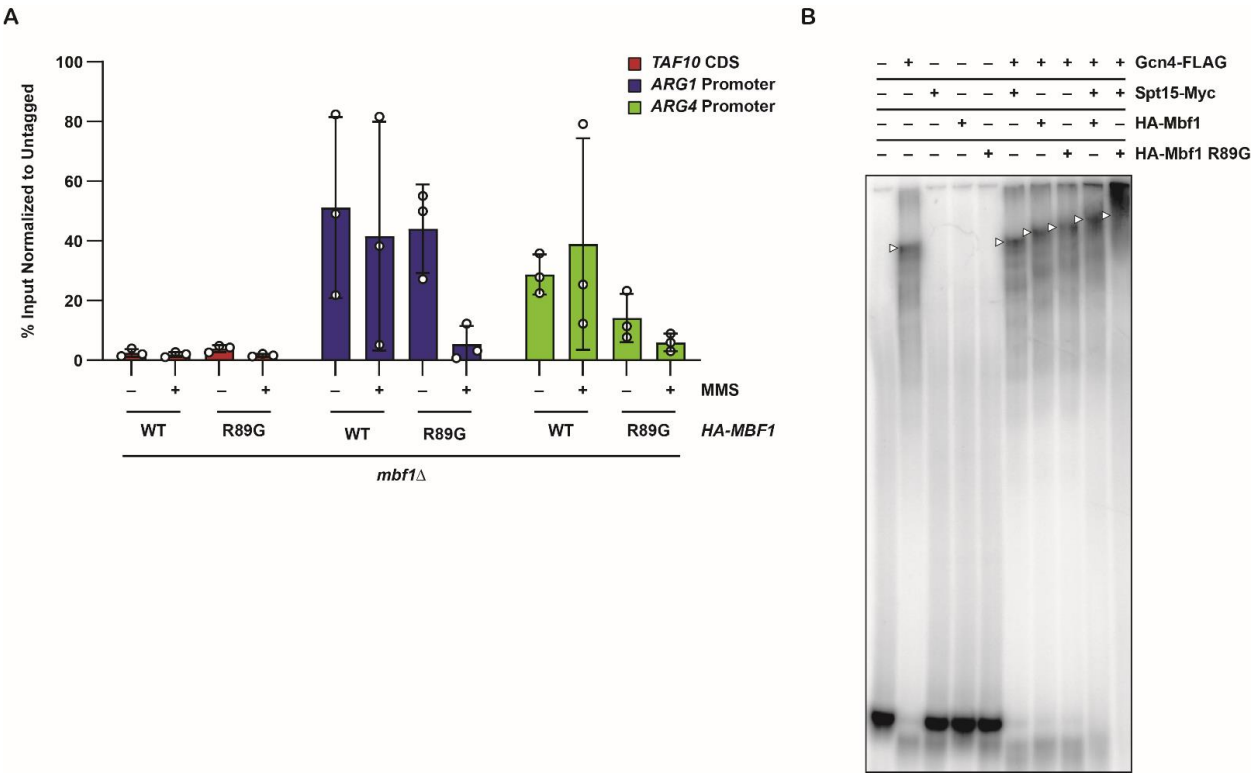

Figure 6: R89G mutation does not affect Mbf1 recruitment to Gcn4 targets
A) CHIP-qPCR of normalized percent input values for the indicated targets for Mbf1 WT and R89G complemented strains. Quantification cycle (C_q) values for immunoprecipitated samples were first normalized to the Cq values for the corresponding input samples to calculate a percent input value. Percent input values were then normalized to the corresponding percent input value calculated for an untagged control; untreated samples were normalized to the untreated control while treated samples were normalized to the treated control. Cells were grown to OD_{600} ~0.6 before treatment with 0.1% MMS for 30 minutes. The control was grown and treated with the same conditions. Shown are the results of three biological replicates. **B)** Gel shift assay of *ARG4* DNA reconstituted with indicated recombinant proteins. Each shifted migration product is marked by a white arrow. Shown is a representative gel of triplicates.

Discussion

Activation of the ISR is a committal step for cells, requiring diversion of valuable resources to produce the response transcripts and proteins to recover from the stress. It follows then that eukaryotes would have evolved additional mechanisms to regulate ISR activation and prevent unnecessary reprogramming of gene expression. De-repression of *GCN4* translation appears to reach threshold much sooner than does phosphorylation of eIF2α, as activity of *GCN4-lacZ* reporters in *mbf1*Δ cells remained comparable to activity in wild-type cells even with greatly reduced levels of phospho-eIF2α (Figure 2A-D). The requirement for Mbf1 may serve to guard against unexpected increases in Gcn4 levels without concordant eIF2α-phosphorylation, in a two-pronged mechanism of ISR activation (Figure 7). Activation of Gcn2, via binding to collided ribosomes in the presence of its coactivators Gcn1 and Gcn20, leads to phosphorylation of eIF2α, de-repression of *GCN4* translation, and translocation of Gcn4 into the nucleus. In parallel, Mbf1 also binds to the collided ribosomes. Ribosome binding then acts as a signaling event to enable Mbf1 to function as a coactivator. As a result, activation of the ISR is only possible when both Gcn4 is present and Mbf1 is competent to act as a coactivator.

Our findings confirm that Mbf1 is a necessary coactivator of Gcn4 for induction of its targets (Figure 1D, E and 2G). Inability to bind the ribosome prevents Mbf1 from participating in this role (Figure 4C, 5C) but does not disrupt targeting of Mbf1 to Gcn4 targets (Figure 6A). Thus, the role of ribosome binding in this process remains unresolved. If signaling on the ribosome modulates the ability of Mbf1 to recruit either Gcn4 or Spt15, that would explain why we observe impaired induction of *ARG1* in strains complemented with the R89G mutant. To address this question, we are currently conducting CHIP-qPCR of tagged-Gcn4 and Spt15 strains.

The key missing piece in the model is the mechanism by which Mbf1 function is regulated. It is clear that Mbf1 is not able to serve as a coactivator by default; the factor is present in the nucleus even under normal conditions (Figure 5D) but accumulation of Gcn4 in an eIF2α-phosphorylation independent manner is insufficient to induce the Gcn4 regulon (Figure 3A, B). Studies on EDF1 and the potato homolog *St*Mbf1 have shown that both are phosphorylated – EDF1 in response to PKC or PKA activation and *St*Mbf1 in response to fungal infection (Mariotti et al., 2004, 2000; Zanetti, 2003). EDF1 also becomes primarily localized to the nucleus upon phosphorylation (Mariotti et al., 2004, 2000). Interestingly, phosphorylation of StMbf1 and PKC-mediated phosphorylation of EDF1 are dependent on Ca2+ signaling (Mariotti et al., 2004, 2000; Zanetti, 2003), suggesting conservation of the regulatory mechanism. It is possible that Mbf1 function is controlled by regulatory phosphorylation, as the region that is phosphorylated in EDF1 and StMBF1 is highly conserved (Mariotti et al., 2000; Wang et al., 2018; Zanetti, 2003).

If Mbf1 is phosphorylated, the identity of the upstream kinase is unknown. It is enticing to speculate if the upstream kinase is Gcn2, which would provide an elegant way to cells to coordinate the activities of both axes of ISR signaling. Conditions that activate Gcn2 are required for Mbf1 coactivation function, as accumulation of Gcn4 in the absence of eIF2α phosphorylation is insufficient to induce the Gcn4 regulon (Figure 3A, B), implying that ribosome collisions are a requisite event. However, although both factors likely report on collision status, the signaling pathway does not necessarily need to be through Gcn2. Experiments with Gcn2 mutants that are constitutively active (Qiu et al., 2002) or in *GCN2* deleted cells would help to resolve if Mbf1 is controlled by a Gcn2-mediated mechanism or the result of other signaling pathways on collided ribosomes.

Likewise, it is unknown if the frame maintenance activity on the ribosome is linked to regulation of Mbf1. Contact between the ribosome and the mRNA through the universally conserved ribosomal protein Rps3 has been found to be important for activation of a different quality control process, No-Go Decay (Simms et al., 2018). Rps3 residues K108, S104, and L113 have been implicated in reading frame maintenance (Wang et al., 2018) and all contact Mbf1 in the collided ribosome structure (Pochopien et al., 2021; Sinha et al., 2020). Our data show that Mbf1 is not a coactivator by default, requiring binding to the ribosome and modification by a ribosomal-mediated signal in order to do so (Figure 3A, B, 4C). Given that both Mbf1 and the ribosome monitor reading frame (Wang et al., 2018), it seems plausible that these residues participate in communication between the two factors. Additional investigation will be needed to explore the consequences of disrupting these interactions on Mbf1 function.

In addition to participating as a coactivator, Mbf1 appears to play a role in Gcn4 stability (Figure 2A, C, D). However, it is unlikely that destabilization of Gcn4 is the primary mechanism for impaired expression of the regulon, as deletion of Gcn4 degradation factors did not fully rescue *ARG1* expression in the absence of Mbf1, even though Gcn4 levels were comparable to levels in the wild-type parent (Figure 2E-G). In this case, Mbf1 factors may have evolved in such a way that binding to Gcn4 simultaneously protects Gcn4 from degradation while bridging interactions with Spt15, as a secondary signal to promote ISR activation. Mbf1 in several organisms bind to bZIP domains (Kabe et al., 1999; Liu et al., 2003; Takemaru et al., 1998, 1997), a highly conserved domain in transcription factors that play many roles in core cellular processes (Amoutzias et al., 2006; Deppmann et al., 2006; Jindrich and Degnan, 2016; Miller, 2009). It has also been posited that Mbf1 factors have coevolved with TBP to preserve their ability to interact with one another (Liu et al., 2007), and the coactivation mechanism appears to

be conserved across eukaryotes (Li et al., 1994; Takemaru et al., 1998, 1997; Tsuda et al., 2004; Wang et al., 2017; Zanetti et al., 2004). Although the bZIP domain is not directly adjacent to the phosphorylated T165 residue in the primary structure of Gcn4, higher order structures may put the two in proximity. Probing crystal structures of Gcn4 or performing protein modeling simulations might provide insights.

We initially thought that regulation of Mbf1 function could be attributed to differential localization of the factor, similar to how EDF1 becomes primarily localized to the nucleus (Mariotti et al., 2004, 2000). However, visualization of Mbf1-mCherry localization by fluorescence microscopy showed no change as a result of MMS treatment (Figure 5D, E). If all or part of the observed nuclear pool of Mbf1 is competent in coactivation function, this would imply their transit to the cytoplasm at some point, since ribosome binding is necessary for Mbf1 coactivation function (Figure 4B, C). One might envision a mechanism where the equilibrium between ribosome bound and free Mbf1 is tuned in such a way that Mbf1 can bind the collided ribosome, become modified, and then dissociate and passively diffuse back into the nucleus. Even an equilibrium that heavily favors the bound state would allow for rapid increase in concentration of Mbf1 available as a coactivator, since Gcn4 levels under ISR-activating conditions are only at ~1-5% of total Mbf1 levels (Ho et al., 2018). Passive diffusion of Mbf1 is possible given its small size of 16.4 kDa, smaller than the threshold of ~40-60 kDa determined in initial studies of the nuclear pore complex (Paine and Feldherr, 1972; Paine, 1975; Peters, 1983). Even the addition of mCherry, at 26.7 kDa, still places the combined mass within the 40-60 kDa threshold. However, if this is the responsible mechanism, it would require the presence of an opposing mechanism to rapidly remove the modifications, as any residually modified Mbf1 would enable a transient increase in Gcn4 levels to activate the ISR. In any case, further

investigation is needed to understand the mechanisms that mediate the seemingly contradictory roles of Mbf1 as both a frame maintenance factor in the cytoplasm and a transcriptional coactivator in the nucleus.

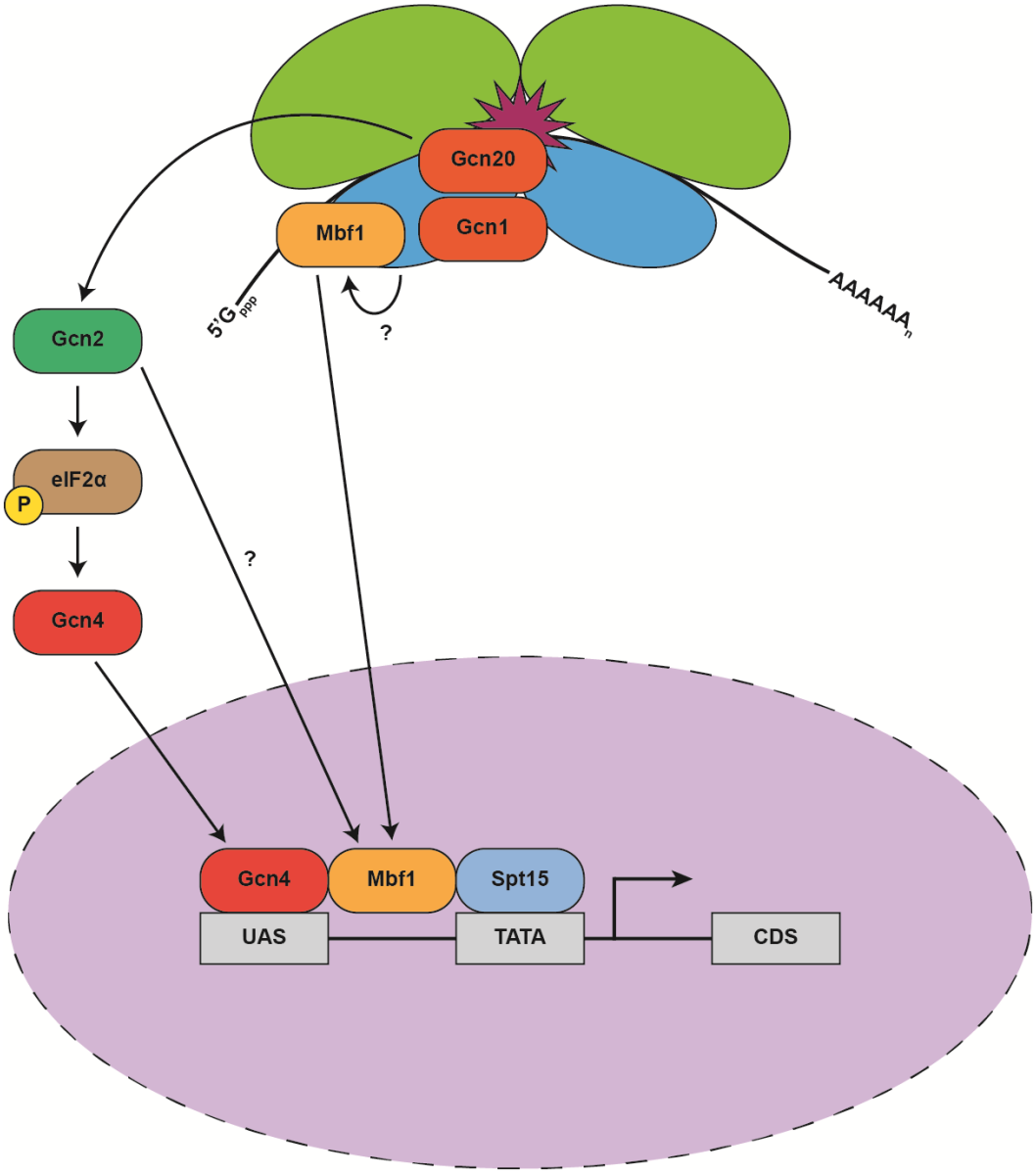

Figure 7: Model for Gcn4 and Mbf1-mediated activation of the ISR
Collided ribosomes are bound by Mbf1 and the coactivators of Gcn2: Gcn1 and Gcn20. Ribosome binding by Gcn1 and Gcn20 leads to activation of Gcn2, while ribosome binding by Mbf1 results in modification of Mbf1, although the identity of the modification or the mechanism by which it occurs are unknown. Activated Gcn2 phosphorylates eIF2α, which in turn leads to production of Gcn4 and its translocation to the nucleus. At the same time, a subset of the ribosome-bound Mbf1 translocates to the nucleus and acts as a coactivator to enable transcription of Gcn4 targets.

Methods and Materials

Yeast Strains and Plasmids

Strains, plasmids, and primers used in this study are listed in Supplementary Tables 1, 2, and 3, respectively. Strains were constructed in either the *BY4741* or *BY4741 GCN4-3XFLAG* background using standard PCR-based techniques. Plasmids were transformed using a lithium acetate method (Gietz et al., 1995). *HA-MBF1* was integrated into the *ADE2* locus using the RNA-ID system (Dean and Grayhack, 2012). FLAG-mCherry was amplified from a pFA6 plasmid containing the construct to add a 6x glycine linker to the 5' end, then inserted at the native *MBF1* locus. All cells with *HA-MBF1* were grown in YPD medium supplemented with additional adenine (YAPD).

RNA-Seq Library Construction and Sequencing

Wild-type, *mbf1*Δ, *gcn2*Δ, and *gcn4*Δ strains were grown in YPD medium to OD_{600} ~0.6. Cultures were split in half, with one collected immediately and the other treated with 0.1% methyl methanesulfonate (MMS) for one hour before collection. Cells were collected by centrifugation and flash frozen on dry ice. RNA was extracted using a hot phenol method (Köhrer and Domdey, 1991) and checked for integrity by denaturing formaldehyde agarose electrophoresis (Sambrook and Russell, 2006).

Total RNA integrity was determined using Agilent Bioanalyzer or 4200 Tapestation. Library preparation was performed with 5 to 10ug of total RNA with a Bioanalyzer RIN score greater than 8.0. Ribosomal RNA was removed by poly-A selection using Oligo-dT beads (mRNA Direct kit, Life Technologies). mRNA was then fragmented in reverse transcriptase buffer by heating at 94 degrees for 8 minutes. Fragments were reverse transcribed using SuperScript III RT enzyme (Life Technologies) and random hexamers, per manufacturer's

instructions, to yield cDNA. A second strand reaction was performed to yield ds-cDNA. cDNA was blunt ended, had an A base added to the 3' ends, and then had Illumina sequencing adapters ligated to the ends. Ligated fragments were then amplified for 12-15 cycles using primers incorporating unique dual index tags. Fragments were sequenced on an Illumina NovaSeq-6000 using paired end reads extending 150 bases.

Differential Gene Expression Analysis

Reads were checked for initial quality using FastQC 0.11.9 (Andrews et al., 2010) and adapters removed via automatic detection by fastp (Chen et al., 2018). Reads were then mapped to the transcriptome using Salmon 1.10.1 (Patro et al., 2017) with libraryType IU, gcBias, seqBias, and validateMappings flags set. The transcriptome was generated by using the R64-3-1 cDNAs from SGD, with 200 nt upstream and downstream of the CDS added. Only those genes whose ORF was classified as verified or unknown were kept. The transcriptome was indexed using Salmon with the k-mers option set to 31.

Salmon quantification files were imported into DESeq2 1.38.3 (Love et al., 2014) using Tximport 1.26.1 (Soneson et al., 2016). Variance stabilized counts, with the blind option set to true, were used for PCA. For pairwise comparisons, the matrix design was set to compare the effect of strain, treatment with MMS, and interaction between strain and treatment with MMS. The wild-type strain and untreated condition were set as the reference levels. Resultant fold changes were adjusted using the ashr package (Stephens, 2017). Genes marked as part of the GCN4 regulon were classified based on the UC and T dataset in Rawal et al. 2018 (Rawal et al., 2018).

For analysis of gene list overlaps, any genes showing a Log_2 fold change ≤ -1 and an adjusted p-value ≤ 0.05 in response to MMS treatment in the wild-type were annotated as MMS-responsive genes. A list of MMS-responsive genes exhibiting impaired expression based on relaxed criteria and a list based on stringent criteria was determined for the *gcn4*Δ, *gcn2*Δ, and *mbf1*Δ strains. Relaxed criteria were defined as any gene showing Log_2 fold change < 0 and adjusted p-value ≤0.05, while stringent criteria were the same except for a Log_2 fold change ≤ -1. Overlaps were tested for significance using a one-tailed Fisher's exact test. Proportional venn diagrams were generated using DeepVenn (Hulsen, 2022).

Treatment conditions for MMS, 4-NQO, rapamycin, and hydroxyurea

Wild-type and *mbf1*Δ strains were grown in YPD medium to OD_{600} 0.6-0.8. Cultures were divided evenly into 5 tubes, with one tube collected immediately as the no treatment sample. MMS, 4-nitroquinoline 1-oxide (4-NQO), rapamycin, and hydroxyurea were added to final concentrations of 0.1%, 5 ug/mL, 1 μg/mL, and 100 mM, respectively. Cells treated with MMS, 4-NQO, and rapamycin were collected after incubation for 30 minutes, while cells treated with hydroxyurea were collected after incubation for an hour. Cells were pelleted by centrifugation and flash frozen on dry ice. Collected pellets were processed for immunoblotting.

Measurement of β-galactosidase activity

Cells were grown in synthetic complete medium minus uracil and histidine and supplemented with additional adenine to OD_{600} ~0.7. Cultures were split into three, with one collected immediately, one treated with 0.1% MMS for 30 minutes, and one treated with 100 mM 3-aminotriazole (3-AT) for one hour. Cells were collected, spheroplasted, and lysed using the same protocol as for luminescence measurement described below. 50 uL of the cleared lysate was aliquoted into a new tube, and 100 uL of Buffer Z (100 mM sodium phosphate, 20 mM KCl,

2 mM $MgSO_4$, 40 mM β-mercaptoethanol) and 30 uL of 4 mg/mL ortho-Nitrophenyl-β-galactoside (ONPG) in Buffer Z was added. After incubation for two hours at 25°C, reactions were stopped by the addition of 180 uL 1M Na_2CO_3. 150 uL of the sample was transferred to a clear 96-well plate and absorbance at 420 nm and 550 nm was measured on an Infinite M200 Pro plate reader (Tecan).

Immunoblotting

Cells were pelleted and lysed in 1 mL of ice-cold lysis buffer (300 mM NaOH, 1% β-mercaptoethanol). Proteins were precipitated through the addition of TCA to a final concentration of 10% by volume and resuspended in HU buffer (8 M Urea, 5% SDS, 200 mM Tris pH 6.8, 100 mM DTT, 1 mM ethylenediaminetetraacetic acid (EDTA), bromophenol blue). Proteins were separated by SDS–PAGE and analyzed by immunoblotting. The following antibodies were used at the following volume by volume dilutions: 1:1000 mouse anti-FLAG M2-HRP (Millipore Sigma), 1:3000 rabbit anti-phospho-eIF2α (Ser51) (Cell Signaling Technology), 1:3000 rabbit anti-Gcn4 (a gift from the Hinnebusch lab), 1:5000 mouse anti-PGK1 (ThermoFisher Scientific), 1:3000 rabbit anti-HA-HRP (Santa Cruz Biotechnology), 1:3000 mouse anti-His-HRP (Santa Cruz Biotechnology), 1:10000 goat anti mouse IgG HRP (ThermoFisher Scientific), 1:5000 goat anti rabbit IgG HRP (ThermoFisher Scientific).

Measurement of Firefly and Renilla Luciferase Luminescence

Luminescence was measured as previously described (Simms et al., 2019). Briefly, cells were grown in synthetic complete medium minus uracil and histidine and supplemented with additional adenine to OD_{600} 0.6-0.8, collected, pelleted, and washed with TE buffer (10 mM Tris pH 7.5, 1mM EDTA). Pellets were then resuspended in 200 µL zymolyase buffer (50 mM Tris pH 7.5, 10 mM MgCl2, 1 M Sorbitol, 30 mM DTT) and incubated with 12.5U of lyticase from

Arthrobacter luteus (Millipore Sigma) at 37°C for 30 minutes. Spheroplasts were lysed by the addition of 50 uL 5X passive lysis buffer (Promega) and pelleted by centrifugation at 4000 × g for 5 minutes at room temperature. Cleared lysates were transferred to 96-well plates and luminescence was measured using the Dual-Luciferase Reporter Assay System (Promega) following manufacturer's instructions on an Infinite F200 Pro plate reader (Tecan).

Polysome Profiling

Cells were grown in YAPD medium at 30°C to OD_{600} 0.6-0.8. Cultures were split in two, with one collected immediately and the other treated with 0.1% MMS for 30 minutes. Cells were collected by rapid vacuum filtration over a membrane and flash frozen with liquid nitrogen. Frozen cells were ground using a mortar and pestle while submerged in liquid nitrogen. After cells were ground into fine powder, the powder was resuspended in polysome-lysis buffer (20 mM Tris pH 7.5, 140 mM KCl, 1.5 mM MgCl2, 0.5 mM DTT, 100 μg/mL cycloheximide, 1% Triton). 1600 μg of RNA were layered over a 10-50% sucrose gradient and centrifuged at 35,000 rpm for 160 minutes in a SW41Ti swinging-bucket rotor. Gradients were fractionated using a Brandel tube-piercing system combined with continuous absorbance reading at 254 nm. 14 equivalent output fractions were collected, and proteins precipitated by the addition of trichloroacetic acid to 20%. Precipitated proteins were washed once with ice-cold acetone and resuspended in HU buffer.

Real-Time Quantitative Reverse Transcription PCR

Total RNA was isolated using a hot phenol method (Köhrer and Domdey, 1991) and checked for integrity by denaturing formaldehyde agarose electrophoresis (Sambrook and Russell, 2006). RNA was then treated with DNase I (ThermoFisher Scientific; cat#EN0525) following manufacturer's instructions. 2 μg of the treated RNA was reversed transcribed using

M-MuLV reverse transcriptase (Promega; cat#M1701) and random hexamers (ThermoFisher Scientific, cat#SO142), following manufacturer's instructions. cDNA was diluted five-fold and added to a reaction mixture containing iTaq Universal SYBR Green Supermix (Bio-Rad; cat#1725120) and the desired primers at 500 nM final concentration. Cq values were determined on a CFX Opus 96 machine (Bio-Rad) using the default iTaq_Univ_SYBR_cDNA protocol (initial denaturation: 95°C for 30 sec; 40 cycles: 95°C for 3 sec, 60°C for 20 sec; melt curve analysis: 65°C for 5 sec, followed by a ramp to 95°C in 0.5°C increments). For CHIP-qPCR, the protocol was the same except the annealing temperature was set to 57°C instead of 60°C. The fold change for each gene was calculated by using the ΔΔCt method, with *TAF10* serving as the control. All measurements were done in biological triplicates.

Fluorescence Microscopy

Cells were grown in YPD medium to OD_{600} 0.6-0.8. Cultures were split in two, with one treated with 0.1% MMS for 30 minutes. After treatment, cells were pelleted by centrifugation and resuspended in 4% paraformaldehyde. After incubation for 15 minutes, cells were washed once with wash buffer (1.2M sorbitol, 100 mM potassium phosphate pH 7.5), resuspended in wash buffer with DAPI added to a final concentration of 1 μg/mL, and then mounted on microscope slides. Slides were visualized on a Nikon Eclipse E600 upright microscope at 60X magnification using NIS-elements software (Nikon) through a Retiga EX charge-couple-device camera (Q-imaging). Separate images were taken for the brightfield, mCherry fluorescence, and DAPI fluorescence. Image analysis was automated in FIJI (Schindelin et al., 2012). To determine total cell area, mCherry images were auto thresholded using Otsu's method (Otsu, 1979), followed by selection of cells using the Analyze Particles tool with the settings 1-15 μM^2 particle size limit and 0.3-1 circularity limit. To determine nuclear area, DAPI images were adjusted

using the Enhance Contrast function with the settings saturated pixels set to 0.3% and normalize, then auto thresholded using the MaxEntropy method (Kapur et al., 1985), followed by selection of nuclei using the Analyze Particles tool with the settings 0.5-4 μM^2 particle size limit and 0.15-1 circularity limit. Selections were checked for overlap to pick nuclei enclosed by a cell, and only selections that overlapped were used to measure intensity in the mCherry images. Background fluorescence was determined by measuring the entire region below the threshold in the mCherry images. Differences in normalized intensities or measured areas were checked for statistical significance using unpaired t-tests for comparisons due to treatment in each strain and one-way ANOVA for comparison across all groups in Prism (GraphPad).

Chromatin Immunoprecipitation – quantitative PCR

Cells were grown in YAPD medium to OD_{600} 0.6-0.8. Cultures were then split in two, with half crosslinked immediately and the other treated with 0.1% MMS for 30 minutes before crosslinking. Cells were crosslinked via the addition of formaldehyde to a final concentration of 1%. After 15 minutes, crosslinking was stopped by the addition of glycine to a final concentration of 300 mM and incubated for an additional 5 minutes. Cells were pelleted, washed once with cold TBS (10 mM Tris pH 7.5, 150 mM NaCl), and flash frozen on dry ice. Pellets were resuspended in FA lysis buffer (50 mM HEPES pH 7.5, 150 mM NaCl, 1 mM EDTA, 1% Triton X-100, 0.1% Na-deoxycholate, 0.1% SDS) with protease inhibitors added, and lysed via bead beating for 7x1 min. cycles in a FastPrep-24 machine (MP-Biomedical). Lysates were cleared via centrifugation and an aliquot taken as the input sample. The remaining sample was sonicated 3 cycles on a S220 focused-ultrasonicator (Covaris) using the following settings: water bath temperature 6.6±1°C, peak power 170, cycles/burst 200, time/burst 120 sec, and duty factor

5. Sonicated samples were then incubated with magnetic anti-HA beads (Pierce) overnight with rotation at 4°C.

After overnight incubation, beads were washed 3 times with low salt buffer (20 mM HEPES pH 8, 150 mM NaCl, 2 mM EDTA, 0.1% Triton X-100, 0.1% SDS), once with high salt buffer (same as the low salt buffer except 500 mM NaCl), once with LiCl buffer (100 mM Tris pH 7.5, 0.5M LiCl, 1% Na-deoxycholate, 1% NP-40), and twice with TE (10 mM Tris pH 8, 1 mM EDTA). DNA-protein complexes were eluted by resuspending the beads in 250 μL elution buffer (TE with 0.1% SDS) and heating at 65°C for 30 minutes with shaking. After elution, output samples were centrifuged, and the supernatant transferred to new tubes. Input samples were resuspended in 250 μL elution buffer, and both sets of samples were incubated at 65°C overnight with shaking to reverse crosslinks.

After crosslink reversal, 250 μL of TE and 100 μg of RNase A (Invitrogen) was added and samples were incubated at 37°C for 2 hours. Next, Proteinase K (Beckman Coulter) was added to a final concentration of 1% and samples were incubated at 55°C for 2 hours. Samples were then purified using DNA Clean and Concentrator columns (Zymo Research), following manufacturer's instructions. Purified DNA was used for qPCR following the protocol described above. Enrichment in expression was calculated by normalizing expression in the immunoprecipitated samples to that of their corresponding input sample using the percent input calculation method described in Solomon et al. (Solomon et al., 2021).

Gel Shift Assays

MBF1, *GCN4*, and *SPT15* were amplified from yeast genomic DNA using primers to add the corresponding peptide tag, as well as the 6xHis and TEV sites. Plasmids were then

constructed in the pProEx-HTb (Thermo Fisher) backbone via Gibson assembly using the Gibson Assembly Master Mix (NEB), following manufacturer's instructions, and transformed into DH5-α cells (NEB). Cells were grown in LB to OD_{600} 0.6, and protein expression induced by the addition of IPTG to a final concentration of 100 μM. After 3 hours of induction, cells were lysed via mechanical disruption by French press. Proteins from cleared lysates were purified using Ni-NTA beads (Qiagen), following manufacturer's instructions. Purified proteins were dialyzed into storage buffer (25 mM Tris pH 7.5, 75 mM NH_4Cl, 2.5 mM $MgCl_2$, 3 mM β-mercaptoethanol, 50% glycerol) and quantified using the Coomassie Plus assay kit (Pierce).

An oligonucleotide encompassing the region surrounding the Gcn4 binding site in the *ARG4* promoter region was radiolabeled with T4 polynucleotide kinase (NEB) and γ-^{32}P-ATP (PerkinElmer), following manufacturer's instructions. The sequence of the oligonucleotide is as follows: TTA GTA GAT GAA TGA CTC ACT TTT TGG ATA AGC TGG CGC AAA TTG AAA CAT GTG AAA AAA AAA AAA AAG GAT TAT AAA AGG TCA GCG AAG. After radiolabeling, the oligonucleotide was annealed to an oligonucleotide harboring the complementary sequence. NEBuffer 3 (NEB) and polyGC (Millipore Sigma) were added to the annealed oligo solution to form a master mix. Master mixes were incubated with various combinations of the recombinant proteins, separated on an 8% TBE native gel, exposed to a phosphor screen, and imaged on a Typhoon Imager (Cytiva).

References

1. Amoutzias G, Veron A, Weiner J, Robinson-Rechavi M, Bornberg-Bauer E, Oliver S, Robertson D. 2006. One Billion Years of bZIP Transcription Factor Evolution: Conservation and Change in Dimerization and DNA-Binding Site Specificity. *Molecular Biology and Evolution* **24**:827–835. doi:10.1093/molbev/msl211

2. Andrews S, Krueger F, Segonds-Pichon A, Biggins L, Krueger C, Wingett S. 2010. FastQC.

3. Buttgereit F, Brand MD. 1995. A hierarchy of ATP-consuming processes in mammalian cells. *Biochemical Journal* **312**:163–167. doi:10.1042/BJ3120163

4. Chen S, Zhou Y, Chen Y, Gu J. 2018. fastp: an ultra-fast all-in-one FASTQ preprocessor. *Bioinformatics* **34**:i884–i890. doi:10.1093/bioinformatics/bty560

5. Cherkasova VA, Hinnebusch AG. 2003. Translational control by TOR and TAP42 through dephosphorylation of eIF2α kinase GCN2. *Genes and Development* **17**:859–872. doi:10.1101/gad.1069003

6. Chi Y, Huddleston MJ, Zhang X, Young RA, Annan RS, Carr SA, Deshaies RJ. 2001. Negative regulation of Gcn4 and Msn2 transcription factors by Srb10 cyclin-dependent kinase. *Genes Dev* **15**:1078–1092. doi:10.1101/gad.867501

7. Costa-Mattioli M, Walter P. 2020. The integrated stress response: From mechanism to disease. *Science (New York, NY)* **368**. doi:10.1126/science.aat5314

8. Dean KM, Grayhack EJ. 2012. RNA-ID, a highly sensitive and robust method to identify cis-regulatory sequences using superfolder GFP and a fluorescence-based assay. *RNA* **18**:2335–2344. doi:10.1261/rna.035907.112

9. Deppmann CD, Alvania RS, Taparowsky EJ. 2006. Cross-Species Annotation of Basic Leucine Zipper Factor Interactions: Insight into the Evolution of Closed Interaction Networks. *Molecular Biology and Evolution* **23**:1480–1492. doi:10.1093/molbev/msl022

10. Dever TE, Feng L, Wek RC, Cigan AM, Donahue TF, Hinnebusch AG. 1992. Phosphorylation of initiation factor 2 alpha by protein kinase GCN2 mediates gene-specific translational control of GCN4 in yeast. *Cell* **68**:585–596. doi:10.1016/0092-8674(92)90193-g

11. Dong J, Qiu H, Garcia-Barrio M, Anderson J, Hinnebusch AG. 2000. Uncharged tRNA Activates GCN2 by Displacing the Protein Kinase Moiety from a Bipartite tRNA-Binding Domain. *Molecular Cell* **6**:269–279. doi:10.1016/S1097-2765(00)00028-9

12. Donnelly N, Gorman AM, Gupta S, Samali A. 2013. The eIF2α kinases: Their structures and functions. *Cellular and Molecular Life Sciences* **70**:3493–3511. doi:10.1007/s00018-012-1252-6

13. Garcia-Barrio M. 2000. Association of GCN1-GCN20 regulatory complex with the N-terminus of eIF2alpha kinase GCN2 is required for GCN2 activation. *The EMBO Journal* **19**:1887–1899. doi:10.1093/emboj/19.8.1887

14. Gietz RD, Schiestl RH, Willems AR, Woods RA. 1995. Studies on the transformation of intact yeast cells by the LiAc/SS-DNA/PEG procedure. *Yeast (Chichester, England)* **11**:355–360. doi:10.1002/yea.320110408

15. Harding HP, Ordonez A, Allen F, Parts L, Inglis AJ, Williams RL, Ron D. 2019. The ribosomal P-stalk couples amino acid starvation to GCN2 2 activation in mammalian cells. *eLife* **8**:1–19. doi:10.7554/eLife.50149

16. Hinnebusch AG. 2005. Translational regulation of GCN4 and the general amino acid control of yeast. *Annual Review of Microbiology* **59**:407–450. doi:10.1146/annurev.micro.59.031805.133833

17. Hinnebusch AG. 1985. A hierarchy of trans-acting factors modulates translation of an activator of amino acid biosynthetic genes in Saccharomyces cerevisiae. *Mol Cell Biol* **5**:2349–2360. doi:10.1128/MCB.5.9.2349

18. Hinnebusch AG. 1984. Evidence for translational regulation of the activator of general amino acid control in yeast. *Proc Natl Acad Sci USA* **81**:6442–6446. doi:10.1073/pnas.81.20.6442

19. Ho B, Baryshnikova A, Brown GW. 2018. Unification of Protein Abundance Datasets Yields a Quantitative Saccharomyces cerevisiae Proteome. *Cell Systems* **6**:192-205.e3. doi:10.1016/j.cels.2017.12.004

20. Hughes TR, Marton MJ, Jones AR, Roberts CJ, Stoughton R, Armour CD, Bennett HA, Coffey E, Dai H, He YD, Kidd MJ, King AM, Meyer MR, Slade D, Lum PY, Stepaniants SB, Shoemaker DD, Gachotte D, Chakraburtty K, Simon J, Bard M, Friend SH. 2000. Functional Discovery via a Compendium of Expression Profiles. *Cell* **102**:109–126. doi:10.1016/S0092-8674(00)00015-5

21. Hulsen T. 2022. DeepVenn -- a web application for the creation of area-proportional Venn diagrams using the deep learning framework Tensorflow.js. doi:10.48550/ARXIV.2210.04597

22. Inglis AJ, Masson GR, Shao S, Perisic O, McLaughlin SH, Hegde RS, Williams RL. 2019. Activation of GCN2 by the ribosomal P-stalk. *Proceedings of the National Academy of Sciences of the United States of America* **116**:4946–4954. doi:10.1073/pnas.1813352116

23. Ishimura R, Nagy G, Dotu I, Chuang JH, Ackerman SL. 2016. Activation of GCN2 kinase by ribosome stalling links translation elongation with translation initiation. *eLife* **5**:1–22. doi:10.7554/eLife.14295

24. Jaimes-Miranda F, Chávez Montes RA. 2020. The plant MBF1 protein family: a bridge between stress and transcription. *Journal of Experimental Botany* **71**:1782–1791. doi:10.1093/jxb/erz525

25. Jelinsky SA, Samson LD. 1999. Global response of Saccharomyces cerevisiae to an alkylating agent. *Proc Natl Acad Sci USA* **96**:1486–1491. doi:10.1073/pnas.96.4.1486

26. Jindrich K, Degnan BM. 2016. The diversification of the basic leucine zipper family in eukaryotes correlates with the evolution of multicellularity. *BMC Evol Biol* **16**:28. doi:10.1186/s12862-016-0598-z

27. Juszkiewicz S, Slodkowicz G, Lin Z, Freire-Pritchett P, Peak-Chew SY, Hegde RS. 2020. Ribosome collisions trigger cis-acting feedback inhibition of translation initiation. *eLife* **9**:1–29. doi:10.7554/eLife.60038

28. Kabe Y, Goto M, Shima D, Imai T, Wada T, Morohashi K, Shirakawa M, Hirose S, Handa H. 1999. The Role of Human MBF1 as a Transcriptional Coactivator. *Journal of Biological Chemistry* **274**:34196–34202. doi:10.1074/jbc.274.48.34196

29. Kapur JN, Sahoo PK, Wong AKC. 1985. A new method for gray-level picture thresholding using the entropy of the histogram. *Computer Vision, Graphics, and Image Processing* **29**:273–285. doi:10.1016/0734-189X(85)90125-2

30. Köhrer K, Domdey HBT-M in E. 1991. [27] Preparation of high molecular weight RNAGuide to Yeast Genetics and Molecular Biology. Academic Press. pp. 398–405. doi:https://doi.org/10.1016/0076-6879(91)94030-G

31. Kornitzer D, Raboy B, Kulka RG, Fink GR. 1994. Regulated degradation of the transcription factor Gcn4. *The EMBO Journal* **13**:6021–6030. doi:10.1002/j.1460-2075.1994.tb06948.x

32. Kubota H, Obata T, Ota K, Sasaki T, Ito T. 2003. Rapamycin-induced translational derepression of GCN4 mRNA involves a novel mechanism for activation of the eIF2α kinase GCN2. *Journal of Biological Chemistry* **278**:20457–20460. doi:10.1074/jbc.C300133200

33. Lee M-W, Kim B-J, Choi H-K, Ryu M-J, Kim S-B, Kang K-M, Cho E-J, Youn H-D, Huh W-K, Kim S-T. 2007. Global protein expression profiling of budding yeast in response to DNA damage. *Yeast* **24**:145–154. doi:10.1002/yea.1446

34. Lee SJ, Swanson MJ, Sattlegger E. 2015. Gcn1 contacts the small ribosomal protein Rps10, which is required for full activation of the protein kinase Gcn2. *Biochemical Journal* **466**:547–559. doi:10.1042/BJ20140782

35. Li FQ, Ueda H, Hirose S. 1994. Mediators of activation of fushi tarazu gene transcription by BmFTZ-F1. *Mol Cell Biol* **14**:3013–3021. doi:10.1128/mcb.14.5.3013-3021.1994

36. Liu Q-X, Jindra M, Ueda H, Hiromi Y, Hirose S. 2003. *Drosophila* MBF1 is a co-activator for Tracheae Defective and contributes to the formation of tracheal and nervous systems. *Development* **130**:719–728. doi:10.1242/dev.00297

37. Liu Q-X, Nakashima-Kamimura N, Ikeo K, Hirose S, Gojobori T. 2007. Compensatory Change of Interacting Amino Acids in the Coevolution of Transcriptional Coactivator MBF1 and TATA-Box–Binding Protein. *Molecular Biology and Evolution* **24**:1458–1463. doi:10.1093/molbev/msm073

38. Love MI, Huber W, Anders S. 2014. Moderated estimation of fold change and dispersion for RNA-seq data with DESeq2. *Genome Biology* **15**:1–21. doi:10.1186/s13059-014-0550-8

39. Mariotti M, De Benedictis L, Avon E, Maier JAM. 2000. Interaction between Endothelial Differentiation-related Factor-1 and Calmodulin in Vitro and in Vivo. *Journal of Biological Chemistry* **275**:24047–24051. doi:10.1074/jbc.M001928200

40. Mariotti M, De Benedictis L, Maier JAM, Ballabio E. 2004. The dual role of endothelial differentiation-related factor-1 in the cytosol and nucleus: modulation by protein kinase A. *Cellular and Molecular Life Sciences (CMLS)* **61**:1069–1074. doi:10.1007/s00018-004-4016-0

41. Marrero Coto J, Ehrenhofer-Murray AE, Pons T, Siebers B. 2011. Functional analysis of archaeal MBF1 by complementation studies in yeast. *Biol Direct* **6**:18. doi:10.1186/1745-6150-6-18

42. Marton MJ, Crouch D, Hinnebusch AG. 1993. GCN1, a translational activator of GCN4 in Saccharomyces cerevisiae, is required for phosphorylation of eukaryotic translation initiation factor 2 by protein kinase GCN2. *Mol Cell Biol* **13**:3541–3556. doi:10.1128/MCB.13.6.3541

43. Marton MJ, Vazquez de Aldana CR, Qiu H, Chakraburtty K, Hinnebusch AG. 1997. Evidence that GCN1 and GCN20, translational regulators of GCN4, function on elongating ribosomes in activation of eIF2alpha kinase GCN2. *Mol Cell Biol* **17**:4474–4489. doi:10.1128/MCB.17.8.4474

44. Meimoun A, Holtzman T, Weissman Z, McBride HJ, Stillman DJ, Fink GR, Kornitzer D. 2000. Degradation of the Transcription Factor Gcn4 Requires the Kinase Pho85 and the SCF ^{CDC4} Ubiquitin–Ligase Complex. *MBoC* **11**:915–927. doi:10.1091/mbc.11.3.915

45. Miller M. 2009. The Importance of Being Flexible: The Case of Basic Region Leucine Zipper Transcriptional Regulators. *CPPS* **10**:244–269. doi:10.2174/138920309788452164

46. Natarajan K, Meyer MR, Jackson BM, Slade D, Roberts C, Hinnebusch AG, Marton MJ. 2001. Transcriptional Profiling Shows that Gcn4p Is a Master Regulator of Gene Expression during Amino Acid Starvation in Yeast. *Molecular and Cellular Biology* **21**:4347–4368. doi:10.1128/mcb.21.13.4347-4368.2001

47. Otsu N. 1979. A Threshold Selection Method from Gray-Level Histograms. *IEEE Trans Syst, Man, Cybern* **9**:62–66. doi:10.1109/TSMC.1979.4310076

48. Paine P, Feldherr C. 1972. Nucleocytoplasmic exchange of macromolecules. *Experimental Cell Research* **74**:81–98. doi:10.1016/0014-4827(72)90483-1

49. Paine PL. 1975. Nucleocytoplasmic movement of fluorescent tracers microinjected into living salivary gland cells. *Journal of Cell Biology* **66**:652–657. doi:10.1083/jcb.66.3.652

50. Pakos-Zebrucka K, Koryga I, Mnich K, Ljujic M, Samali A, Gorman AM. 2016. The integrated stress response. *EMBO reports* **17**:1374–1395. doi:10.15252/embr.201642195

51. Patro R, Duggal G, Love MI, Irizarry RA, Kingsford C. 2017. Salmon provides fast and bias-aware quantification of transcript expression. *Nature methods* **14**:417–419. doi:10.1038/nmeth.4197

52. Peters R. 1983. Nuclear envelope permeability measured by fluorescence microphotolysis of single liver cell nuclei. *Journal of Biological Chemistry* **258**:11427–11429. doi:10.1016/S0021-9258(17)44241-4

53. Pochopien AA, Beckert B, Kasvandik S, Berninghausen O, Beckmann R, Tenson T, Wilson DN. 2021. Structure of Gcn1 bound to stalled and colliding 80S ribosomes. *Proceedings of the National Academy of Sciences of the United States of America* **118**. doi:10.1073/pnas.2022756118

54. Qiu H, Hu C, Dong J, Hinnebusch AG. 2002. Mutations that bypass tRNA binding activate the intrinsically defective kinase domain in GCN2. *Genes Dev* **16**:1271–1280. doi:10.1101/gad.979402

55. Rawal Y, Chereji RV, Valabhoju V, Qiu H, Ocampo J, Clark DJ, Hinnebusch AG. 2018. Gcn4 Binding in Coding Regions Can Activate Internal and Canonical 5′ Promoters in Yeast. *Molecular Cell* **70**:297-311.e4. doi:10.1016/j.molcel.2018.03.007

56. Russell JB, Cook GM. 1995. Energetics of bacterial growth: balance of anabolic and catabolic reactions. *Microbiological Reviews* **59**:48–62. doi:10.1128/MR.59.1.48-62.1995

57. Sambrook J, Russell DW. 2006. Separation of RNA According to Size: Electrophoresis of RNA through Agarose Gels Containing Formaldehyde. *Cold Spring Harbor Protocols* **2006**:pdb.prot4050. doi:10.1101/pdb.prot4050

58. Sattlegger E, Hinnebusch AG. 2005. Polyribosome binding by GCN1 is required for full activation of eukaryotic translation initiation factor 2α kinase GCN2 during amino acid starvation. *Journal of Biological Chemistry* **280**:16514–16521. doi:10.1074/jbc.M414566200

59. Schindelin J, Arganda-Carreras I, Frise E, Kaynig V, Longair M, Pietzsch T, Preibisch S, Rueden C, Saalfeld S, Schmid B, Tinevez J-Y, White DJ, Hartenstein V, Eliceiri K, Tomancak P, Cardona A. 2012. Fiji: an open-source platform for biological-image analysis. *Nat Methods* **9**:676–682. doi:10.1038/nmeth.2019

60. Shemer R, Meimoun A, Holtzman T, Kornitzer D. 2002. Regulation of the Transcription Factor Gcn4 by Pho85 Cyclin Pcl5. *Mol Cell Biol* **22**:5395–5404. doi:10.1128/MCB.22.15.5395-5404.2002

61. Simms CL, Kim KQ, Yan LL, Qiu J, Zaher HS. 2018. Interactions between the mRNA and Rps3/uS3 at the entry tunnel of the ribosomal small subunit are important for no-go decay. *PLoS Genetics* **14**:1–25. doi:10.1371/journal.pgen.1007818

62. Simms CL, Yan LL, Qiu JK, Zaher HS. 2019. Ribosome Collisions Result in +1 Frameshifting in the Absence of No-Go Decay. *Cell Reports* **28**:1679-1689.e4. doi:10.1016/j.celrep.2019.07.046

63. Sinha NK, Ordureau A, Best KM, Saba JA, Zinshteyn B, Sundaramoorthy E, Fulzele A, Garshott DM, Denk T, Thoms M, Paulo JA, Harper JW, Bennett EJ, Beckmann R, Green R, Harper W, Bennett EJ, Beckmann R, Green R. 2020. EDF1 coordinates cellular responses to ribosome collisions. *eLife* **9**:1–84. doi:10.7554/ELIFE.58828

64. Solomon ER, Caldwell KK, Allan AM. 2021. A novel method for the normalization of ChIP-qPCR data. *MethodsX* **8**:101504. doi:10.1016/j.mex.2021.101504

65. Soneson C, Love MI, Robinson MD. 2016. Differential analyses for RNA-seq: Transcript-level estimates improve gene-level inferences. *F1000Research* **4**:1–23. doi:10.12688/F1000RESEARCH.7563.2

66. Stephens M. 2017. False discovery rates: A new deal. *Biostatistics* **18**:275–294. doi:10.1093/biostatistics/kxw041

67. Takemaru K, Harashima S, Ueda H, Hirose S. 1998. Yeast Coactivator MBF1 Mediates GCN4-Dependent Transcriptional Activation. *Molecular and Cellular Biology* **18**:4971–4976. doi:10.1128/mcb.18.9.4971

68. Takemaru K, Li F-Q, Ueda H, Hirose S. 1997. Multiprotein bridging factor 1 (MBF1) is an evolutionarily conserved transcriptional coactivator that connects a regulatory factor and TATA element-binding protein. *Proc Natl Acad Sci USA* **94**:7251–7256. doi:10.1073/pnas.94.14.7251

69. Tsuda K, Tsuji T, Hirose S, Yamazaki K. 2004. Three Arabidopsis MBF1 Homologs with Distinct Expression Profiles Play Roles as Transcriptional Co-activators. *Plant and Cell Physiology* **45**:225–231. doi:10.1093/pcp/pch017

70. Wang J, Zhou J, Yang Q, Grayhack EJ. 2018. Multi-protein bridging factor 1(Mbf1), Rps3 and Asc1 prevent stalled ribosomes from frameshifting. *eLife* **7**:1–26. doi:10.7554/eLife.39637

71. Wang Y, Wei X, Huang J, Wei J. 2017. Modification and functional adaptation of the MBF1 gene family in the lichenized fungus Endocarpon pusillum under environmental stress. *Sci Rep* **7**:16333. doi:10.1038/s41598-017-16716-4

72. Wek RC. 2018. Role of eIF2α Kinases in Translational Control and Adaptation to Cellular Stress. *Cold Spring Harb Perspect Biol* **10**:a032870. doi:10.1101/cshperspect.a032870

73. Wek SA, Zhu S, Wek RC. 1995. The histidyl-tRNA synthetase-related sequence in the eIF-2 alpha protein kinase GCN2 interacts with tRNA and is required for activation in response to starvation for different amino acids. *Mol Cell Biol* **15**:4497–4506. doi:10.1128/MCB.15.8.4497

74. Wu CCC, Peterson A, Zinshteyn B, Regot S, Green R. 2020. Ribosome Collisions Trigger General Stress Responses to Regulate Cell Fate. *Cell* **182**:404-416.e14. doi:10.1016/j.cell.2020.06.006

75. Yan LL, Simms CL, McLoughlin F, Vierstra RD, Zaher HS. 2019. Oxidation and alkylation stresses activate ribosome-quality control. *Nature Communications* **10**:1–15. doi:10.1038/s41467-019-13579-3

76. Yan LL, Zaher HS. 2021. Ribosome quality control antagonizes the activation of the integrated stress response on colliding ribosomes. *Molecular Cell* **81**:614-628.e4. doi:10.1016/j.molcel.2020.11.033

77. Zanetti ME. 2003. Phosphorylation of a member of the MBF1 transcriptional co-activator family, StMBF1, is stimulated in potato cell suspensions upon fungal elicitor challenge. *Journal of Experimental Botany* **54**:623–632. doi:10.1093/jxb/erg061

78. Zanetti ME, Chan RL, Godoy AV, Gonzalez DH, Casalongue CA. 2004. Homeodomain-leucine Zipper Proteins Interact with a Plant Homologue of the Transcriptional Co-activator Multiprotein Bridging Factor 1. *BMB Reports* **37**:320–334. doi:10.5483/BMBRep.2004.37.3.320

79. Zhu S, Sobolev AY, Wek RC. 1996. Histidyl-tRNA Synthetase-related Sequences in GCN2 Protein Kinase Regulate in Vitro Phosphorylation of eIF-2. *Journal of Biological Chemistry* **271**:24989–24994. doi:10.1074/jbc.271.40.24989

Supplementary Figures and Tables

Supplementary Table 1: Yeast strains used in this study

Name	Genotype	Reference/Source
BY4741 (MATa)	*MATa his3Δ1 leu2Δ0 met15Δ0 ura3Δ0*	Dharmacon
mbf1Δ	*BY4741; mbf1Δ::NAT*	This Study
gcn2Δ	*BY4741; gcn2Δ::KAN*	Horizon
gcn4Δ	*BY4741; gcn4Δ::KAN*	Horizon
GCN4-3XFLAG	*BY4741; GCN4-3XFLAG KAN, ARG4-Myc HIS3*	This Study
mbf1Δ GCN4-3XFLAG	*GCN4-3XFLAG; mbf1Δ::NAT*	This Study
pcl5Δ GCN4-3XFLAG	*GCN4-3XFLAG; pcl5Δ::LEU2*	This Study
pho85Δ GCN4-3XFLAG	*GCN4-3XFLAG; pho85Δ::LEU2*	This Study
HA-MBF1	*mbf1Δ GCN4-3XFLAG; ade2::MET15 HA-MBF1*	This Study
HA-MBF1 R89G	*mbf1Δ GCN4-3XFLAG; ade2::MET15 HA-mbf1 R89G*	This Study
MBF1-mCherry	*BY4741; MBF1-6xGly-FLAG-mCherry HIS3*	This Study
mbf1 R89G-mCherry	*BY4741; mbf1 R89G-6x-Gly-FLAG-mCherry HIS3*	This Study

Supplementary Table 2: Plasmids used in this study

Name	Genotype	Reference/Source
p180	Gcn4-lacZ	(Hinnebusch, 1985)

pCUP-Empty	pAG426 CUP-ccDB	This Study
pCUP-GCN4-FLAG	pAG 426 CUP-GCN4-FLAG	This Study
pRL-$(CGA)_4$-FL	pDB RL-$(CGA)_4$-FL	(Simms et al., 2019)
pProEx-MBF1	pProEx HTb His_6-TEV-HA-MBF1	This Study
pProEx-GCN4	pProEx HTb His_6-TEV-GCN4-FLAG	This Study
pProEx-SPT15	pProEx HTb His_6-TEV-SPT15-Myc	This Study

Supplementary Table 3: Primers used in this study

Name	**Genotype**	**Reference/Source**
MBF1-HA-F	TTA GAA GTG TCA ACA ACG TAT CTA CCA ACT GGT ACC GCT ATA TTT GCA TAC GTT TTT CAG	This Study
MBF1-HA-R	AGG GCT GCA GTG CTA AGC TTC CAA ACT ACC ATA AAG ATC CTG AAT CAT AAT ATA TAC GTG	This Study
EKD-HA-MBF1-F	AGT GAA GTA CAC ACG TAT ATA TTA TGA TTC AGG ATC TTT ATG GTA GTT TGG AAG CTT AGC	This Study
EKD-HA-MBF1-R	GGA ATA GAA GAA GGA TCT GAA AAA CGT ATG CAA ATA TAG CGG TAC CAG TTG GTA GAT ACG	This Study
GCN4-FLAG-F	GAA AAT GAG GTT GCC AGA TTA AAG AAA TTA GTT GGC GAA CGC GGG GGA GGC GGG GGT GGA	This Study
GCN4-FLAG-R	AAT GAA ATA AAA AAT ATA AAA TAA AAG GTA AAT GAA AGA ATT CGA GCT CGT TTA AAC	This Study

ARG4-MYC-F	CGG GGG TGG AGA ACA AAA ACT CAT CTC AGA AGA GGA TCT GTA GGG CGC GCC ACT TCT AAA	This Study
ARG4-MYC-F2	CAA TTG GAT AAT TTG AAA TCC CAA TTA AAT GGG GGA GGC GGG GGT GGA GAA CAA AAA CTC	This Study
ARG4-MYC-F3	GCT ACT GGT GGA ACC GCT AAA TCT GCT GTA TTG AAG CAA TTG GAT AAT TTG AAA TCC CAA	This Study
ARG4-MYC-R	CCA GAC CTG ATG AAA TTC TTG CGC ATA ACG TCG CCA TGA ATT CGA GCT CGT TTA AAC TGG	This Study
ARG4-MYC-R2	TAA GTA TTT AAA GAA GGG TTG ATG AAG TCC TAG AAG TAC CAG ACC TGA TGA AAT TCT TGC	This Study
ARG4-MYC-R3	CAC AAT CTC GAA AAT ATA ATA CTA ATA ACA AAA TAA GTA TTT AAA GAA GGG TTG ATG AAG	This Study
GCN4-CUP-F	AAA CAC AAC ATA TCC AGT CAC TAT GGC GGC CGC AAA TAA AAT GTC CGA ATA TCA GCC	This Study
GCN4-CUP-R	TTA CAT GAC TCG AGG TCG ACG GTA TCG ATA AGC TTC TAC TTG TCA TCG TCA TCC TTG T	This Study
CUP-GCN4-R	TTA AAG CAA ATA AAC TTG GCT GAT ATT CGG ACA TTT TAT TTG CGG CCG CCA TAG TGA	This Study
CUP-GCN4-F	ATC ATG ACA TCG ACT ACA AGG ATG ACG ATG ACA AGT AGA AGC TTA TCG ATA CCG TCG	This Study
6xHis-TEV-HA-Mbf1-F	ATC CCA ACG ACC GAA ACC CTG TAT TTT CAG GGC TCT GAC TGG GAT ACA AAT ACT ATT	This Study

6xHis-TEV-HA-Mbf1-R	TAG TCA GGA ACA TCG TAT GGG TAG TCG ACC TGC AGC GTA CGT TTC TTC TTT GGA GCT C	This Study
pProEx-HTb-Mbf1-F	AGG TCG ACT ACC CAT ACG ATG TTC CTG ACT ATG CGT AGG AGA AGA TTT TCA GCC TGA	This Study
6xHis-TEV - GCN4-FLAG-F	TAC GAT ATC CCA ACG ACC GAA AAC CTG TAT TTT CAG GGC TCC GAA TAT CAG CCA AGT	This Study
6xHis-TEV - GCN4-FLAG-R	GCG TTC TGA TTT AAT CTG TAT CAG GCT GAA AAT CTT CTC CTA CTT GTC ATC GTC ATC	This Study
pProEx-HTb-GCN4-F	ATC ATG ACA TCG ACT ACA AGG ATG ACG ATG ACA AGT AGG AGA AGA TTT TCA GCC TGA	This Study
6xHis-TEV-SPT15-Myc-F	GAT TAC GAT ATC CCA ACG ACC GAA AAC CTG TAT TTT CAG GGC GCC GAT GAG GAA CGT	This Study
6xHis-TEV-SPT15-Myc-R	AGA TGA GTT TCT GCT CTC CAC CCC CGC CTC CCC CCA TTT TTC TAA ATT CAC TTA GCA C	This Study
pProEx-HTb-SPT15--F	GTG GAG AGC AGA AAC TCA TCT CAG AAG AGG ATC TGT AGG AGA AGA TTT TCA GCC TGA	This Study
ARG1-qPCR-F	TGA ACG TGG TCT TCC AGT CA	This Study
ARG1-qPCR-R	CAG TCA ATG GAG CCT GTT CG	This Study
TAF10-qPCR-F	CGGGTTTAACGTAGCAGATG	This Study
TAF10-qPCR-R	CGCCTGACTGTTGTTAGCAT	This Study
ARG1-CHIP-F	TAA TCT GAG CAG TTG CGA GA	This Study
ARG1-CHIP-R	ATG TTC CTT ATC GCT GCA CA	This Study

ARG4-CHIP-F	GTT CTT GTG GTG GTT ACT CA	This Study
ARG4-CHIP-R	CCC TAG CTA AAG AAA GGT AG	This Study
Mbf1-6xGly-F	GGT AAC AAC ATC GGT TCG CCT TTG GGA GCT CCA AAG AAG AAA GGG GGA GGC GGG GGT GGA	This Study
Mbf1-6xGly-R	TTC ATT GAT GAC ATG CAG TGC GAA AAG AAA GGA ACA AAT GGA ATT CGA GCT CGT TTA AAC	This Study

Chapter 7

Conclusions and Future Directions

Abstract

The focus of my thesis work has been to broaden our understanding of how disruptions to normal ribosome functioning are recognized and utilized as signals to activate various response pathways. By harnessing the genetic tractability of the budding yeast *Saccharomyces cerevisiae*, we uncover that disruption of canonical translation initiation activates a conserved stress response pathway known as the integrated stress response (ISR). In addition, we find that translation of the key effector of the ISR occurs via a non-canonical mechanism. Using in vitro approaches in tandem with mass spectrometry analysis, we show that N1-methylpseudouridine – the modification used in the SARS-CoV-2 mRNA vaccines – is translated faithfully, a reassuring sign for future RNA therapeutics. Finally, using various biochemical and computational methods, we investigate the role of the factor Mbf1 in activation of the ISR and the mechanisms that regulate its function, confirming the centrality of ribosome collisions to this process. By completing this work, we have gained new insight into the mechanisms that enable the translational machinery to sense the environment and reprogram gene expression in response.

Summary

Loss of eIF4E in yeast results in induction of the integrated stress response in an eIF2*α* phosphorylation-independent manner

Canonical initiation in eukaryotes begins with the formation of 43S preinitiation complexes (43S PICs), which are composed of the 40S ribosomal subunit, ternary complex (TC) – a complex of initiator methionyl-tRNA, GTP, and the initiation factor eIF2, and several other initiation factors (Hinnebusch and Lorsch, 2012; Pelletier and Sonenberg, 2019). In parallel, the cap-binding initiation factor eIF4E, helicase eIF4A, and scaffolding factor 4G form a complex known as eIF4F on the transcript and recruit the 43S PIC to begin scanning. Under stress

conditions, initiation is repressed by the action of two different response pathways. Integrated stress response (ISR) signaling leads to a reduction in ternary levels, inhibiting 43S PIC formation (Hinnebusch, 2005; Pakos-Zebrucka et al., 2016; Wek, 2018), while shutoff of the TOR pathway derepresses eIF4E-binding proteins, which sequester eIF4E from eIF4G and prevent formation of eIF4F (Gingras et al., 2001). Given that stress response genes must be translated under these conditions, it follows that they would be resistant to such inhibition. The mechanisms that these genes utilize to recruit ribosomes have not been widely characterized. In addition, it is known that crosstalk exists between these two pathways (Cherkasova and Hinnebusch, 2003; Kubota et al., 2003), but the mechanisms by which the communication occurs is not well understood.

Here we search for these mechanisms in *Saccharomyces cerevisiae* by using a temperature-sensitive allele of eIF4E (4E-ts; *cdc33-ts4-2*) (Altmann et al., 1989), which allowed us to mimic the action of 4E-BPs without altering TOR signaling. Characterization of transcripts that remained translated even under restrictive conditions, by RNA-seq and ribosome profiling, revealed that the ISR was activated when eIF4E activity was lost. Immunoblot analysis showed accumulation of Gcn4 without concomitant eIF2α phosphorylation in 4E-ts cells under restrictive conditions, suggesting that *GCN4* translation was derepressed via a non-canonical mechanism (Hinnebusch, 2005). These results were recapitulated in strains deleted for the eIF2α kinase Gcn2, further supporting a novel mechanism. Immunoblot analysis of eIF2γ levels appeared to implicate decreased ternary complex levels as responsible for observed Gcn4 accumulation. However, neither overexpression of eIF2γ nor overexpression of the eIF2γ maturation factor Cdc123 was sufficient to restore *GCN4* translational control. Finally, dual luciferase assays of various reporter constructs harboring the *GCN4* 5'UTR showed it to be insufficient for cap-

independent initiation, as no increase in relative luminescence was observed under restrictive conditions for reporters bearing an in frame stop codon between the luciferases. Together, our findings suggest that additional factors, such as eIF4E, participate in the communication between the ISR and TOR pathways.

N1-methylpseudouridine found within COVID-19 mRNA vaccines produces faithful protein products

The mRNA vaccines against SARS-CoV-2 (Baden et al., 2021; Polack et al., 2020) have shown the viability of RNA therapeutics. However, synthesis of RNA for use in the clinic requires the incorporation of modified nucleotides to bypass antiviral defenses that repress translation (Akira et al., 2006; Anderson et al., 2010; Freund et al., 2019; Karikó et al., 2012, 2011, 2008, 2005, 2004; Weissman et al., 2000). The SARS-CoV-2 vaccines incorporate the modification N1-methylpseudouridine (m1Ψ) since it was determined to be even less immunogenic and better translated than the originally studied pseudouridine (Ψ) modification (Andries et al., 2015; Parr et al., 2020; Svitkin et al., 2017). However, how m1Ψ is decoded by the ribosome is unknown. Studies on the effects of Ψ on translational fidelity have reported conflicting results, with some groups reporting readthrough of stop codons (Adachi and Yu, 2020; Fernández et al., 2013; Karijolich and Yu, 2011; Parisien et al., 2012), while others have reported minimal effects on miscoding (Eyler et al., 2019; Hoernes et al., 2019, 2016; Nir et al., 2022; Svidritskiy et al., 2016).

We sought to address this knowledge gap by investigating the effect of m1Ψ on translational fidelity. To characterize how ribosomes decode m1Ψ, we performed peptidyl transfer kinetics experiments with synthetic mRNAs harboring either Ψ or m1Ψ in a well-defined reconstituted bacterial system. We found that m1Ψ in the codon decreased the rate and endpoint

of peptide bond formation, but unlikely to be significant enough to affect protein yield. Peptidyl transfer surveys with all 19 near/non-cognate aminoacylated tRNA isoacceptors showed no significant difference between U and m1Ψ-containing mRNA, indicating that m1Ψ does not alter the fidelity of tRNA selection. We also did not see increased reactivity with near-cognates, and suppression of near stop recognition, for the m1Ψ mRNA. Mass spectrometry analysis of SARS-CoV-2 spike protein produced in HEK 293 cells from electroporation of m1Ψ modified mRNA did not detect an increase in miscoded peptide frequency. In addition, complementary dual luciferase assays in HEK 293 cells using the same mRNA also failed to show any increase in miscoding frequency, suggesting that transcripts containing m1Ψ are still translated with high fidelity. To examine the effects of m1Ψ on duplex stability, we conducted high-resolution melt analysis and found that m1Ψ did not stabilize mismatched duplexes, in accordance with our tRNA selection data. In order to understand how m1Ψ might be read by other enzymes, we conducted primer extension assays with M-MLV and the synthetic mRNA from before. We also deep sequenced AMV and M-MLV reverse transcribed products. In both cases, m1Ψ increased the number of errors made by the reverse transcriptases, although at far lower frequency than did Ψ. Combined, our results show mRNAs containing m1Ψ are translated faithfully and that RNA therapeutics utilizing the modification will produce the intended protein product.

Mbf1 acts in conjunction with Gcn4 to activate the Integrated Stress Response

The Gcn2-Gcn4 axis of integrated stress response (ISR) activation has been well characterized (Hinnebusch, 2005), with recent evidence supporting a model for ribosome collision-mediated activation of Gcn2 (Harding et al., 2019; Hughes et al., 2000; Inglis et al., 2019; Ishimura et al., 2016; Lee et al., 2015; Natarajan et al., 2001; Pochopien et al., 2021; Sattlegger and Hinnebusch, 2005; Wu et al., 2020; Yan and Zaher, 2021). However, a previous

study reported that Gcn4-mediated transcription of its targets required the presence of an additional factor, Mbf1, in order to recruit TATA binding protein (TBP) (Takemaru et al., 1998), indicating the presence of another arm of ISR signaling. Cryo-EM studies have revealed that Mbf1 also binds to collided ribosomes (Pochopien et al., 2021; Sinha et al., 2020), suggesting that Gcn2 and Mbf1 both report on collided ribosomes to activate the ISR, but the mechanisms that regulate the role of Mbf1 in this process have not yet been characterized.

Here we conducted transcriptomic analysis of *mbf1*Δ, *gcn2*Δ, and *gcn4*Δ strains and find significant overlaps in those genes that exhibit impaired expression, suggesting that Mbf1 is necessary for induction of Gcn4 targets during MMS stress. Immunoblot analysis revealed that cells lacking Mbf1 were defective in accumulation of Gcn4 in response to MMS. This defect did not appear to be due to differences in *GCN4* translational derepression, based on *GCN4-lacZ* reporters, but due to differences in stability, based on cycloheximide chase assays. However, stabilization of Gcn4 levels did not rescue ISR activation – as judged by induction of the Gcn4 target gene *ARG1* – suggesting that Mbf1 necessity is via its coactivation function. We find that induction of Gcn4 in an eIF2α-independent manner is also not sufficient to activate the ISR, indicating that phosphorylation of eIF2α, or conditions that lead to activation of Gcn2, is necessary for the response. We confirm that a previously identified frameshifting mutant, Mbf1 R89G does not bind ribosomes, based on the observation that the mutant factor does not comigrate with polysomes upon treatment with MMS. Critically, *mbf1*Δ cells complemented with Mbf1 R89G remain unable to activate the ISR, suggesting that ribosome binding is a key event in enabling Mbf1 coactivation function.

While our observations have provided important details about the role of Mbf1 in this process, outstanding questions still remain regarding the mechanism by which ribosome binding

alters Mbf1 function. Visualization of a Mbf1-mCherry reporter by fluorescence microscopy did not show any differences in localization as a result of treatment with MMS. Meanwhile, chromatin immunoprecipitation-quantitative PCR showed that recruitment of the R89G mutant to Gcn4 targets was unimpaired. Furthermore, purified recombinant Mbf1 R89G is able to bind both Gcn4 and Spt15, as seen by gel shift assay. Regardless, our work has resolved several mechanistic details on how Mbf1 acts as a secondary signal in activation of the ISR.

Future Directions

The primary focus of our efforts is uncovering the mechanism by which Mbf1 function is regulated and the contribution of the ribosome to this process. One of the key questions to resolve is the mechanism by which abrogation of ribosome binding prevents activation of the ISR. Both Mbf1 binding to Gcn4 and Mbf1 recruitment of Spt15 are necessary for induction of Gcn4 targets (Takemaru et al., 1998). Examination of Mbf1 recruitment to Gcn4 targets by chromatin immunoprecipitation – quantitative PCR (CHIP-qPCR) shows that R89G mutant Mbf1, which is not able to bind the ribosome, is not defective in recruitment. Furthermore, gel shift assays of recombinant protein purified from *E. coli* incubated with a radiolabeled oligonucleotide encompassing the Gcn4 binding region of *ARG4* shows that the R89G mutant is able to bind both Gcn4 and Spt15. These observations are seemingly contradictory, as Mbf1 does not appear to serve as a transcriptional coactivator by default given that complementation with the R89G mutant does not rescue ISR activation during treatment with MMS, and induction of Gcn4 in an eIF2α-phosphorylation independent manner is insufficient to induce the Gcn4 regulon. If binding to the collided ribosome alters the ability of Mbf1 to bind either Gcn4 or Spt15, this would provide a mechanism for the necessity of ribosome binding in Mbf1 function as a coactivator. CHIP-qPCR experiments of tagged-Gcn4 and Spt15 strains are currently

ongoing to determine if the recruitment of either factor is affected in strains complemented with the R89G mutant.

Another key question to resolve is the signaling that occurs on Mbf1. It is currently unknown if Mbf1 activity is regulated by a post-translational modification (PTM). Our current hypothesis is that binding to the collided ribosome alters the phosphorylation status of Mbf1. EDF1, the human homology of Mbf1, has been shown to be phosphorylated in response to either activation of protein kinase C (PKC) or protein kinase A (PKA) (Mariotti et al., 2004, 2000). Likewise, potato Mbf1 (*St*Mbf1) has been shown to be phosphorylated in response to challenge by a fungal pathogen (Zanetti, 2003). For both of these homologs, the region that is phosphorylated is highly conserved (Figure 1) (Mariotti et al., 2004, 2000; Wang et al., 2018; Zanetti, 2003), suggesting that yeast Mbf1 is liable to have a conserved phosphorylation site. Furthermore, PKC-mediated phosphorylation of EDF1 and phosphorylation of StMbf1 are both dependent on Ca^{2+} signaling, indicating that the regulatory mechanism may also be conserved (Mariotti et al., 2004, 2000; Zanetti, 2003). Indeed, complementation with any of the three *A. thaliana* Mbf1s (Tsuda et al., 2004), or *D. melanogaster* Mbf1 (Liu et al., 2003), can partially rescue growth on the histidine starvation inducer 3-aminotriazole (3-AT). By mutating conserved serine and threonine residues, and checking ISR activation in these cells, we can assess if phosphorylation on these sites contributes to Mbf1 function in the ISR. Here, T69 and S95 immediately stand out as universally conserved sites (Figure 1). In parallel, we plan to use an unbiased proteomics approach to identify all PTMs present on Mbf1, which would be informative on alternative modifications that occur on Mbf1, their location, and if their presence is dependent on the induction of ribosome collisions.

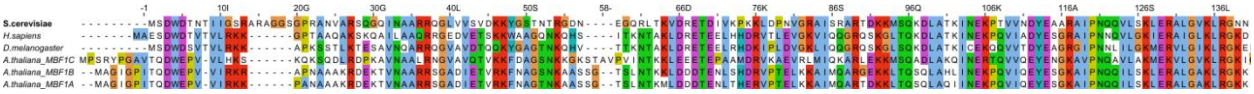

Figure 1: Conservation of Mbf1
Conserved residues are colored. *S. cerevisiae* Mbf1 was used as the reference for numbering.

If Mbf1 is indeed regulated by phosphorylation, the identities of the upstream kinase and the downstream phosphatase are unknown. Since it appears that modification of Mbf1 occurs on the ribosome, the two factors are also likely to associate with ribosomes. Mbf1 binds to the collided ribosome via various contacts with the ribosomal protein Rps3 (Pochopien et al., 2021; Sinha et al., 2020). However, a BioID experiment to search for proteins in proximity to Rps3 yielded only one kinase, Ste20, and no phosphatases (Schmitt et al., 2021). It is possible that the factors we seek do not bind to ribosomes under normal conditions and only bind collided ribosomes, similar to Mbf1. BioID experiments using either tagged Rps3 or tagged Mbf1 in cells treated with methyl methanesulfonate (MMS), an inducer of collisions, may capture the identities of the factors. Concurrently, it would be prudent to generate PKC and PKA deletion strains, the kinases responsible for EDF1 phosphorylation, in the event that BioID fails to provide any insights. As for the identity of the phosphatase, phosphatase 2 (PP2A) stands out as a candidate given that it has been shown to stabilize Gcn4 under conditions of abundant methionine. The phosphatase does so by dephosphorylating the critical T165 residue that targets Gcn4 for degradation (Meimoun et al., 2000; Shemer et al., 2002; Walvekar et al., 2020). A shared Gcn4-Mbf1 phosphatase would be an elegant way to link regulation of the two pathways together, preventing activation of the canonical stress response program while enabling Gcn4 to carry out alternative transcriptional functions.

Another line of inquiry is investigating if the frame maintenance activity on the ribosome is linked to regulation of Mbf1. Genetic interaction experiments showed epistasis between loss of Mbf1 and mutation of the K108 residue in the ribosomal protein Rps3 on frameshifting (Wang et al., 2018), suggesting that monitoring of reading frame may begin on the ribosome and the signal transmitted to Mbf1. As a result, it is plausible that signaling on the ribosome that alters Mbf1 function in the ISR is linked to or transmitted through this residue. Investigating how mutation of this residue affects ISR activation may provide clues as to how the ribosome participates in regulating Mbf1 function. In addition to K108, residues S104, and L113 have also been implicated in reading frame maintenance (Wang et al., 2018) and contact with Mbf1 in the collided ribosome structure (Pochopien et al., 2021; Sinha et al., 2020), providing additional targets for study.

Conclusion of the thesis

The goal of my dissertation was to expand our understanding of how cells utilize ribosomes as sensors of internal conditions. My studies were particularly focused on how disruptions to typical ribosome functioning are recognized and converted into signals that lead to changes in gene expression. In that regard, we find that disruption of canonical translation initiation leads to activation of the integrated stress response (ISR). The activation of the ISR in this regard appeared to be via a novel mechanism, as it occurred in the absence of the canonical eIF2α phosphorylation signal. We also find that the N1-methylpseudouridine, the modification used in the SARS-CoV-2 mRNA vaccines, appears to be decoded similar to uridine and not disruptive to ribosome function. However, the main focus of my research has been understanding the role of Mbf1 in activation of the ISR. As a coactivator of Gcn4, its presence is necessary for activation of the ISR. We show that this activity is dependent on contact with collided ribosomes, further

supporting the idea that disruptions in ribosome function are monitored by the cell as key signaling events to activate response pathways.

Even at the conclusion of my work, several important questions still remain. We still do not understand the mechanisms by which the translational machinery enables communication between the integrated stress response and the TOR pathway. We also do not understand the mechanisms that regulate Mbf1 function and how the ribosome is involved in this process. Regardless, I am confident that future studies will continue to unravel the mechanisms that enable cells to utilize the translational machinery as a powerful signaling system, capturing signals from the environment and relaying this information to the other genetic machinery to enable cells to dynamically respond to an ever-changing environment.

References

1. Adachi H, Yu YT. 2020. Pseudouridine-mediated stop codon readthrough in s. cerevisiae is sequence context–independent. *Rna* **26**:1247–1256. doi:10.1261/RNA.076042.120

2. Akira S, Uematsu S, Takeuchi O. 2006. Pathogen recognition and innate immunity. *Cell* **124**:783–801. doi:10.1016/j.cell.2006.02.015

3. Altmann M, Sonenberg N, Trachsel H, Universitat M Der, Bern C-. 1989. Translation in Saccharomyces cerevisiae: initiation factor 4E-dependent cell-free system. *Molecular and Cellular Biology* **9**:4467–4472. doi:10.1128/MCB.9.10.4467

4. Anderson BR, Muramatsu H, Nallagatla SR, Bevilacqua PC, Sansing LH, Weissman D, Karikó K. 2010. Incorporation of pseudouridine into mRNA enhances translation by diminishing PKR activation. *Nucleic Acids Research* **38**:5884–5892. doi:10.1093/nar/gkq347

5. Andries O, Mc Cafferty S, De Smedt SC, Weiss R, Sanders NN, Kitada T. 2015. N1-methylpseudouridine-incorporated mRNA outperforms pseudouridine-incorporated mRNA by providing enhanced protein expression and reduced immunogenicity in mammalian cell lines and mice. *Journal of Controlled Release* **217**:337–344. doi:10.1016/j.jconrel.2015.08.051

6. Baden LR, El Sahly HM, Essink B, Kotloff K, Frey S, Novak R, Diemert D, Spector SA, Rouphael N, Creech CB, McGettigan J, Khetan S, Segall N, Solis J, Brosz A, Fierro C, Schwartz H, Neuzil K, Corey L, Gilbert P, Janes H, Follmann D, Marovich M, Mascola J, Polakowski L, Ledgerwood J, Graham BS, Bennett H, Pajon R, Knightly C, Leav B, Deng

W, Zhou H, Han S, Ivarsson M, Miller J, Zaks T. 2021. Efficacy and Safety of the mRNA-1273 SARS-CoV-2 Vaccine. *New England Journal of Medicine* **384**:403–416. doi:10.1056/nejmoa2035389

7. Cherkasova VA, Hinnebusch AG. 2003. Translational control by TOR and TAP42 through dephosphorylation of eIF2α kinase GCN2. *Genes and Development* **17**:859–872. doi:10.1101/gad.1069003

8. Eyler DE, Franco MK, Batool Z, Wu MZ, Dubuke ML, Dobosz-Bartoszek M, Jones JD, Polikanov YS, Roy B, Koutmou KS. 2019. Pseudouridinylation of mRNA coding sequences alters translation. *Proceedings of the National Academy of Sciences of the United States of America* **116**:23068–23074. doi:10.1073/pnas.1821754116

9. Fernández IS, Ng CL, Kelley AC, Wu G, Yu YT, Ramakrishnan V. 2013. Unusual base pairing during the decoding of a stop codon by the ribosome. *Nature* **500**:107–110. doi:10.1038/nature12302

10. Freund I, Eigenbrod T, Helm M, Dalpke AH. 2019. RNA modifications modulate activation of innate toll-like receptors. *Genes* **10**. doi:10.3390/genes10020092

11. Gingras A-C, Raught B, Gygi SP, Niedzwiecka A, Miron M, Burley SK, Polakiewicz RD, Wyslouch-Cieszynska A, Aebersold R, Sonenberg N. 2001. Hierarchical phosphorylation of the translation inhibitor 4E-BP1. *Genes Dev* **15**:2852–2864. doi:10.1101/gad.912401

12. Harding HP, Ordonez A, Allen F, Parts L, Inglis AJ, Williams RL, Ron D. 2019. The ribosomal P-stalk couples amino acid starvation to GCN2 2 activation in mammalian cells. *eLife* **8**:1–19. doi:10.7554/eLife.50149

13. Hinnebusch AG. 2005. Translational regulation of GCN4 and the general amino acid control of yeast. *Annual Review of Microbiology* **59**:407–450. doi:10.1146/annurev.micro.59.031805.133833

14. Hinnebusch AG, Lorsch JR. 2012. The mechanism of eukaryotic translation initiation: new insights and challenges. *Cold Spring Harbor perspectives in biology* **4**. doi:10.1101/cshperspect.a011544

15. Hoernes TP, Clementi N, Faserl K, Glasner H, Breuker K, Lindner H, Hüttenhofer A, Erlacher MD. 2016. Nucleotide modifications within bacterial messenger RNAs regulate their translation and are able to rewire the genetic code. *Nucleic Acids Research* **44**:852–862. doi:10.1093/nar/gkv1182

16. Hoernes TP, Heimdörfer D, Köstner D, Faserl K, Nußbaumer F, Plangger R, Kreutz C, Lindner H, Erlacher MD. 2019. Eukaryotic translation elongation is modulated by single natural nucleotide derivatives in the coding sequences of mRNAs. *Genes* **10**:1–12. doi:10.3390/genes10020084

17. Hughes TR, Marton MJ, Jones AR, Roberts CJ, Stoughton R, Armour CD, Bennett HA, Coffey E, Dai H, He YD, Kidd MJ, King AM, Meyer MR, Slade D, Lum PY, Stepaniants SB, Shoemaker DD, Gachotte D, Chakraburtty K, Simon J, Bard M, Friend SH. 2000.

Functional Discovery via a Compendium of Expression Profiles. *Cell* **102**:109–126. doi:10.1016/S0092-8674(00)00015-5

18. Inglis AJ, Masson GR, Shao S, Perisic O, McLaughlin SH, Hegde RS, Williams RL. 2019. Activation of GCN2 by the ribosomal P-stalk. *Proceedings of the National Academy of Sciences of the United States of America* **116**:4946–4954. doi:10.1073/pnas.1813352116

19. Ishimura R, Nagy G, Dotu I, Chuang JH, Ackerman SL. 2016. Activation of GCN2 kinase by ribosome stalling links translation elongation with translation initiation. *eLife* **5**:1–22. doi:10.7554/eLife.14295

20. Karijolich J, Yu YT. 2011. Converting nonsense codons into sense codons by targeted pseudouridylation. *Nature* **474**:395–399. doi:10.1038/nature10165

21. Karikó K, Buckstein M, Ni H, Weissman D. 2005. Suppression of RNA recognition by Toll-like receptors: The impact of nucleoside modification and the evolutionary origin of RNA. *Immunity* **23**:165–175. doi:10.1016/j.immuni.2005.06.008

22. Karikó K, Muramatsu H, Keller JM, Weissman D. 2012. Increased erythropoiesis in mice injected with submicrogram quantities of pseudouridine-containing mRNA encoding erythropoietin. *Molecular Therapy* **20**:948–953. doi:10.1038/mt.2012.7

23. Karikó K, Muramatsu H, Ludwig J, Weissman D. 2011. Generating the optimal mRNA for therapy: HPLC purification eliminates immune activation and improves translation of nucleoside-modified, protein-encoding mRNA. *Nucleic Acids Research* **39**:1–10. doi:10.1093/nar/gkr695

24. Karikó K, Muramatsu H, Welsh FA, Ludwig J, Kato H, Akira S, Weissman D. 2008. Incorporation of pseudouridine into mRNA yields superior nonimmunogenic vector with increased translational capacity and biological stability. *Molecular therapy : the journal of the American Society of Gene Therapy* **16**:1833–1840. doi:10.1038/mt.2008.200

25. Karikó K, Ni H, Capodici J, Lamphier M, Weissman D. 2004. mRNA Is an Endogenous Ligand for Toll-like Receptor 3. *Journal of Biological Chemistry* **279**:12542–12550. doi:10.1074/jbc.M310175200

26. Kubota H, Obata T, Ota K, Sasaki T, Ito T. 2003. Rapamycin-induced translational derepression of GCN4 mRNA involves a novel mechanism for activation of the eIF2α kinase GCN2. *Journal of Biological Chemistry* **278**:20457–20460. doi:10.1074/jbc.C300133200

27. Lee SJ, Swanson MJ, Sattlegger E. 2015. Gcn1 contacts the small ribosomal protein Rps10, which is required for full activation of the protein kinase Gcn2. *Biochemical Journal* **466**:547–559. doi:10.1042/BJ20140782

28. Liu Q-X, Jindra M, Ueda H, Hiromi Y, Hirose S. 2003. *Drosophila* MBF1 is a co-activator for Tracheae Defective and contributes to the formation of tracheal and nervous systems. *Development* **130**:719–728. doi:10.1242/dev.00297

29. Mariotti M, De Benedictis L, Avon E, Maier JAM. 2000. Interaction between Endothelial Differentiation-related Factor-1 and Calmodulin in Vitro and in Vivo. *Journal of Biological Chemistry* **275**:24047–24051. doi:10.1074/jbc.M001928200

30. Mariotti M, De Benedictis L, Maier JAM, Ballabio E. 2004. The dual role of endothelial differentiation-related factor-1 in the cytosol and nucleus: modulation by protein kinase A. *Cellular and Molecular Life Sciences (CMLS)* **61**:1069–1074. doi:10.1007/s00018-004-4016-0

31. Meimoun A, Holtzman T, Weissman Z, McBride HJ, Stillman DJ, Fink GR, Kornitzer D. 2000. Degradation of the Transcription Factor Gcn4 Requires the Kinase Pho85 and the SCF ^{CDC4} Ubiquitin–Ligase Complex. *MBoC* **11**:915–927. doi:10.1091/mbc.11.3.915

32. Natarajan K, Meyer MR, Jackson BM, Slade D, Roberts C, Hinnebusch AG, Marton MJ. 2001. Transcriptional Profiling Shows that Gcn4p Is a Master Regulator of Gene Expression during Amino Acid Starvation in Yeast. *Molecular and Cellular Biology* **21**:4347–4368. doi:10.1128/mcb.21.13.4347-4368.2001

33. Nir R, Hoernes TP, Muramatsu H, Faserl K, Karikó K, Erlacher MD, Sas-Chen A, Schwartz S. 2022. A systematic dissection of determinants and consequences of snoRNA-guided pseudouridylation of human mRNA. *Nucleic Acids Research* **50**:4900–4916. doi:10.1093/nar/gkac347

34. Pakos-Zebrucka K, Koryga I, Mnich K, Ljujic M, Samali A, Gorman AM. 2016. The integrated stress response. *EMBO reports* **17**:1374–1395. doi:10.15252/embr.201642195

35. Parisien M, Yi C, Pan T. 2012. Rationalization and prediction of selective decoding of pseudouridine-modified nonsense and sense codons. *Rna* **18**:355–367. doi:10.1261/rna.031351.111

36. Parr CJC, Wada S, Kotake K, Kameda S, Matsuura S, Sakashita S, Park S, Sugiyama H, Kuang Y, Saito H. 2020. N 1-Methylpseudouridine substitution enhances the performance of synthetic mRNA switches in cells. *Nucleic Acids Research* **48**:E35. doi:10.1093/nar/gkaa070

37. Pelletier J, Sonenberg N. 2019. The Organizing Principles of Eukaryotic Ribosome Recruitment. *Annual review of biochemistry* **88**:307–335. doi:10.1146/annurev-biochem-013118-111042

38. Pochopien AA, Beckert B, Kasvandik S, Berninghausen O, Beckmann R, Tenson T, Wilson DN. 2021. Structure of Gcn1 bound to stalled and colliding 80S ribosomes. *Proceedings of the National Academy of Sciences of the United States of America* **118**. doi:10.1073/pnas.2022756118

39. Polack FP, Thomas SJ, Kitchin N, Absalon J, Gurtman A, Lockhart S, Perez JL, Pérez Marc G, Moreira ED, Zerbini C, Bailey R, Swanson KA, Roychoudhury S, Koury K, Li P, Kalina W V., Cooper D, Frenck RW, Hammitt LL, Türeci Ö, Nell H, Schaefer A, Ünal S, Tresnan DB, Mather S, Dormitzer PR, Şahin U, Jansen KU, Gruber WC. 2020. Safety and Efficacy of the BNT162b2 mRNA Covid-19 Vaccine. *New England Journal of Medicine* **383**:2603–2615. doi:10.1056/nejmoa2034577

40. Sattlegger E, Hinnebusch AG. 2005. Polyribosome binding by GCN1 is required for full activation of eukaryotic translation initiation factor 2α kinase GCN2 during amino acid starvation. *Journal of Biological Chemistry* **280**:16514–16521. doi:10.1074/jbc.M414566200

41. Schmitt K, Kraft A-A, Valerius O. 2021. A Multi-Perspective Proximity View on the Dynamic Head Region of the Ribosomal 40S Subunit. *IJMS* **22**:11653. doi:10.3390/ijms222111653

42. Shemer R, Meimoun A, Holtzman T, Kornitzer D. 2002. Regulation of the Transcription Factor Gcn4 by Pho85 Cyclin Pcl5. *Mol Cell Biol* **22**:5395–5404. doi:10.1128/MCB.22.15.5395-5404.2002

43. Sinha NK, Ordureau A, Best KM, Saba JA, Zinshteyn B, Sundaramoorthy E, Fulzele A, Garshott DM, Denk T, Thoms M, Paulo JA, Harper JW, Bennett EJ, Beckmann R, Green R, Harper W, Bennett EJ, Beckmann R, Green R. 2020. EDF1 coordinates cellular responses to ribosome collisions. *eLife* **9**:1–84. doi:10.7554/ELIFE.58828

44. Svidritskiy E, Madireddy R, Korostelev AA. 2016. Structural Basis for Translation Termination on a Pseudouridylated Stop Codon. *Journal of Molecular Biology* **428**:2228–2236. doi:https://doi.org/10.1016/j.jmb.2016.04.018

45. Svitkin Y V., Cheng YM, Chakraborty T, Presnyak V, John M, Sonenberg N. 2017. N1-methyl-pseudouridine in mRNA enhances translation through eIF2α-dependent and independent mechanisms by increasing ribosome density. *Nucleic Acids Research* **45**:6023–6036. doi:10.1093/nar/gkx135

46. Takemaru K, Harashima S, Ueda H, Hirose S. 1998. Yeast Coactivator MBF1 Mediates GCN4-Dependent Transcriptional Activation. *Molecular and Cellular Biology* **18**:4971–4976. doi:10.1128/mcb.18.9.4971

47. Tsuda K, Tsuji T, Hirose S, Yamazaki K. 2004. Three Arabidopsis MBF1 Homologs with Distinct Expression Profiles Play Roles as Transcriptional Co-activators. *Plant and Cell Physiology* **45**:225–231. doi:10.1093/pcp/pch017

48. Walvekar AS, Kadamur G, Sreedharan S, Gupta R, Srinivasan R, Laxman S. 2020. Methylated PP2A stabilizes Gcn4 to enable a methionine-induced anabolic program. *Journal of Biological Chemistry* **295**:18390–18405. doi:10.1074/jbc.RA120.014248

49. Wang J, Zhou J, Yang Q, Grayhack EJ. 2018. Multi-protein bridging factor 1(Mbf1), Rps3 and Asc1 prevent stalled ribosomes from frameshifting. *eLife* **7**:1–26. doi:10.7554/eLife.39637

50. Weissman D, Ni H, Scales D, Dude A, Capodici J, McGibney K, Abdool A, Isaacs SN, Cannon G, Karikó K. 2000. HIV Gag mRNA Transfection of Dendritic Cells (DC) Delivers Encoded Antigen to MHC Class I and II Molecules, Causes DC Maturation, and Induces a Potent Human In Vitro Primary Immune Response. *The Journal of Immunology* **165**:4710–4717. doi:10.4049/jimmunol.165.8.4710

51. Wek RC. 2018. Role of eIF2α Kinases in Translational Control and Adaptation to Cellular Stress. *Cold Spring Harb Perspect Biol* **10**:a032870. doi:10.1101/cshperspect.a032870

52. Wu CCC, Peterson A, Zinshteyn B, Regot S, Green R. 2020. Ribosome Collisions Trigger General Stress Responses to Regulate Cell Fate. *Cell* **182**:404-416.e14. doi:10.1016/j.cell.2020.06.006

53. Yan LL, Zaher HS. 2021. Ribosome quality control antagonizes the activation of the integrated stress response on colliding ribosomes. *Molecular Cell* **81**:614-628.e4. doi:10.1016/j.molcel.2020.11.033

54. Zanetti ME. 2003. Phosphorylation of a member of the MBF1 transcriptional co-activator family, StMBF1, is stimulated in potato cell suspensions upon fungal elicitor challenge. *Journal of Experimental Botany* **54**:623–632. doi:10.1093/jxb/erg061